Measurement of Treatment Response and Survival Prediction in Malignant Pleural Mesothelioma

Andrew Craig Kidd
B.Sc.(Med.Sci.) MBChB MRCP(UK)

Submitted in fulfilment of the requirements for the degree of Doctor of Philosophy

Institute of Infection, Immunity and Inflammation
College of Medical and Veterinary Life Sciences
University of Glasgow

July 2022

Summary

Malignant pleural mesothelioma (MPM) is a rare cancer of the mesothelial cells of the visceral and parietal pleurae that is heterogeneous in terms of biology, prognosis and response to systemic anti-cancer therapy (SACT). The primary tumour forms an unusual, complex shape which makes survival prediction and response measurement uniquely challenging. Computed tomography (CT) imaging is the bedrock of radiological quantification and response assessment, but it has major limitations that translate into low sensitivity and high inter-observer variation when classifying response using Response Evaluation Classification In Solid Tumours (mRECIST) criteria. Magnetic resonance imaging (MRI) tools have been developed that overcome some of these problems but cost and availability of MRI mean that optimisation of CT and better use for data acquired by this method are important priorities in the short term. In this thesis, I conducted 3 studies focused on, 1) development of a semi-automated volumetric segmentation method for CT based on recently positive studies in MRI, 2) training and external validation of a deep learning artificial intelligence (AI) tool for fully automated volumetric segmentation based on CT data, and, 3) use of non-tumour imaging features available from CT related to altered body composition for development of new prognostic models, which could assist in selection of patients for treatment and improving tolerance to treatment by targeting the systemic consequences of MPM.

The aim of Chapter 3 is to develop a semi-automated MPM tumour volume segmentation method that would serve as the ground truth for the training of a fully automated AI algorithm. A semi-automated approach to pleural tumour segmentation has been developed using MRI scans which calculated volumetric measurements from seed points - defined by differential tumour enhancement - placed within a pre-defined volume of pleural tumour. I extrapolated this MRI method using contrast-enhanced CT scans in 23 patients with MPM. Radiodensity values – defined by Hounsfield units (HU) - were calculated for the different thoracic tissues by placing regions of interest (ROI) on visible areas of pleural tumour with similar ROIs placed on other thoracic tissues. Pleural volume contours were drawn on axial CT slices and propagated throughout the volume by linear interpolation using volumetric software (Myrian Intrasense® software

v2.4.3 (Paris, France)). Seed points based on the radiodensity range of pleural tumour were placed on representative areas of tumour with regions grown. There were similarities in median thoracic tissue HU values: pleural tumour, 52 [IQR 46 to 60] HU; intercostal muscle, 20.4 [IQR 11.9 to 32.3] HU; diaphragm, 40.4 [IQR 26.4 to 56.4] HU and pleural fluid, 11.8 [IQR 8.3 to 17.8] HU. There was also reduced definition between MPM tumour and neighbouring structures. The mean time taken to complete semi-automated volumetric segmentations for the 8 CT scans examined was 25 (SD 7) minutes. The semi-automated CT volumes were larger than the MRI volumes with a mean difference between MRI and CT volumes of -457.6 cm^3 (95% limits of agreement -2741 to +1826 cm^3). The complex shape of MPM tumour and overlapping thoracic tissue HU values precluded HU threshold-based region growing and meant that semi-automated volumetry using CT was not possible in this thesis.

Chapter 4 describes a multicentre retrospective cohort study that developed and validated an automated AI algorithm – termed a deep learning Convolutional Neural Network (CNN) - for volumetric MPM tumour segmentation. Due to the limitations of the semi-automated approach described in Chapter 3, manually annotated tumour volumes were used to train the CNN. The manual segmentation method ensured that all the parietal pleural tumour was included in the respective volumes. Although the manual CT volumes were consistently smaller than semi-automated MRI volumes (average difference between AI and human volumes 74.8 cm^3), they were moderately correlated (Pearson's r=0.524, p=0.0103). There was strong correlation (external validation set r=0.851, p<0.0001) and agreement (external validation set mean AI minus human volume difference of +31 cm^3 between human and AI tumour volumes). AI segmentation errors (4/60 external validation set cases) were associated with complex anatomical features. There was agreement between human and AI volumetric responses in 20/30 (67%) cases. There was agreement between AI volumetric and mRECIST classification responses in 16/30 (55%) cases. Overall survival (OS) was shorter in patients with higher AI-defined pre-chemotherapy tumour volumes (HR=2.40, 95% CI 1.07 to 5.41, p=0.0114).

Survival prediction in MPM is difficult due to the heterogeneity of the disease. Previous survival prediction models have not included measures of body composition which are prognostic in other solid organ cancers. In Chapter 5, I explore the impact of loss of skeletal muscle and adipose tissue at the level of the third lumbar vertebra (L3) and the loss of skeletal muscle at the fourth thoracic (T4) vertebrae on survival and response to treatment in patients with MPM receiving chemotherapy. Skeletal and adipose muscle areas at L3 and T4 were quantified by manual delineation of relevant muscle and fat groups using ImageJ software (U.S. National Institutes of Health, Bethesda, MD) on pre-chemotherapy and response assessment CT scans, with normalisation for height. Sarcopenia at L3 was not associated with shorter OS at the pre-chemotherapy (HR 1.49, 95% CI 0.95 to 2.52, p=0.077) or response assessment time points (HR 1.48, 95% CI 0.97 to 2.26, p=0.0536). A higher visceral adipose tissue index (VFI) measured at L3 was associated with shorter OS (HR 1.95, 95% CI 1.05 to 3.62, p=0.0067). In multivariate analysis, obesity was associated with improved OS (HR 0.36, 95% CI 0.20 to 0.65, p<0.001) while interval VFI loss (HR 1.81, 95% CI 1.04 to 3.13, p=0.035) was associated with reduced OS. Overall loss of skeletal muscle index at the fourth thoracic vertebra (T4SMI) during treatment was associated with poorer OS (HR 2.79, 95% CI 1.22 to 6.40, p<0.0001). Skeletal muscle index on the ipsilateral side of the tumour at the fourth thoracic vertebra (Ipsilateral T4SMI) loss was also associated with shorter OS (HR 2.91, 95% CI 1.28 to 6.59, p<0.0001). In separate multivariate models, overall T4SMI muscle loss (HR 2.15, 95% CI 102 to 4.54, p=0.045) and ipsilateral T4SMI muscle loss (HR 2.85, 95% CI 1.17 to 6.94, p=0.021) were independent predictors of OS. Response to chemotherapy was not associated with decreasing skeletal muscle or adipose tissue indices.

Table of Contents

Summary **1**

Table of Contents **4**

List of Tables **13**

List of Figures **15**

Acknowledgments **22**

Declaration **23**

List of Abbreviations **24**

Publications relating to this thesis **32**

Presentations to Learned Societies **34**

Chapter 1: Introduction **37**

1.1 General introduction **37**

1.2 Malignant pleural mesothelioma **38**

1.2.1 Histological sub-types of MPM 39

1.3 Detection and staging of MPM **40**

1.3.1 Limitations of CT in detecting MPM 40

1.4 Systemic anti-cancer therapy in MPM **42**

1.4.1 Chemotherapy 42

1.4.2 Immunotherapy 42

1.4.2.1 Immunotherapy as first-line treatment in MPM 43

1.4.2.2 Immunotherapy as second-line treatment in MPM 43

1.5 Tumour response assessment **44**

1.5.1 Response Evaluation Criteria In Solid Tumours 45

1.5.2 Modified Response Evaluation Criteria in Solid Tumours 45

1.6 Tumour volumetry in other thoracic malignancies **47**

1.7 Previous volumetric techniques in MPM **47**

1.8 Artificial Intelligence in imaging **50**

1.8.1 Convolutional neural networks 51

1.8.2 Artificial Intelligence in MPM 52

1.9 Survival prediction in MPM..... 52

1.9.1 Performance status..... 53

1.9.2 Systemic inflammation..... 55

1.9.3 Limitations of survival prediction models in MPM 55

1.10 Cancer cachexia 56

1.11 Principal constituents of cancer cachexia 57

1.11.1 Weight loss 58

1.11.2 Anorexia..... 58

1.11.3 Systemic inflammation..... 59

1.11.4 Sarcopenia 60

1.11.4.1 Sarcopenia in MPM 61

1.11.5 Adipopenia..... 62

1.12 Body composition measurement..... 63

1.12.1 Skeletal muscle mass measurement using DEXA 63

1.12.2 Skeletal muscle mass measurement using CT 64

1.12.3 Software programmes used to measure body composition 64

1.12.4 Definition of sarcopenia: measurements at L3 67

1.12.5 Definition of sarcopenia in mesothelioma: L3 versus T4..... 68

1.12.5.1 Fourth thoracic vertebra..... 69

1.13 Overall aim and hypothesis of thesis 71

1.13.1 Chapter 3: Semi-automated segmentation of MPM tumour volume 71

1.13.2 Chapter 4: Volumetric MPM tumour assessment using human and deep learning algorithmic segmentations 71

1.13.3 Chapter 5: Prevalence, pattern and prognostic significance of altered body composition in patients with chemotherapy-treated MPM 72

2 Chapter 2: Methods..... 74

2.1 Semi-automated segmentation of MPM tumour volume 74

2.1.1 Study objectives and outcome measures 74

2.1.2 Study population 76

2.1.3 Study procedures 78

2.1.3.1 Collection of study data 78

2.1.3.2 Clinical data 78

2.1.4 Image analyses 79

2.1.4.1 Summary of MRI method 79

2.1.5 CT method 81

2.1.5.1 Radiodensity analyses 81

2.1.5.2 Pleurae 83

2.1.5.3 Other thoracic structures 83

2.1.5.4 Contour mask 84

2.1.5.5 Semi-automated segmentation using radiodensity thresholds 86

2.1.6 CT image acquisition and anonymisation 86

2.1.7 Statistical analyses 86

2.1.7.1 Primary objectives 86

2.1.7.2 Secondary objectives 87

2.2 Volumetric MPM tumour assessment using human and deep learning algorithmic segmentations 88

2.2.1 Study objectives and outcome measures 88

2.2.2 Study population 90

2.2.2.1 Original study population 90

2.2.2.2 Final version 93

2.2.3 Eligibility criteria 94

2.2.4 Study procedures 95

2.2.4.1 Clinical data 95

2.2.5 CT image acquisition and anonymisation 95

2.2.6 Treatment response evaluation using mRECIST 96
2.2.7 Manual tumour segmentation 98
2.2.8 CT image transfer 100
2.2.9 Development of the convolutional neural network 100
2.2.10 Human and AI volumetric response classification 101
2.2.11 Statistical analyses 101
2.2.11.1 Training and internal validation set 101
2.2.11.2 External validation set 102
2.3 Prevalence, pattern and prognostic significance of altered body composition in patients with chemotherapy-treated MPM 103
2.3.1 Study objectives 103
2.3.1.1 Primary objective and outcome measures 103
2.3.1.2 Secondary objectives and outcome measures 103
2.3.2 Study population 107
2.3.3 Eligibility criteria 107
2.3.4 Study procedures 108
2.3.4.1 Clinical data 108
2.3.4.2 Weight and height measurements 109
2.3.5 CT image acquisition and anonymisation 109
2.3.6 Body composition analyses 109
2.3.6.1 Skeletal muscle at the third lumbar vertebra 109
2.3.6.2 Skeletal muscle at the fourth thoracic vertebra 111
2.3.6.3 Skeletal muscle at the ipsilateral fourth thoracic vertebra 112
2.3.6.4 Adipose tissue at the third lumbar vertebra 113
2.3.7 Body composition index changes 115
2.3.8 Chemotherapy response evaluation 116
2.3.9 Tumour volume 116
2.3.10 Statistical analyses 116
2.3.10.1 Primary objective 116

2.3.10.2 Secondary objectives 116

3 Chapter 3: Semi-automated segmentation of MPM tumour volume 119

3.1 Introduction 119

3.2 Methods 121

3.3 Results 122

3.3.1 Study population 122

3.3.2 Primary objectives 123

3.3.2.1 Radiodensity measurements 123

3.3.2.2 Comparison of radiodensities in pleural tumour and other tissues 125

3.3.2.3 Segmentation attempt 1 127

3.3.2.4 Segmentation attempts 2 to 5 128

3.3.2.5 Segmentation attempts 6 and 7 130

3.3.2.6 Radiodensity measurements using axial views 130

3.3.2.7 Segmentation attempts using median pleural tumour ROI in axial views 133

3.3.2.8 Time taken for volume analyses 137

3.3.3 Secondary objectives 137

3.3.3.1 Correlation and agreement analyses between semi-automated CT and MRI volumes 137

3.3.3.2 Abandonment of a semi-automated segmentation approach 139

3.4 Discussion 140

3.4.1 Heterogeneity of Hounsfield units in thoracic tissues 140

3.4.2 Comparison to MRI method 140

3.4.3 ROI measurements in coronal and axial views 141

3.4.4 Comparison to other semi-automated CT segmentation methods 142

3.4.5 Possible clinical implications 145

3.4.6 Study limitations and strengths 145

3.5 Conclusion 148

4 Chapter 4: Volumetric MPM tumour assessment using human and deep learning algorithmic segmentations 150

4.1 Introduction 150

4.2 Methods 152

4.3 Results 153

4.3.1 Study population 153

4.3.2 Training and internal validation 155

4.3.2.1 Manual CT tumour volumes 155

4.3.2.2 Comparison between manual CT and semi-automated MRI tumour volumes 155

4.3.2.3 Reproducibility 157

4.3.2.4 Human versus AI volumes 158

4.3.3 External validation 159

4.3.3.1 Human versus AI volumes 159

4.3.3.1.1 Human versus AI pre-chemotherapy volumes 160

4.3.3.1.2 Human versus AI response assessment volumes 161

4.3.4 Visual inspection of outlying volumes 162

4.3.5 Changes in tumour volume following chemotherapy by human and AI 163

4.3.6 mRECIST versus AI volumetric response 166

4.3.7 Survival analyses 170

4.4 Discussion 172

4.4.1 Manual CT method 172

4.4.2 Comparison to the MRI method 172

4.4.3 AI and ground truth tumour volumes 174

4.4.4 Tumour volume comparison to other studies 175

4.4.5 CNN model performance 175

4.4.6 Reproducibility 175

4.4.7 Analysis of anatomical features associated with AI segmentation errors 176

4.4.8 Survival analyses 177

4.4.9 Differences in mRECIST-, human- and AI-defined volumetric response classification 178

4.4.10 Thresholds for AI and mRECIST response classification 179

4.4.11 Comparison with other computer-generated tumour volumes. 180

4.4.12 Possible clinical implications 180

4.4.13 Study limitations and strengths 181

4.5 Conclusions 183

5 Chapter 5: Prevalence, pattern and prognostic significance of altered body composition in patients with chemotherapy-treated MPM 185

5.1 Introduction 185

5.2 Methods 187

5.3 Results 188

5.3.1 Study population 188

5.3.2 Primary objective 191

5.3.2.1 Prevalence and pattern of sarcopenia and adipopenia at L3 191

5.3.2.1.1 Sarcopenia 191

5.3.2.1.2 Adipopenia 191

5.3.2.2 Prevalence and pattern of sarcopenia at T4 192

5.3.3 Secondary objectives 193

5.3.3.1.1 L3 measures and systemic inflammation and tumour volume 193

5.3.3.1.2 T4 measures and systemic inflammation and tumour volume 195

5.3.3.1.3 Survival at L3 and T4 200

5.3.3.1.4 Reproducibility at L3 215

5.3.3.1.5 Reproducibility at T4 215
5.3.4 Exploratory objectives 216
5.3.4.1 Ipsilateral T4 and survival 216
5.3.4.2 Chemotherapy treatment completion and response to treatment 218
5.3.4.2.1 Relationship between chemotherapy treatment completion and response to treatment at L3 218
5.3.4.2.2 Relationship between chemotherapy treatment completion and response to treatment at T4 220
5.3.4.3 Sex-and BMI-specific differences 223
5.3.4.3.1 Sex-specific differences at L3 223
5.3.4.3.2 Sex-and BMI-specific differences at T4 225
5.3.4.4 Correlation between L3 and T4 227
5.4 Discussion 229
5.4.1 Skeletal muscle measurements at the L3 and T4 229
5.4.2 Thresholds for sarcopenia 229
5.4.3 Body composition differences between male and female patients 230
5.4.4 Correlations between T4SMI and L3SMI 232
5.4.5 Sarcopenia survival outcomes 233
5.4.6 Adipopenia 235
5.4.7 Treatment tolerance 237
5.4.8 Response assessment 239
5.4.9 Systemic inflammation 240
5.4.10 Tumour volume 241
5.4.11 Potential clinical implications 242
5.4.12 Study limitations and strengths 243
5.5 Conclusions 245
6 Chapter 6: Conclusions 247

6.1 Limitations of semi-automated tumour segmentation in MPM.. 248

6.2 Development of automated tumour volumetry in MPM 248

6.3 The prognostic significance of altered body composition in MPM 249

6.4 Future work 251

References 253

List of Tables

Table 1.1 Eighth edition of the TNM staging system for MPM..... 41

Table 1.2 WHO/ECOG Performance Status 54

Table 1.3 Examples of body composition software programmes 66

Table 2.1 Objectives and outcome measures of the semi-automated segmentation of MPM tumour volume study..... 75

Table 2.2 Objectives and outcome measures of volumetric MPM tumour assessment using human and deep learning algorithmic segmentations study... 89

Table 2.3 Original studies included in the first Automatic RECIST reporting in Mesothelioma using Deep Learning Artificial Intelligence protocol 91

Table 2.4 mRECIST standardised window settings..... 97

Table 2.5 Primary and secondary objectives and associated outcome measures of the altered body composition study 104

Table 2.6 Exploratory objectives and outcome measures of the altered body composition study 106

Table 3.1 Clinicopathological data of 23 patients with MPM who had contemporaneous contrast-enhanced CT and MRI scans.....122

Table 3.2 Pleural tumour ROI HU values obtained in the coronal plane of contrast-enhanced CT scans 123

Table 3.3 Other thoracic tissues ROI HU values obtained in the coronal plane of contrast-enhanced CT scans 124

Table 3.4 Subjective visual analysis of ROIs in coronal plane slices of contrast-enhanced CT scans 131

Table 3.5 Comparison of pleural tumour ROIs in coronal and axial planes of contrast-enhanced CT scans 134

Table 4.1 Clinicopathological data in patients with MPM divided according to training and internal validation (scan n=123) and external validation sets (scan n=30) 154

Table 4.2 Manually segmented pleural tumour volume differences between two human readers 157

Table 4.3 Response to treatment defined by human and AI volumes and mRECIST in 30 patients with MPM (n=60 scans) 166

Table 5.1 Clinicopathological characteristics in patients with MPM who received chemotherapy.....190

Table 5.2 Body composition measurements at L3 (n=91) and T4 (n=111).....192

Table 5.3 Inflammatory indices between pre-chemotherapy and response assessment time points in a single centre sub-group of 47 patients with MPM .197

Table 5.4 Correlation matrices of p-values of T4 skeletal muscle indices and inflammatory indices of a single centre sub-group of 47 patients with MPM....198

Table 5.5 Chi square of decreased T4SMI percentage change and increasing inflammatory indices between pre-chemotherapy and response assessment inflammatory indices in a single centre sub-group of 47 patients with MPM 199

Table 5.6 Hazard ratios from Log Rank test for T4SMI indices between males and females 205

Table 5.7 Univariate and multivariate analyses of factors contributing to overall survival in 111 patients with MPM.....207

Table 5.8 Hazard ratios from Log Rank test for pre-chemotherapy and response assessment adipose tissue indices in 91 patients with MPM.....209

Table 5.9 Univariate and multivariate analyses of factors contributing to overall survival in 91 patients with MPM 213

Table 5.10 Sex-specific differences in skeletal muscle and adipose indices at L3 in 91 patients with MPM 224

Table 5.11 Body composition analyses at T4 in 111 patients with MPM 226

List of Figures

Figure 1.1 Contrast-enhanced coronal CT image of a patient with MPM. A large malignant pleural effusion (red P) and pleural enhancement (white arrows) are visible 44

Figure 1.2 Axial contrast-enhanced CT image of a patient with MPM demonstrating mRECIST. The blue lines represent measurements taken perpendicular to the chest wall and the vertebral column 46

Figure 1.3 Pathophysiology of cancer cachexia 57

Figure 1.4 Axial CT scan slices of two patients in the TRACERx study delineated by me demonstrating the differences in adiposity between patients. Subcutaneous (green), visceral (yellow) and intra-muscular (blue) adipose tissue compartments are visible. The red represents skeletal muscle. The image was created on Slice-O-Matic® software v5.0 (TomoVision, Montreal, Canada) 63

Figure 1.5 Single axial contrast-enhanced CT image of a patient with MPM demonstrating the muscles at the third lumbar vertebra (L3) which include the psoas (A), erector spinae (B), quadratus lumborum (C), transversus abdominis (D), internal obliques (E), external 67

Figure 1.6 Single axial contrast-enhanced CT image of a patient with MPM demonstrating the muscles at the fourth thoracic vertebra (T4) which includes the pectoralis (A), intercostals (B), sub-scapularis (C), infraspinatus (D), trapezius(E) and erector spinae (F) 69

Figure 2.1 Flowchart of patients included in semi-automated segmentation of MPM tumour study 77

Figure 2.2 Coronal plane of contrast-enhanced MRI scans illustrating the semi-automated SI-tuned pleural tumour segmentation method 80

Figure 2.3 Coronal plane of contrast-enhanced CT scans with ROIs placed on areas representative of pleural tumour across three different slices (highlighted by the green dots) 82

Figure 2.4 Coronal CT scan slice illustrating thoracic tissues 84

Figure 2.5 Example of contouring of pleural tumour in the axial slice of a contrast-enhanced CT scan. The yellow area contains what was interpreted as pleural tumour 85

Figure 2.6 Example of the difference in pleural tumour resolution between a contrast-enhanced CT scan (left) and contrast-enhanced MRI (right) in the same patient. The white arrow denotes pleural enhancement..... 85

Figure 2.7 Flowchart of pleural tumour volumes included in the original Automatic RECIST reporting in Mesothelioma using Deep Learning Artificial Intelligence protocol (n=468 patients) 92

Figure 2.8 Flowchart of pleural tumour volumes included in final Automatic RECIST reporting in Mesothelioma using Deep Learning Artificial Intelligence protocol (n=108 patients) 93

Figure 2.9 Example of manual pleural tumour segmentation when viewed in the axial plane in Panel A, the coronal plane in Panel B and in 3-D in Panel C. Pleural tumour is highlighted in green 99

Figure 2.10 Axial slices of CT scans demonstrating the third lumbar vertebra (L3). Panel A demonstrates the delineation of the external skeletal muscle area (SMA) on ImageJ software, defined by the area included in the dotted yellow line. Panel B demonstrates the skeletal muscle threshold selection using a HU range of -29 to +150 HU. Panel C demonstrates the delineation of the internal SMA, defined by the area included in the dotted yellow line. Panel D demonstrates skeletal muscle HU threshold selection.....110

Figure 2.11 Axial slices of CT scans demonstrating fourth thoracic vertebra (T4). Panel A demonstrates the delineation of the external skeletal muscle area (SMA) on ImageJ software, defined by the area included in the dotted yellow line. Panel B demonstrates the skeletal muscle threshold selection (HU range, -29 to +150 HU). Panel C demonstrates the delineation of the internal SMA, defined by the area included in the dotted yellow line. Panel D demonstrates skeletal muscle HU threshold selection 111

Figure 2.12 Axial slices of CT scans demonstrating fourth thoracic vertebra (T4). Panel A demonstrates the delineation of the external skeletal muscle area (SMA)

on the ipsilateral side of MPM tumour, defined by the area included in the dotted yellow line. Note the straight yellow line separating the ipsilateral and contralateral muscle compartments. Panel B demonstrates the skeletal muscle threshold selection (HU range, -29 to +150 HU). Panel C demonstrates the delineation of internal SMA, defined by the area included in the dotted yellow line. Panel D demonstrates skeletal muscle HU threshold selection 112

Figure 2.13 Axial slices of CT scans demonstrating L3. Panel A demonstrates the delineation of the external adipose tissue on ImageJ software, defined by the area included in the dotted yellow line. Panel B demonstrates the adipose tissue threshold selection using established adipose tissue HU ranges of -190 to -30 HU. Panel C demonstrates the delineation of external adipose tissue area. Panel D demonstrates adipose tissue HU threshold selection. Panel E and F demonstrates internal adipose tissue area (defined by the area included in the dotted yellow line) and HU threshold selection, respectively 114

Figure 3.1 Violin plots illustrating overlapping HU values of all thoracic tissues. The dotted lines inside the violins represent the median and 25th and 75th percentile HU values. The red dotted lines across the plot represent the minimum and maximum HU values for pleural tumour 125

Figure 3.2 Violin plots illustrating overlapping HU values of pleural tumour and adjacent thoracic tissues, including intercostal muscle, pleural fluid and diaphragm. The dotted lines inside the violins represent the median and 25th and 75th percentile HU values. The red dotted lines across the plot represent the minimum and maximum HU values for pleural tumour 126

Figure 3.3 Segmentation attempt illustrating erroneous extrusion of the contour mask (white arrows) 127

Figure 3.4 Segmentation attempt illustrating under-segmentation of pleural tumour (in blue). There are light grey areas of pleural tumour that should have been entirely blue (white arrows) 128

Figure 3.5 Segmentation attempt illustrating under-segmented pleural tumour (in blue). There are light grey areas of pleural tumour that should have been entirely blue (white arrow) 129

Figure 3.6 Segmentation attempt illustrating both erroneous contour mask propagation (in blue, overlying pleural effusion) and extra-pleural segmentation errors (white arrow) 129

Figure 3.7 Segmentation attempt illustrating over-segmentation with bleeding into the pleural fluid (blue area highlighted by white arrows) 130

Figure 3.8 Example of pleural tumour (white arrows) when viewed in axial (A) and coronal (B) planes in the same patient. The contrast is clearer on Panel A compared to Panel B.....132

Figure 3.9 Radiodensity measurements in the axial plane with the red marker placed on an area representative of pleural tumour.....133

Figure 3.10 Segmentation attempt 8 illustrating over-segmentation (in blue) with inclusion of non-pleural tumour (white arrows) in the final volume using seed point thresholds of +/- 22 HU.....135

Figure 3.11 Difficulties in interpreting pleural tumour. Panel A illustrates the similarities between pleural tumour (red arrow) and atelectasis (white arrow). Panel B illustrates the difficulties in differentiating between different tissues, e.g., pleural fluid (red P), atelectasis (white arrow) and tumour (red arrows). Panel C illustrates non-confluence of pleural tumour (red arrows) which resulted in software limitations and time spent returning to edit the completed contour mask. Panel C also illustrates atelectasis (white arrow). Panel D illustrates calcified tumour (white arrow) which was not included in the segmented volumes and pleural tumour (red arrows) 136

Figure 3.12 Bland-Altman plot (Panel A) and Spearman's correlation (Panel B) comparing primary tumour volume measured using semi-automated segmentation CT scans versus semi-automated segmentation MRI scans in 8 patients with MPM.....138

Figure 4.1 Bland-Altman plot (Panel A) and Pearson's correlation (Panel B) comparing tumour volume measured using manual segmentation CT scan versus semi-automated segmentation MRI in 23 patients with MPM 156

Figure 4.2 Bland-Altman analysis (Panel A) and Spearman's correlation (Panel B) between human and AI training and interval validation set volumes (n=80 scans) 158

Figure 4.3 Bland-Altman analysis (Panel A) and Spearman's correlation (Panel B) between human and AI external validation set volumes in 60 scans 159

Figure 4.4 Bland-Altman analysis (Panel A) and Spearman's correlation (Panel B) between pre-chemotherapy (PC) human and AI external validation set volumes in 60 scans.....160

Figure 4.5 Bland-Altman analysis (Panel A) and Spearman's correlation (Panel B) between response assessment (Res) human and AI external validation set volumes in 60 scans 161

Figure 4.6 Examples of the scans out-with the 95% limits of agreement. Panel A illustrates under-segmentation by the AI in pre-chemotherapy images with tumour in the left lung fissure (yellow arrow) not included in the final volume. Panel B illustrates over-segmentation with the AI erroneously including lung atelectasis above the right hemidiaphragm (yellow arrow). Panel C illustrates over-segmentation with the AI erroneously including contralateral benign pleural thickening by the AI (yellow arrow) 162

Figure 4.7 Bland-Altman analysis (Panel A) and Spearman's correlation (Panel B) between human and AI percentage volume change in the 60 volumes in the external validation set.....163

Figure 4.8 Comparison of human- and AI-defined volume responses for each patient (rows 1 to 30) in the external validation set. Partial response is green, stable disease is amber and progressive disease is red 164

Figure 4.9 Comparison of human- and AI-defined volume responses for each patient (rows 1 to 30) in the external validation set. Progressive disease (PD) is red and Non-PD is blue 165

Figure 4.10 Comparison of mRECIST- and AI-defined volume responses for each patient (rows 1 to 30) in the external validation set. Partial response is green, stable disease is amber and progressive disease is red 167

Figure 4.11 Comparison of mRECIST- and AI-defined volume responses for each patient (rows 1 to 30) in the external validation set. Progressive disease (PD) is red and Non-PD is blue 168

Figure 4.12 Classification of percentage human volume changes into mRECIST (Panel A) and AI-defined (Panel B) progressive disease (PD), stable disease (SD) and partial response (PR) in the external validation set 169

Figure 4.13 Kaplan-Meier curves and number at risk tables illustrating overall survival stratified by, Panel A) pre-chemotherapy human tumour volume ≥366 cm3 and, Panel B) pre-chemotherapy AI tumour volume ≥427 cm3, Panel C) human volume-defined progressive disease (PD) and Non-PD, Panel D) AI volume-defined PD and Non-PD, and, Panel E) mRECIST-defined PD and Non-PD.....171

Figure 5.1 Flowchart of body composition study 189

Figure 5.2 Heatmap of adjusted p-values summarising associations of L3 skeletal muscle and adipose indices and inflammatory indices and tumour volume in 91 patients with MPM.....194

Figure 5.3 Heatmap of adjusted p-values summarising associations of total T4 skeletal muscle index percentage change (Panel A) and ipsilateral T4SMI percentage change (Panel B) and inflammatory indices and tumour volume in 111 patients with MPM.....196

Figure 5.4 Kaplan-Meier curves and number at risk tables illustrating no survival differences in overall survival (OS) and L3 muscle index differences at pre-chemotherapy (Panel A) and response assessment (Panel B) time points and in patients who lose skeletal muscle at L3 during chemotherapy (Panel C).....201

Figure 5.5 Kaplan-Meier curves and number at risk tables illustrating no survival differences in overall survival (OS) and pre-chemotherapy (Panel A) and response assessment (Panel B) fourth thoracic vertebra skeletal muscle indices. Panel C illustrates poorer OS in patients who lost thoracic skeletal muscle during chemotherapy (Panel C).....203

Figure 5.6 Kaplan-Meier curves and number at risk tables illustrating poorer OS in those patients with higher disease stage losing skeletal muscle at T4 during

chemotherapy (Panel A) and in those patients with higher pre-chemotherapy tumour volume losing thoracic skeletal muscle during chemotherapy (Panel B) 204

Figure 5.7 Kaplan-Meier curves and number at risk tables illustrating the survival advantage afforded by not losing total fat (Panel A) and visceral fat (Panel B) between pre-chemotherapy and response assessment time points. Subcutaneous fat tissue loss was not associated with overall survival (Panel C).....211

Figure 5.8 Kaplan-Meier curves and number at risk tables illustrating overall survival stratified by muscle losing and non-losing groups, Panel A) pre-chemotherapy ipsilateral (to tumour) T4SMI, Panel B), response assessment ipsilateral T4SMI, and, Panel C) ipsilateral T4SMI percentage change between pre-chemotherapy and response assessment scans 217

Figure 5.9 Scatterplot illustrating mRECIST-defined response assessment criteria and percentage changes between pre-chemotherapy and response assessment scans in, Panel A) total fat index (TFI), and, Panel B) visceral fat index (VFI) in 91 patients with MPM 219

Figure 5.10 Violin plots illustrating fourth thoracic vertebra skeletal muscle index (T4SMI) and ipsilateral (to tumour) T4SMI percentage changes between pre-chemotherapy and response assessment scans and response assessment criteria according to, Panels A) and, Panel B) mRECIST, and, Panel C) and, Panel D) human volumes in 111 patients with MPM.....222

Figure 5.11 Correlations between third lumbar vertebra skeletal muscle index (L3SMI) and fourth thoracic vertebra skeletal muscle index (T4SMI) at the pre-chemotherapy time points in all patients (Panel A), male (Panel B) and female patients (Panel C), and at response assessment time points in all patients (Panel D), male (Panel E) and female patients (Panel F) 228

Acknowledgments

I will be forever grateful to Professor Kevin G. Blyth for his guidance, expert supervision and mentorship during my four-and-a-half-year tenure with the Glasgow Pleural Disease Unit (GPDU). My thanks also go to Professor Anthony Chalmers for his supportive co-supervision and to Dr Mariam Jamal-Hanjani and Dr Barry Laird for their expert guidance. I would like to thank the University of Glasgow, University College London and NHS Greater Glasgow and Clyde for my employment as a Clinical Research Fellow.

I am indebted to my good friend Dr Geoffrey Martin for his assistance in the inter-observer work as well as his support throughout and after my research fellowship. This work could not have been undertaken without the assistance of my former GPDU colleagues Dr Selina Tsim and Dr Jenny Ferguson and radiology collaborator Dr Gordon Cowell. The artificial intelligence work would not have been possible without the work of Owen Anderson and Keith Goatman and the rest of the team at Canon Medical Research Europe. I also wish to express my gratitude to my research nurse colleague Patricia Clark who provided me with invaluable insights into the practicalities and governance of clinical research. I would also like to thank Rosie Woodward and the Glasgow Clinical Research Imaging Facility radiographers for their support in facilitating the radiographic images used in this thesis. I also extend my thanks to Dr Marcin Skrzypski for his body composition software teaching during my visits to the University College London Cancer Institute.

Finally, I must acknowledge all the patients who participated in the Diagnostic and Prognostic Biomarkers in the Rational Assessment of Mesothelioma study, the Prediction of Resistance to Chemotherapy in Malignant Pleural Mesothelioma study and the Automatic RECIST reporting in Mesothelioma using Deep Learning Artificial Intelligence study.

This thesis is dedicated to my late father, James Alexander Kidd. I was not able to share my undergraduate or postgraduate journeys with him, but his interest in science was the catalyst that ignited my pursuit of knowledge.

Declaration

The work presented in this thesis was undertaken during my tenure as a Clinical Research Fellow at the Glasgow Pleural Disease Unit, Queen Elizabeth University Hospital, Glasgow and at the Institute of Cancer Sciences, College of Medical and Veterinary Life Sciences, at the University of Glasgow. I was supervised by Professor Kevin Blyth and Professor Anthony Chalmers.

The work reported in this thesis was undertaken by me with the assistance of colleagues who I have made explicit reference to as well as the extent of their contributions in the text of this thesis.

Work relating to this thesis has been published in or submitted to peer-reviewed journals and presented at national and international conferences.

The writing of this thesis constitutes my own work, written solely by me.

Signed:

Andrew Craig Kidd, June 2022

List of Abbreviations

ACTRII	Activin Type 2 Receptors
AGRP	Agouti-Related Peptide
AI	Artificial Intelligence
AMPK	5' Adenosine Monophosphate-activated Protein Kinase
ASCO	American Society of Clinical Oncology
AU	Arbitrary Units
BAPE	Benign Asbestos Pleural Effusion
BAT	Brown Adipose Tissue
BMI	Body Mass Index
BSA	Body Surface Area
BTS	British Thoracic Society
CALGB	Cancer and Leukaemia Group B
C4d	Complement Component 4d
CI	Confidence Interval
CM	Centimetre
CM^2	Centimetre Squared
CM^2/M^2	Centimetre Squared Per Metre Squared

CM^3	Centimetre Cubed
CMRE	Canon Medical Research Europe
CNN	Convolutional Neural Network
CNV	Copy Number Variations
COPD	Chronic Obstructive Pulmonary Disease
CR	Complete Response
CRP	C-Reactive Protein
CRUK	Cancer Research United Kingdom
CT	Computed Tomography
CTLA-4	Cytotoxic T-Lymphocyte–Associated Protein 4
CTPA	Computed Tomography Pulmonary Angiogram
CXR	Chest Radiograph
DCE-CT	Dynamic Contrast-Enhanced Computed Tomography
DCE-MRI	Dynamic Contrast-Enhanced Magnetic Resonance Imaging
DEXA	Dual-Energy X-ray Absorptiometry
DIAPHRAGM	Diagnostic and Prognostic Biomarkers in the Rational Assessment of Mesothelioma
DICOM	Digital Imaging and Communications in Medicine

DICOM-RT	Digital Imaging and Communications in Medicine Radiotherapy
DNA	Deoxyribonucleic Acid
ECOG	Eastern Cooperative Oncology Group
eGFR	Estimated Glomerular Filtration Rate
EORTC	European Organisation for Research and Treatment of Cancer
ESMO	European Society for Medical Oncology
FDG	Fluorodeoxyglucose
FFPE	Formalin-Fixed Paraffin-Embedded
G	Grams
G/L	Grams Per Litre
GTV	Gross Tumour Volume
HASTE	Half-Fourier Single-Shot Fast Spin-Echo Sequence
HRA	Health Research Authority
HU	Hounsfield Units
IASLC	International Association for the Study of Lung Cancer
ICC	Intraclass Correlation Coefficient
IL-6	Interleukin-6

IQR	Interquartile Range
KG	Kilogram
KG/M^2	Kilogram Per Metre Squared
KS	Karnofsky Performance Status
L3	Third Lumbar Vertebra
L3SMA	Skeletal Muscle Area at the Third Lumbar Vertebra
L3SMI	Skeletal Muscle Index at the Third Lumbar Vertebra
L3TFI	Total Fat Index at L3 at the Third Lumbar Vertebra
L3VFI	Visceral Fat Index at L3 at the Third Lumbar Vertebra
L5	Fifth Lumbar Vertebra
LMR	Lymphocyte-to-monocyte ratio
M	Metre
M^2	Metre Squared
MARS2	Mesothelioma and Radical Surgery 2
MDT	Multi-Disciplinary Team
MG	Milligrams
MG/L	Milligrams Per Litre
MGPS	Modified Glasgow Prognostic Score

ML	Millilitre
ML/MIN	Millilitres Per Minute
MM	Millimetre
mPFS	Median Progression Free Survival
MPM	Malignant Pleural Mesothelioma
MRECIST	Modified Response Evaluation Criteria in Solid Tumours
MRI	Magnetic Resonance Imaging
MTV	Metabolic Tumour Volume
NCI	US National Cancer Institute
NHS	National Health Service
NHSGGC	NHS Greater Glasgow and Clyde
NLR	Neutrophil-to-Lymphocyte ratio
Non-PD	Non-Progressive Disease
NSCLC	Non-Small Cell Lung Cancer
OS	Overall Survival
PACS	Picture Archiving and Communication System
PD	Progressive Disease
PD-1	Programmed Cell Death Protein 1

PD-L1	Programmed Death Ligand Protein 1
PET	Positron Emission Tomography
PLR	Platelet-to-Lymphocyte Ratio
POMC	Proopiomelanocortin
PR	Partial Response
PREDICT-Meso	Pre-malignant Drivers Combined with Target-Drug Validation in Mesothelioma
PRISM	Prediction of Resistance to Chemotherapy in Malignant Pleural Mesothelioma
PS	Performance Status
QEUH	Queen Elizabeth University Hospital
R&D	Research and Development
REC	Research Ethics Committee
RECIST	Response Evaluation Criteria in Solid Tumours
REE	Resting Energy Expenditure
ROI	Region of Interest
SACT	Systemic Anti-Cancer Therapy
SAT	Subcutaneous Adipose Tissue
SCC	Squamous Cell Carcinoma

SCLC	Small Cell Lung Cancer
SD	Standard Deviation
SD	Stable Disease
SFA	Subcutaneous Fat Area
SFI	Subcutaneous Fat Index
SMA	Skeletal Muscle Area
SMI	Skeletal Muscle Index
SI	Signal Intensity
SUV	Standardised Uptake Value
SUV_{MAX}	Maximum Standardised Uptake Value
SWAMP	South West Area Mesothelioma and Pemetrexed
T4	Fourth Thoracic Vertebra
T4SMI	Skeletal Muscle Index at the Fourth Thoracic Vertebra
T5	Fifth Thoracic Vertebra
T10	Tenth Thoracic Vertebra
T12	Twelfth Thoracic Vertebra
TFA	Total Fat Area
TFI	Total Fat Index

TGF	Transforming Growth Factor
TGV	Total Glycolytic Volume
TLG	Total Lesion Glycolysis
TMATV	Total Metabolic Active Tumour Volume
TNF	Tumour Necrosis Factor
TNF-α	Tumour Necrosis Factor-alpha
TNM	TNM Classification of Malignant Tumours
TRACERx	TRAcking Cancer Evolution through therapy (Rx)
TTB	Total Tumour Burden
UCP1	Uncoupling Protein 1
UG/L	Micrograms Per Litre
VAT	Visceral Adipose Tissue
VFA	Visceral Fat Area
VFI	Visceral Fat Index
WAT	White Adipose Tissue
WCC	White Cell Count
WHO	World Health Organisation

Publications relating to this thesis

1. Kidd AC, Anderson O, Cowell GW, Weir AJ, Voisey JP, Evison M, Tsim S, Goatman KA, Blyth KG. Fully automated volumetric measurement of malignant pleural mesothelioma by deep learning AI: validation and comparison with modified RECIST response criteria

   Thorax 2021; doi:10.1136/thoraxjnl-2021-217808

2. Armato SG III, Nowak AK, Francis RJ, Katz SI, Kholmatov M, Blyth KG, Gudmundsson E, Kidd AC, Gill R. Imaging in pleural mesothelioma: a review of the 15th International Conference of the International Mesothelioma Interest Group

   Lung Cancer 2021; 164: 76-83

3. Estimating the false positive prediction rate in automated volumetric measurements of malignant pleural mesothelioma

   Anderson O, Kidd AC, Goatman KA, Weir AJ, Voisey JP, Dilys V, Siebert JP, Blyth KG

   Biomedical Engineering Systems and Technologies. BIOSTEC 2020. Communications in Computer and Information Science, vol 1400. Springer, Cham. https://doi.org/10.1007/978-3-030-72379-8_7

4. A comparison between MRI and CT in the assessment of primary tumour volume in mesothelioma

   Tsim S, Cowell GW, Kidd AC, Woodward R, Alexander L, Kelly C, Foster JE, Blyth KG

   Lung Cancer 2020; 150: 12–20

5. Fully automated volumetric measurement of malignant pleural mesothelioma from computed tomography images by deep learning: preliminary results of an internal validation

   Anderson O, Kidd AC, Goatman KA, Weir AJ, Voisey J, Dilys V, Siebert JP, Blyth KG

   Bioimaging 2020; RP-21: Full Paper

6. Cancer cachexia in thoracic malignancy: a narrative review

   Kidd AC, Skrzypski M, Jamal-Hanjani M, Blyth KG

   Current Opinion in Supportive and Palliative Care 2019; 13(4): 316–22

7. Survival prediction in mesothelioma using a scalable lasso regression model: instructions for use and initial performance using clinical predictors

   Kidd AC, McGettrick M, Tsim S, Halligan DL, Bylesjo M, Blyth KG

   BMJ Open Respiratory Research 2017; 5(1): e000240

Presentations to Learned Societies

1. Prognostic significance of loss of skeletal muscle in patients with malignant pleural mesothelioma receiving chemotherapy

   Kidd AC, Winter A, Miller L, Baird W, Dick C, Pearce D, Sloan W, Cowell G, Noble C, Smith A, Westwood P, Hopkins T, Williams N, Walter H, King A, Fennell D, Blyth KG

   Accepted for oral presentation at the rescheduled virtual International Conference of the International Mesothelioma Interest Group, May 2021

2. Thoracic skeletal muscle loss is prognostic in malignant pleural mesothelioma

   Kidd AC, Winter A, Miller L, Baird W, Dick C, Pearce D, Sloan W, Cowell GW, Noble C, Smith A, Westwood P, Hopkins T, Williams N, Walter H, King W, Fennell D, Blyth KG

   Accepted for ePoster presentation at the British Thoracic Society Winter Meeting, February 2021

3. Mesothelioma is associated with ipsilateral thoracic muscle loss

   Kidd AC, Winter A, Miller L, Baird W, Dick C, Pearce D, Sloan W, Cowell GW, Noble C, Smith A, Westwood P, Hopkins T, Williams N, Walter H, King W, Fennell D, Blyth KG

   Accepted for ePoster presentation at the European Respiratory Society Congress, September 2020

4. Technical limitation of semi-automated volumetric analysis using CT in patients with malignant pleural mesothelioma

   Kidd AC, Tsim S, Blyth KG

   Accepted for poster presentation at the European Respiratory Society, October 2019

5. Can we treat mesothelioma cachexia?

   Kidd AC

   Invited oral presentation at the 17th Annual British Thoracic Oncology Group Conference, January 2019

6. Survival prediction in malignant pleural mesothelioma: fundamental limitations of routinely available clinic predictors

   Kidd AC, McGettrick M, Tsim S, Halligan DL, Bylesjo M, Blyth KG

   Accepted for poster presentation at the British Thoracic Society Winter Meeting, December 2017

Chapter 1

INTRODUCTION

Chapter 1: Introduction

1.1 General introduction

Malignant pleural mesothelioma (MPM) is a rare and incurable tumour of mesothelial cells of the pleurae associated with antecedent asbestos exposure. The median survival time is approximately 12-months(1). The first-line treatment of MPM in NHS England and Wales is doublet chemotherapy(2) which affords an additional 3-month survival advantage(3). In February 2022, the Scottish Medicines Consortium (SMC) approved the use of nivolumab and ipilimumab immunotherapy as a first-line treatment for adults with unresectable MPM in NHS Scotland(4). Nivolumab has been approved in the second-line treatment setting in NHS England and Wales(5).

All systemic anti-cancer therapies (SACT) have toxic side effects and it is important to have objective measures of response to treatment to justify the continuation of treatment. Response assessment in solid organ cancers has traditionally been measured using Response Evaluation Criteria for Solid Tumours (RECIST) criteria. In MPM, modified Response Evaluation Criteria for Solid Tumours (mRECIST) criteria have been developed to provide objectivity when assessing treatment response(6), but there are shortcomings with these criteria. An automated approach specific to the distinct morphological complexities of MPM tumour is imperative.

SACT requires the maintenance of adequate fitness during treatment. Fitness is regularly assessed in the clinical setting by means of clinical examination, biochemical laboratory tests and anthropometric measurements. Patients receiving SACT commonly develop cancer cachexia which is a complex syndrome resulting in changes in body weight and composition(7). Sarcopenia – the loss of skeletal muscle mass - is a principal component of cancer cachexia and is prognostically significant in other solid organ cancers. Adipopenia – the loss of adipose tissue – is another feature of the cachexia syndrome. Although encountered frequently in the clinical setting, very few research studies have determined the significance of altered body composition in patients with MPM.

The general aim of my thesis is to develop and examine radiological biomarkers to measure treatment response and predict survival in patients with chemotherapy-treated MPM.

1.2 Malignant pleural mesothelioma

Malignant pleural mesothelioma (MPM) is an incurable cancer of the mesothelial cells of the pleurae(8). MPM is associated with prior exposure to asbestos fibres(9). Exposure can be via industrial use of asbestos or through second-hand exposure such as spousal contact(10). Exposure to asbestos can occur after contact with naturally occurring asbestos deposits and community contamination through asbestos mines, processing plants and manufacturing facilities(9). Asbestos fibres are broadly classified into serpentine (from serpentinite rocks) and amphibole fibres. The former is mostly chrysotile (white) asbestos, and the latter is divided into amosite (brown), crocidolite (blue), tremolite, actinolite and anthophyllite(8, 9).

Ancient uses of asbestos have been documented as early as 4000 B.C. with asbestos fibres being used as lamp wicks(11). The Romans used asbestos fibres in tablecloths(12). MPM was first identified in the late 1940s and mid-1950s(13, 14). During this time, asbestos was being extensively used in industry due to its low-cost and fire-retardant properties. The locomotive, boiler-making and shipbuilding industries boasted a predominance of asbestos use(15). Importation and industrial use of amosite and crocidolite asbestos was banned in 1985 and chrysotile asbestos was banned from industrial use in 1999 in the United Kingdom(16) and in 2005 by the European Union(17). Following exposure to asbestos fibres, MPM can manifest up to 30 to 40 years later. The large increase in annual deaths in the UK observed due to MPM over the last fifty years reflect this latent period and have been attributed to the peak of imported asbestos to the UK up until the 1970s(18).

MPM occurs mostly in males with a median age around 70 years old in high-income countries(19), with almost 50,000 deaths occurring in Europe between 1994 and 2016(20). Earlier predictions suggested that after 2020, deaths related

to MPM would start to decline(21). In 2019, there were 2,369 mesothelioma-related deaths in the United Kingdom(22). Data extrapolated on asbestos use in 59 countries in 2017 estimated the worldwide rate of MPM deaths to be 38,400 per year(23). In post-industrial nations, the incidence has levelled off through asbestos bans. However, despite the ban of the use of asbestos in the United Kingdom, residual asbestos remains in households and workplaces today with exposure occurring through damaged asbestos cement materials. MPM will continue to be a burdensome disease for several decades to come due to the continued mining and processing of asbestos in large countries such as Russia and China(24, 25).

1.2.1 **Histological sub-types of MPM**

The three histologic sub-types of MPM are epithelioid, sarcomatoid and biphasic. The epithelioid sub-type is the most common, accounting for up to 70% of cases(20, 26). It is characterised by oval tumour cell proliferation on histopathological examination following tissue biopsy(27). The sarcomatoid sub-type approximates 20% of all cases of MPM(28, 29). Spindle cell proliferation and the formation of oval nuclei are histological characteristics(27). Biphasic MPM has features of both the epithelioid and sarcomatoid sub-types(20).

Epithelioid sub-type is associated with a better prognosis compared to the other sub-types(30-32). Blyth and Murphy retrospectively assessed 370 patients in the West of Scotland and determined that overall survival (OS) was longest in epithelioid sub-types compared to sarcomatoid and biphasic sub-types (HR 1.75, p=0069 and HR 1.93, p<0.0001, respectively)(32). Sarcomatoid confers the worst prognosis with a median survival time of 3.5 to 8 months(33). The European Organization for Research and Treatment of Cancer (EORTC)(34) prognostic scoring system and subsequent validation studies include sarcomatoid histology as an independent predictor of early mortality(35-37). The authors of the Cancer and Leukaemia Group B (CALGB) prognostic scoring system also determined non-epithelioid history to be an independent survival predictor(38). Nowak and colleagues assessed 93 patients with MPM and concluded that sarcomatoid histology was the most significant determinant of OS(39). In their study of 367

patients with MPM, Billè and colleagues reported that sarcomatoid MPM was an independent prognostic factor for OS (HR 7.86, p<0.001)(31).

1.3 Detection and staging of MPM

Disease stage is prognostic in patients with MPM(40-44) and is an important determinant of prospective treatment strategies. MPM is staged according to the tumour, node and metastasis (TNM) classification. The International Association for the Study of Lung Cancer (IASLC) published the eighth edition of the staging classification in 2018(45). This has been summarised in Table 1.1.

1.3.1 **Limitations of CT in detecting MPM**

Although CT is the primary imaging modality in assessing 'T' stage in MPM, it is limited in the assessment of primary tumour. MPM grows as an irregular, circumferential rind within the pleural cavity, extending axially in the thoracic cage. Distinguishing between atelectasis, pleural fluid, pleural thickening and calcified pleural plaques further complicates the accurate assessment of primary tumour volume in MPM(46). CT has limited accuracy in distinguishing between potentially resectable (T3) and technically unresectable (T4) disease, including reliable identification of tumour extension into the diaphragm(47). This is important in patients in whom surgery is being considered, as tested recently in the randomised Mesothelioma and Radical Surgery 2 (MARS 2) trial which is due to read out in 2023(48). There is wide variability in the diagnostic performance of CT reported in the pleural malignancy literature with sensitivities and specificities ranging from 58% to 93% and 78 to 96%, respectively(49-52).

Table 1.1 Eighth edition of the TNM staging system for MPM

TNM	**Descriptor**
Tx	Primary tumour cannot be assessed
T0	No evidence of primary tumour
T1	Tumour involving ipsilateral parietal pleura +/- visceral pleura
T2	Tumour involving any of the ipsilateral pleural surfaces plus: • Confluent visceral pleural tumour, and/or • Involvement of diaphragmatic muscle, and/or • Invasion of the lung parenchyma
T3	Tumour involving the ipsilateral pleural surfaces plus: • Invasion of the endothoracic fascia, and/or • Extension into the mediastinal fat, and/or • Solitary soft tissue chest wall invasion, and/or • Non-transmural pericardial involvement
T4	Tumour involving the ipsilateral pleural surfaces plus: • Any rib involvement, and/or • Peritoneal invasion through the diaphragm, and/or • Mediastinal organ invasion, and/or • Contralateral pleura extension, and/or • Spine or brachial plexus invasion, and/or • Transmural pericardial involvement, and/or
Nx	Nodes cannot be assessed
N0	No evidence of nodal involvement
N1	Ipsilateral bronchopulmonary, hilar or mediastinal nodes
N2	Contralateral bronchopulmonary, hilar or mediastinal nodes or ipsilateral or contralateral supraclavicular nodes
Mx	Presence of metastases cannot be assessed
M0	No distant metastases
M1	Distant metastases

1.4 Systemic anti-cancer therapy in MPM

1.4.1 Chemotherapy

Chemotherapy exerts its cytotoxicity directly on cancer cells and has been the mainstay of systemic anti-cancer therapy (SACT) following the discovery of the marrow-suppressive effects of nitrogen mustards in the First World War(53). In patients with MPM, combination chemotherapy with pemetrexed - a folate antimetabolite - and cisplatin - a platinum-based alkylating agent - affords a three-month survival advantage in patients with MPM (12.1 versus 9.3 months, p=0.020)(3). Patients receiving raltitrexed - another folate antimetabolite - and cisplatin had a superior survival advantage compared to single agent cisplatin (8.8 months versus 11.4 months, p=0.048)(54). The addition of bevacizumab - an anti-angiogenesis recombinant humanised monoclonal antibody - to doublet chemotherapy offers a modest survival benefit compared to combination chemotherapy alone (18.8 months versus 16.1 months, p=0.0167)(55).

The efficacy of second-line treatments in patients previously exposed to platinum-based therapy is unproven. Previously studied second-line agents include chemotherapies such as histone deacetylase inhibitors, e.g., vorinostat(56), tyrosine kinase inhibitors, e.g., sorafenib(57) and dasatinib(58), and further single agent chemotherapy, e.g., pemetrexed(59). A recent study assessed vinorelbine versus supportive care in the second-line setting, demonstrating a median progression free survival of 4.2 months versus 2.8 months, respectively (p=0.0017)(60).

1.4.2 Immunotherapy

Over recent years, immune checkpoint inhibitors which block inhibitory signals of T-cell activation have been increasingly investigated and reported in the thoracic malignancy literature. The programmed cell death protein 1 (PD-1) inhibitors nivolumab(61) and pembrolizumab(62) and the programmed death ligand (PD-L1) inhibitors durvalumab(63) and atezolizumab(64) have been shown to improve overall survival (OS) in patients with non-small cell lung cancer

(NSCLC). In patients with small cell lung cancer (SCLC), improved survival outcomes have been reported with combination treatment with chemotherapy and the PD-L1 inhibitor atezolizumab(65).

1.4.2.1 Immunotherapy as first-line treatment in MPM

The Checkmate 743 study assessing ipilimumab – a monoclonal antibody against CTLA-4 – in combination with nivolumab – a human monoclonal immunoglobulin G4 antibody to PD-1 – in patients with MPM reported a significant survival advantage compared to combination chemotherapy alone (18.1 months versus 14.1 months, p=0.002)(66). There was a very large benefit of immunotherapy over chemotherapy in the non-epithelioid group. In the recently published Checkmate 743 study update, Peters and colleagues reported a 3-year survival benefit with the combination of nivolumab and ipilimumab compared to traditional chemotherapy in patients with MPM who are not eligible for surgery(67). The Scottish Medicines Consortium recently accepted combination nivolumab and ipilumumab as a first-line treatment for unresectable MPM(4).

1.4.2.2 Immunotherapy as second-line treatment in MPM

Second-line nivolumab monotherapy has been investigated in the NivoMis and MERIT trials with median OS rates of 11.8 and 17.3 months, respectively(68, 69). In the MAPS-2 study, nivolumab monotherapy had a median progression free survival (mPFS) of 4.0 months(70). Avelumab, a PD-L1 blocker, was studied in 53 patients and had a response rate of 9.4% and a mPFS of 3.9 months(71). The CONFIRM study recently reported preliminary results demonstrating improved OS with nivolumab (9.2 months versus 6.6 months, p=0.018)(72). In NHS England and Wales, single agent nivolumab has been licensed under interim treatment options published during the COVID-19 pandemic as a second-line treatment (rather than second-line chemotherapy)(5).

1.5 Tumour response assessment

Assessment of treatment response is important in determining efficacy of toxic therapies and suitability to second-line and more novel anti-cancer treatments in MPM.

Venous-phase contrast-enhanced computed tomography (CT) is widely used in clinical practice for the diagnosis of MPM and assessment of response to chemotherapy and other anti-cancer agents(73). Radiological features of MPM include parietal and visceral pleural enhancement and chest wall and diaphragmatic infiltration. Some of these features are illustrated in Figure 1.1.

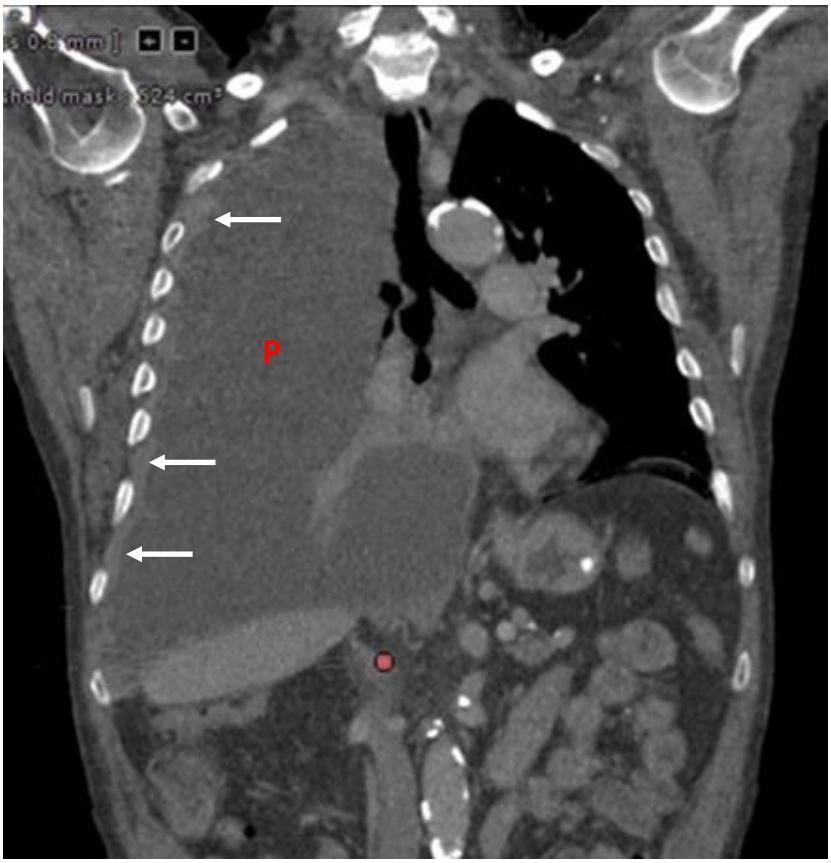

Figure 1.1 Contrast-enhanced coronal CT image of a patient with MPM. A large malignant pleural effusion (red P) and pleural enhancement (white arrows) are visible

1.5.1 **Response Evaluation Criteria In Solid Tumours**

Early objective reporting of treatment response was first standardised in the 1980s with the recommendation of bidimensional tumour measurements – defined as the sum of the longest diameter of the lesion and its perpendicular diameter - at pre- and post-treatment time points(74). The World Health Organisation (WHO), US National Cancer Institute (NCI) and the European Organisation for Research and Treatment of Cancer (EORTC) defined simplified response assessment criteria, termed Response Evaluation Criteria in Solid Tumours (RECIST) which were based on the sum of the unidimensional measurements of the longest diameter of tumours of 'target lesions'(75). According to RECIST criteria, a maximum of ten lesions can be measured with a maximum of five measurements in each organ. RECIST 1.0(75) and RECIST 1.1(76) are the gold standard response assessment tools in patients with solid organ cancers.

1.5.2 **Modified Response Evaluation Criteria in Solid Tumours**

The principal limitation with the RECIST criteria is the assumption of tumour sphericity which under-classifies tumour response(77) and does not take into account equivalent percentage changes in the three-dimensions of a tumour(78).

Modified Response Evaluation Criteria in Solid Tumours (mRECIST) classification was developed in MPM to assuage such assumptions with readers measuring tumour thickness perpendicular to the chest wall or mediastinum in two positions at three separate levels on thoracic CT scans(6). The summed value of these measurements define response assessment with a reduction of ≥30% on two occasions four weeks apart defining partial response (PR) and an increase of ≥20% from the pre-treatment scan defining progressive disease (PD)(6). Those who do not fulfil the criteria for PR nor PD are defined as having stable disease. Figure 1.2 provides an example of mRECIST measurements.

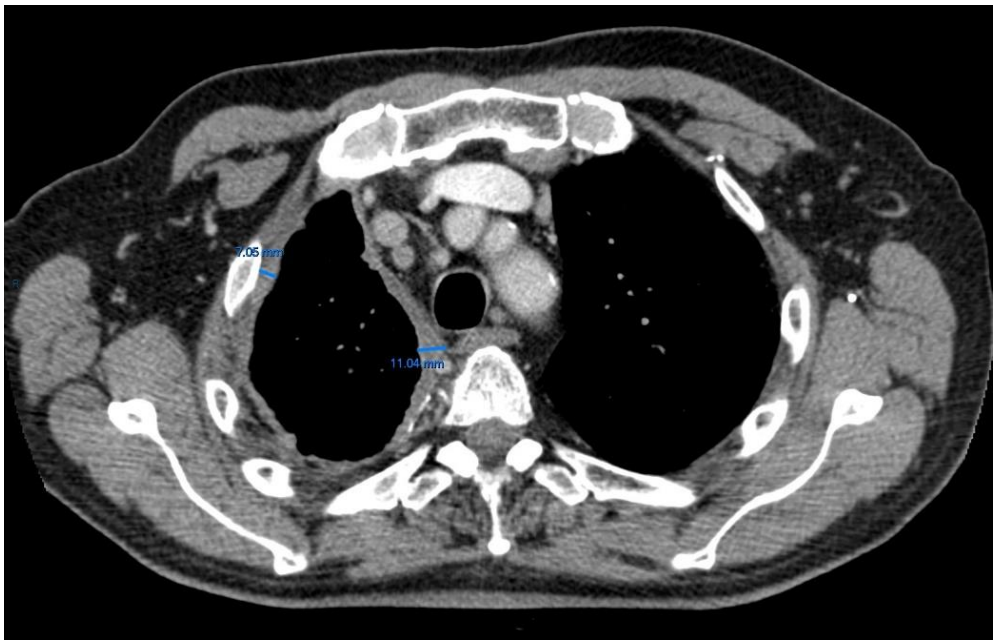

Figure 1.2 Axial contrast-enhanced CT image of a patient with MPM demonstrating mRECIST. The blue lines represent measurements taken perpendicular to the chest wall and the vertebral column

However, disparities in treatment response have been reported when applying the bidimensional WHO criteria and unidimensional mRECIST criteria in the same patients with MPM(79). Differences in OS have been observed depending on whether tumour volumetry or mRECIST criteria are applied in the same patient cohort(80). Additionally, significant inter-observer variability has been reported when applying mRECIST criteria in patients with MPM with 95% limits of agreement for inter-observer differences spanning a range as high as 30%(81). As previously mentioned, mRECIST criteria defines partial response to treatment as a 30% volume decrease from the pre-treatment scan and progressive disease as a 20% increase in tumour volume between interval scans. Inter-observer variation may directly translate into different response classification based on the same imaging appearances. An important study by Oxnard and colleagues applied RECIST response criteria to thickness measurements of MPM models(82). Their modelling suggested that more appropriate response thresholds to the non-spherical shape of MPM would be partial response defined as a 66% volume decrease and progressive disease defined as a 73% volume increase, with these requiring prospective validation(82). As a result, novel methods that measure the volume of primary tumour in patients with MPM have been sought.

1.6 Tumour volumetry in other thoracic malignancies

Different tumour volumetric measurement techniques have been reported in patients with thoracic malignancy. In patients with NSCLC, mathematical modelling(83, 84) and radiodensity correction methods(85) have also been described. Volumetric parameters using ^{18}F-fluorodeoxyglucose positron emission tomography computed tomography (^{18}F-FDG PET CT) have been reported to be significant prognostic indicators in patients with NSCLC(86). Other PET CT parameters have included maximum standardized uptake value (SUV_{max})(87), total metabolic active tumour volume (TMATV) and total tumour burden (TTB) measurements(88).

Tumour volume is a predictor of prognosis in patients with thoracic malignancy. In patients with NSCLC, metabolic tumour volume has been reported as prognostically significant in early(89) and later stage disease(90-92). Similar outcomes have been reported in SCLC(93-96). Other studies have reported correlation between OS and the sphericity of gross tumour volume (GTV) in NSCLC(97) as well as shape and textural analyses(98).

1.7 Previous volumetric techniques in MPM

Higher tumour volume is prognostically significant in patients with MPM(80, 99-104). In the mesothelioma literature, recent advances in CT tumour volumetry have resulted in new approaches to the traditional T staging techniques of the 7th(105) and 8th(45) versions of the TNM staging systems. These have included three-dimensional CT volumetric approaches to response assessment which are described as follows.

In their landmark study published in 1998, Pass and colleagues manually delineated pleural tumour using a track-and-ball mouse on 48 patients' pre-resection and post-resection CT scans with computer software reconstructing the tumour in three dimensions to provide volume in cubic centimetres(99). The patients had cytoreductive debulking by extra-pleural pneumonectomy (n=25) or pleurectomy/decortication (n=23). Patients with pre-operative tumour volume

<100cm^3 had a longer median OS (22 months versus 11 months, p=0.03)(99). Patients with pre-operative tumour volumes >52 cm^3 had shorter progression-free intervals (8 months versus 11 months, p=0.02).

Zhao and colleagues developed a sequential segmentation approach that involved dissecting pleural tumour from other anatomical structures in the thoracic cage. They reported an accuracy of 80.6% with absolute differences in the percentage change between the manual and automated results of 6.7% in the 8 patients studied(106).

Three-dimensional interpretation of two-dimensional cross sections by counting the number of evenly spaced dots overlying tumour – also termed Cavalieri's geometrical principle of stereology – has been investigated by Ak and colleagues (107). They demonstrated that patients with non-progressive disease - defined as stable disease or objective response - had a longer median OS compared to patients with progressive disease (14 v 16 v 10 months, respectively, p=0.008). This technique has since been superseded by digital volumetric approaches to tumour segmentation.

Liu and colleagues used a semi-automated computer algorithm. After dichotomising tumour volume into crude 'increase' and 'decrease' change groups, volumetric change after two cycles of chemotherapy predicted OS in the 30 patients investigated(80).

Frauenfelder and colleagues used Myrian® software – originally designed as a hepatic volumetric measurement tool – to compare tumour volume measurements to mRECIST criteria using pre- and post-chemotherapy CT scans of 30 patients with MPM(108). Their semi-automated method involved contouring the outer part of the pleura every fourth to fifth slice followed by automatic linear algorithmic interpolation between the marked slices to provide tumour volume. High inter-rater reliability (0.99) and inter-observer agreement (general κ 0.9) were reported for absolute tumour volumes. However, low inter-rater reliability (ICC=0.55) and low inter-observer agreement for tumour response classification (general κ 0.33) was reported when compared to RECIST criteria.

A novel method involving computerised delineation of the pleural space through automated segmentation of lung parenchyma and the hemi-thoracic cavity followed by a semi-automated segmentation method to define the liver boundary was reported by Sensakovic and colleagues(109). Three readers delineated five axial sections in 31 patients' CT scans. The median Jaccard similarity co-efficient (J-index) was 0.517 between the human readers and 0.484 between the manual- and computer-defined segmentations.

Labby and colleagues adapted the Sensakovic method by adding an interpolation component – defined as a 'watershed segmentation' which divided the segmented disease into three-dimensional regions based on morphology and spatial proximity – to 281 serial CT scans from 81 chemotherapy-treated patients, and reported volume change to be an independent predictor of OS (104).

Chaisaowong and colleagues segmented pleural thickening from thoracic tissue using a 3-D modelling approach(110). However, their method was limited by growth pattern assumptions.

Rusch and colleagues conducted a feasibility study assessing the use of CT-derived volumetric assessment of pleural tumour in MPM, with mean tumour volumes of 91.2 cm^3, 245.3 cm^3 and 511.3 cm^3 conferring respective median OS rates of 37, 18 and 8 months(102).

Gill and colleagues employed a semi-automated volumetric approach based on automated radiodensity-thresholds provided by Vitrea Enterprise suite 6.0® (Vital Images®, Minnesota, USA) and human reader manual delineation, with absolute volume differences of 173.7cm^3 to 860.6 cm^3 reported between human readers(111). This was blamed on 'perception errors' and limited distinction between tumour and adjacent tissues(111).

Chen and colleagues reported a Dice coefficient of 0.825 after comparing manual segmentation on 45 baseline and follow-up CT scans with a semi-automated random walk segmentation method involving the placement of seed points in areas representative of pleural tumour(112). The Dice coefficient - also

known as the Dice score, Sørensen–Dice coefficient or F1 score - is a performance metric for image segmentation by deep learning algorithms which is widely reported in AI literature and detailed later in Section 1.8.2 of this chapter. A higher J-index (0.79) and Dice similarity coefficient (0.88) were observed by Brahim and colleagues upon assessing their semi-automated, multi-stage thoracic cavity segmentation and texture analysis approach(113).

In their study of tumour volume in MPM, calculated by the sum of the maximal tumour thickness and tumour extent grade of the pleural circumference which was measured at the level of the carina, Paajanen and colleagues divided tumour size into tertiles with the median OS in the lowest, middle and highest tumour volume groups being 14.0, 11.1 and 5.4 months, respectively (p=0.016)(103).

1.8 Artificial Intelligence in imaging

Despite the advent of three-dimensional measurements, accurate and reproducible measurements of primary tumour volume in MPM have remained problematic. Tumour volume has yet to be incorporated into clinical practice for prognostication and staging. As previously highlighted, manual oversight and contouring are time-consuming and prone to inter-observer variability. Limitations of primary tumour volumetric assessment in MPM has led to the development of automated and semi-automated approaches to CT image interpretation, including deep learning approaches.

Deep learning is a sub-category of machine learning that forms the basis for artificial intelligence (AI) image interpretation(114). AI was first defined as “the science and engineering of making intelligent machines” by John McCarthy in 1955(115). Deep learning is broadly defined as the “simulation of human behaviour by machines”(116). Deep learning algorithms are designed to include multiple layers of algorithms that are stratified into hierarchies of data importance(117). The accumulation of data from real-world inputs ‘trains’, or rather, mathematically improve its ‘fit’, as it seeks to match the input

provided(118). The network provides outputs that are adaptive as it continues to 'learn' from these inputs(119).

Deep learning algorithms are used in every-day life. Social media platforms utilise deep learning to power their virtual assistants(120) and to analyse data(121). Other uses include chatbot agents such as those deployed in banking(122) and healthcare settings(123). The commercial sector uses deep learning to predict customer behaviour(124, 125). Deep learning algorithms can extract information from text(126), detect fraud(127) and filter spam messages on email communications(128). Deep learning also forms the basis of facial recognition technology(129). In the medical setting, deep learning can be utilised to extract medical information from electronic health records(130) and to facilitate matching of patients to clinical trials(131).

Deep learning has also been applied to medical images(132). Image interpretation by expert human readers is required as a first step in this process; this human 'input' is commonly known as ground truth in the AI literature. In intelligent medical imaging, ground truth is determined by clinicians who identify anatomical structures such as bone, lung and normal pleurae(133, 134). Accurate ground truth enables the artificial algorithm to 'image label' each tissue to provide appropriate outputs by algorithms(135).

1.8.1 **Convolutional neural networks**

Advances in deep learning methods have resulted in the development of convolutional neural networks (CNN)(136). A CNN is a multi-layered convolutional filter that can be trained to identify image features that correspond with given image classifications or image labels(137). Deep CNNs have been widely utilised in the machine learning community, including Visual Geometry Group(138), GoogleNet(139), Residual Net(140) and U-Net(141). CNNs have been proven to out-perform humans when trained on very large datasets(142). Commercial object detection and recognition datasets are trained on millions of images, for example, ImageNET (n=14,197,122)(143), Open Images (n=9,178,275)(144), Microsoft Common Objects in Context (n=2,500,000)(145) and OpenLORIS-Object (n=1,106,424)(146). Deep learning techniques have been

applied in medical imaging(147), including U-net architecture in lung segmentation(148) and in patients with thoracic malignancies(149, 150). U-Net architecture was first described by Ronneberger and colleagues and is a deep learning method that identifies label-specific regions of an image(141). The network is shaped like a U-curve and is broadly divided into convolutional encoding and decoding units. Convolutional encoding facilitates image analysis and feature combination at different scales of the image. The network is also coupled with 'skip connections' to maintain detailed features. Although similarly sized datasets are not available in medicine, U-net architecture can operate with limited training images(141, 151).

1.8.2 **Artificial Intelligence in MPM**

Gudmundsson and colleagues were the first authors to report automated segmentation of pleural thickening in patients with MPM utilising U-Net architecture(136). Their method involved differentiating between pleural thickening and normal thoracic tissue in 131 slices from 43 CT scans. After testing the CNN against human-measured segmentations of MPM tumour in two separate validation datasets, the CNN demonstrated superior performance (Dice coefficient 0.662 to 0.800). The Dice coefficient was described earlier in Section 1.7.1 of this chapter and equals 1.0 if the two datasets are identical and 0.0 if there are no similarities. Dice is more precise in reporting on exact region overlap on the image files. One of the limitations of the Gudmundsson paper was that the CNN often included pleural effusions in the predicted tumour volumes. The authors refined their deep CNN-based method in a subsequent publication, with a focus on pleural effusions(152). Another imitation was that requirement of a human user having to manually define the side of the MPM tumour.

1.9 Survival prediction in MPM

Survival in MPM is heterogenous with a median survival of 9 to 12 months(20). Survival prediction in MPM is made difficult by the heterogeneity of the disease. Factors predictive of survival have been reported since the late 1990s and are largely based on routinely available clinicopathological data. As described

earlier in this chapter, survival in MPM is dependent on the histological sub-type(30-34, 38, 39), disease stage(38, 153) and tumour volume(80, 99-104). Other predictors include older age(38, 154-156), male sex(34, 36, 156), poorer performance status(30, 34, 36), low haemoglobin(36, 38) and elevated inflammatory indices(34, 36, 38). Performance status and inflammatory indices will be discussed in more detail here.

1.9.1 **Performance status**

Performance status (PS) is universally used as a surrogate metric for patients' fitness to undergo specific treatments, including surgery, radiotherapy and systemic anti-cancer therapy (SACT). The Eastern Cooperative Oncology Group Performance Status (ECOG PS) grading system is the most commonly used scale and ranges from 0 (normal functioning) to 5 (dead)(157). Table 1.2 provides the scale-points and descriptions of activity on each scale. The Karnofsky score (KS) is another scoring system used and ranges from 0 (dead) to 100 (normal functioning)(158).

The British Thoracic Society (BTS) guidelines state that patients with MPM being considered for first-line chemotherapy require a PS of 0 or 1(2). The American Society of Clinical Oncology (ASCO) MPM treatment guidelines recommend first-line SACT for patients with a PS ≤2(159). The European Society for Medical Oncology (ESMO) MPM guidelines stipulate that patients with PS 0 to 2 should be considered for SACT(160).

Patients with a PS of 2 are a heterogenous cohort and are often excluded from clinical trials, e.g., Checkmate 743(66). The licensing of nivolumab and ipilimumab in Scotland will follow this(4). Only patients with a PS of 1 or 0 are directed to nivolumab and ipilimumab in the European Society for Medical Oncology (ESMO) MPM guidelines(160). This is reflected in day-to-day clinical practice. If patients at risk of losing fitness or already determined to have a PS ≥2 are targeted, the life prolonging benefits for treatments like nivolumab and ipilimumab could be extended to more cases.

PS features in all the MPM prediction scores. In the regression tree of the CALGB score, PS was the most significant prognostic factor(30). In the Brims decision tree model, patients with a PS ≥2 were included in Group 4 (the group with the worst survival) and patients with PS 0 or 1 went into Group 3(30). Their data demonstrated that PS superseded histology, i.e., sub-type only mattered if PS was 0 or 1, with a similar effect for haemoglobin <12 ug/L(30). Cedres and colleagues assessed 189 patients with MPM - 85% had been offered first-line chemotherapy – and reported median OS of 28.8 months for patients with PS 0, 18.8 months for those with PS 1 and 2.4 months for those who were PS 2 (p=0.001)(161). Rahouma and colleagues assessed 114 patients with MPM who received platinum chemotherapy and reported superior OS in the PS 0 to 1 group compared to the PS ≥2 group (p=0.024)(162). The same authors reported that patients with PS 0 or 1 completed 3 or more cycles of chemotherapy.

Table 1.2 WHO/ECOG Performance Status

Grade	**Description of activity**
0	Fully active Able to carry on all pre-disease performance without restriction
1	Restricted in physically strenuous activity Ambulatory and able to carry out light or sedentary work
2	Ambulatory and capable of all self-care Unable to carry out any work activities Up and about >50% of waking hours
3	Capable of only limited self-care Confined to bed or chair >50% of waking hours
4	Completely disabled Cannot carry on any self-care Totally confined to bed or chair
5	Dead

1.9.2 **Systemic inflammation**

Systemic inflammation is prognostic in patients with MPM. Elevated white cell count (WCC) is prognostic in the EORTC model(34) and in the external validation studies of this model(35, 36). In their study of 33,432 patients with solid organ cancers, Templeton and colleagues concluded that the prognostic effect of neutrophil:lymphocyte ratio (NLR) was higher in mesothelioma compared to other malignancies (HR 2.35, p=0.001)(163). Three studies by Kao and colleagues have reported the prognostic significance of NLR in patients with MPM(164), including 173 patients receiving systemic treatment(165) and 85 patients who had an extra-pleural pneumonectomy(166). Pinato and colleagues examined 171 patients with MPM and reported that NLR was an independent predictor of OS (HR 2.0, p=0.008)(167). The same authors also reported that modified Glasgow Prognostic Score (mGPS, a composite of serum albumin and C-reactive protein (CRP)) was also an independent predictor of OS (HR 2.6, p<0.001)(167). Low serum albumin(168) and lymphocyte-to-monocyte ratio (LMR)(169) are also prognostic in separate studies of patients with MPM. Pre-treatment CRP has been associated with subsequent clinical benefit from multi-modality treatments incorporating surgical resection(170). Elevated NLR and PLR have also been shown to affect disease-free survival(171).

1.9.3 **Limitations of survival prediction models in MPM**

In a study on which I was first author, our research group identified the limitations of routinely available clinical data in accurately predicting MPM prognosis(172). This was important and directly informed the decision to investigate additional predictors of survival, which are explored in Chapter 4 (in which tumour volume is related to survival) and in Chapter 5 (regarding altered body composition). In this single centre study with a validation set of 100 patients with MPM, age, PS, pre-chemotherapy WCC and pre-chemotherapy albumin were reported to be prognostically significant(172), almost matching the predictors reported by Brims and colleagues(30) which is included in the British Thoracic Society (BTS) guidelines for the 'Investigation and Management of MPM'(2). However, a validation set D_{XY} - a quantification score numerically equivalent to a C-statistic or area under the cure (AUC) score) ranging from 0 to

1, with increasing concordance between observed (0) and predicted (1) outcomes - was only 0.221 which suggested that our survival prediction model only provided a 22% improvement upon what would have been expected by chance. This highlighted the inadequacy of survival prediction models based on clinical data in accurately predicting outcomes in MPM. Moreover, the aforementioned survival prediction scores and studies that have validated these scores do not include survival predictors such as tumour genomics, tumour volumetry and body composition metrics such as skeletal muscle mass and adipose tissue mass which are integral to the cancer cachexia syndrome. I therefore focused on body composition measures which I will report in Chapter 5 in parallel to my work on tumour volumetry methods in Chapters 3 and 4.

1.10 Cancer cachexia

Cancer cachexia was defined by an international panel of experts in 2011 as “a multifactorial syndrome defined by ongoing loss of skeletal muscle mass - with or without loss of fat mass - that cannot be reversed by conventional nutritional support and leads to progressive functional impairment”(7).

Cachexia results in reduced tolerance to chemotherapy(173-176), reduced quality of life(177) and shorter survival(173, 178-186). Similarly, sarcopenic patients are at risk of treatment-related toxicities(187) and shorter survival(179, 188, 189). There are few data relating to the significance of cancer cachexia in MPM(190). The detection of cachexia is not just important for prognostic models. It could be actionable with improved tolerance to therapies, especially in the high-risk PS 2 cases who are often not treated.

The prevalence of cancer cachexia in advanced malignancies ranges between 50% and 80%(191-195). Limited prevalence data exist regarding cancer cachexia in patients with MPM. In their study assessing Actin A in patients with MPM(196), Paajanen and colleagues used the Fearon definition of ≥5% weight loss over the past 6 months, BMI <20 kg/m^2 and weight loss >2% or skeletal muscle index (SMI) consistent with sarcopenia and weight loss >2%(7). They reported cachexia in 12/21 (57%) of the patients studied(196).

1.11 Principal constituents of cancer cachexia

Cancer cachexia results from a complex interplay between tumour and host and is driven by pro-inflammatory and catabolic mediators, or 'cachexokines'. I have provided a visual guide to the multi-system involvement of this syndrome in Figure 1.3. This is an amalgam of pathological mechanisms described in detail by Fearon and colleagues(7), Baracos and colleagues(197), Porporato(198) and Biswas and colleagues(199).

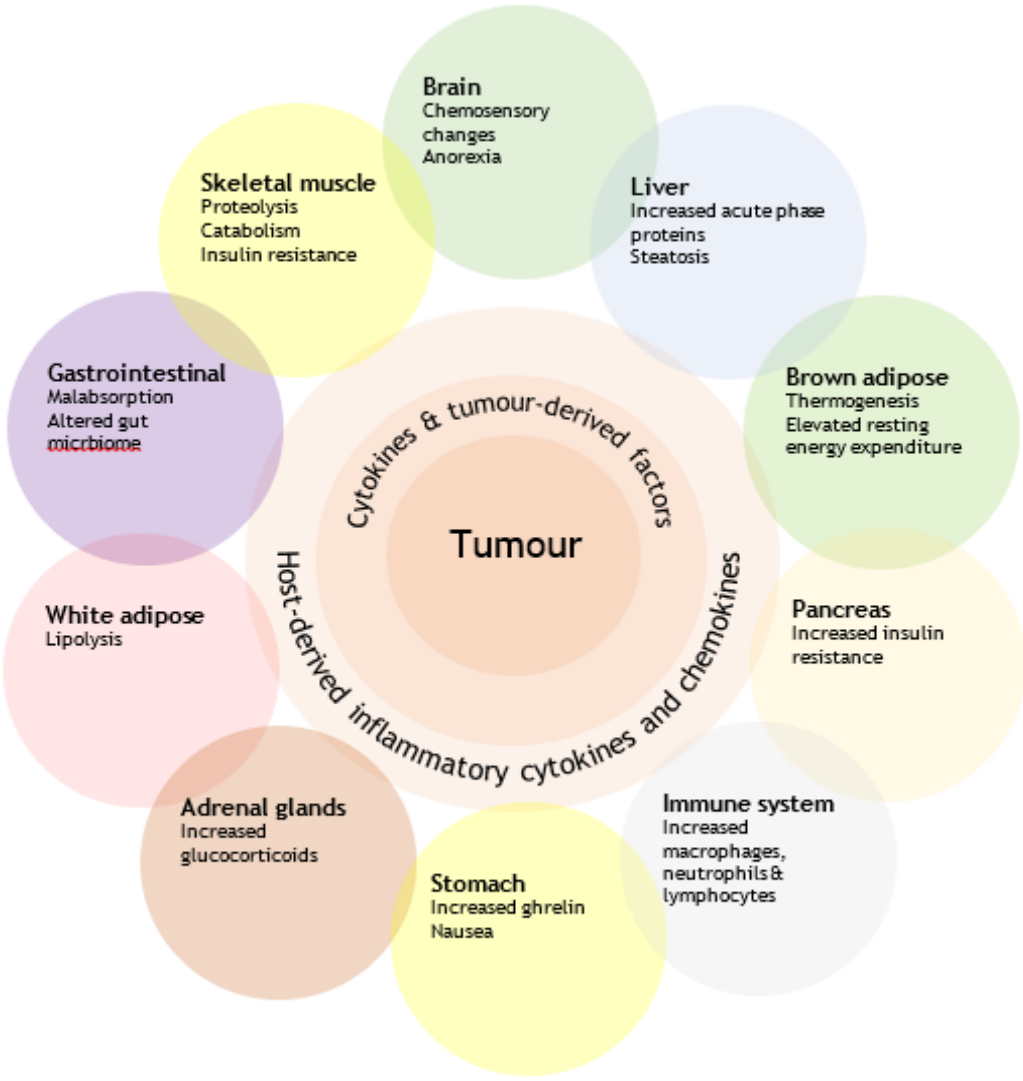

Figure 1.3 Pathophysiology of cancer cachexia

A detailed description of the biochemistry and pathophysiology of the cancer cachexia syndrome is beyond the scope of this thesis. However, the principal constituents are weight loss, anorexia, systemic inflammation and altered body composition.

1.11.1 **Weight loss**

Weight loss is a central tenet of cancer cachexia. In the early 1990s, an international clinical research group sponsored by the National Cancer Institute defined weight loss in the context of cancer cachexia as “a 5-pound weight loss in the preceding 2 months and/or an estimated daily caloric intake of <20 calories per kg, a desire by the patient to increase his or her appetite and gain weight, and the physician’s opinion that weight gain would be beneficial for the patient”(200). The importance of weight loss was again emphasised by Loprinzi in 1995 who stated that “cancer cachexia is most often defined by criteria based on weight loss, i.e., involuntary weight loss greater than 10%”(201).

The current definition of cancer cachexia is based upon the rate of weight loss as well as attainment of a low body mass index (BMI)(7). Martin and colleagues published a scoring matrix based on weight loss and BMI in patients with locally advanced or metastatic cancer that predicted OS independent of cancer type, tumour stage, age, sex and PS(186).

Weight loss is common in patients with thoracic malignancies(181, 202, 203) and is prognostic in patients with non-small cell lung cancer (NSCLC)(204) and small cell lung cancer (SCLC)(205). Weight gain in patients with advanced NSCLC receiving chemotherapy has been shown to be beneficial(206). The impact of weight loss in patients with MPM has been less conclusive, with previous studies reporting an adverse association with prognosis(30, 36, 38, 207) whilst other authors concluding that weight loss is not an important determinant of survival(34, 208), including the before-mentioned survival prediction study on which I was first author(172). The reliance of weight loss on the cachexia definition can make retrospective studies difficult since these data may not be reliably recorded in routine clinical records.

1.11.2 **Anorexia**

Another important constituent of the cancer cachexia syndrome is anorexia. Anorexia is derived from the Greek: *an*, meaning ‘without’, and *orexia*, meaning ‘appetite’. In the context of cancer cachexia, anorexia has been defined as

"food intake insufficient to meet the metabolic needs of the tumour-bearing host"(209). It is common in patients with thoracic malignancies, including NSCLC(210) and SCLC(211). In patients with MPM, pre-treatment anorexia is prognostic of OS(164). The complex biology of anorexia has been described in previous studies and is beyond the scope of this thesis(212, 213). A brief overview is provided here.

Peripheral signalling provides feedback to the hypothalamus which polices metabolic changes in skeletal and adipose tissues(214) as well as behaviours that results in energy intake(215). In animal models, arcuate neurons such as pro-opiomelanocortin (POMC) and agouti-related peptide (AgRP) are central to the pathogenesis of anorexia(216). Additionally, altered feedback to the hypothalamus from peripheral tissues has also been shown to be deleterious(217). Proinflammatory cytokines from tumours and systemic inflammation(218) also have an important role in the anorexia syndrome(216, 219).

Anorexia is poorly understood in the cachexia syndrome as evidenced by enigmas such as elevated ghrelin levels (ghrelin is an appetite stimulant) in patients with advanced lung cancer and anorexia(220, 221). The enigma is that patients with the cachexia syndrome do not experience increased appetite. Clinical trials have assessed the impact of anamorelin(222) - a ghrelin receptor agonist - in patients with lung malignancy. Nabilone(223) - a tetrahydrocannabinol mimic and appetite stimulant via central cannabinoid 1 receptors(224) – has also been investigated in this patient population. There is an ongoing study assessing the use of anamorelin in patients with MPM (New Zealand Clinical Trials Number: U1111-1240-6828)(225).

1.11.3 **Systemic inflammation**

Systemic inflammation plays an important role in the cancer cachexia syndrome. Although there are no human studies which assess systemic inflammation in the context of cancer cachexia in patients with MPM, elevated measures of systemic inflammation are associated with poor outcomes in patients with MPM and have been detailed in Section 1.9.2 earlier in this chapter. Blood tests are almost

always collected in chemotherapy-treated patients, including at prior to commencement of chemotherapy, which make them suitable datapoints for retrospective studies seeking to understand cachexia syndrome in mesothelioma.

There are few studies assessing inflammation in patients with MPM and cachexia. Duong and colleagues demonstrated a tumour growth rate reduction by inducing macrophage depletion in MPM-bearing mice, thus preventing cachexia induced by immunotherapy(226). Tumour-associated macrophages inhibit the activity of anti-tumour T cells and confer a poor prognosis(227, 228). Systemic inflammation is also subject to recent targeted therapeutic approaches in patients with NSCLC and cancer cachexia. Interleukin-6 (IL-6) - a pro-inflammatory cytokine - is currently subject to ongoing clinical trials investigating the role of IL-6 monoclonal antibodies, including clazakizumab (NCT00866970) and inflixamab (NCT00040885).

1.11.4 **Sarcopenia**

Sarcopenia is the loss of skeletal muscle mass. The term sarcopenia is derived from the Greek: *sarx*, meaning ‘flesh’, and *penia*, ‘poverty’. The complex pathophysiology of sarcopenia is described in numerous comprehensive reviews and is beyond the scope of this thesis(194, 197, 199, 229, 230). A brief overview focused on thoracic malignancy is provided here.

The development of sarcopenia in patients receiving chemotherapy involves the deleterious effects of circulating inflammatory mediators such as tumour necrosis factor-alpha (TNF-α)(194) and IL-6(231, 232) on muscular biology(229), including protein synthesis suppression(233) and protein degradation(234). Chemotherapy - including cisplatin(235) which is used as a treatment in MPM - also releases proinflammatory cytokines (236, 237) and is associated with elevated levels of glucocorticoids(238) as well as promoting mechanisms that drive oxidative stress(239).

Myocyte-released myokines – signalling molecules of the transforming growth factor (TGF) superfamily, including myostatin and activin A(240, 241) - promote catabolism of skeletal muscle(242). Myostatin has been found to be contributory

to sarcopenia in murine models(243), including the Lewis lung carcinoma model(244).

The prevalence of sarcopenia in the thoracic malignancy literature is widely varied. For example, in patients with early-stage NSCLC, sarcopenia measured pre-operatively has been reported in 13.9 to 55.8% of cases(245-250). Sarcopenia is prognostically significant in patients with thoracic malignancy(251-253). Pre-operative sarcopenia has been associated with poorer outcomes in most studies of patients with radically treatable NSCLC(245, 246, 248, 254). In patients with more advanced NSCLC, sarcopenia prior to commencing palliative SACT has been shown to have increased mortality compared to patients without sarcopenia(176, 255). The prevalence of sarcopenia in patients with SCLC is even less well defined SCLC(249) but has been associated with poor outcomes(256).

1.11.4.1 Sarcopenia in MPM

There are few studies assessing sarcopenia in MPM(190, 257). There are also no data to support the impact of sarcopenia measured at L3 on treatment outcomes in patients with MPM. Jeffery and colleagues assessed 18 patients with MPM and reported that those patients with dual-energy X-ray absorptiometry (DEXA)-defined muscle loss had shorter OS compared to those who did not lose muscle (7 muscle-losing patients versus 0 non-muscle losing patients died less than 12 months from the second body composition scan, p=0.002)(257). A group from Switzerland assessing sarcopenia and pre-cardial adipose tissue in pre-operative CT scans with sarcopenia(190). In the 278 patients with MPM who had surgery, those with sarcopenia – defined as skeletal muscle area below the 33rd percentile - had a higher three-year mortality compared to those without sarcopenia (23.9 months versus 31.7 months, p=0.041)(190).

The pathophysiology of sarcopenia in MPM is poorly understood. A recent study of 22 patients with MPM concluded that elevated activin A – a glycoprotein which regulates muscle growth - correlated with CT-determined baseline tumour size (r=0.549, p=0.010) and post-chemotherapy tumour size (r=0.743, p=0.0006)(196). The authors postulated that muscle growth is negatively

regulated by activins via activin type 2 receptors (ActRII) and are prognostically significant in other solid organ cancers, including lung cancer. In the NSCLC setting, bimagrumab - an antagonist to activin type II receptors which stimulates skeletal muscle growth – was the subject of a Phase II clinical trial(258). Higher expression of irisin – another myokine – has been shown to be prognostic in patients with NSCLC(259).

1.11.5 **Adipopenia**

The current consensus definition of cancer cachexia states that the syndrome can occur "with or without loss of fat mass"(7), also termed adipopenia. Adipopenia can be quantified using imaging software that measures body composition metrics and is demonstrated in Figure 1.4(260). It is associated with shorter OS and sarcopenia in advanced cancer(261). It is seldom studied in the thoracic malignancy literature.

The pathophysiology of adipopenia is poorly understood in the cancer cachexia syndrome(262, 263). It may occur prior to the development of sarcopenia through lipolysis – lipid breakdown by hydrolysis - resulting in circulating free fatty acids and ubiquitin ligase-induced skeletal muscle atrophy(231). Adipose tissue is divided into white and brown adipose tissue (WAT and BAT, respectively). WAT stores energy in the form of triglycerides and BAT regulates lipid oxidation and thermogenesis(264). Studies have discussed the pathophysiological changes that results in adipose tissue browning(265, 266). BAT is thermogenic and regulates energy expenditure through heat dissipation(267). Irisin - briefly mentioned in section 1.11.4.1 of this chapter - is related to WAT browning and can increase uncoupling protein 1 (Ucp1) expression which is central to non-shivering thermogenesis in adipocytes mitochondria(268). WAT browning is associated with altered glucose homeostasis(269) and considered to be contributory to hypermetabolism in patients with cancer cachexia(266, 270-272), including patients with lung cancer(273). Elevated resting energy expenditure (REE) has been reported in patients with metastatic NSCLC(274, 275). Higher REE and circulating TNF-receptor 75 and cortisol have been demonstrated in patients with SCLC

compared to NSCLC(276). An *in vitro* study reported reduced chemosensitivity in NSCLC cells through BAT-mediated cell proliferation(277).

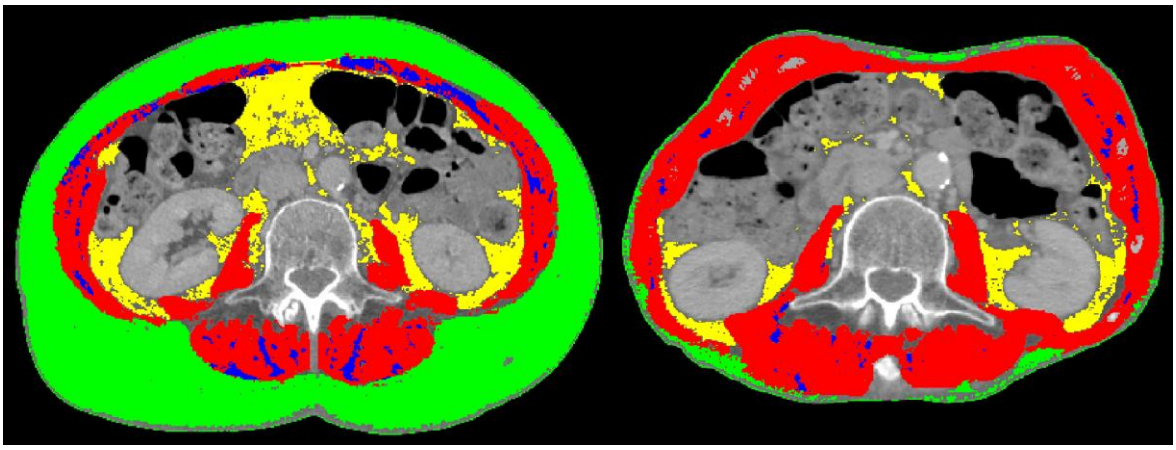

Figure 1.4 Axial CT scan slices of two patients in the TRACERx study delineated by me demonstrating the differences in adiposity between patients. Subcutaneous (green), visceral (yellow) and intra-muscular (blue) adipose tissue compartments are visible. The red represents skeletal muscle. The image was created on Slice-O-Matic® software v5.0 (TomoVision, Montreal, Canada)

1.12 Body composition measurement

Body composition is defined as the proportion of muscle, adipose tissue, bone and water content in the human body. It can be assessed using different imaging modalities. Dual-energy x-ray absorptiometry (DEXA) and CT are examples of this, and although DEXA is considered the gold standard for anthropomorphic measurements of total appendicular lean tissue mass(278, 279), CT has the significant advantage of facilitating relevant data as part of already routine tumour assessment imaging.

1.12.1 Skeletal muscle mass measurement using DEXA

Dual-energy x-ray absorptiometry (DEXA) has been used for cancer cachexia evaluation in patients with thoracic malignancy(280-283). Jeffery and colleagues used DEXA to measure pre-sarcopenia - defined as appendicular skeletal muscle mass 7.26 kg/m^2 for men and 5.45 kg/m^2 for women - and reported this in over

half of the 61 patients studied(283). In the clinical setting, DEXA is not routinely available. DEXA also measures lean body mass in grams which is not equivalent to muscle mass(284).

1.12.2 Skeletal muscle mass measurement using CT

Computed tomography (CT) is a routinely available imaging modality used for diagnostic and response assessment purposes. CT is based on Hounsfield units (HU) which are attenuations of tissue relative to water. Water has 0 HU. Tissues denser than water such as muscle and adipose tissue have HU values >0 and materials less dense than water such as air have HU values <0(285-287). A further advantage of CT is that it can be used to differentiate different body tissues. There are well-published and validated HUs for skeletal muscle and adipose tissue in the sarcopenia literature(288). I will use CT for this reason, and as such, it is important to consider what software solutions are available to measure skeletal muscle and adipose tissue.

1.12.3 Software programmes used to measure body composition

I have detailed the different software packages available for the purposes of body composition measurement in Table 1.3. Different software programmes have been compared in multiple previous studies, demonstrating high levels of agreement(289-292). Particularly excellent agreement for cross-sectional muscle area measurements has been reported using sliceOmatic®(TomoVision®, Magog, Canada) and ImageJ software (U.S. National Institutes of Health, Bethesda, MD)(292). Excellent agreement levels between OsiriX® (Pixmeo SARL®, Geneva, Switzerland) and ImageJ have been observed for paraspinal muscle measurements on MRI(293).

As part of my learning of body composition measurement techniques, I attended University College London (UCL) during my tenure as a Clinical Research Fellow recruiting patients to the TRAcking Cancer Evolution through therapy (Rx) (TRACERx) study(294). TRACERx uses multi-region whole-exome sequencing to assess the clinical significance of intra-tumour heterogeneity in patients with

radically-treatable NSCLC, and to advance the understanding of cancer evolution in this cohort. I provided second reader measurements using Slice-O-Matic software (TomoVision®, Montreal, Canada) on CT scans as part of a TRACERx sub-study assessing body composition changes. This is demonstrated in Figure 1.4 of this chapter. My experiences with this body composition software aided my learning and development of the techniques required to accurately determine different body compartments. ImageJ software was chosen as the body composition platform for analysis of skeletal muscle and adipose tissue in this thesis because it was readily available, free to download and easy to use. I have described this in further detail in Chapter 2, Section 2.3.6.

Table 1.3 Examples of body composition software programmes

Software	**Software developers**	**Examples of study populations**
Aquarius NET server	TeraRecon Inc., San Mateo, CA, USA	Patients who underwent abdominal wall reconstruction(295)
Aquarius iNutrition	TeraRecon, San Mateo, CA, USA	Healthy population(296)
FatSeg	Biomedical Imaging Group Rotterdam of Erasmus MC, Rotterdam, Netherlands, using MeVisLab (Mevis Medical Solutions, Bremen, Germany)	Patients with colorectal cancer(297)
ImageJ	U.S. National Institutes of Health, Bethesda, MD	Patients with head and neck cancer(298)
MeVisLab	MeVisLab, v2.2.1, Bremen, Germany	Healthy population(299)
OsiriX	Pixmeo SARL, Geneva, Switzerland	Patients with prostate cancer(300)
PACS	PACS, Centricity® 4.1, GE Healthcare, Barrington, IL, USA	Patients with multiple myeloma(301)
sliceOmatic	TomoVision, Montreal, Canada	Patients with non-metastatic colorectal and breast cancers(302)
Synapse Vincent	FUJIFILM Co. Ltd., Tokyo, Japan	Patients with prostate cancer(303)
VikingSlice	Aalborg University Hospital	Patients with chronic pancreatitis(304)

1.12.4 Definition of sarcopenia: measurements at L3

Mourtzakis and colleagues developed and validated regression equations for extrapolating data from a single third lumbar vertebra (L3) cross-sectional CT image to predict whole body composition of adipose tissue and skeletal muscle mass area (SMA, cm^2)(305). SMA can be divided by height squared (m^2) to provide skeletal muscle index (SMI, cm^2/m^2).

The third lumbar vertebra (L3) contains the spinal vertebrae, large and small intestines, kidney and liver. It also contains visceral, subcutaneous and intra-muscular adipose tissue as well as the psoas, erector spinae, quadratus lumborum, transversus abdominus, internal and external obliques and rectus abdominus muscle groups. This is illustrated in Figure 1.5.

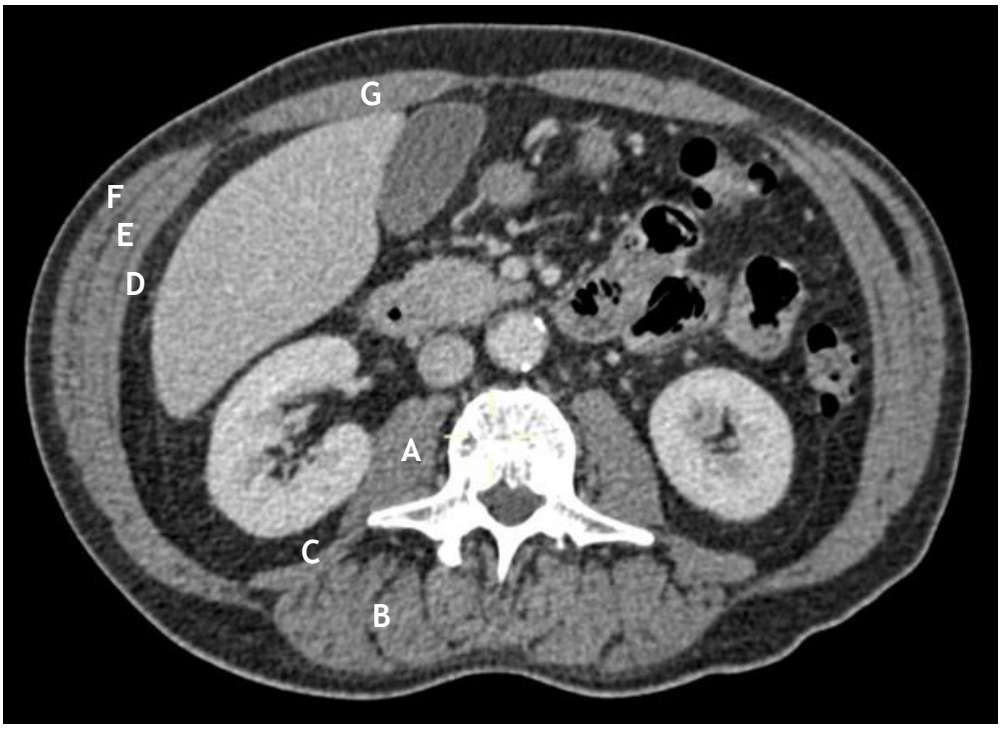

Figure 1.5 Single axial contrast-enhanced CT image of a patient with MPM demonstrating the muscles at the third lumbar vertebra (L3) which include the psoas (A), erector spinae (B), quadratus lumborum (C), transversus abdominis (D), internal obliques (E), external

Authors have proposed different cut-offs and definitions for sarcopenia using a single mid-axial CT image slice at L3 using body composition software tools based on their populations' skeletal muscle mass and target outcomes(306, 307). However, the most used sex- and BMI-specific sarcopenia cut-offs at L3 were devised by Martin and colleagues and are defined as: SMI 43 cm^2/m^2 for males with a BMI <25 kg/m^2 and SMI <53 cm^2/m^2 for males with a BMI ≥25 kg/m^2; SMI <41 cm^2/m^2 for females regardless of BMI category(186).

1.12.5 **Definition of sarcopenia in mesothelioma: L3 versus T4**

In patients with thoracic malignancy, CT scans often do not extend inferiorly to include L3. In one epidemiological survey of mostly patients with thoracic malignancy, only 65% of patients had CT scans which included L3 for evaluation of skeletal muscle mass(308). As a result, those researching skeletal muscle loss in thoracic malignancies have sought alternative skeletal muscle area measurements. Derstine and colleagues reported excellent correlation between muscle area measurements performed at multiple levels from the tenth thoracic vertebra (T10) to the fifth lumbar vertebra (L5) supporting the validity of calculating SMI at different axial levels(309). There are no data to support the measurement of sarcopenia at different thoracic levels in patients with MPM.

1.12.5.1 Fourth thoracic vertebra

The fourth thoracic vertebra (T4) has been investigated as a surrogate of sarcopenia in patients with thoracic and other malignancies(310-314). This is illustrated in Figure 1.6.

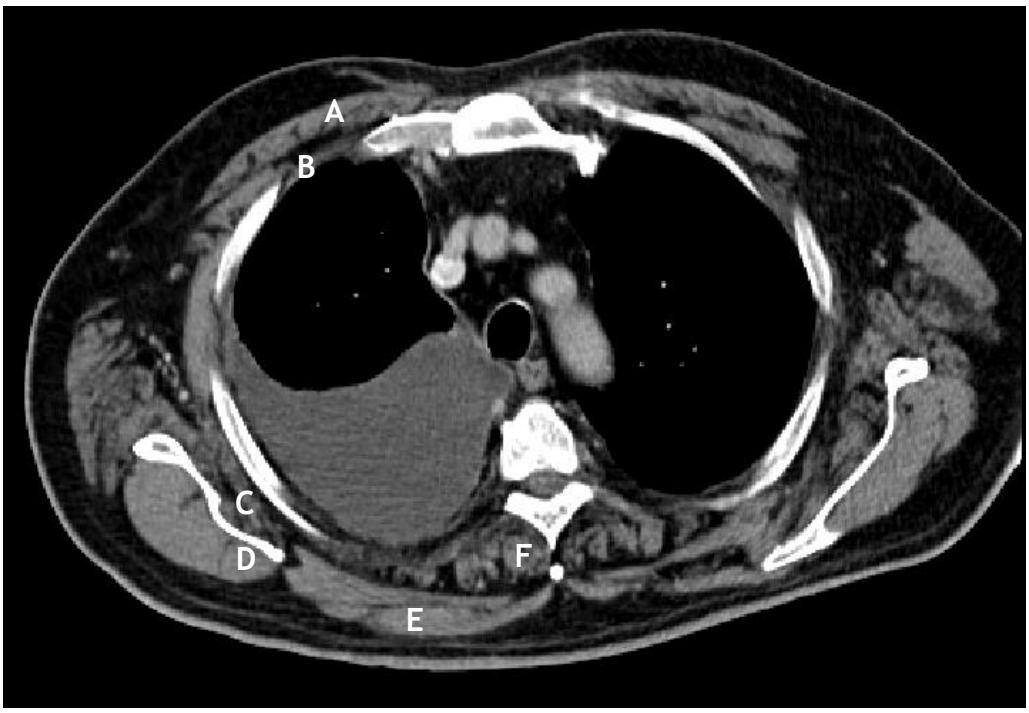

Figure 1.6 Single axial contrast-enhanced CT image of a patient with MPM demonstrating the muscles at the fourth thoracic vertebra (T4) which includes the pectoralis (A), intercostals (B), sub-scapularis (C), infraspinatus (D), trapezius(E) and erector spinae (F)

Sarcopenia measured at T4 is prognostically important and associated with treatment-related adverse outcomes in other cancers. In a study of 117 male patients diagnosed with SCLC, sarcopenia at T4 – defined as those in the lowest quartile of T4 skeletal muscle index (T4SMI) values – was found to have lower median progression-free survival than non-sarcopenic patients (6.0 vs. 7.5 months, p=0.009)(311). Hua and colleagues assessed 301 patients with breast cancer who received post-operative adjuvant radiotherapy and concluded that patients with higher T4SMI had longer median OS compared to those with lower T4SMI (62.4 months versus 68.5 months, p=0.025)(313). In 213 patients with head and neck cancers, CT-measured T4SMI and L3SMI measurements were combined

into a single score for SMI difference and was an independent predictor of early termination of treatment (OR 0.96, p=0.021)(314). Conversely, in their study of 86 patients with advanced NSCLC, Wysham and colleagues did not find that thoracic sarcopenia (measured at T4) correlated with adverse outcomes (HR 0.94, p=0.66)(315).

Sarcopenia measured at T4 has also been investigated in non-cancer patient cohorts. Rozenberg and colleagues determined that thoracic muscle cross-sectional–area - measured at the carina which corresponds roughly –o T4 - was associated with metrics of frailty in 527 patients who underwent lung transplantation(316). Moon and colleagues measured the cross-sectional area of the pectoralis, paraspinal, serratus and latissimus muscles at T4 in 180 patients with idiopathic pulmonary fibrosis and concluded that male patients in the lowest quartile of T4SMI values had lower OS (p=0.035)(317). Low skeletal muscle radiation attenuation at T4 – a radiological marker of myosteatosis, or skeletal muscle fat infiltration – was associated with post-operative pneumonia following liver surgery in a study of 180 patients (OR 3.65, p<0.01)(312).

1.13 Overall aim and hypothesis of thesis

The overall aim of this thesis is to develop, validate and describe the significance of radiological biomarkers for treatment response measurement and survival prediction in patients with malignant pleural mesothelioma (MPM). The materials and methods for these clinical research studies will be detailed in Chapter 2. The results will be presented in three results chapters. The individual hypotheses for each results chapter are summarised below.

1.13.1 Chapter 3: Semi-automated segmentation of MPM tumour volume

Volumetric tumour measurement is established in other solid tumour types. In MPM, semi-automated tumour volumetric measurements based on magnetic resonance imaging (MRI) have recently been shown to outperform traditional T-staging in predicting survival in MPM. However, MRI is not routinely performed in clinical practice and computed tomography (CT) remains the primary imaging modality of response assessment in MPM. The null hypothesis of this study is that a semi-automated contrast-enhanced CT tumour segmentation method cannot be extrapolated from contrast-enhanced MRI to serve as the ground truth for a future MPM volumetric AI algorithm.

1.13.2 Chapter 4: Volumetric MPM tumour assessment using human and deep learning algorithmic segmentations

The delivery of more accurate volumetric measurements is important due to the limitations of modified Response Evaluation Criteria In Solid Tumours (mRECIST) criteria which is inaccurate and associated with poor reproducibility. A fully automated approach to MPM pleural tumour segmentation would directly address major limitations of human readers, including high inter-observer variation and costs. The null hypothesis of this study is that a volumetric AI algorithm cannot improve human response classification in patients with MPM treated with chemotherapy.

1.13.3 Chapter 5: Prevalence, pattern and prognostic significance of altered body composition in patients with chemotherapy-treated MPM

Altered body composition such as the loss of skeletal muscle and adipose tissue mass results in reduced tolerance to chemotherapy and shorter survival in patients with solid organ cancers. Accurate and reproducible measurements of skeletal muscle and adipose tissue mass may be able to facilitate the identification of those patients most-at-risk of developing complications related to systemic anti-cancer therapy (SACT), including those patients with a PS ≥2. Few data exist relating to skeletal muscle and adipose tissue loss in patients with MPM. The null hypothesis of this study is that altered body composition is not prognostically significant in patients with chemotherapy-treated MPM.

Chapter 2

METHODS

2 Chapter 2: Methods

This chapter outlines the design and data collection for the three studies that aimed to address the hypothesis of this thesis. The Chief Investigator for all the studies was Professor Kevin G. Blyth, Queen Elizabeth University Hospital, Glasgow, United Kingdom.

2.1 Semi-automated segmentation of MPM tumour volume

A single centre retrospective cohort study was performed at the Queen Elizabeth University Hospital, Glasgow (QEUH). The study sponsor was NHS Greater Glasgow and Clyde (NHSGGC). Patients were recruited prospectively to an initial pilot study and subsequently to an MRI sub-study of the Diagnostic and Prognostic Biomarkers in the Rational Assessment of Mesothelioma (DIAPHRAGM) study (ISRCTN10079972) between January 2013 and October 2016. The Chief Investigator for DIAPHRAGM was Professor Kevin G. Blyth, Queen Elizabeth University Hospital, Glasgow, United Kingdom. Ethical approval was granted by the West of Scotland Research Ethics Service (12/WS/0219, 13/WS/0240).

2.1.1 Study objectives and outcome measures

This single centre cohort study aimed to determine whether a semi-automated magnetic resonance imaging (MRI) method could be successfully adapted for deployment on routinely acquired computed tomography (CT) scans in patients with chemotherapy-treated malignant pleural mesothelioma (MPM). The first step was to determine Hounsfield unit (HU) values of different thoracic tissues using CT scans of patients with MPM. This was to facilitate a method of semi-automated tumour region-growing by which HUs replaced the SI unit values used in the original MRI method. The second step involved manual delineation of pleural tumour on CT scans. The final step was to determine the accuracy of pleural tumour coverage afforded by the semi-automated segmentation process through subjective visual inspection and assessment of inter-observer agreement plus an assessment of the time taken to perform the task. Table 2.1 summarises the study objectives and outcome measures.

Table 2.1 Objectives and outcome measures of the semi-automated segmentation of MPM tumour volume study

Study objectives	**Outcome measures**
Primary objectives	
To determine the difference in Hounsfield units between different thoracic tissues using CT scans of patients with MPM	Radiodensity of pleurae (HU) Radiodensity of lung, bone, intercostal muscle, pleural fluid, diaphragm, spleen and liver (HU)
To determine the feasibility and accuracy of a semi-automated method for MPM primary tumour volumetry based on radiodensity-tuned segmentation of contrast-enhanced CT scans	Accurate coverage of pleural tumour in patients based on subjective visual assessment Time taken to complete volume analysis (minutes)
Secondary objectives	
To determine correlation and agreement between semi-automated CT and MRI volumes	Tumour volume on CT (cm^3) Tumour volume on MRI (cm^3) Correlation (Spearman Rho) Agreement (Bland-Altman)
To determine whether a semi-automated volumetric CT method is reproducible	Tumour volume on CT (cm^3)
CT: computed tomography; HU: Hounsfield units; MPM: malignant pleural mesothelioma; MRI: magnetic resonance imaging	

2.1.2 **Study population**

Patients included in this chapter were selected from the Diagnostic and prognostic biomarkers in the rational assessment of Mesothelioma (DIAPHRAGM) study(318). DIAPHRAGM was a prospective, multicentre, observational study that recruited 747 patients over 3 years from 23 UK sites at first presentation of MPM. This study included an MRI sub-study which recruited 58 patients with suspected MPM. These patients had contemporaneous CT and MRI prior to histological sampling. Of these, MPM was confirmed in 31/58(319). 8/31 patients were excluded. Of these, 2/8 had arterial phase CT pulmonary angiograms and 6/8 were co-enrolled into the Prediction of Resistance to Chemotherapy in Malignant Pleural Mesothelioma (PRISM) study and were included in the external validation set of the volumetric study described in Chapter 4 of this thesis. 23 patients were included in the final analyses and are illustrated in a study flowchart in Figure 2.1.

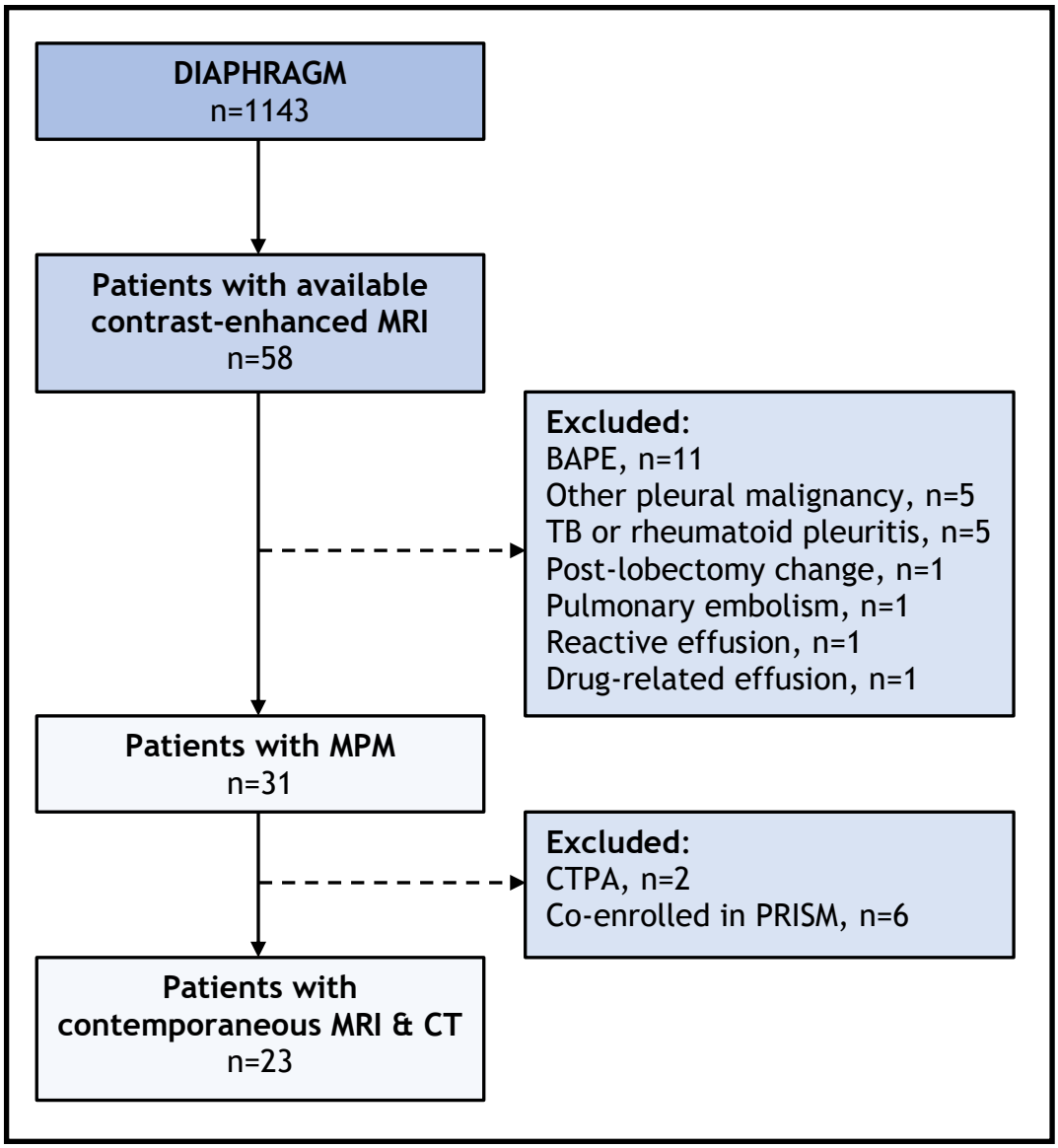

Figure 2.1 Flowchart of patients included in semi-automated segmentation of MPM tumour study

BAPE: benign asbestos pleural effusion

2.1.3 **Study procedures**

2.1.3.1 Collection of study data

Clinical data were entered onto a Microsoft Excel data collection sheet. Each patient was associated with a study number and their data entered on to the appropriate row. Patient identifiers were entered and data recorded in a linked anonymised format. All image analyses were performed in Glasgow using the same methods and the same reporters for all subjects. The scans were anonymised and issued a study number.

2.1.3.2 Clinical data

Data were extracted retrospectively from the study database and supplemented by electronic records, including demographics (age, sex), Eastern Cooperative Oncology Group performance status (ECOG PS)(157, 320), disease stage according to the eighth TNM classification for malignant pleural mesothelioma(45) and histological sub-type (epithelioid, biphasic, sarcomatoid or not specified). ECOG PS was not recorded consistently and a best estimate of ECOG PS was recorded based on MDT outcome documentation, pre-chemotherapy clinic letters or inferences made from functional descriptions in pre-chemotherapy clinic letters.

2.1.4 **Image analyses**

2.1.4.1 Summary of MRI method

The semi-automated threshold-based segmentation method used in this chapter has been adapted from a previously published study investigating MRI perfusion-tuned segmentation(319). This work was done by Dr Selina Tsim. I learned this method so that I could adapt it to CT. I have presented the MRI method for completeness.

Three coronal MRI slices (anterior, midpoint and posterior) were assessed using Myrian Intrasense® software v2.4.3 (Paris France). Multiple regions of interest (ROI) were distributed across parietal pleurae and mean signal intensity and standard deviation (SD) measured. Free-hand parietal pleural tumour delineations were drawn every 8 to 10 slices (slice thicknesses were 2.33 to 5mm). This technique was semi-automatic: 8 to 10 slices accurately defined pleural tumour within an acceptable time. Propagation of the contour mask resulted in a completed contour mask of the entire image series. A contour mask is a free-hand drawing performed which grossly defines the pleura. Signal intensity (SI) threshold-based segmentation – defined as the median of the SI ranges divided by 2 – was achieved through seed points placed on areas of pleural tumour within the contour mask, resulting in a final pleural tumour volume (cm^3). A seed point is an area representative of pleural tumour within a contour mask from which SI threshold-based regions are grown. Figure 2.2 provides a visual summary of the MRI method.

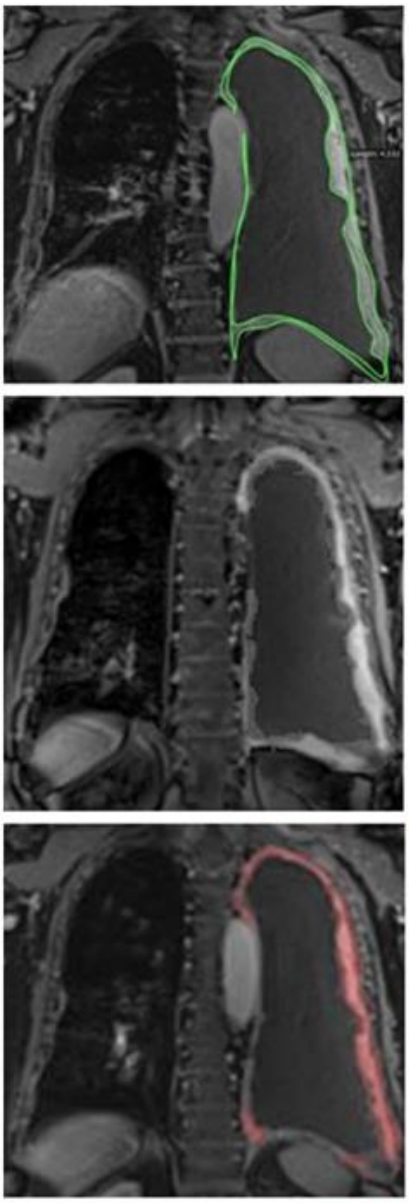

Figure 2.2 Coronal plane of contrast-enhanced MRI scans illustrating the semi-automated SI-tuned pleural tumour segmentation method

2.1.5 **CT method**

I performed the CT method which was extrapolated from the MRI method. Hounsfield unit (HU) threshold-based segmentation was employed rather than SI threshold-based segmentation. HU were identified through radiodensity analyses.

2.1.5.1 Radiodensity analyses

I performed the radiodensity analyses using Myrian Intrasense® software v2.4.3 (Paris, France). Anonymised Digital Imaging and Communications in Medicine (DICOM) files were imported into Myrian Intrasense® software. Fifteen regions of interest (ROIs) were placed using a track-and-ball mouse and cursor on representative areas of pleural tumour on 3 coronal plane CT scan slices as per the MRI signal intensity (SI) method described by Tsim and colleagues(319). Median intensity and interquartile range [IQR] were documented for each ROI in HU. I was blinded to clinical and histopathological data.

The coronal planes were defined into separate slices as follows:

- Mid-point: CT slice with the longest continuous cranio-caudal length of parietal pleura
- Anterior: CT slice half-way from the mid-point coronal slice to the most anterior slice with distinguishable parietal pleura
- Posterior: CT slice half-way from the mid-point coronal slice to the most posterior slice with distinguishable parietal pleura

This has been outlined in Figure 2.3.

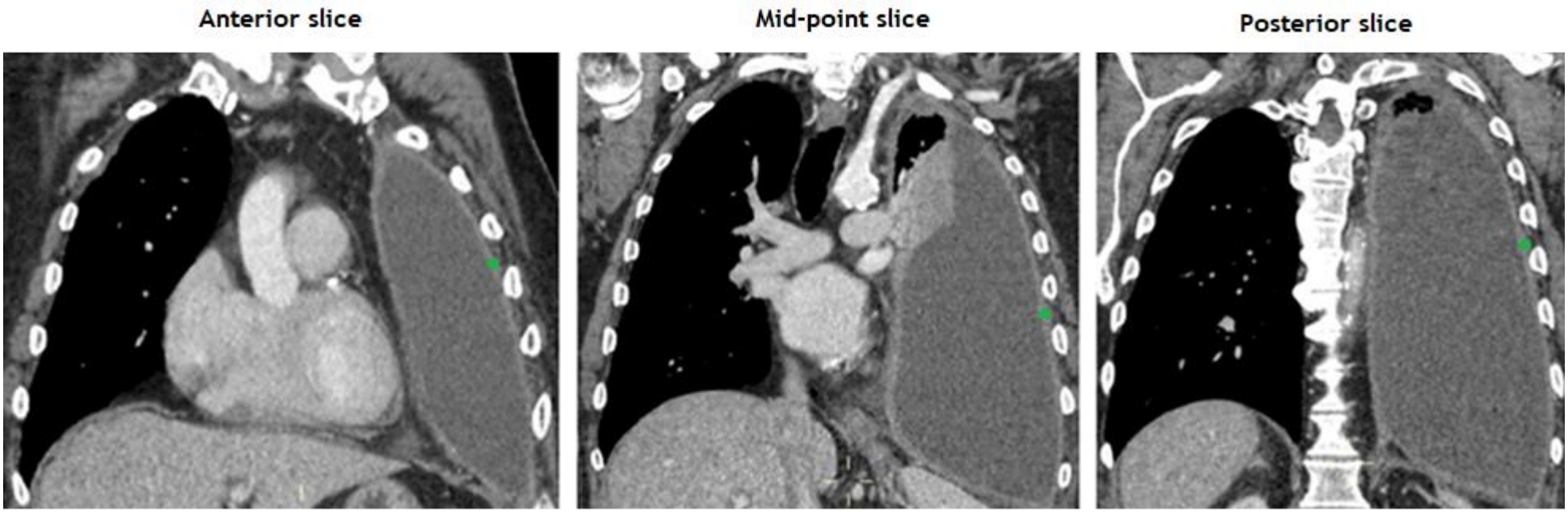

Figure 2.3 Coronal plane of contrast-enhanced CT scans with ROIs placed on areas representative of pleural tumour across three different slices (highlighted by the green dots)

2.1.5.2 Pleurae

The thoracic cavity contains visceral and parietal pleurae. During the development of the SI-threshold MRI method, efforts were made to obtain non-nodular and macro-nodular disease ROI measurements solely in the parietal pleura. To facilitate the development of the HU-threshold CT method, I mirrored this ROI measurement technique by including only parietal pleural tumour in the ROIs. The parietal pleura was defined as the anatomical membrane internal to and parallel with the ribcage and immediately adjacent to aerated lung.

2.1.5.3 Other thoracic structures

Three ROIs were placed on the corresponding tissues and median intensity and interquartile range [IQR] were documented for each ROI in HU. This has been illustrated in Figure 2.4. The external, internal and innermost intercostal muscles were identified as the thin muscle layer present in the intercostal space and parallel with the ribs. Pleural fluid was identified as an accumulation of fluid in the pleural cavity which usually manifests as a crescent-shaped opacity in the dependent parts of the thorax on CT scans. Lung was identified as the aerated space that filled the mediastinum between the ribs, intercostal muscles and pleurae. Ribs were identified as the curved bones that caged the thorax and their high attenuation manifested as a bright white structure on CT scans. Calcified pleural plaques were identified as areas of high attenuation in the parietal pleurae. The right and left hemi-diaphragms were identified as the dome-shaped muscles separating the thoracic and abdominal cavities. In cases where the diaphragmatic muscles were not immediately obvious, diaphragmatic crurae were identified and measured. The liver was identified as the organ immediately infero-posterior to the right hemi-diaphragm in the right upper quadrant. The spleen was identified as the oval organ immediately infero-posterior to the left hemi-diaphragm in the left upper quadrant.

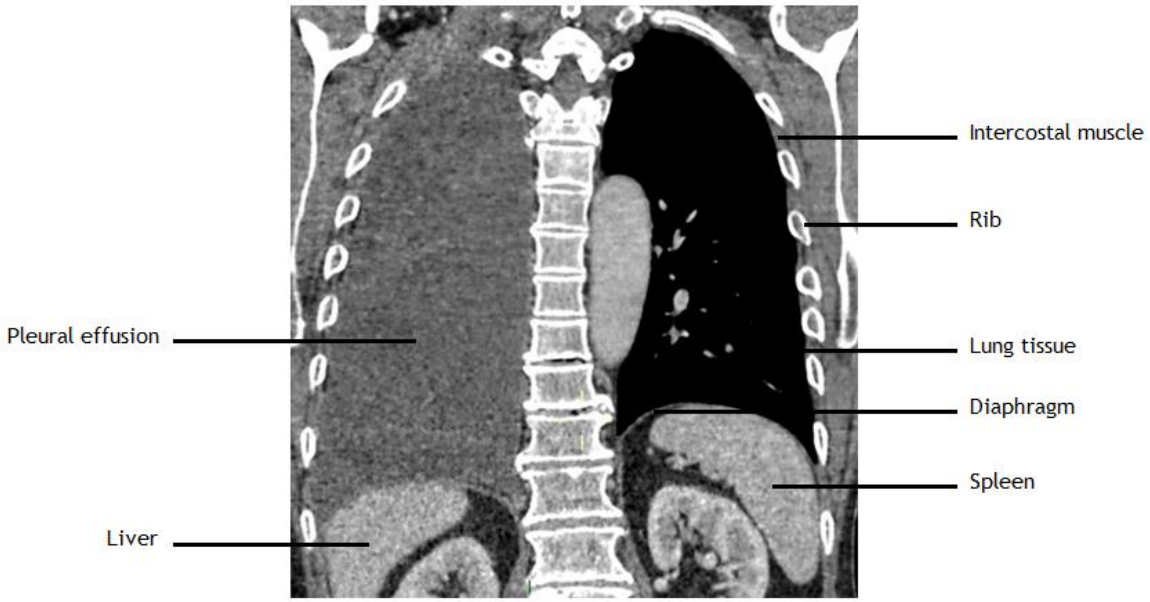

Figure 2.4 Coronal CT scan slice illustrating thoracic tissues

2.1.5.4 Contour mask

I created contour masks using Myrian Intrasense® software v2.4.3 (Paris, France). Areas of visible parietal pleurae were defined and delineated using a free-hand drawing tool. This is illustrated in Figure 2.5. The first 20 apical slices were delineated followed by manual delineations every 5 slices. The final 20 basal slices were also segmented. This resulted in approximately 75 slices per image series. More apical and basal slices were delineated due to the complexity of pleural tumours in these anatomical areas. The higher resolution MRI scans acquired in the same patients served as guide to the contour mask drawing process. This has been illustrated in Figure 2.6. Semi-automated linear interpolation by Myrian Intrasense® software v2.4.3 (Paris, France) extended the contours I had drawn throughout the image series, resulting in a complete contour mask containing pleural tumour. If there were areas of where pleural tumour was not included, manual adjustments to the contour mask were made.

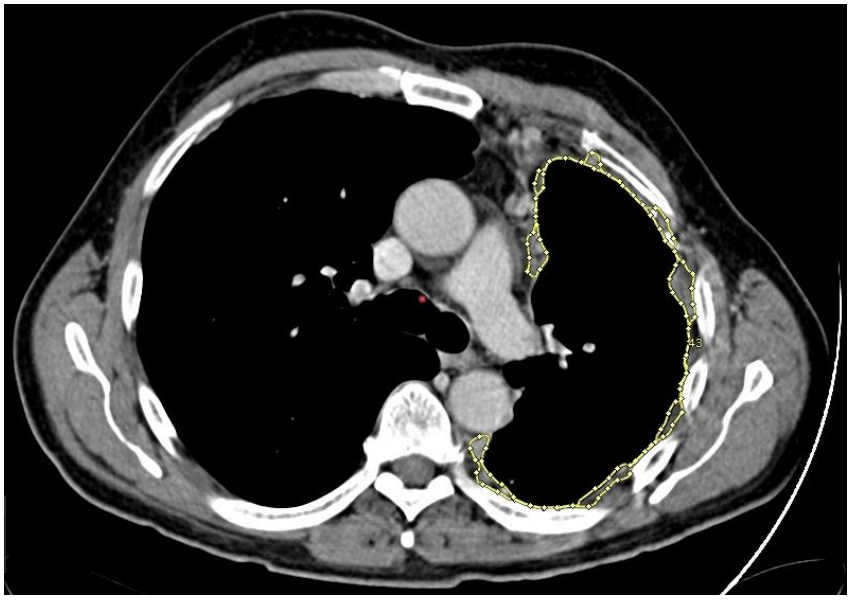

Figure 2.5 Example of contouring of pleural tumour in the axial slice of a contrast-enhanced CT scan. The yellow area contains what was interpreted as pleural tumour

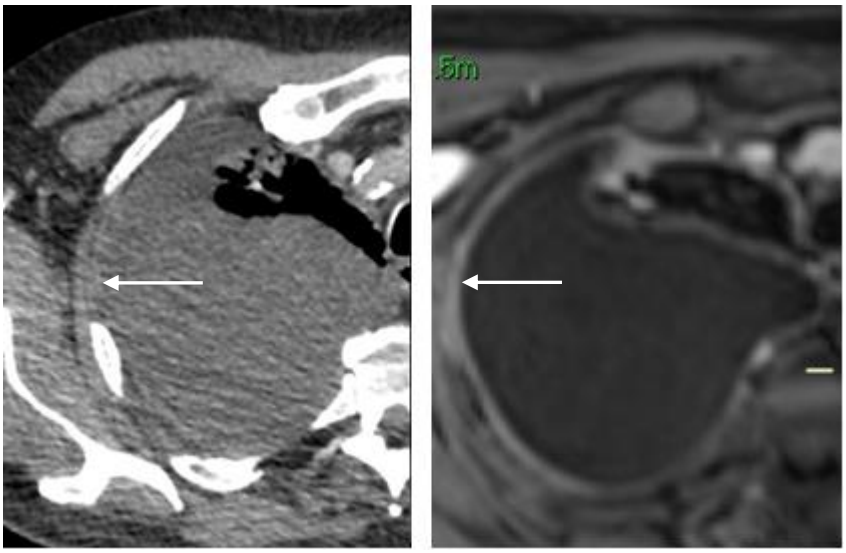

Figure 2.6 Example of the difference in pleural tumour resolution between a contrast-enhanced CT scan (left) and contrast-enhanced MRI (right) in the same patient. The white arrow denotes pleural enhancement

2.1.5.5 Semi-automated segmentation using radiodensity thresholds

After completion of the contour mask, a semi-automated region-growing step was attempted using region growing limits. HU threshold limits were based on the radiodensity range (minimum to maximum) measured in the pleural ROIs in all 23 patients. These data were then summarised by generating a median pleural radiodensity value in HU for all the ROIs in all the patients (n=154 ROIs). This value was divided by 2 to provide a seed point estimate which was placed in areas representative of pleural tumour in the contour mask.

2.1.6 **CT image acquisition and anonymisation**

CT scans with thoracic views obtained as part of routine care were included. Image acquisition followed intravenous injection of iodine-based contrast media (75 to 95ml) with portal-venous phase images obtained 65 seconds following contrast injection. Different scanners were used and included Canon Medical Aquilion and GE Medical Systems BrightSpeed, LightSpeed or Optima 660. Multi-slice helical axial images had been reconstructed with a contiguous minimum slice of 1 mm and a maximum slice thickness of 2 mm.

2.1.7 **Statistical analyses**

Statistical tests were performed in SPSS v24.0 (Chicago, USA) and GraphPad v9.1.0 (San Diego, USA). No formal sample size calculations were performed as the study design was exploratory. Data were tested for normal distribution using the Kolmogorov–Smirnov test. Individual data are summarised by median [interquartile range, IQR] or mean (standard deviation, SD) depending on their distribution.

2.1.7.1 Primary objectives

To determine the difference in Hounsfield units (HU) between different thoracic tissues using CT scans of patients with MPM, median HU values (range) were

generated. Violin plots were drawn to visualise the spread of the data and identify reasons for the observed results, e.g., overlapping HU values determined by the median, 25th and 75th percentiles and minimum and maximum HUs. Accuracy of pleural tumour coverage was based on subjective visual assessment. Time efficiency was determined by the median time taken to complete each volume analysis in minutes.

2.1.7.2 Secondary objectives

Spearman's Rho test was used for correlation and agreement evaluated using Bland-Altman plots between semi-automated CT and MRI volumes. To assess reproducibility, intra-class correlation coefficient (ICC) was used to determine human inter- and intra-observer variability.

2.2 Volumetric MPM tumour assessment using human and deep learning algorithmic segmentations

This study, which was called Automatic RECIST reporting in Mesothelioma using Deep Learning Artificial Intelligence, was a multicentre retrospective cohort study based at the Queen Elizabeth University Hospital, Glasgow (QEUH), Wythenshawe Hospital and University Hospitals of Leicester NHS Trust. The study sponsor was NHS Greater Glasgow and Clyde (NHSGGC). The NHS Greater Glasgow and Clyde (NHSGGC) Safe Haven granted approval for access to unconsented anonymised imaging data required for this project on 12th April 2018 (Ref: GSH/18/ON/001).

2.2.1 Study objectives and outcome measures

The objectives and associated outcome measures for this study are detailed in Table 2.2. The training and internal validation sets were used to generate the detailed ground truth needed to report correlation and agreement and inter-observer reliability between human readers and the later convolutional neural network (CNN) outputs.

The external validation set used to compare the CNN against modified Response Evaluation Criteria in Solid Tumours (mRECIST) classifications as well as the analysis of the prognostic value of the CNN volumetric measurements versus human reader-defined tumour volume and mRECIST classifications.

Table 2.2 Objectives and outcome measures of volumetric MPM tumour assessment using human and deep learning algorithmic segmentations study

Study objectives	**Outcome measures**
Training and internal validation	
To generate detailed ground truth needed for the CNN by fully manual annotations using contrast-enhanced CT scans of patients with MPM, based on learning from Chapter 4	Pleural tumour volume on CT (cm^3)
To determine correlation and agreement between human and CNN output volumes	Pleural tumour volume on CT (cm^3) Correlation (Spearman Rho) Agreement (Bland-Altman)
To assess inter- and intra-observer variations for later comparison with CNN output volumes	Pleural tumour volume on CT (cm^3)
External validation	
Comparison between classifications of treatment response as defined by human volume, CNN volume and mRECIST	Pleural tumour volume on CT (cm^3) Agreement (Cohen's Kappa)
Analysis of anatomical features associated with CNN segmentation errors	Visual inspection
Survival analyses based on treatment response as defined by human volumes, CNN volumes and mRECIST	Pleural tumour volume on CT (cm^3) Overall survival (days)
CNN: convolutional neural network; CT: computed tomography; MPM: malignant pleural mesothelioma mRECIST: modified Response Evaluation Criteria In Solid Tumours; PD: progressive disease; non-PD: non-progressive disease	

2.2.2 **Study population**

2.2.2.1 Original study population

The first version of the study protocol stipulated that patients were to be recruited from one of the following three clinical studies which have been detailed below and in Table 2.3 and Figure 2.7:

- Diagnostic and Prognostic Biomarkers in the Rational Assessment of Mesothelioma (DIAPHRAGM)(318)
- The South West Area Mesothelioma and Pemetrexed trial (SWAMP)(321)
- Prediction of ResIstance to chemotherapy using Somatic copy number variation in Mesothelioma (PRISM)(322)

The DIAPHRAGM study has been summarised in Chapter 2, Section 2.1.2. The South West Area Mesothelioma and Pemetrexed (SWAMP) trial was a multicentre prospective observational study evaluating biomarkers of chemotherapy response and prognostication(321). The Prediction of Resistance to chemotherapy using Somatic Copy Number Variation in Mesothelioma (PRISM) study is an ongoing retrospective cohort study which aims to define a genomic classifier that predicts chemo-resistance in patients with MPM(322).

Table 2.3 Original studies included in the first Automatic RECIST reporting in Mesothelioma using Deep Learning Artificial Intelligence protocol

Study	**Eligibility Criteria**	**Patients**
DIAPHRAGM REC Ref: 13/WS/0240	Inclusion: Suspected MPM requiring biopsy, recruited in Glasgow Exclusion: eGFR <30 ml/min, MRI contraindicated	n=25
SWAMP REC Ref: 08/H0102/46	Inclusion: Diagnosis of MPM, chemotherapy planned Exclusion: No measurable disease, prognosis <3 months	n=65
PRISM REC Ref: 16/WS/0207, Amendment 348	Inclusion: MPM diagnosis, previous chemotherapy, CT images available Exclusion: Insufficient tumour for genomic analyses	n=380
eGFR: estimated glomerular filtration rate; MPM: malignant pleural mesothelioma; REC: research ethics committee		

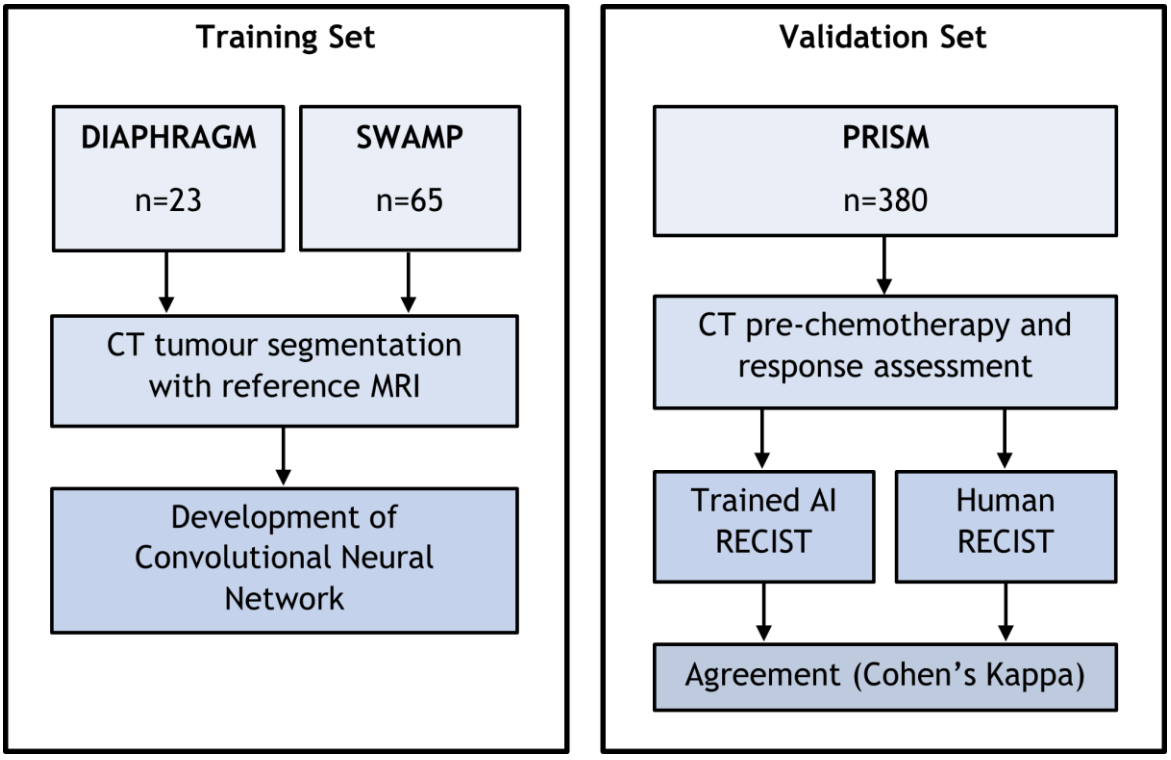

Figure 2.7 Flowchart of pleural tumour volumes included in the original Automatic RECIST reporting in Mesothelioma using Deep Learning Artificial Intelligence protocol (n=468 patients)

Unfortunately, due to data access restrictions, acquisition of images from the SWAMP study was not possible. NHSGGC made a formal application to the Health Research Authority (HRA) via the NHS Research Scotland Permissions Coordinating Centre to address this, but subsequent associated project delays prevented this data being included. Following discussions with the Trial Management Group, this problem was addressed by re-distributing the training and validation sets to include subjects from the DIAPHRAGM and PRISM studies only. This removed the capability to test the algorithm on data obtained from a fully independent study but preserved a fully reserved external validation set which was comprised of scans from three different study centres. This was a smaller size than originally planned with only Glasgow cases used in the training and internal validation set.

2.2.2.2 Final version

The second and final version of the study protocol recruited patients from two studies which have been detailed below and in Figure 2.8:

- DIAPHRAGM
- PRISM

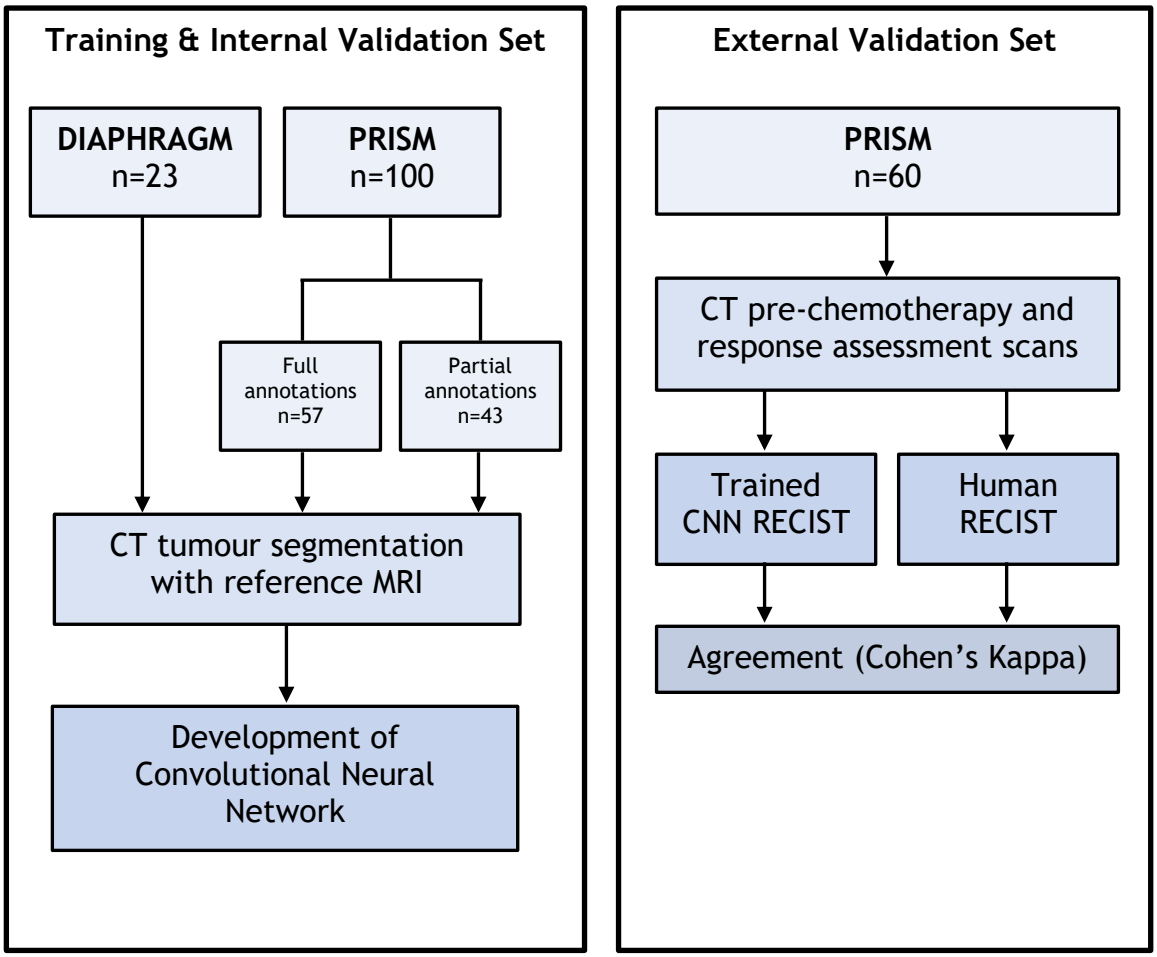

Figure 2.8 Flowchart of pleural tumour volumes included in final Automatic RECIST reporting in Mesothelioma using Deep Learning Artificial Intelligence protocol (n=108 patients)

The training and internal validation set comprised 123 annotated pleural tumour volumes from 108 patients in the DIAPHRAGM study (n=23) and PRISM (n=57) study sets. 80/123 were full manual volumes and 43/123 were partially annotated volumes, which I have described in more detail in Section 2.2.8 of this chapter. The external validation set 60 pleural tumour volumes (n=30 volumes at pre-chemotherapy and n=30 from response assessment time points) from 30 patients in the PRISM study only (n=10 patients from each of the three participating study centres).

2.2.3 **Eligibility criteria**

The following eligibility criteria were applied to all cases selected for the present study:

- Inclusion criteria:
    - Recruited to DIAPHRAGM or PRISM studies (Glasgow, Leicester or Wythenshawe patients)
    - Histological diagnosis of MPM
    - Venous-phase contrast-enhanced CT scan available
- Exclusion criteria:
    - Contrast-enhanced CT acquisition performed as CT pulmonary angiography (i.e., arterial-phase scans)

In the training and internal validation set, PRISM study patients were solely recruited from Glasgow. DIAPHRAGM cases were also included in the training and internal validation set because they had contemporaneous contrast-enhanced magnetic resonance imaging (MRI) scans which were used to aid in the delineation of tumour from adjacent soft tissue structures on CT scans. The advantage of MRI is that it offers superior soft tissue contrast(323, 324). Only pre-chemotherapy CT scans were assessed in the training and internal validation set. Patients in the external validation set were solely recruited from the PRISM study and included patients from Glasgow, Leicester or Wythenshawe. Both pre-chemotherapy and response assessment CT scans were assessed.

2.2.4 **Study procedures**

2.2.4.1 Clinical data

Clinical data were entered onto a Microsoft Excel data collection sheet. Each patient was associated with a study number and their data entered on to the appropriate row. Patient identifiers were entered and data recorded in a linked anonymised format. Clinical data was transferred to the QEUH in Glasgow from the other participating centres using a secure file transfer portal (University of Glasgow, https://transfer.gla.ac.uk/).

Data were extracted from study databases and supplemented by electronic records, including demographics (age, sex), Eastern Cooperative Oncology Group performance status (ECOG PS)(157, 320), disease stage according to the eighth TNM classification for MPM(45), histological sub-type (epithelioid, biphasic, sarcomatoid or not specified), date of diagnosis, type of chemotherapy received, chemotherapy intent, dates of chemotherapy, number of chemotherapy cycles received, reason for chemotherapy cessation and dates of pre-chemotherapy and response assessment CT imaging. Data regarding ECOG PS were inconsistently recorded and steps to provide a best estimate have been described in Chapter 2, Section 2.1.3.2. Overall survival (OS, days) was recorded from the date of pre-chemotherapy CT to death from any cause.

2.2.5 **CT image acquisition and anonymisation**

All image analyses were performed in Glasgow using the same methods and the same reporters for all subjects. The pre-chemotherapy CT scan was the last scan performed before administration of chemotherapy. The response assessment scan was defined as the CT scan on which the treating oncologist made their assessment of response to chemotherapy. This scan was not less than four-weeks after completion of the first chemotherapy cycle.

All CT scans were anonymised by the supplying site and issued the appropriate study number. Transfer of linked anonymised imaging data from the non-

Glasgow sites was done using the University of Glasgow secure file transfer portal (https://transfer.gla.ac.uk/). NHSGGC Research Radiography staff downloaded the linked anonymised CT images onto a secure encrypted external hard drive for the purposes of chemotherapy response evaluation and manual tumour segmentation.

2.2.6 **Treatment response evaluation using mRECIST**

Modified Response Evaluation Criteria in Solid Tumours (mRECIST) reporting was used in all subjects incorporating recent guidance on how to standardise this method when applied to CT imaging(325, 326). A Consultant Radiologist with expertise in MPM response assessment (Dr Gordon Cowell) reported all CT scans independently and was blinded to outcome data. Standardised window settings were reported as detailed in Table 2.4. I have provided further detail and an accompanying image of mRECIST measurements in Chapter 1, Section 1.5.2 and Figure 1.2, respectively.

Partial response (PR) was defined as a ≥30% reduction of tumour thickness on two occasions four-weeks apart. Progressive disease (PD) was defined as increase of >20% in tumour thickness over the two measurements. Stable disease (SD) included patients who did not meet the criteria for PR or PD.

Table 2.4 mRECIST standardised window settings

Pre-chemotherapy CT scans	**Response Assessment CT scans**
Target lesions: 5 lesions each with 2 diameter measurements (10 fields)	Target lesions: 5 lesions each with 2 diameter measurements (10 fields)
Sum of longest diameters of target lesions	Sum of longest diameters of target lesions
Non-target lesions: Yes/No	Percentage change in sum of longest diameters
Extra-thoracic disease: Yes/No	Non-target lesion response: CR, PR, SD, PD
	Overall disease response: CR, PR, SD, PD
	Extra-thoracic disease response: CR, PR, SD, PD
CR: complete response; PD: progressive disease; PR: partial response; SD: stable disease	

2.2.7 **Manual tumour segmentation**

I performed the human tumour annotations using Myrian Intrasense® software v2.4.3 (Paris, France) to generate the reference ground truth annotations. Pleural tumour boundaries were contoured on visible pleural tumour using a track-ball mouse and cursor on every axial slice in the CT image series. This is illustrated in Figure 2.5. Pleural tumour volume was calculated using the summed axial pleural tumour areas and slice thickness. Figure 2.9 provides an overview of the manual segmentation process.

80/123 volumetric studies were performed using a fully manual segmentation method. In the training and external validation set, an additional 43/123 scans were sparsely annotated with contours drawn only every fifth slice in 43/123 CT scans. This method was preceded by an interim analysis by an EngD Research Engineer (Owen Anderson) from Canon Medical Research Europe (CMRE) which highlighted high correlation between adjacent pleural tumour CT scan slices. This process facilitated the enrichment of the number of the patients in the training and internal validation set. Each full annotation took approximately 2.5 hours to complete. A second human reader with PhD training in MPM imaging (Dr Selina Tsim) generated annotations using the same method for inter-observer data.

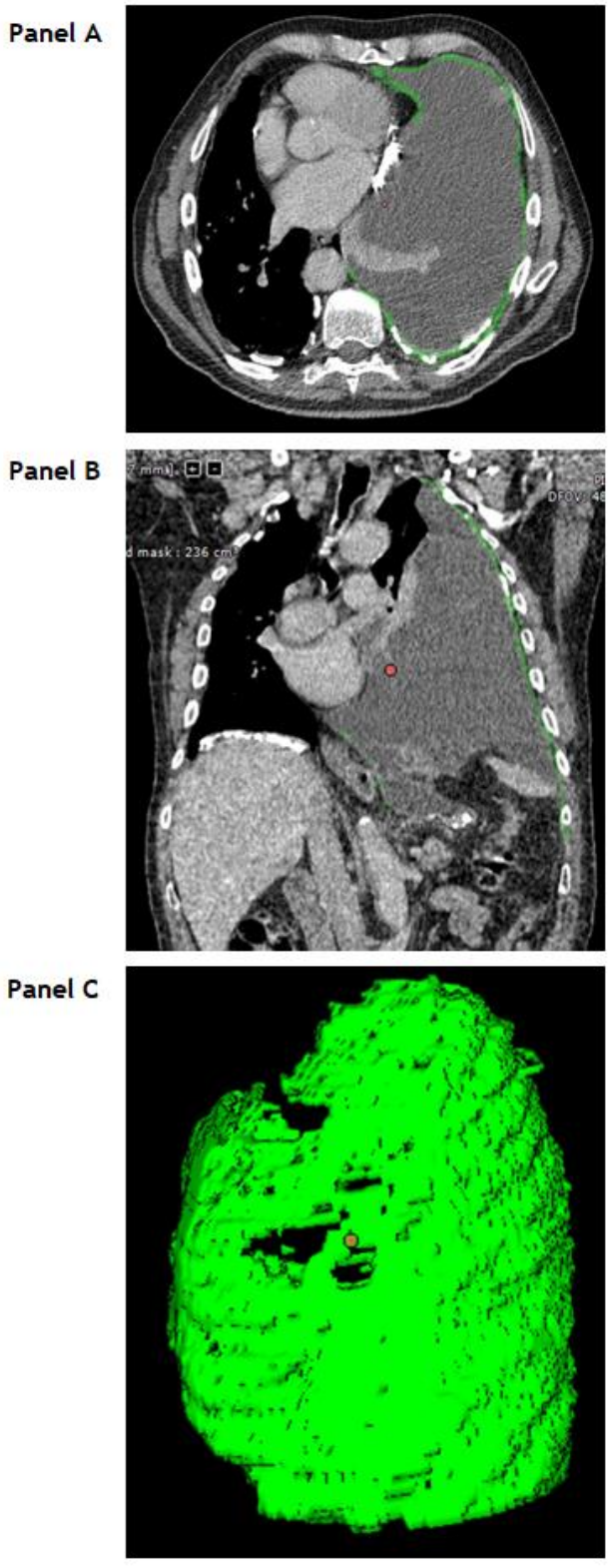

Figure 2.9 Example of manual pleural tumour segmentation when viewed in the axial plane in Panel A, the coronal plane in Panel B and in 3-D in Panel C. Pleural tumour is highlighted in green

2.2.8 **CT image transfer**

All anonymised images and segmented pleural tumour volumes were exported to the Canon Medical Research Europe team in Digital Imaging and Communications in Medicine Radiotherapy (DICOM-RT) format for AI training and development using the University of Glasgow secure file transfer port**al** **(**https://transfer.gla.ac.uk/).

2.2.9 **Development of the convolutional neural network**

The convolutional neural network (CNN) volumetric measurements were performed by an EngD Research Engineer (Owen Anderson) from CMRE using in-house and Amazon Web Service graphics processing units. A comprehensive description of the CNN model has been described by our group previously(327). I have summarised the method as follows. A convolutional neural network (CNN) with a two-dimensional U-Net architecture was employed(141). Three consecutive CT scan slices were added to a pre-trained network. CT Hounsfield unit (HU) intensities were clipped to -1025 to +1100 HU and normalised to a range of -1 to +1. The probability that each pixel contained tumour was predicted by the raw CNN output. A binary mask of the tumour pixels was created after a pre-determined threshold was applied to this map. The pre-determined threshold was defined using a sub-set of the training data. A predicted volumetric segmentation was created after this step and repeated on all the slices in the CT image series. Internal validation was achieved by seven CNN models which were trained by the computer scientists using seven-fold division of the training data. The subsequent volumetric measurements increased validity and provided confidence estimation.

2.2.10 Human and AI volumetric response classification

Human and AI response classifications were based on percentage volume change between pre-chemotherapy and response assessment time points. They were calculated as: ((post-chemotherapy tumour volume minus pre-chemotherapy tumour volume) divided by pre-chemotherapy tumour volume) multiplied by 100 (%). Volumetric partial response (PR) and progressive disease (PD) were defined as a 30% decrease in tumour volume and 20% increase between the two time points, respectively. Patients were classified as having stable disease (SD) if the percentage volume change did not meet the PR or PD criteria.

2.2.11 Statistical analyses

Statistical tests were performed in SPSS v24.0 (Chicago, USA) and GraphPad v9.1.0 (San Diego, USA). The study design was exploratory and no formal sample size calculations were performed. Data were tested for normal distribution using the Kolmogorov–Smirnov test. Normally and non-normally distributed data were summarised by mean (standard deviation, SD) and median [interquartile range, IQR], respectively.

2.2.11.1 Training and internal validation set

Initial performance of the CNN determined overlap between manual and automated regions was calculated by the Dice score separately by an EngD Research Engineer (Owen Anderson) from CMRE. This has not been included in this thesis but was presented by Owen Anderson at the 13th International Joint Conference on Biomedical Engineering Systems and Technologies in 2020 and subsequently published in the Bioimaging journal(327). The Dice score is a measure of performance commonly reported in the AI literature and has been described in more detail in Chapter 1, Sections 1.7 and 1.8.2.

Correlation between human and AI volumes using CT scans of patients with MPM was determined by Spearman's Rho test. Agreement between human and AI volumes using CT scans of patients with MPM was determined using Bland-Altman

plots. Intra-class correlation coefficient (ICC) determined reproducibility between human and AI readers. For inter-observer data, I randomly chose 13 pleural tumour volumes which were delineated by a respiratory physician with expertise in MPM (Dr Selina Tsim). For intra-observer data, I randomly chose 10 training set scans and repeated delineations of these scans at least three weeks after my original delineations.

2.2.11.2 External validation set

Paired volume data were compared using the Wilcoxon matched-pairs signed rank test. Agreement between chemotherapy response classification by human volumetry, AI volumetry and mRECIST was calculated using Cohen's Kappa statistic. The Kruskal-Wallis test compared differences in volume between the AI- and mRECIST-defined PR, SD and PD groups. Dunn's test was used for multiple comparisons. Overall survival (OS, days) was determined using Kaplan-Meier methodology and compared using the log-rank test. Cases with scans having interval periods between pre-chemotherapy and response assessment time points exceeding 100 days were excluded from the survival analyses. Post-hoc subjective visual analysis of CNN segmentation errors determined whether anatomical features could account for these.

2.3 Prevalence, pattern and prognostic significance of altered body composition in patients with chemotherapy-treated MPM

A multicentre retrospective cohort study was performed. NHS Greater Glasgow and Clyde (NHSGGC) were the study sponsors. The NHS Greater Glasgow and Clyde (NHSGGC) Safe Haven granted approval for access to unconsented anonymised imaging data required for this project on 12th April 2018 (Ref: GSH/18/ON/001). This covered both local NHS Research and Development (R&D) and Research Ethics Committee (REC) approvals. The study protocol was approved by the NHSGGC Biorepository Clinical Governance Group. This extended the existing ethical approval in place for Biorepository projects (Biorepository Application 348).

2.3.1 **Study objectives**

2.3.1.1 Primary objective and outcome measures

The primary objective of this study was to determine the prevalence and pattern of altered body composition at the third lumbar (L3) and fourth thoracic vertebrae (T4) in patients with MPM who went on to receive chemotherapy.

2.3.1.2 Secondary objectives and outcome measures

The secondary objectives were to determine, a) the prognostic significance of sarcopenia and adipopenia at L3 and sarcopenia at T4, and, b) the reproducibility of skeletal muscle and adipose tissue indices. Table 2.5 summarises the primary and secondary objectives and outcome measures. Table 2.6 summarises the exploratory objectives and outcome measures.

Table 2.5 Primary and secondary objectives and associated outcome measures of the altered body composition study

Study objectives	**Outcome measures**
Primary objective	
To define the prevalence and pattern of skeletal muscle and adipose tissue loss during chemotherapy at L3 in patients with MPM who went on to receive chemotherapy	Presence of L3SMI (cm^2/m^2) loss, Y/N Presence of L3VFI (cm^2/m^2) loss, Y/N Presence of L3TFI (cm^2/m^2) loss, Y/N where loss was defined as minus 1 standard deviation if the data were normally distributed or data below the 25th percentile if non-normally distributed
To define the prevalence and pattern of skeletal muscle loss during chemotherapy at T4 in patients with MPM who went on to receive chemotherapy	Presence of T4SMI (cm^2/m^2) loss, Y/N where loss was defined as minus 1 standard deviation if the data were normally distributed or data below the 25th percentile if non-normally distributed
Secondary objectives	
To determine if L3SMI, L3VFI, L3TFI and T4SMI correlate with measures of pre-chemotherapy systemic inflammation and tumour volume	L3SMI (cm^2/m^2) L3VFI (cm^2/m^2) L3TFI (cm^2/m^2) T4SMI (cm^2/m^2) Measures of inflammation: WCC, neutrophils, platelets, lymphocytes, NLR, PLR, albumin, mGPS MPM tumour volume CT (cm^3)

To determine the prognostic significance of sarcopenia and adipopenia at L3 and sarcopenia at T4	Presence of sarcopenia as defined by: L3SMI (cm^2/m^2) loss, Y/N T4SMI cm^2/m^2) loss, Y/N Presence of adipopenia as defined by: L3VFI (cm^2/m^2) loss, Y/N L3TFI (cm^2/m^2) loss, Y/N where loss was defined as minus 1 standard deviation if the data were normally distributed or data below the 25^{th} percentile if non-normally distributed Overall survival (OS), days
To determine the reproducibility of L3SMI, L3VFI and L3TFI measurements by different observers	L3SMI (cm^2/m^2) L3VFI (cm^2/m^2) L3TFI (cm^2/m^2)
To determine the reproducibility of T4SMI measurements by different observers	T4SMI (cm^2/m^2)
CRP: C-reactive protein; L3: third lumbar vertebra; L3SMI: skeletal muscle index at L3; L3TFI: total fat index at L3; L3VFI: visceral fat index at L3; mGPS: modified Glasgow Prognostic Score; NLR: neutrophil:lymphocyte ratio; PLR: platelet:lymphocyte ratio; T4: fourth thoracic vertebra; T4SMI: skeletal muscle index at T4; WCC: white cell count	

Table 2.6 Exploratory objectives and outcome measures of the altered body composition study

Exploratory objectives	**Outcome measures**
To determine the difference between ipsilateral and contralateral T4SMI loss	Ipsilateral T4SMI (cm^2/m^2) Contralateral T4SMI (cm^2/m^2)
To determine the prognostic significance of ipsilateral T4SMI loss	Presence of ipsilateral T4SMI loss (cm^2/m^2), Y/N Overall survival (OS), days
To determine correlation between L3SMI and T4SMI and response to treatment	Presence of L3SMI (cm^2/m^2) loss, Y/N Presence of T4SMI (cm^2/m^2) loss, Y/N
To determine correlation between L3SMI and T4SMI	L3SMI (cm^2/m^2) T4SMI (cm^2/m^2)
To determine if sex- and BMI-specific differences exist at L3 and T4	L3SMI (cm^2/m^2) in males L3SMI (cm^2/m^2) in females L3VFI (cm^2/m^2) in males L3VFI (cm^2/m^2) in females L3TFI (cm^2/m^2) in males L3TFI (cm^2/m^2) in females T4SMI (cm^2/m^2) in males T4SMI (cm^2/m^2) in females L3SMI (cm^2/m^2) in BMI <25 kg/m^2 L3SMI (cm^2/m^2) in BMI ≥25 kg/m^2 L3VFI (cm^2/m^2) in BMI <25 kg/m^2 L3VFI (cm^2/m^2) in BMI ≥25 kg/m^2 L3TFI (cm^2/m^2) in BMI <25 kg/m^2 L3TFI (cm^2/m^2) in BMI ≥25 kg/m^2 T4SMI (cm^2/m^2) in BMI <25 kg/m^2 T4SMI (cm^2/m^2) in BMI ≥25 kg/m^2
BMI: body mass index; L3: third lumbar vertebra; L3SMI: skeletal muscle index at L3; T4: fourth thoracic vertebra; T4SMI: skeletal muscle index at T4; Ipsilateral & Contralateral T4SMI: skeletal muscle index at T4 on ipsilateral and contralateral side of tumour, respectively	

2.3.2 **Study population**

Patients were selected from the Prediction of Resistance to chemotherapy using Somatic Copy Number Variation in Mesothelioma (PRISM) study which is a multicentre MPM biomarker study assessing a genomic predictor classifier of chemotherapy resistance described in Section 2.2.2.1 of this chapter. Potentially eligible patients were identified retrospectively using existing databases at the study centres.

2.3.3 **Eligibility criteria**

The following eligibility criteria were applied to all cases selected for the present study:

- Inclusion criteria:
    - Histological diagnosis of MPM
    - Cisplatin (or carboplatin) plus pemetrexed chemotherapy received
    - Pre-chemotherapy and response assessment venous-phase contrast-enhanced CT images available for analysis
    - Height and weight metrics available at pre-chemotherapy time point
- Exclusion criteria:
    - Non-availability of pre-chemotherapy and response assessment venous-phase contrast-enhanced CT images
    - Non-availability of height and weight metrics available at pre-chemotherapy time point

2.3.4 **Study procedures**

2.3.4.1 Clinical data

The coordinating study centre was the Queen Elizabeth University Hospital (QEUH) in Glasgow. Data and imaging were collected from Wythenshawe Hospital and University of Leicester Hospitals NHS Trust. Clinical data were entered onto a Microsoft Excel data collection sheet. Each patient was associated with a study number and their data entered on to the appropriate row. Patient identifiers were entered and data recorded in a linked anonymised format. Clinical data was transferred to Glasgow from the other participating centres using a secure file transfer portal (https://transfer.gla.ac.uk/).

Data were extracted retrospectively from study databases and supplemented by electronic records, including demographics (age, sex), Eastern Cooperative Oncology Group performance status (ECOG PS)(157, 320), histological sub-type (epithelioid, biphasic, sarcomatoid or not specified), disease stage according to the eighth TNM classification for malignant pleural mesothelioma(45) and details of chemotherapy (outlined in Section 2.2.4.1 of this chapter). Data regarding ECOG PS have been further described in Section 2.1.3.2 of this chapter. Overall survival (OS, days) was recorded from the date of pre-chemotherapy CT to death from any cause.

The systemic inflammatory response can be defined by single measures. Pre-chemotherapy blood laboratory value data were collected and included haemoglobin, white cell count, neutrophils, platelets and lymphocytes. The latter haematological indices are included in the neutrophil:lymphocyte ratio (NLR) – calculated by dividing the number of neutrophils by number of lymphocytes - and platelet:lymphocyte ratio (PLR) – defined by dividing the number of platelets by number of lymphocytes. Laboratory value data collected also included acute phase proteins C-reactive protein (CRP) and albumin and the integrated modified Glasgow Prognostic Score (mGPS) which combines CRP and albumin(328). A single centre sub-group of patients also had available response assessment blood laboratory results, including white cell count, neutrophils, lymphocytes, platelets, albumin and CRP.

2.3.4.2 Weight and height measurements

Weight and height measurements were collected retrospectively. Body mass index (BMI) was calculated as: (weight (kg) divided by height squared (m^2)). The World Health Organisation (WHO) categories were used and have been summarised as follows(329):

- Underweight: BMI <18.5 kg/m^2
- Normal: BMI 18.5–24.9 kg/m^2
- Overweight: 25–29.9 kg/m^2
- Obese: BMI ≥30 kg/m^2

2.3.5 **CT image acquisition and anonymisation**

CT image acquisition and anonymisation has been described in Sections 2.2.6 of this chapter.

2.3.6 **Body composition analyses**

A freely available image processing software called ImageJ (U.S. National Institutes of Health, Bethesda, MD)(330) was used for body composition analyses.

2.3.6.1 Skeletal muscle at the third lumbar vertebra

The third lumbar vertebra (L3) was identified by counting down from the first rib and counting upwards from the pelvic bones. Images were saved at the mid-point of the spinous process. Adequate image penetration and image contrast were evidenced by visualising lumbar vertebral bodies with both trabecular and cortical bone demonstrated. The L3 muscle groups included the following muscle groups: psoas, erector spinae, quadratus lumborum, transversus abdominis, internal obliques, external obliques, rectus abdominus.

The L3 skeletal muscle area measurement method is illustrated in Figure 2.10. The external musculature was delineated by the segmented line tool on ImageJ software (U.S. National Institutes of Health, Bethesda, MD; see Figure 2.10: Panel A). Established Hounsfield unit (HU) skeletal muscle thresholds of -29 to +150 HU were applied(288), and area measured (cm^2, see Figure 2.10, Panel B). The internal musculature was delineated (see Figure 2.10, Panel C) with the same HU thresholds set and area measured (see Figure 2.10, Panel D). The external and internal musculature areas were subtracted to provide the L3 skeletal muscle area (L3SMA, cm^2).

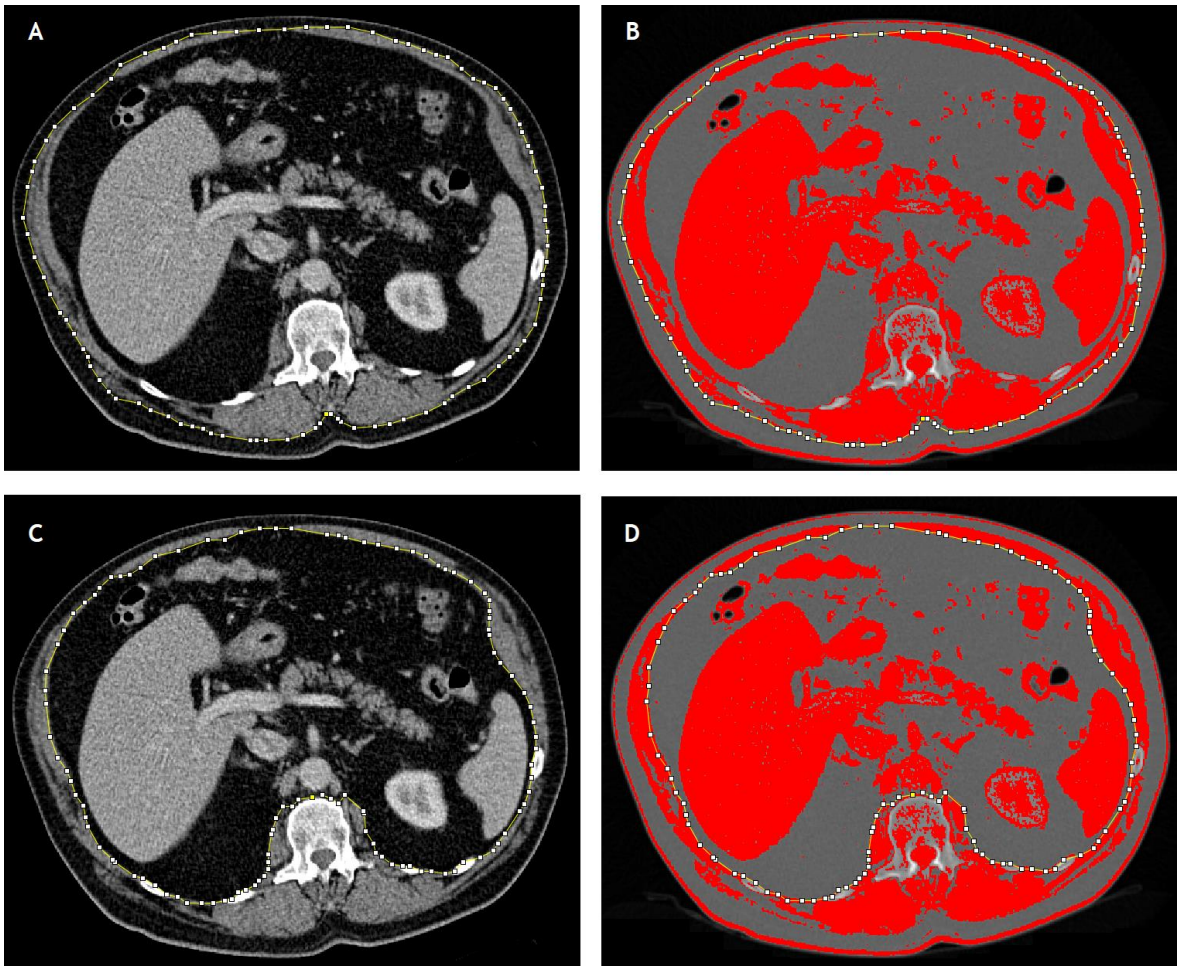

Figure 2.10 Axial slices of CT scans demonstrating the third lumbar vertebra (L3). Panel A demonstrates the delineation of the external skeletal muscle area (SMA) on ImageJ software, defined by the area included in the dotted yellow line. Panel B demonstrates the skeletal muscle threshold selection using a HU range of -29 to +150 HU. Panel C demonstrates the delineation of the internal SMA, defined by the area included in the dotted yellow line. Panel D demonstrates skeletal muscle HU threshold selection

2.3.6.2 Skeletal muscle at the fourth thoracic vertebra

The fourth thoracic vertebra (T4) was identified by counting down from the first rib and counting upwards from the twelfth thoracic vertebra. Images were saved at the mid-point of the spinous process. Adequate image penetration and image contrast were evidenced by visualising thoracic vertebral bodies with both trabecular and cortical bone demonstrated. The T4 muscle groups included the following muscle groups: pectoralis, intercostal, serratus, latissimus and paraspinal muscles. Figure 2.11 illustrates the skeletal muscle HU threshold method for total T4 skeletal muscle area measurement which is described in detail in Section 2.3.6.1 of this chapter.

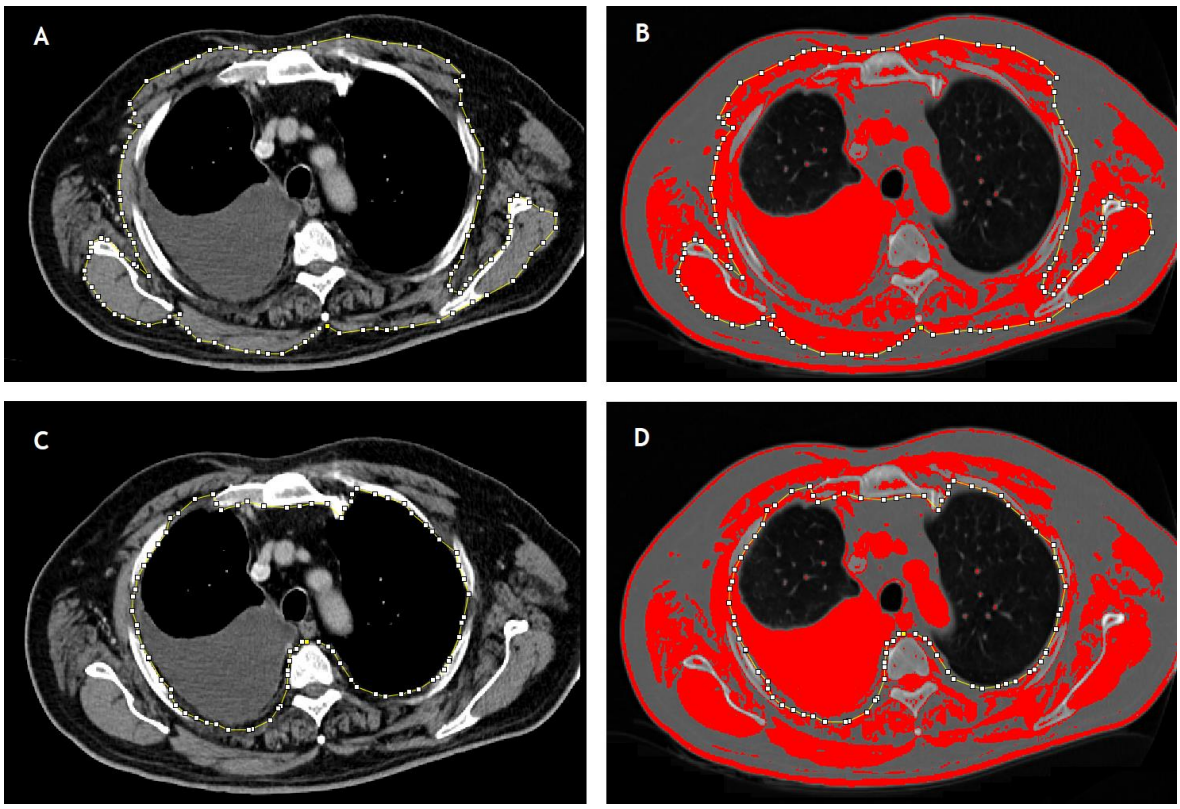

Figure 2.11 Axial slices of CT scans demonstrating fourth thoracic vertebra (T4). Panel A demonstrates the delineation of the external skeletal muscle area (SMA) on ImageJ software, defined by the area included in the dotted yellow line. Panel B demonstrates the skeletal muscle threshold selection (HU range, -29 to +150 HU). Panel C demonstrates the delineation of the internal SMA, defined by the area included in the dotted yellow line. Panel D demonstrates skeletal muscle HU threshold selection

2.3.6.3 Skeletal muscle at the ipsilateral fourth thoracic vertebra

Ipsilateral T4 was defined as the side of the thorax containing pleural tumour. The border between ipsilateral and contralateral compartments was defined as a straight line drawn posterio-anteriorly from the mid-point of the vertebral body to the midpoint of the sternum. Figure 2.12 illustrates the same skeletal muscle HU threshold method for skeletal muscle area measurement described in Section 2.3.6.2 of this chapter. The contralateral fourth thoracic vertebra (Contralateral T4) muscle area was calculated subtracting the ipsilateral T4 muscle area (cm^2) from the total T4 muscle area.

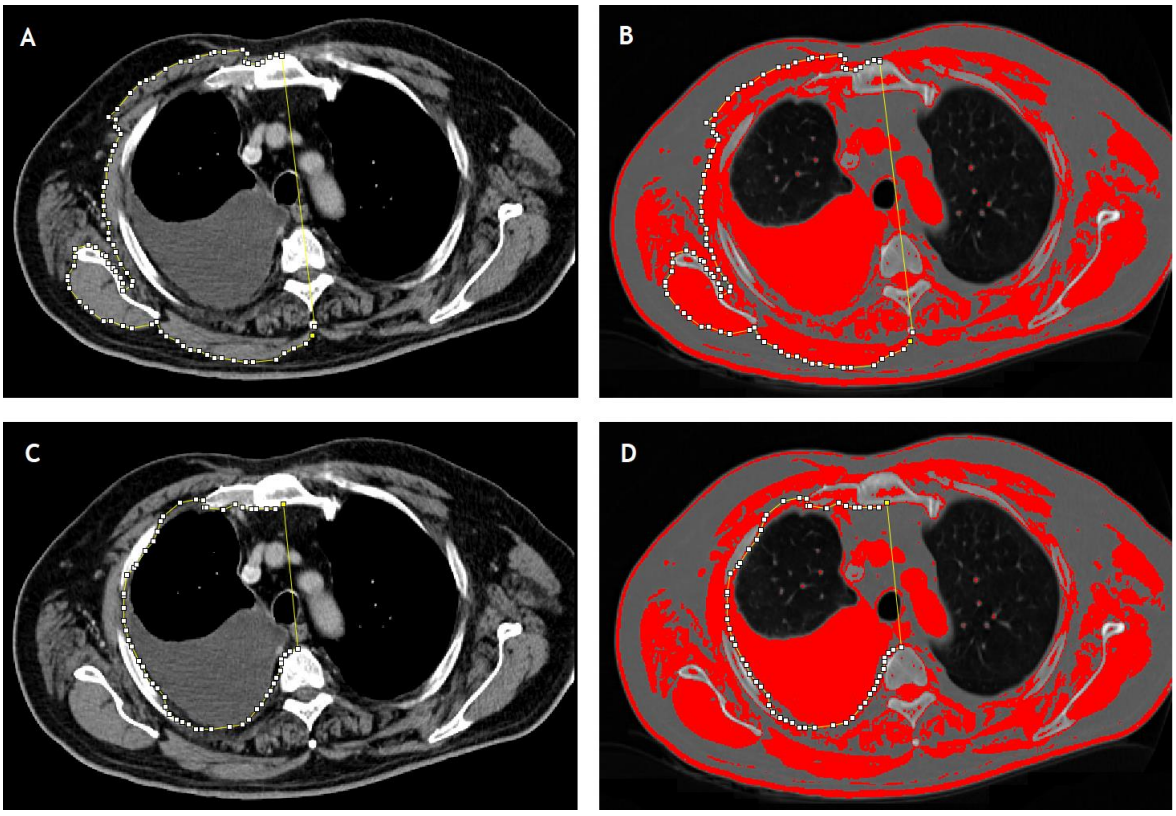

Figure 2.12 Axial slices of CT scans demonstrating fourth thoracic vertebra (T4). Panel A demonstrates the delineation of the external skeletal muscle area (SMA) on the ipsilateral side of MPM tumour, defined by the area included in the dotted yellow line. Note the straight yellow line separating the ipsilateral and contralateral muscle compartments. Panel B demonstrates the skeletal muscle threshold selection (HU range, -29 to +150 HU). Panel C demonstrates the delineation of internal SMA, defined by the area included in the dotted yellow line. Panel D demonstrates skeletal muscle HU threshold selection

2.3.6.4 Adipose tissue at the third lumbar vertebra

Image analysis for adipose tissue was based on a single image at L3 on contrast-enhanced CT scans defined as per Section 2.3.6.1 of this chapter. The exterior skin was delineated (see Figure 2.13, Panel A). Established HU thresholds for adipose tissue (-190 to -30 HU) were applied(305), and area measured (cm^2, see Figure 2.13: Panel B). The external musculature was delineated (see Figure 2.13, Panel C) and subcutaneous adipose tissue HU thresholds were applied (see Figure 2.13: Panel D). Subcutaneous adipose area (SFA, cm^2) was calculated by subtracting the exterior skin and external musculature areas. The internal musculature was delineated (see Figure 2.13: Panel E) with adipose tissue HU thresholds applied and area measured (see Figure 2.13, Panel F). Visceral adipose area (SFA, cm^2) was calculated by subtracting the external and internal musculature areas (cm^2). Total fat area (TFA, cm^2) was calculated as the sum of visceral adipose area (VFA, cm^2) and subcutaneous adipose area (SFA, cm^2).

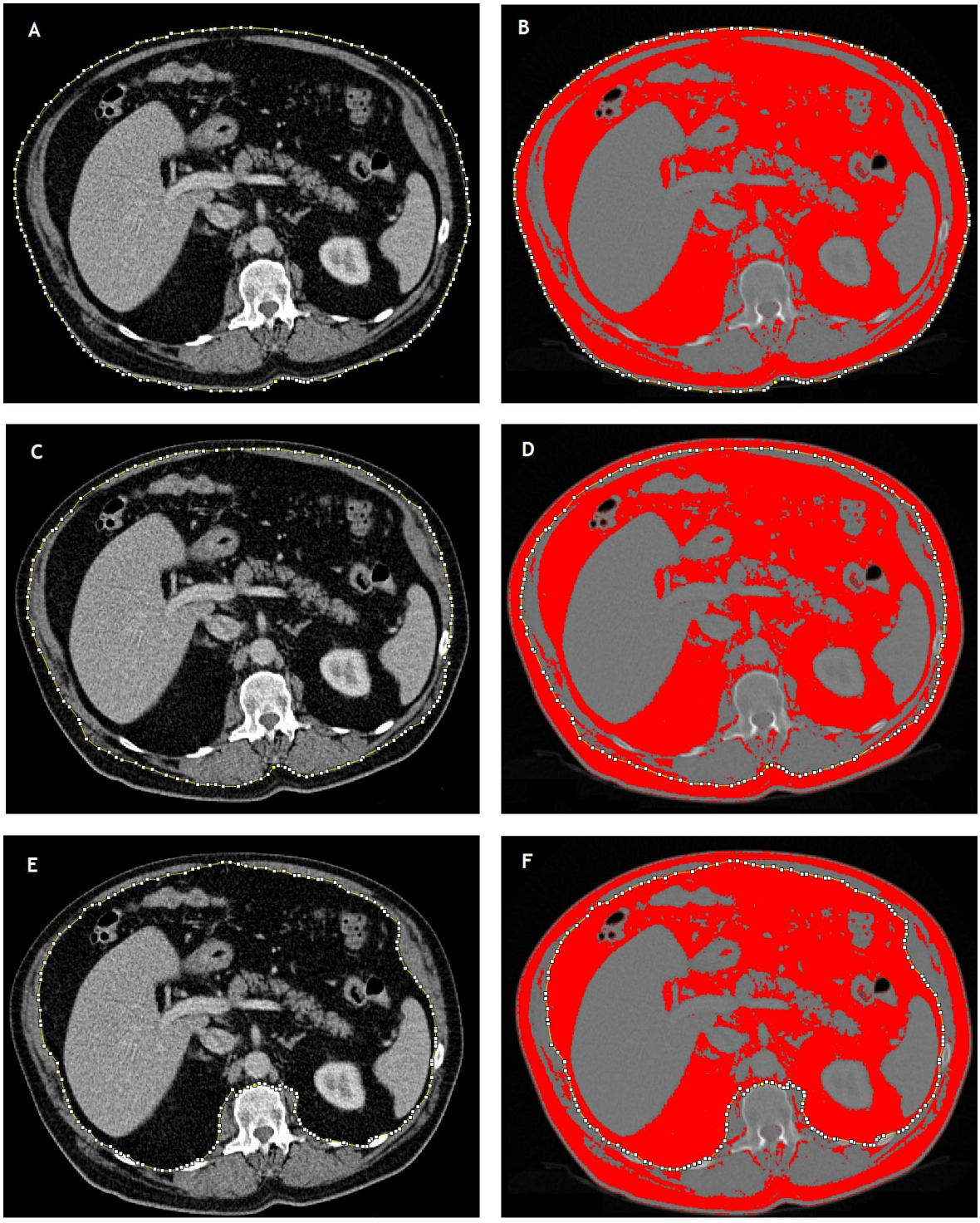

Figure 2.13 Axial slices of CT scans demonstrating L3. Panel A demonstrates the delineation of the external adipose tissue on ImageJ software, defined by the area included in the dotted yellow line. Panel B demonstrates the adipose tissue threshold selection using established adipose tissue HU ranges of -190 to -30 HU. Panel C demonstrates the delineation of external adipose tissue area. Panel D demonstrates adipose tissue HU threshold selection. Panel E and F demonstrates internal adipose tissue area (defined by the area included in the dotted yellow line) and HU threshold selection, respectively

2.3.7 **Body composition index changes**

Body composition indices were calculated by dividing the relevant muscle or adipose tissue areas (cm^2) by height squared (m^2) to provide skeletal muscle index (SMI, cm^2/m^2) or adipose tissue indices, including total fat index (TFI, cm^2/m^2), visceral fat index (VFI, cm^2/m^2) and subcutaneous fat index (SFI, cm^2/m^2).

I used published sex- and BMI-specific cut-offs for sarcopenia at L3 as follows(186):

- L3 skeletal muscle index (L3SMI) <41 cm^2/m^2 in females
- L3SMI <53 cm^2/m^2 if BMI ≥25 kg/m^2 and L3SMI <43 cm^2/m^2 if BMI <25 kg/m^2 in males

No sarcopenia thresholds exist for skeletal muscle index at T4 (T4SMI) or Ipsilateral or Contralateral T4SMI. I made an *a priori* decision to dichotomise patients into muscle losing and non-losing groups based on thresholds of mean minus 1 standard deviation if the data were normally distributed or data below the 25th percentile if non-normally distributed. There are also no thresholds for T4SMI or T4SMI Ipsilateral changes between pre-chemotherapy and response assessment time points. Percentage changes between pre-chemotherapy and response assessment time points were computed for each case as: ((response assessment SMI minus pre-chemotherapy SMI) divided by pre-chemotherapy SMI) multiplied by 100 (%). I made an *a priori* decision to dichotomise patients into muscle losing and non-losing groups based on thresholds of mean minus 1 standard deviation if the data were normally distributed or data below the 25th percentile if non-normally distributed. The same thresholds were used for percentage changes between pre-chemotherapy and response assessment time points at L3SMI and for all the adipose tissue indices.

2.3.8 **Chemotherapy response evaluation**

Chemotherapy response evaluation was performed by a Consultant Radiologist (Dr Gordon Cowell) using mRECIST described in Section 2.2.6 of this chapter.

2.3.9 **Tumour volume**

I performed manual pleural tumour segmentations on pre-chemotherapy CT scans using Myrian Intrasense® software v2.4.3 (Paris, France). This method has been described in detail in Section 2.2.7 of this chapter.

2.3.10 **Statistical analyses**

Statistical analyses were performed using SPSS v24.0 (Chicago, USA) and GraphPad v9.1.0 (San Diego, USA). Sample size calculations were not performed due to the exploratory study design. Data were tested for normal distribution using the Kolmogorov–Smirnov test. Descriptive data have been presented as percentage, mean (standard deviation, SD) for normally distributed and median [interquartile range, IQR] for non-normally distributed variables.

2.3.10.1 Primary objective

The prevalence of skeletal muscle and adipose tissue loss at L3 and skeletal muscle loss at T4 was determined as: (number of patients in the muscle or adipose tissue losing group divided by the total number of patients) multiplied by 100 (%).

2.3.10.2 Secondary objectives

The proportion of cases in muscle losing and non-muscle losing groups was compared using X^2 or Fisher's exact test, where appropriate. Mean or median values for groups were compared using the unpaired Student's t-test for normally

distributed data or the Mann-Whitney U test for non-normally distributed data. Differences in T4SMI change and mRECIST-defined partial response (PR), stable disease (SD) and progressive disease (PD) groups were compared by ANOVA Correlations between variables and muscle indices were calculated by Parson's or Spearman's correlation, where appropriate. No factors with $r>0.8$ were included in the same multivariable model to account for co-linearity. Factors with values of $p<0.05$ in univariate analyses were included in the multivariate analysis with the Cox proportional hazards model. Overall survival (OS, days) was generated using Kaplan-Meier methodology and compared using the log-rank test. Correlation between L3SMI and T4SMI was determined by Spearman's Rho test. For inter-observer data of L3, I randomly selected 35 CT scans which were annotated independently by a respiratory physician (Dr Geoffrey Martin). For intra-observer data, I re-annotated 35 randomly selected scans, three weeks after my original annotations. For inter-observer data of T4, I randomly selected 35 CT scans which were annotated independently by a clinical fellow (Dr Jenny Ferguson). For intra-observer data, I re-annotated 35 randomly selected scans, three weeks after my original annotations.

Chapter 3

SEMI-AUTOMATED SEGMENTATION OF MPM TUMOUR VOLUME

3 Chapter 3: Semi-automated segmentation of MPM tumour volume

3.1 Introduction

Response assessment in patients with malignant pleural mesothelioma (MPM) is important in determining prognosis and suitability for traditional chemotherapies agents as well as emerging immunotherapies. An alternative to the modified Response Evaluation Criteria in Solid Tumours (mRECIST) classification is required due to high inter-observer variation(78) and tumour over-classification(82). Tumour volumetry has become established in lung(331) and other malignancies(332-334) and overcomes the limitation of arbitrary unidimensional measurements made on serial computed tomography (CT) scans to provide a more reliable assessment of tumour volume.

Volumetric segmentation of pleural tumour in MPM has been studied by several previous group(46, 80, 99, 104, 108), including using magnetic resonance imaging (MRI)(319). MRI is a medical imaging modality that generates anatomical images using magnetic field gradients and radio waves(335). It affords clearer soft tissue definition when compared to CT(336). Research from our own study group has demonstrated that MRI-measured T-volume is superior to TNM8-defined T-stage as a survival predictor (HR 4.03, p=0.006)(319). However, MRI is not used routinely in clinical practice and is not suitable in every patient, for example, due to claustrophobia or pre-existing metalwork in the body.

CT remains the primary initial cross-sectional imaging modality in the evaluation of patients with suspected MPM(2). CT does have technical limitations, but due to the availability, cost and familiarity among radiologists (in the short to medium term at least), better tools are required to use the data acquired by CT, including development of an automated approach to pleural tumour volumetry in MPM. Recent studies have reported semi-automated(109, 112, 113, 337) and automated approaches to CT volumetry in patients with MPM(136). However, these approaches require human annotations which have wide inter-observer

variability(102, 104) and have struggled to differentiate complex pleural tumours from other anatomical structures in the thorax(113, 338). Automated CT volumetry has the potential to obviate the need for time-consuming and potentially inaccurate annotations drawn by human readers but has yet to be established in MPM. This first step in volumetric automation is the training of artificial intelligence (AI) algorithms using human-defined – or ground –ruth - volumes.

This chapter describes the attempt to deploy a recently reported semi-automated method of volumetric MPM tumour assessment developed using MRI on contrast-enhanced CT scans to serve as ground truth for a future AI algorithm.

3.2 Methods

A detailed description of the methods is provided in Chapter 2, Section 2.1.

The objectives and associated outcome measures for this study are detailed in Chapter 2, Section 2.1.1. To summarise, the primary objective was to determine the feasibility of semi-automated MPM volumetry based on radiodensity-tuned segmentation of contrast-enhanced CT scans (originally developed on MRI). The secondary objectives were to assess correlation and agreement between CT and MRI volumes and the reproducibility of the method.

3.3 Results

3.3.1 **Study population**

23 patients were included and have been summarised in Table 3.1. The median age was 71 [IQR 71 to 83] years and the majority were male (87%). Epithelioid mesothelioma was the most common histological sub-type (70%). Patients mostly had earlier stage disease (TNM8 stage I disease 70%) with an ECOG Performance status of 0 (13%) or 1 (61%). Over one fifth of patients had a PS of 2 (22%).

Table 3.1 Clinicopathological data of 23 patients with MPM who had contemporaneous contrast-enhanced CT and MRI scans

	Median [IQR] or n (%)
Age at diagnosis, years	71 [71–83]
Male gender	20 (87%)
Histological sub-type	
Epithelioid	16 (70%)
Biphasic	3 (13%)
Sarcomatoid	2 (9%)
Not available	2 (9%)
Disease stage	
I	16 (70%)
II	0 (0%)
III	1 (4%)
IV	0 (0%)
Not available	6 (26%)
ECOG Performance status	
0	3 (13%)
1	14 (61%)
2	5 (22%)
3	1 (4%)
ECOG: Eastern Cooperative Oncology Group	

3.3.2 **Primary objectives**

3.3.2.1 Radiodensity measurements

The total number of pleural ROIs assessed was 154. The median radiodensity in Hounsfield unit (HU) values in these ROIs was 52 [IQR 46 to 60] HU, see Table 3.2. The HU threshold limits used for subsequent region growing for generation of pleural volumes was the median value of seed placed in the contour mask +/- 11 HU.

Table 3.2 Pleural tumour ROI HU values obtained in the coronal plane of contrast-enhanced CT scans

	Pleural tumour HU
Minimum	21
25th Percentile	46
Median	52
75th Percentile	60
Maximum	100
HU: Hounsfield unit	

The median HU in areas of intercostal muscle, diaphragm and pleural fluid were 20.4 [IQR 11.9 to 32.3] HU, 40.4 [IQR 26.4 to 56.4] HU and 11.8 [IQR 8.3 to 17.8] HU, respectively (see Table 3.3). Lung, rib and pleural plaque were -827.9 [IQR -863.9 to -791.5] HU, 438 [IQR 382.2 to 481.2] HU and 639.6 [IQR 538.5 to 763.3] HU, respectively.

Table 3.3 Other thoracic tissues ROI HU values obtained in the coronal plane of contrast-enhanced CT scans

	Intercostal muscle HU	**Pleural fluid HU**	**Diaphragm HU**	**Liver HU**	**Spleen HU**	**Rib HU**	**Pleural plaque HU**	**Lung HU**
Minimum	3.3	1.2	7.8	16.4	12.5	293.8	249	-1003
25th Percentile	11.9	8.3	26.4	73.3	85.7	382.2	538.5	-863.9
Median	20.4	11.8	40.4	95.9	104	438	639.6	-827.9
75th Percentile	32.3	17.8	56.4	107.8	118.7	491.2	763.3	-791.5
Maximum	53.3	35.1	87.1	138.7	175.3	703.1	1007	17.3
HU: Hounsfield unit								

3.3.2.2 Comparison of radiodensities in pleural tumour and other tissues

There was significant overlap between the radiodensities of the pleurae and adjacent structures as illustrated in Figures 3.1 and 3.2.

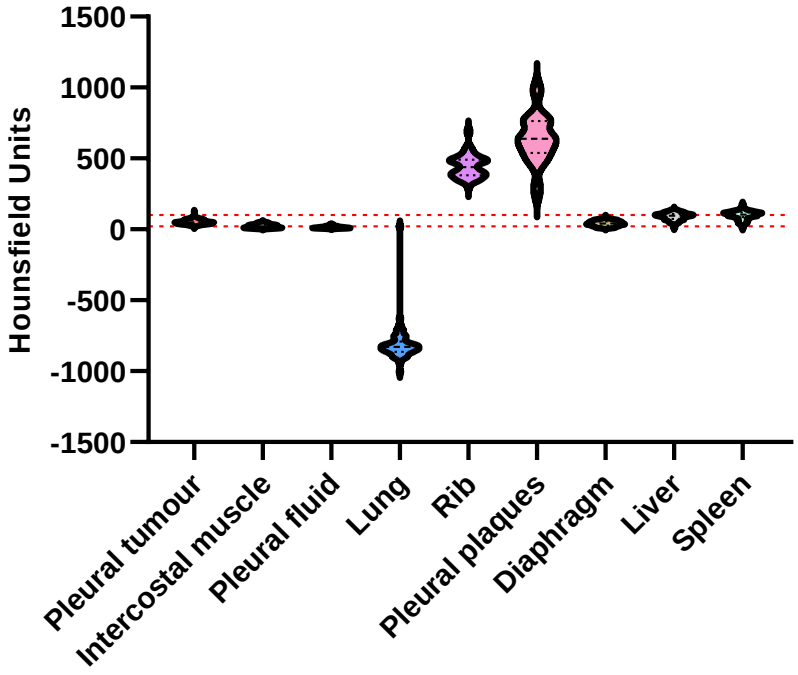

Figure 3.1 Violin plots illustrating overlapping HU values of all thoracic tissues. The dotted lines inside the violins represent the median and 25th and 75th percentile HU values. The red dotted lines across the plot represent the minimum and maximum HU values for pleural tumour

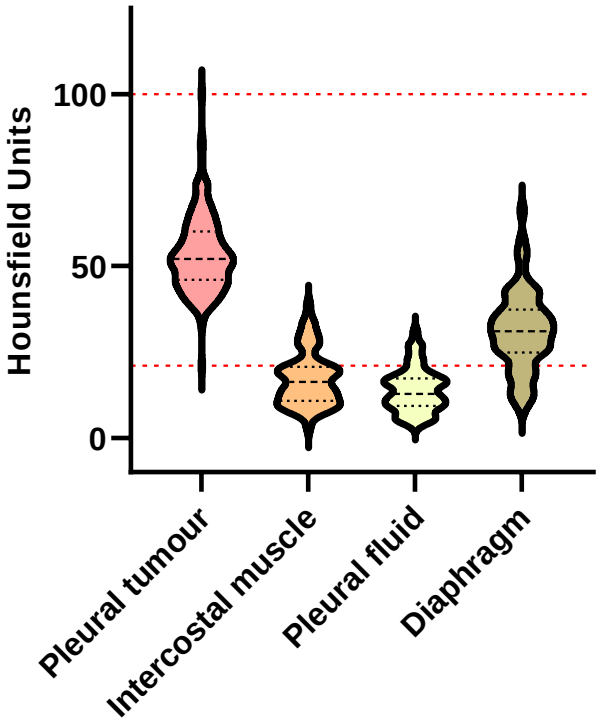

Figure 3.2 Violin plots illustrating overlapping HU values of pleural tumour and adjacent thoracic tissues, including intercostal muscle, pleural fluid and diaphragm. The dotted lines inside the violins represent the median and 25th and 75th percentile HU values. The red dotted lines across the plot represent the minimum and maximum HU values for pleural tumour

3.3.2.3 Segmentation attempt 1

Despite the similarities in HUs between pleural tumour and different thoracic tissues, semi-automated volumetric segmentation was attempted. In my first attempt, freehand contours were drawn every 10 slices to include 36 axial slices. This process took 35 minutes. After propagating the contour mask, areas were visible within the semi-automated volumes that included anatomical structures out-with pleural tumour. These presented as areas of artefact – or 'ghost images' - superimposed on the CT image. This has been illustrated in Figure 3.3. I considered the complex shapes of the lung and chest wall to be possible reasons for this phenomenon as well as a relatively light segmentation schedule which the software was unable to semi-automate in the linear interpolation step to make an accurate contour mask. The threshold mask volume based on the 36 contoured axial slices was approximately 493 cm^3, but when the HU-thresholds of +/- 11 HU were applied to 2 areas representative of pleural tumour, the final tumour volume was much lower at 116 cm^3. This has been illustrated in Figure 3.4.

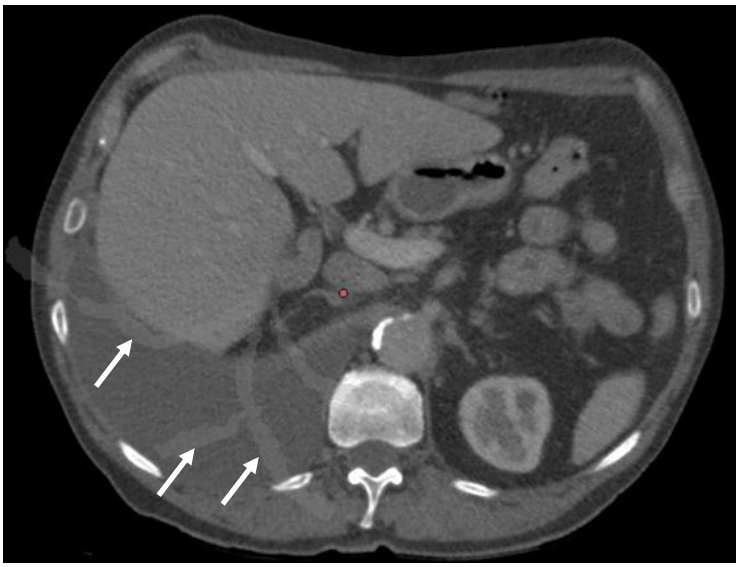

Figure 3.3 Segmentation attempt illustrating erroneous extrusion of the contour mask (white arrows)

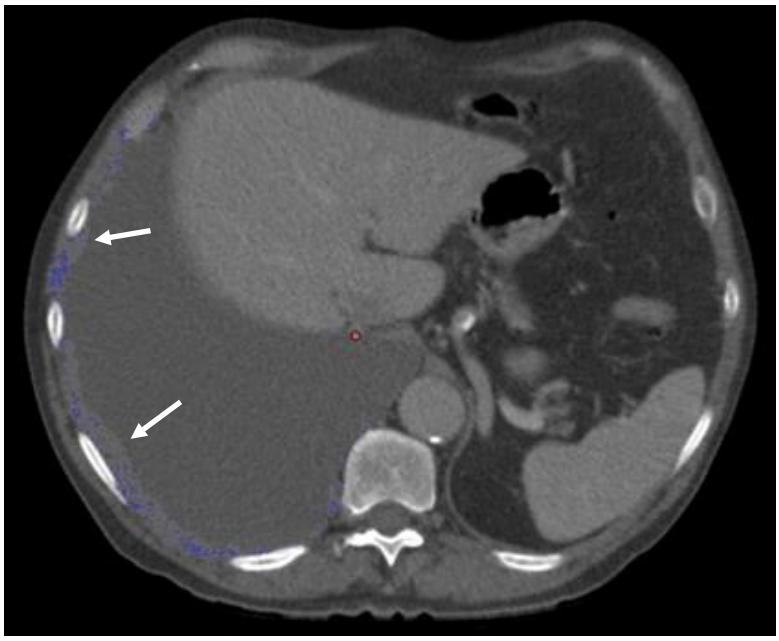

Figure 3.4 Segmentation attempt illustrating under-segmentation of pleural tumour (in blue). There are light grey areas of pleural tumour that should have been entirely blue (white arrows)

3.3.2.4 Segmentation attempts 2 to 5

I made two further attempts at contouring pleural tumour on the first 20 apical and last 20 basal slices with contours drawn every 5 slices in between these. This resulted in approximately 75 contoured slices and took 120 minutes. The semi-automated contour masks in these cases appeared to have fewer of the superimposed 'ghost artefacts'. However, propagation errors were still evident in the apical and basal areas. The threshold mask volumes measured 647 cm^3, but when 2 seed points +/- 11 HU were applied, the volumes were approximately 234 cm^3. Figure 3.5 illustrates this under-segmentation.

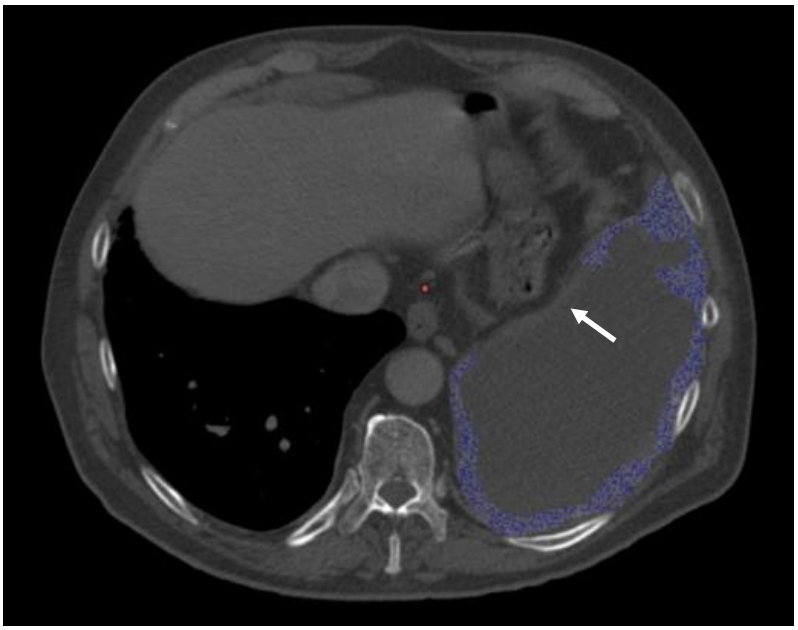

Figure 3.5 Segmentation attempt illustrating under-segmented pleural tumour (in blue). There are light grey areas of pleural tumour that should have been entirely blue (white arrow)

A third attempt was made with more slices contoured (108/390 axial slices). However, the 'ghost artefacts' and under-segmentation of pleural tumour were still evident and have been illustrated in Figure 3.6.

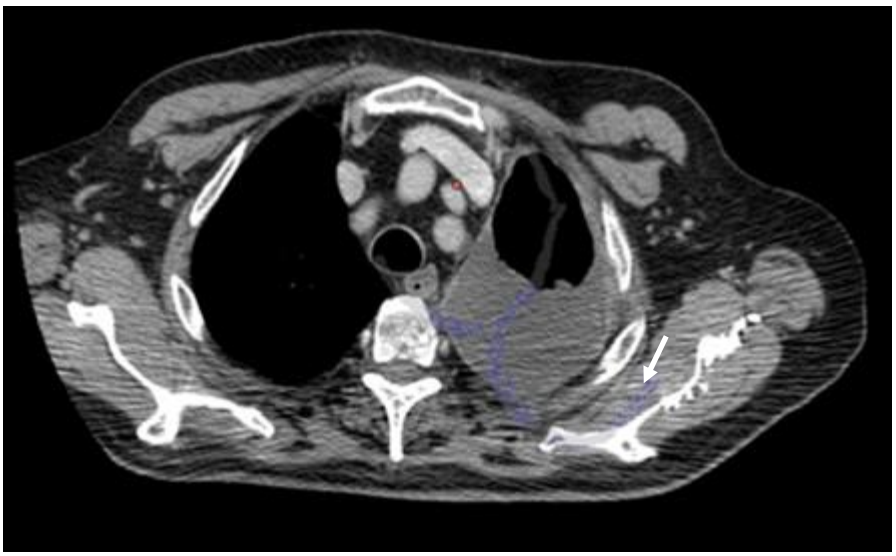

Figure 3.6 Segmentation attempt illustrating both erroneous contour mask propagation (in blue, overlying pleural effusion) and extra-pleural segmentation errors (white arrow)

3.3.2.5 Segmentation attempts 6 and 7

A sixth attempt was made with the first 20 apical and last 20 basal slices contoured and contours drawn every other slice, resulting 200/312 axial slices contoured. The threshold mask volume measured 966 cm^3, but when 3 seed points +/- 11 HU were placed, the volume increased to 3340 cm^3. After visual inspection of this inflated volumetric measurement, segmented areas bled into the neighbouring pleural fluid and other thoracic structures not contained within the contour mask. This has been illustrated in Figure 3.7.

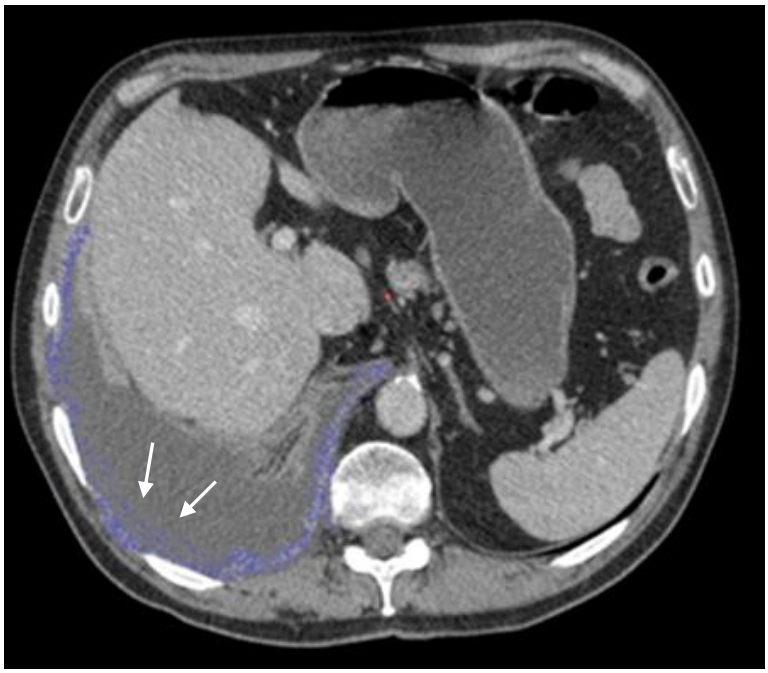

Figure 3.7 Segmentation attempt illustrating over-segmentation with bleeding into the pleural fluid (blue area highlighted by white arrows)

3.3.2.6 Radiodensity measurements using axial views

To further explore the pleural tumour segmentation issues encountered with the HU-specific seed points, I performed a detailed visual inspection of pleural tumour in the coronal plane. Identifiable areas of pleural tumour were often only visible in two or three areas. One scan had no areas of visible pleural tumour in the three coronal slices assessed. This has been summarised in Table 3.4.

Table 3.4 Subjective visual analysis of ROIs in coronal plane slices of contrast-enhanced CT scans

Case	Number of ROIs	Description
1	8	Minimal pleural tumour visible in mid-point slice
2	5	Minimal pleural tumour in anterior and mid-point slice
3	7	Minimal pleural tumour in mid-point slice
4	10	Pleural tumour visible in all areas
5	12	Pleural tumour only visible at costophrenic angle
6	3	Two areas of pleural tumour visible in mid-slice
7	15	Pleural tumour visible in all areas
8	2	Small area of pleural tumour in anterior and mid-point slices
9	5	Minimal pleural tumour in mid-point slice
10	2	Pleural tumour visible in all areas
11	9	Minimal pleural tumour in mid-point slice
12	3	Pleural tumour only visible in apical area
13	3	Pleural tumour visible in all areas
14	0	No areas of pleural tumour identified
15	4	Pleural tumour mainly in the posterior slice
16	10	Small volume pleural tumour in all slices
17	4	Small volume pleural tumour in all slices
18	5	Small volume pleural tumour in all slices
19	10	Limited areas of pleural tumour in anterior and mid-point slices
20	4	Limited areas of pleural tumour in anterior and mid-point slices
21	11	Limited pleural tumour in mid-point slice
22	12	Pleural tumour in posterior slice
23	10	Pleural tumour in anterior slice
ROI: region of interest		

In the clinical setting, assessment of CT scans in axial plane is more commonplace. After reviewing pleural tumour in both the coronal and axial planes in a selection of CT scans, it became apparent that the yield of pleural tumour ROI measurements would increase if I measured ROIs in the axial plane. An example of the differences in pleural tumour visibility in the axial versus coronal planes has been illustrated in Figure 3.8.

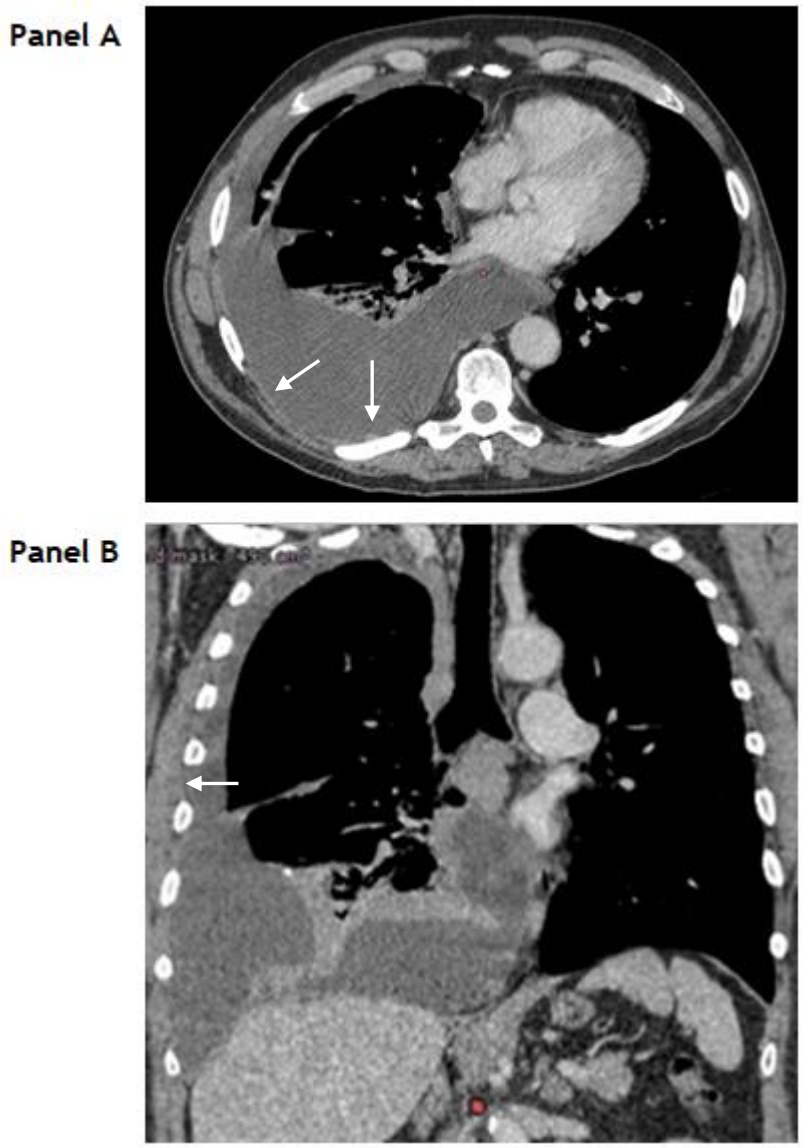

Figure 3.8 Example of pleural tumour (white arrows) when viewed in axial (A) and coronal (B) planes in the same patient. The contrast is clearer on Panel A compared to Panel B

I re-assessed all the CT scans in the axial view to enhance the pleural tumour radiodensity data. Fifteen ROIs were distributed cranio-caudally on areas of what I considered representative of pleural tumour. This has been illustrated in Figure 3.9. Mean intensity and standard deviation (SD) were documented for each ROI in HU. HU threshold limits used for subsequent region growing were derived using the ranges (maximum to minimum) of the pleural tumour ROIs in all 23 patients and divided by two to facilitate region growing either side of the seed points placed on representative areas of pleural tumour.

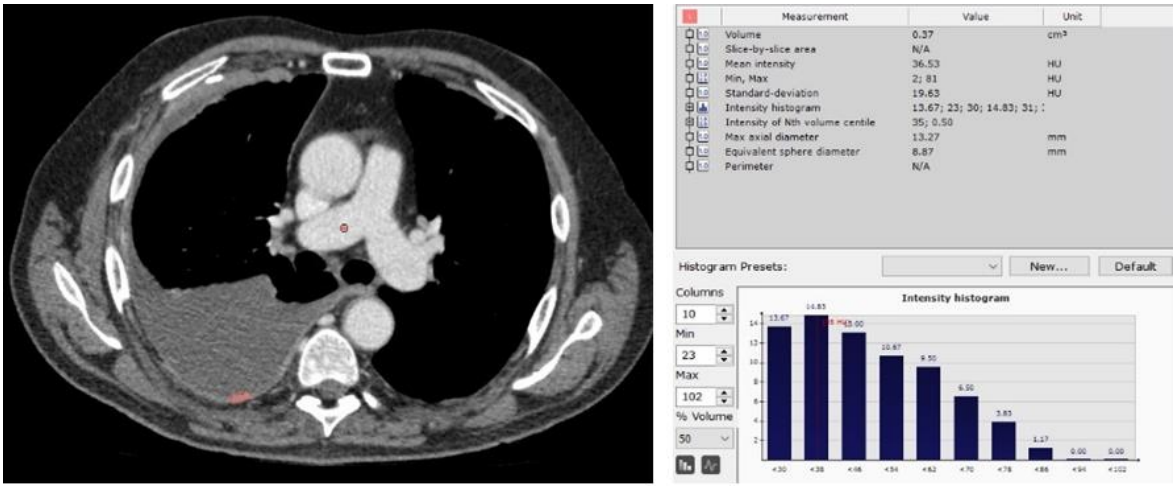

Figure 3.9 Radiodensity measurements in the axial plane with the red marker placed on an area representative of pleural tumour

3.3.2.7 Segmentation attempts using median pleural tumour ROI in axial views

The median radiodensity in HU in areas of pleural tumour was 49.3 [IQR 39.8 to 62.7] HU. Table 3.5 summarises the median and range differences in HUs between coronal and axial planes.

Table 3.5 Comparison of pleural tumour ROIs in coronal and axial planes of contrast-enhanced CT scans

Case	**Coronal**			**Axial**		
	ROI n=154	**Median HU**	**HU range**	**ROI n=269**	**Median HU**	**HU range**
1	8	55.1	31	12	50.8	102
2	5	54.8	23	15	52.5	61
3	7	65.4	19	12	51.5	60
4	10	54.5	43	15	59.5	27
5	12	46.8	22	14	49.3	39
6	3	79.7	48	2	36.9	6
7	15	53.8	32	15	40.6	56
8	2	54.0	10	5	27.6	189
9	5	65.4	32	15	62.4	54
10	2	54.0	18	14	54.9	38
11	9	55.4	33	8	32.8	20
12	3	66.3	16	15	52.8	59
13	3	52.3	15	3	29.3	13
14	0	N/A	N/A	8	47.6	59
15	4	46.5	12	8	44.6	22
16	10	48.4	18	15	40.4	47
17	4	49.5	10	7	38.7	21
18	5	46.8	47	12	49.5	44
19	10	53.3	35	15	58.8	73
20	4	46.5	9	14	49.2	36
21	11	49.8	20	15	35.8	53
22	12	51.5	33	15	59.7	50
23	10	51.7	26	15	54.7	47
ROI: region of interest; HU: Hounsfield unit						

Repeat measurements were not taken for the other thoracic tissues as these were easily identifiable in the three coronal plane slices. The new HU threshold limits used for subsequent region growing based on 23 patients (ROI n=269) was +/- 22 HU.

I made a further semi-automated segmentation attempt using these new data. However, I continued to encounter the aforementioned issues with artefact, or 'ghost areas'. Moreover, seed points based on axial HU-threshold limits of +/- 22 HU resulted in a greater proportion of over-segmentation of pleural tumour and bleeding into other non-pleural tumour tissues which have been illustrated in Figure 3.10.

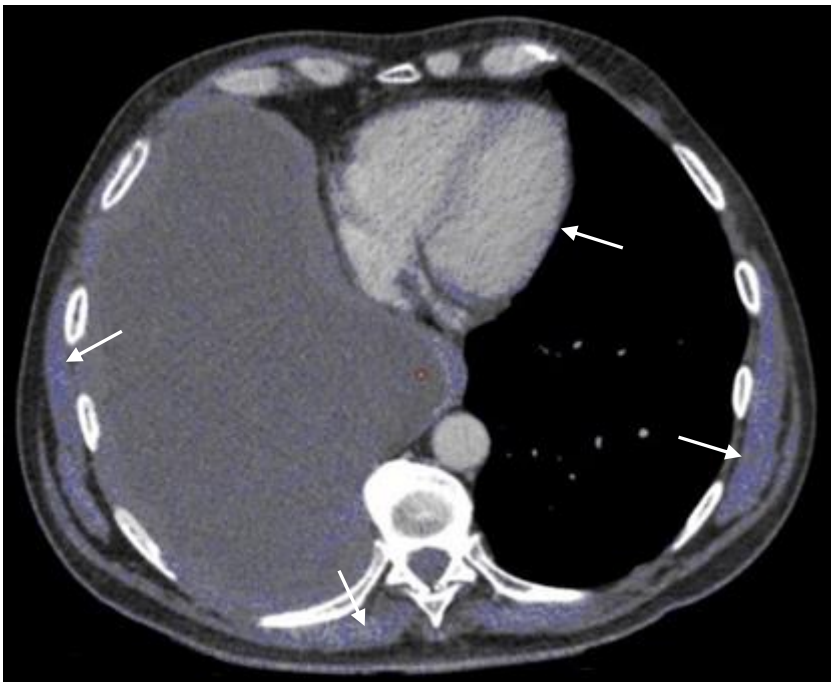

Figure 3.10 Segmentation attempt 8 illustrating over-segmentation (in blue) with inclusion of non-pleural tumour (white arrows) in the final volume using seed point thresholds of +/- 22 HU

Anatomical difficulties in interpretating pleural tumour also contributed to the repeated failed attempts of a semi-automated approach to pleural tumour segmentation. Detailed illustrations and descriptions of the anatomical difficulties are included in Figure 3.11. I have presented the images without segmentation colour to demonstrate the subtle differences in greyscale.

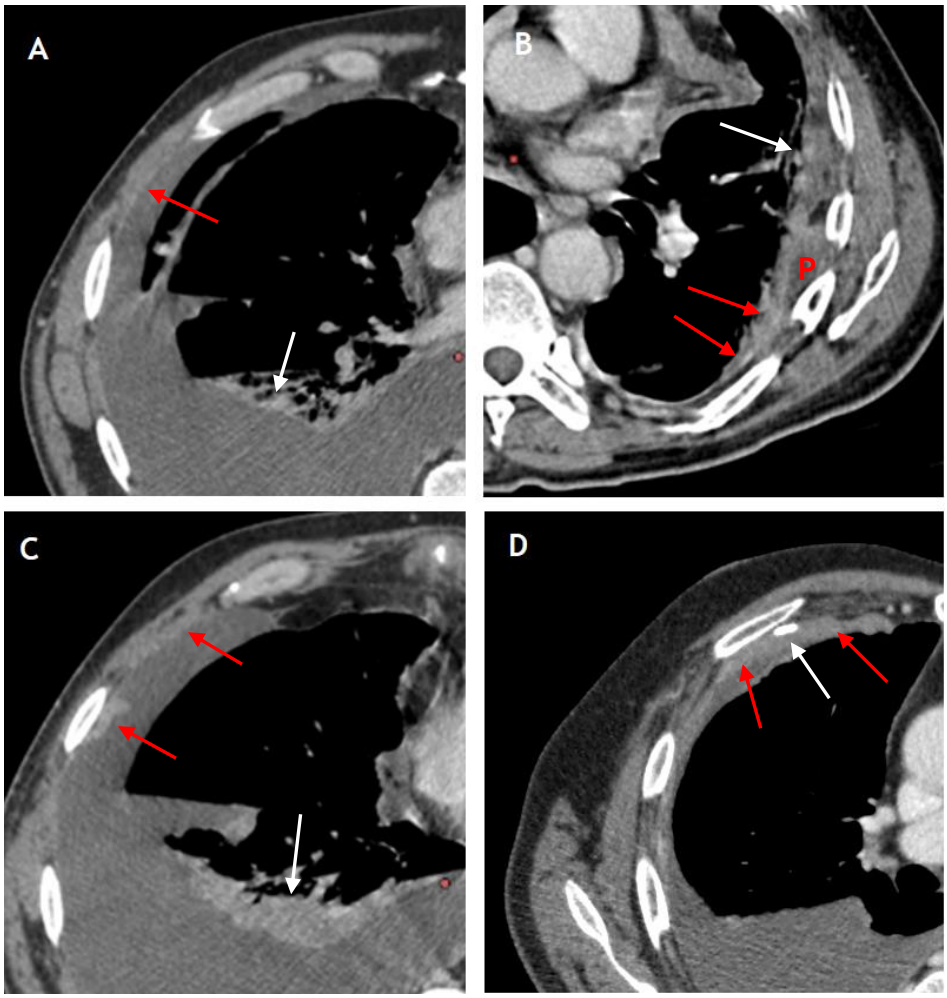

Figure 3.11 Difficulties in interpreting pleural tumour. Panel A illustrates the similarities between pleural tumour (red arrow) and atelectasis (white arrow). Panel B illustrates the difficulties in differentiating between different tissues, e.g., pleural fluid (red P), atelectasis (white arrow) and tumour (red arrows). Panel C illustrates non-confluence of pleural tumour (red arrows) which resulted in software limitations and time spent returning to edit the completed contour mask. Panel C also illustrates atelectasis (white arrow). Panel D illustrates calcified tumour (white arrow) which was not included in the segmented volumes and pleural tumour (red arrows)

3.3.2.8 Time taken for volume analyses

The mean time taken to complete semi-automated segmentation for the CT scans (n=8) was 25 (SD 7) minutes, with the mean number of CT slices delineated 77 (SD 21).

3.3.3 **Secondary objectives**

3.3.3.1 Correlation and agreement analyses between semi-automated CT and MRI volumes

The median semi-automated CT and MRI volumes (n=8) were 204 [IQR 124 to 1852] cm^3 and 368 [IQR 238 to 502] cm^3, respectively. The semi-automated CT volumes were larger than the MRI volumes with a mean difference between MRI and CT volumes of -457.6 cm^3 (95% limits of agreement -2741 to +1826 cm^3, see Figure 3.12: Panel A). There was a strong correlation between CT and MRI volumes (r=0.738, p=0.0458, see Figure 3.12: Panel B).

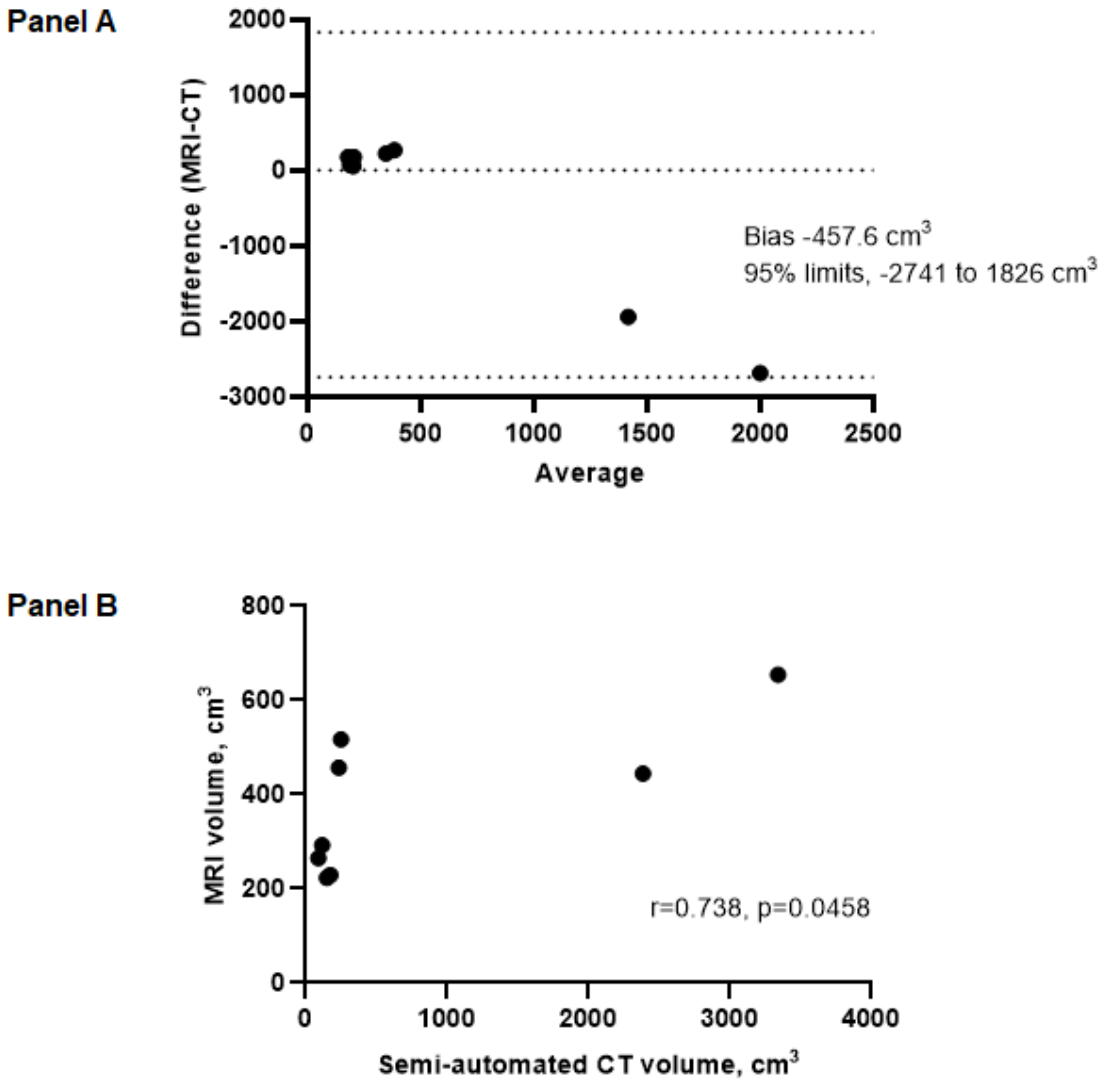

Figure 3.12 Bland-Altman plot (Panel A) and Spearman's correlation (Panel B) comparing primary tumour volume measured using semi-automated segmentation CT scans versus semi-automated segmentation MRI scans in 8 patients with MPM

3.3.3.2 Abandonment of a semi-automated segmentation approach

Following subjective interpretation of the 8 segmented CT volumes, and the very wide 95% limits of agreement following the correlation analysis, I met with a Myrian Intrasense® software engineer to determine a solution to the semi-automated segmentation errors. The first step involved installing an update to the Myrian Intrasense® software. However, the semi-automated segmentation errors persisted despite this. The main reasons for the semi-automated segmentation errors were determined to be the complexity of pleural tumour in patients with MPM and the inability to obtain feasible HU-defined threshold limits (+/- 11 HU and +/- 22 in the coronal and axial planes, respectively) due to overlapping thoracic tissue HU values. As such, further semi-automated segmentation attempts were abandoned in favour of a fully manual segmentation approach which is described in more detail in Chapter 2, Section 2.2.7.

The failure of my primary objective to develop a semi-automated region-growing step for tumour segmentation using contrast-enhanced CT scans meant that it was not possible to proceed with the secondary outcome of intra-observer agreement.

3.4 Discussion

3.4.1 Heterogeneity of Hounsfield units in thoracic tissues

The first aim of this chapter was to determine the radiodensities of different thoracic tissues. To recap, Hounsfield units (HU) are radiodensities of tissues relative to water, which has 0 HU(285). Tissues denser than water will have HUs >0. This was reflected in the present study where the median [interquartile range, IQR] pleural tumour (measured in the axial plane) and pleural effusion radiodensities were 49.3 [IQR 39.8 to 62.7] HU and 11.8 [8.3 to 17.8] HU, respectively. I observed overlapping radiodensities between pleural tumour 49.3 [IQR 39.8 to 62.7] HU, intercostal muscle (20.4 [11.9 to 32.3] HU), diaphragm (40.4 [26.4 to 56.4] HU) and pleural fluid (11.8 [8.3 to 17.8] HU). My thoracic radiodensity values were analogous to those described by Corson and colleagues who reported the following median radiodensity values: pleural tumour 56 [IQR 23 to 91] HU, intercostal muscle 61 [37 to 85] HU and pleural fluid 4 [-24 to 30] HU(339). Similarly, Mirvis and colleagues reported a median radiodensity of pleural tumour of 44 HU in their study of 9 patients with MPM(340). Luerken and colleagues determined differences in contrast-enhanced multi-detector-computed-tomography radiodensities in 28 patients with MPM and reported MPM tumour radiodensities that were larger than my measurements (56.7 HU in the arterial-phase and 75.4 HU in the portal-venous phase, respectively(341)). After plotting median HU values alongside IQR values, overlapping HU distributions were obvious. When HU-defined seed points were applied to the propagated contour masks, seeding into structures and thoracic tissue compartments adjacent to pleural tumour resulted in inaccurate tumour volumes.

3.4.2 Comparison to MRI method

I extrapolated my CT method from the MRI method developed by Tsim and other colleagues from our own study group who determined mean signal intensity (SI) values on T1-weighted dynamic contrast-enhanced MRI (DCE-MRI)(342). DCE-MRI is a functional imaging technique that can be used to measure tissue

perfusion(342, 343), including MPM pleural tumour(344). Tsim and colleagues determined that pleural tumour has an intermediate signal intensity on T1-weighted MRI of 99 arbitrary units (AU) which was greater than that of pleural fluid and intercostal muscles(319). The diaphragm muscles have a low signal intensity(345) as does lung parenchyma with signal intensities ranging from -132 to -158 AU, depending on normalisation relative to water or muscle(346). As such, there were no overlapping signal intensities between different thoracic tissues using the Tsim and colleagues MRI method.

DCE-MRI has recently been shown to predict response to treatment in patients with MPM(347). Very few data exist regarding dynamic contrast-enhanced CT scans (DCE-CT) in MPM(348-350). DCE-CT sequentially measures tissue density over time on an image series(351). Gudmundsson and colleagues reported differences in tissue blood flow and tissue blood volume on DCE-CT between chemotherapy-treated and untreated patients with MPM(348). The thoracic tissue HU measurements I made were obtained without CT perfusion data. Further studies assessing DCE-CT perfusion metrics would yield further data that may serve to facilitate more accurate identification of pleural tumour using CT.

3.4.3 **ROI measurements in coronal and axial views**

There is no gold standard approach to region of interest (ROI) selection when determining the radiodensity range of pleural tumour. I employed a strategic approach to define ROIs to ensure standardisation across the dataset. In the coronal plane this involved ROI measurements in pre-defined anterior, mid-point and posterior slices. In the axial plane, I sequentially identified pleural tumour working down the images series in a cranial-caudal direction. Accurate identification of pleural tumour was difficult when assessed in the coronal view and resulted in less ROIs to define population values for pleural tumour HU that could be later used to define threshold limits for subsequent region growing. Attempts to mitigate this problem using contemporaneous MRI were unsuccessful.

The identification of pleural tumour from other thoracic tissues was made easier when viewed in the axial plane and resulted in a greater number of ROIs distributed across each CT scan, enriching the pleural tumour radiodensity data. The median HUs in axial and coronal views were similar (49.3 [IQR 39.8–62.7] HU and 52 [46-60] HU, respectively). However, the median ranges of axial plane-defined HU thresholds were wider than those obtained in the coronal plane. The reason for this is unclear. One possible explanation may relate to the smaller number of ROIs afforded by assessment in the coronal view, with a larger margin of error. For example, 5/23 scans assessed in the coronal view included only 2 or 3 ROIs and there were no obvious areas of pleural tumour in one scan. A further explanation may be the inclusion of areas of pleural tumour where prior pleurodesis had occurred. Typically, this would manifest as visible areas of high attenuation on CT(352). I made a conscious effort not to include visible areas of high attenuation in my ROI measurements. However, pleurodesis can result in more subtle changes such as pleural thickening and pleural nodularity(352). A study examining positron emission tomography (PET CT) and CT in 9 patients who had prior talc pleurodesis for malignant pleural effusions reported a mean pleural HU value of 230 HU (range 140 to 380 HU)(353). If I did include areas of pleurae exposed to pleurodesis, higher HU values will have been recorded. Another explanation may relate to the way that Myrian Intrasense© software determined mean radiodensity within a ROI measurement volume. The HU value obtained from each ROI measurement was a mean value of the different voxels – voxels are 3-D analogues of pixels(354) - contained within each ROI. This is evident on the 'intensity histogram' visible in Figure 3.9 which includes minimum and maximum voxels of 2 HU and 83 HU, respectively. I made efforts to keep the volumes of the measured ROIs low, for example, the ROI volume in Figure 3.9 was 0.37 cm^3. However, my ROIs may have included voxels of adjacent non-pleural tissues with divergent HU values such as intercostal muscle (20.4 [IQR 11.9 to 32.3] HU) and air (-827.9 [IQR -863.9 to -791.5] HU).

3.4.4 **Comparison to other semi-automated CT segmentation methods**

Authors have described pleural tumour volumetric thresholding and region growing in MPM. Frauenfelder and colleagues – who also used Myrian Intrasense®

software - employed a semi-automatic thresholding and region growing method on normal lung tissue and associated anatomy with subsequent semi-automatic parietal pleurae segmentation on every fourth to fifth CT slice followed by inter-slice interpolation(108). They reported high inter-observer agreement between absolute tumour volumes. They did acknowledge the requirement for manual input from human readers which is a limitation. My method differed to the Frauenfelder method in its sole use of a semi-automated region growing method to pleural tumour, without prior fixing of lung tissue. My final tumour volumes required to be exportable to serve as the ground truth for a convolutional neural network (CNN) described in the next chapter. It is unclear whether prior fixing of lung tissue would have been compatible with these later processes. Regardless of this, I was unable to achieve the same results as the Frauenfelder team.

Sensakovic and colleagues also described a mixed semi-automated and automated approach. They employed a computerised segmentation of lung tissue and the hemi-thoraces as well as semi-automated liver segmentation to define MPM in the pleural space followed by classification of tissues into categories based on pixel HUs, with pleural tumour HU values ranging from 0 to 100 HU(109). They reported a mean difference between the computerised method and human measurements of −59 (SD 17) cm^2 and 95% limits of agreement for the differences of −40 to 28 cm^2. Two of their human observers demonstrated superior mean differences of −36 (SD 11) cm^2 with 95% limits of agreement for the differences of −26 to 19 cm^2. They described the lung bases and pleural effusions as being particularly problematic. I was able to apply my clinical knowledge of MPM to help distinguish pleural fluid and calcified tumour and pleural plaques. I also focused on the first and last 20 slices in each image series with more detailed delineations applied to the pleural cupulae and diaphragmatic recesses, respectively.

Similar pleural tumour HU thresholds (20 to 80 HU) were utilised by Gill and colleagues who reported a semi-automated volumetric approach initiated by software-automated segmentation with the requirement for subsequent manual human user delineations, including correction for the presence of pleural

effusions(111). As previously mentioned, my median pleural tumour HU values were 49.3 [IQR 39.8 to 62.7] HU and 52 [IQR 46 to 60] HU when determined in axial and coronal planes, respectively. When seed points of +/- 11 HU were placed in areas of representative of pleural tumour, this would have captured tissue with HUs of approximately 39 to 61 HUs. The maximum intercostal muscle and pleural fluid HUs were 53.5 HU and 35.1 HU, respectively. Erroneous inclusion of these structures would have been possible. When seed points of +/- 22 HU following re-assessment in the axial plane were applied, the expected HU will have been approximately 28 to 72 HU. This broader range of tissue capture would explain why diaphragm (40.4 HU) and pleural fluid (maximum HU value, 35 HU) were erroneously included in the final volume on my eighth segmentation attempt.

I did not proceed to assess inter-observer variability due to the flaws and inaccuracies of my semi-automated method attempts. Other authors have reported high inter-observer variability, including Gill and colleagues who reported absolute differences in volumes of 173 to 860 cm^3(111). MPM disease-specific pathological features such as pleural effusions and pleurodesis were again reported to be problem areas. I have outlined the pitfalls of potentially including areas of pleural tumour exposed to pleurodesis in my ROI measurements in Section 3.4.3 of this discussion.

There is no standardised approach to the number of contours or seed points applied to respective contour masks. Chen and colleagues placed 20 to 30 seed points in areas representative of pleural tumour across six to ten axial CT scan slices in their computer-aided random walk-based method(112). I placed two to three seed points per each segmented image series. When I attempted to place further seed points, tumour over-segmentation occurred. The reason for this is not entirely clear, however it was likely due to limitations caused by the complex morphology of the MPM tumours, resulting in seepage of what the software perceived as pleural tumour into adjacent structures with similar HUs such as intercostal muscle and pleural fluid. Lauk and colleagues used the Frauenfelder technique on Myrian Intrasense® software, contouring pleural tumour every fifth to tenth CT slices with adjustments made if necessary(355).

They did not assess inter-observer variation. The mean number of contours in my analysis was 77 (SD 21), with a minimum of 36 and maximum of 108. I initially delineated every five to ten slices before sequentially increasing the number of CT slice delineations to correct for the linear interpolation errors I encountered. This culminated in a final contour mask attempt where I had delineated every other axial CT slice.

Despite my best efforts, and meetings with the Myrian Intrasense® software engineers to solve the aforementioned issues, I was unable to find a solution to the limitations of HU-based region growing of MPM tumour. The decision to move to a manual method was based on the premise that automated segmentation methods are restricted to pixel HU data while human readers can use a much broader pallet of visual clues and clinical experience to estimate a volume even when the radiodensity fundamentals could not in isolation support the contour masks drawn.

3.4.5 **Possible clinical implications**

Although MRI has been shown to be superior to CT in soft tissue enhancement, it is not as routinely available as CT in clinical practice. MRI is also not suitable in all patients, for example, those with metal implants or those who experience claustrophobia. MRI is also more expensive than CT but has technical advantages. Therefore, the development of an automated approach to pleural tumour volumetry using CT in patients with MPM is important. Volumetric methods using CT are increasingly being reported in the mesothelioma literature and have been shown to be superior to mRECIST at predicting pleural tumour and assessing response to treatment(108). The results from this chapter directly led to the manual volumetric segmentation method descried in the next chapter.

3.4.6 **Study limitations and strengths**

The main limitation of this study was the small sample size of 23 patients. However, the pleural tumour HU threshold values were determined on >200

regions of interest. It also important to highlight that median pleural tumour HU values were almost identical when assessed in the coronal and axial views, suggesting that my ROI measurement technique was reproducible.

Nodular and circumferential pleural thickening are commonly associated with pleural malignancy(356) and contrast-enhanced CT remains the first-line imaging modality for assessment for MPM(2). However, there are wide ranging sensitivities and specificities for the identification of pleural tumour on CT in the thoracic malignancy literature(49-52). Although I used my knowledge of CT features in MPM when measuring HU of pleural tumour with efforts made to include only these in my pleural tumour ROIs, it is possible that non-malignant parietal pleura may have been included in these ROIs, and as a direct consequence, the semi-automated tumour volumes that were grown from the seed points applied. Research from our own research group determined that early contrast enhancement, based on tumoral blood vessel density, is a sensitive biomarker for determining pleural malignancy using MRI scans(342). A similar biomarker is not available in CT but would be a useful clinical tool. If the inclusion of non-malignant parietal pleura was a limiting factor in the present study, the impact would have been consistent across the dataset.

Another limitation is the potential for pleural tumour ROIs to have included areas previously exposed to pleurodesis, resulting in higher radiodensity values as described in Section 3.4.2 of this discussion. Although I excluded any areas with visibly high attenuation in my ROIs (i.e., talc deposits), I was not able to fully control for this in my dataset. It is important to note that assessment of pleural tumour radiodensities were solely made from patients included in the DIAPHRAGM study which were mostly diagnostic CT scans, i.e., scans were performed early in the diagnostic pathway which will have likely preceded any pleural interventions involving surgical pleurodesis or the administration of talc. Another tissue with higher radiodensities is calcified pleural tumour which had a median radiodensity of 639 [IQR 538 to 763] HU in the present study. The maximum pleural tumour HU in both the coronal and axial measurements views was 189 HU, evidencing that no calcified pleural plaques were included in the ROI measurements.

My ROI dataset was mostly comprised of patients with earlier disease stage, i.e., TNM8 stage 1. It is uncertain whether pleural tumour ROI values are dependent on the stage of the disease. The natural history of MPM is the extension of a rind-like growth around the pleurae with interlobar fissure involvement and chest wall invasion in later stages. Radiodensities can differentiate benign from malignant pulmonary nodules(357) as well as the invasiveness(358) and likelihood of recurrence in early stage lung cancer(359). However, it is unclear whether HU values correspond to different disease stages in solid organ cancers. Veeratterapillay and colleagues concluded that HU values did not correlate with disease stage in their cohort of patients with renal cancer(360). Conversely, higher HU values were inversely related to growth deceleration in patients with meningiomas(361). In patients with gastric(362) and lung cancers(363), decreasing HU values following chemotherapy is predictive of response to treatment. No data exist relating to HU differences according to stage or treatment response in MPM. Corson and colleagues reported higher radiodensities of MPM tumour compared to my data, with 97.5% centile and maximum radiodensities of 181 HU and 355 HU, respectively(339). My maximum pleural tumour radiodensity was 100 HU. However, the Corson study did not provide details on the disease stages of the patients on their cohort, neither did the Mirvis(340) or Leurken studies(341). The inclusion of patients with early-stage disease stage in the present study also meant that pleural tumour was more difficult to visualise due to smaller tumour volumes associated with this. I will demonstrate that patients in the DIAPHRAGM study had a smaller volume of measurable disease than patients in the PRISM study later in this thesis (Chapter 4, Sections 4.3.2.4 and 4.3.3.1), as the PRISM study scans were obtained later in patient's respective cancer pathways.

Another limitation was that the study dataset was composed of mostly patients with the epithelioid sub-type of MPM. A sizeable minority (30%) of patients did not have available histological data. Authors have reported CT imaging features that can differentiate between different histological MPM sub-types, for example, the sarcomatoid MPM sub-type is more likely to involve extension into the lung parenchyma(364) and volume loss on the ipsilateral side of the tumour(356). Conversely, Escalon and colleagues demonstrated no statistically

differences between histological sub-type and CT imaging features(365). Radiodensity differences have failed to distinguish tumour sub-types in patients with renal(366) and breast cancers(367). A future study with a more diverse range of mesothelioma sub-types would increase the generalisability of the findings and could potentially provide further insights into whether there are variations in pleural tumour radiodensities dependent on the MPM sub-type being investigated.

3.5 Conclusion

In this chapter, the methods for an attempted semi-automated segmentation approach to tumour segmentation using CT scans have been described. It was not possible to accurately deploy a semi-automated volumetric analysis method for MPM developed using MRI on contrast-enhanced CT images. Reduced definition between tumour and neighbouring structures was a major contributor. A manual segmentation method was chosen to serve as the ground truth for the development of an automated volumetric approach described in the next chapter.

Chapter 4

VOLUMETRIC MPM TUMOUR ASSESSMENT USING HUMAN AND DEEP LEARNING ALGORITHMIC SEGMENTATIONS

4 Chapter 4: Volumetric MPM tumour assessment using human and deep learning algorithmic segmentations

4.1 Introduction

Computed tomography (CT) scans taken before and during treatment are routinely used to determine response to systemic anti-cancer therapy (SACT). In solid tumours, Response Evaluation Classification In Solid Tumours (RECIST) criteria have traditionally provided objectivity in response assessment to SACT. Modified Response Evaluation Classification In Solid Tumours (mRECIST) was developed in malignant pleural mesothelioma (MPM) to tackle the limitations of RECIST which assumes that tumours have spherical growth patterns(6). The mRECIST reader makes unidimensional tumour thickness measurements perpendicular to the chest wall in two positions at three levels on thoracic CT scans to provide a summed value that broadly classifies response to treatment. The mRECIST method has poor reproducibility, with up to 30% variability reported between observers(81). This wide variation can cross response thresholds based on the same data. In the clinical setting, response assessment is often made through subjective assessment of serial cross-sectional images, neglecting the use of mRECIST criteria altogether.

Accurate and time-efficient methods of response assessment are required to improve response assessment in MPM. Semi-automated methods have been explored but remain time-consuming and are prone to inter-observer differences(102, 111). In Chapter 3, I demonstrated the limitations of a semi-automated volumetry method after being unable to adapt a successful method defined using MRI to CT data, primarily because of insufficient soft tissue contrast on the CT images. More recent volumetric methods have focused on utilising advancements in artificial intelligence (AI), specifically deep learning methods such as convolutional neural networks (CNN)(136). Some CNNs have been proven to out-perform humans when trained on very large datasets(142). Commercial object detection and recognition datasets are trained on millions of images(143-146). Similarly sized datasets are not yet routinely available in the

medical setting. However, detailed ground truth allows CNN algorithms to ‘learn’ more efficiently, using the thousands of pixels in each image and their surrounding context(141, 151).

This chapter describes a multicentre retrospective cohort study which aims to develop a volumetric AI algorithm to improve human response classification in patients with chemotherapy-treated MPM.

4.2 Methods

A detailed description of the methods is provided in Chapter 2, Section 2.2.

The objectives and associated outcome measures for this study are detailed in Chapter 2, Section 2.2.1. To summarise, the objectives of the training and internal validation set were to generate the detailed ground truth needed (based on learning from Chapter 3) and to report correlation and agreement and inter- and intra-observer variations for comparisons with the deep learning outputs. I undertook the following analyses to address these, while the CNN was built by Owen Anderson and Keith Goatman from Canon Medical Research Europe (CMRE). The CNN performance was also assessed by Owen Anderson and Keith Goatman using Dice overlap. In the external validation set, the objectives were to compare the CNN against mRECIST as this set involved paired scans obtained at the pre-chemotherapy and response assessment time points and analysis of the prognostic value of the CNN volume measures versus human read-outs of volume and mRECIST classifications.

4.3 Results

4.3.1 Study population

Tables 4.1 summarises the clinical characteristics of the training and internal validation and external validation sets. The mean age at diagnosis in the training and internal validation and external validation sets were 70 (SD 8) and 69 (SD 7) years, respectively. Most patients in training and internal validation and external validation sets were male (71/80 (89%) and 22/30 (73%), respectively) and had an ECOG Performance Status (ECOG PS) of 0 (20/80 (25%) and 6/30 (20%), respectively) or ECOG PS 1 (47/80 (59%) and 15/30 (50%), respectively). Epithelioid MPM was the predominant histological sub-type (77% in both sets). There was also a predominance of early-stage disease, with 35% and 40% of patients having stage I disease in the training and internal validation and external validation sets, respectively. A sizeable minority had stage III and IV disease (22% in the training and internal validation set and 27% in the external validation set). All patients received doublet chemotherapy cisplatin or carboplatin and pemetrexed with a median number of cycles of 4 [3.75 to 4].

In the external validation set, the median interval between the last dose of chemotherapy and response assessment scan was 22 [IQR 10 to 62] days. The median interval between the last dose of chemotherapy and response assessment scan in 4/30 was >100 days.

Table 4.1 Clinicopathological data in patients with MPM divided according to training and internal validation (scan n=123) and external validation sets (scan n=30)

	Training and internal validation set (scan n=123) Mean (SD) or n (%)	**External validation set (scan n=30) Mean (SD) or n (%)**
Age at diagnosis, years	70 (SD 8)	69 (SD 7)
Male gender	71 (89%)	22 (73%)
ECOG PS		
0	20 (25%)	6 (20%)
1	47 (59%)	15 (50%)
2	11 (14%)	2 (7%)
Not available	2 (3%)	7 (23%)
Histological sub-type		
Epithelioid	62 (77%)	23 (77%)
Non-epithelioid	15 (19%)	5 (17%)
Not available	3 (4%)	2 (7%)
Disease stage		
I	28 (35%)	12 (40%)
II	2 (3%)	4 (13%)
III	11 (14%)	3 (10%)
IV	6 (8%)	5 (17%)
Not available	33 (41%)	6 (20%)
ECOG PS: Eastern Cooperative Oncology Group performance status		

4.3.2 **Training and internal validation**

4.3.2.1 Manual CT tumour volumes

The mean number of CT scan slices in the images series was 225. The mean CT volume (n=23) was 279.4 (SD 94.6) cm^3. The mean time taken to segment pleural tumour was 151 (SD 19) minutes, or approximately 2.5 hours.

4.3.2.2 Comparison between manual CT and semi-automated MRI tumour volumes

The mean MRI volume (n=23) was 354.2 (SD 140.6) cm^3. CT volumes were consistently smaller than MRI volumes (mean difference between AI minus human scans 74.8 (SD 122) cm^3, 95% limits of agreement -313 to 164 cm^3, see Figure 4.1: Panel A). The data were moderately correlated (Pearson's r 0.524, 95% CI 0.142 to 0.769, p=0.0103, see Figure 4.1: Panel B).

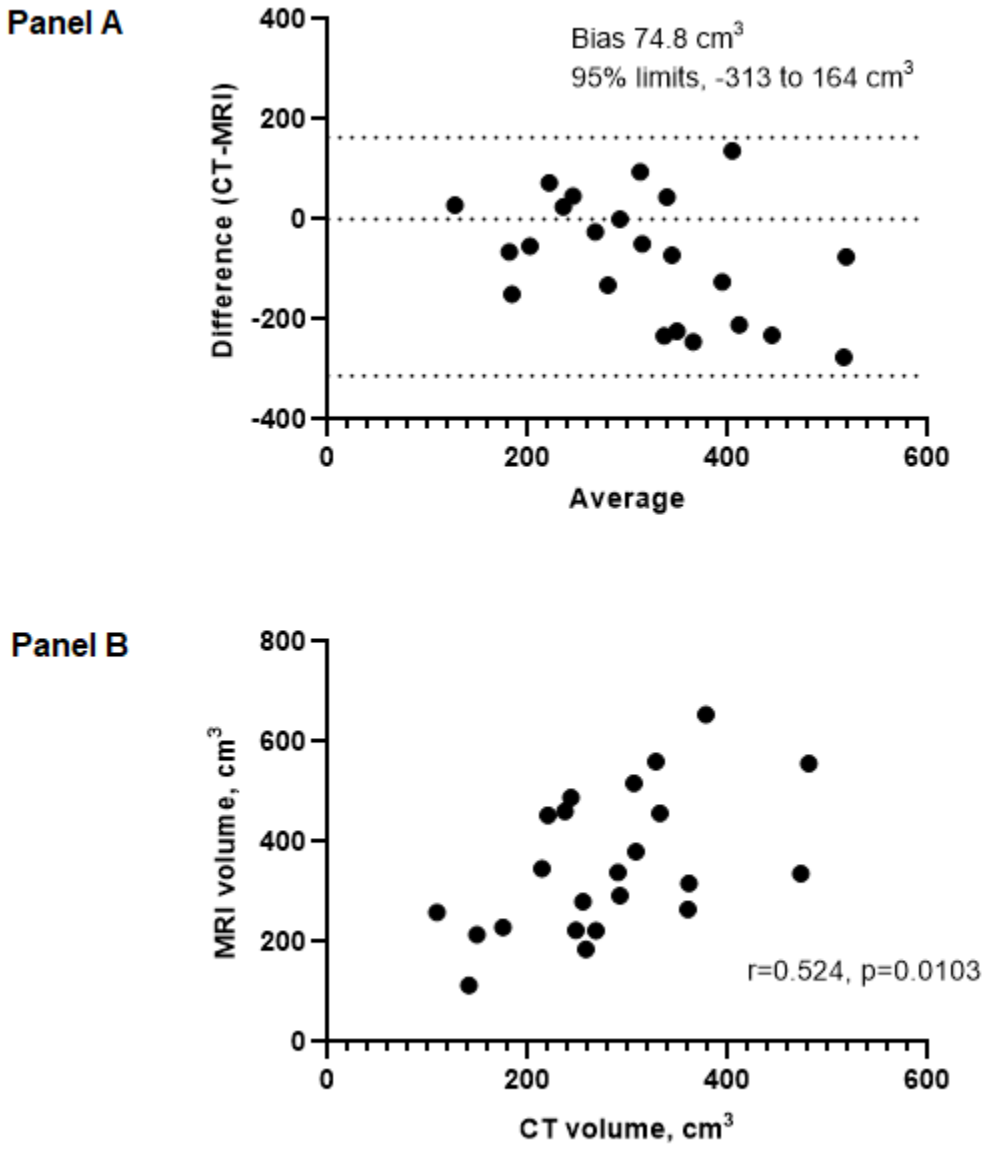

Figure 4.1 Bland-Altman plot (Panel A) and Pearson's correlation (Panel B) comparing tumour volume measured using manual segmentation CT scan versus semi-automated segmentation MRI in 23 patients with MPM

4.3.2.3 Reproducibility

There was moderate human inter-observer agreement (ICC 0.732, p=0.001), with a mean absolute difference of 65.7 (SD 73.8) cm^3. There was excellent human intra-observer agreement (ICC 0.997, p<0.0001), with a mean difference of 29.6 (SD 19.1) cm^3. These data have been summarised in Table 4.2. AI inter-observer analyses would have to involve comparison with a different algorithm. There is no AI intra-observer variation.

Table 4.2 Manually segmented pleural tumour volume differences between two human readers

Reader 1 volume (cm^3)	**Reader 2 volume (cm^3)**	**Volume difference (cm^3)**
237	172	65
292	225	67
306	239	67
360	309	51
220	208	12
473	597	-124
258	174	84
361	213	148
175	123	52
308	154	154
268	171	97
378	220	158
248	224	24

4.3.2.4 Human versus AI volumes

The median human and AI volumes were 330 [IQR 248.5 to 464] cm^3 and 474.5 [IQR 354 to 694] cm^3, respectively. AI volumes were larger than human volumes with a mean difference between AI and human volumes of +142 cm^3 (95% limits of agreement -226 to 511 cm^3, see Figure 4.2: Panel A). There was a strong correlation between human and AI volumes (training set r=0.847, 95% CI 0.768 to 0.901, p<0.0001, see Figure 4.2: Panel B).

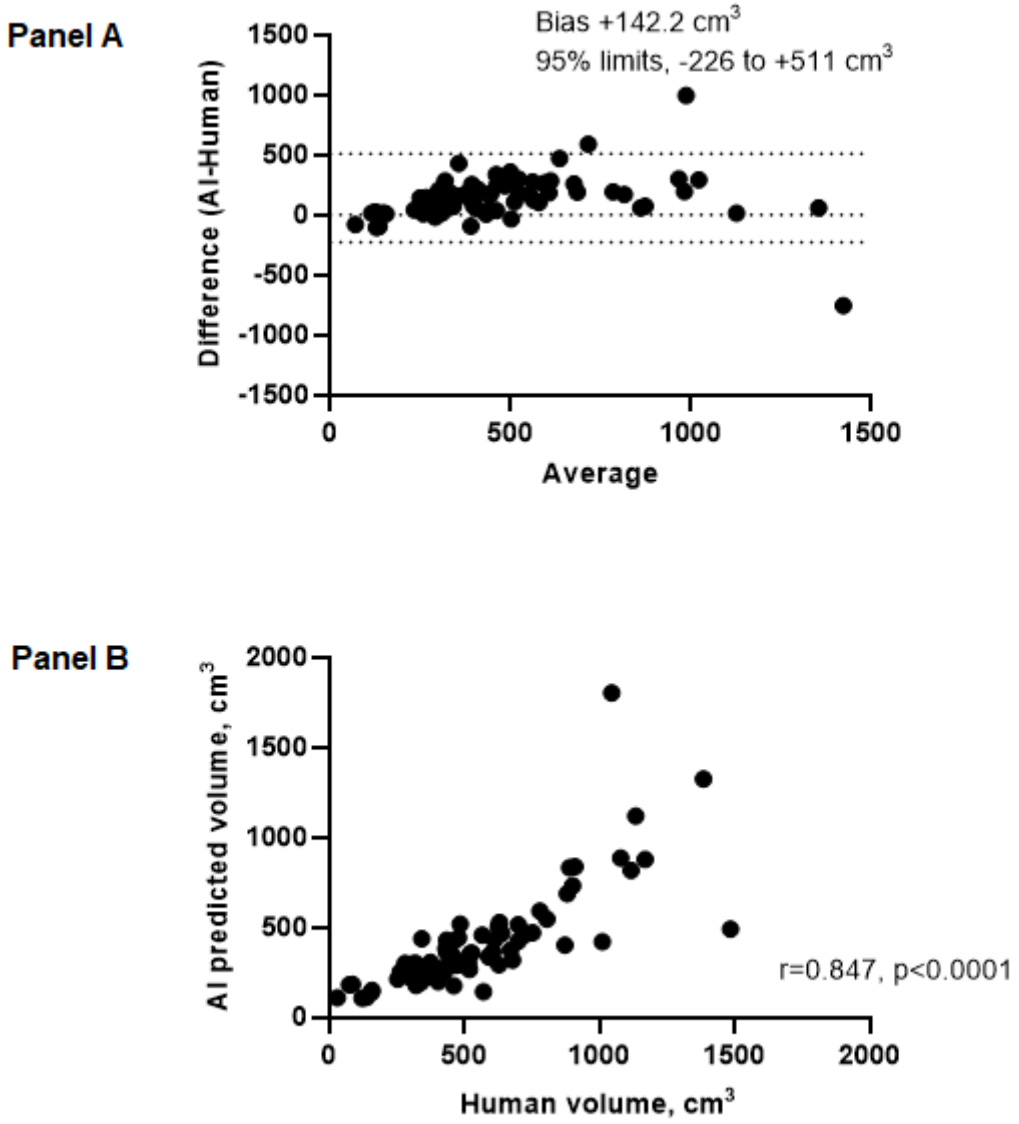

Figure 4.2 Bland-Altman analysis (Panel A) and Spearman's correlation (Panel B) between human and AI training and interval validation set volumes (n=80 scans)

4.3.3 **External validation**

4.3.3.1 Human versus AI volumes

In the external validation set, the median human and AI tumour volumes were 336.5 [IQR 227.8 to 637] cm^3 and 394 [IQR 217 to 679] cm^3, respectively. There was a mean difference between AI minus human of +31 cm^3 on the Bland-Altman plots (95% limits of agreement 345 to +407 cm^3, see Figure 4.3: Panel A). There was a strong correlation between human and AI volumes (r=0.851, 95% CI 0.759 to 0.910, p<0.0001, see Figure 4.3: Panel B).

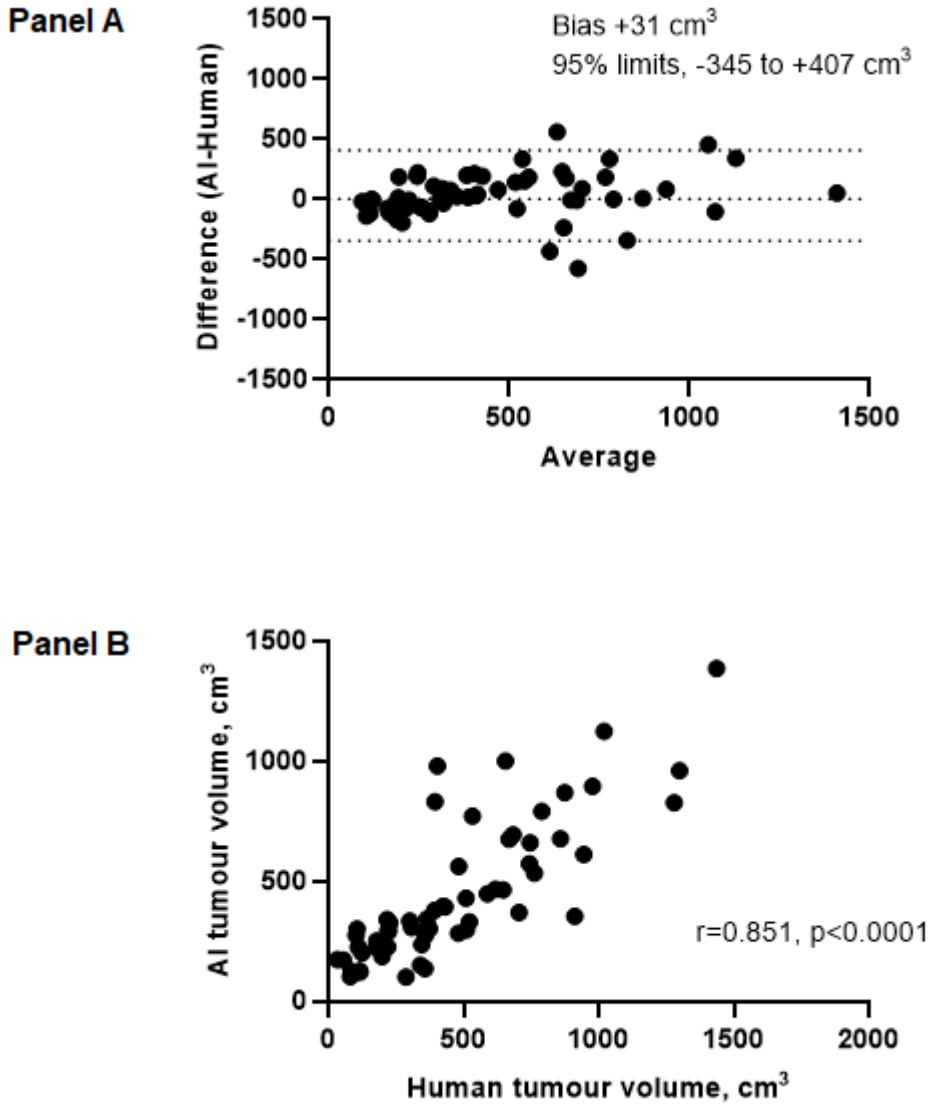

Figure 4.3 Bland-Altman analysis (Panel A) and Spearman's correlation (Panel B) between human and AI external validation set volumes in 60 scans

4.3.3.1.1Human versus AI pre-chemotherapy volumes

At the pre-chemotherapy time point, there was a mean difference between AI minus human of +29.1 cm^3 on the Bland-Altman plots (95% limits of agreement -312.9 to +371.1 cm^3, see Figure 4.4: Panel A). Pre-chemotherapy human and AI volumes were also strongly correlated (r=0.837, 95% CI 0.683 to 0.920, see Figure 4.4: Panel B).

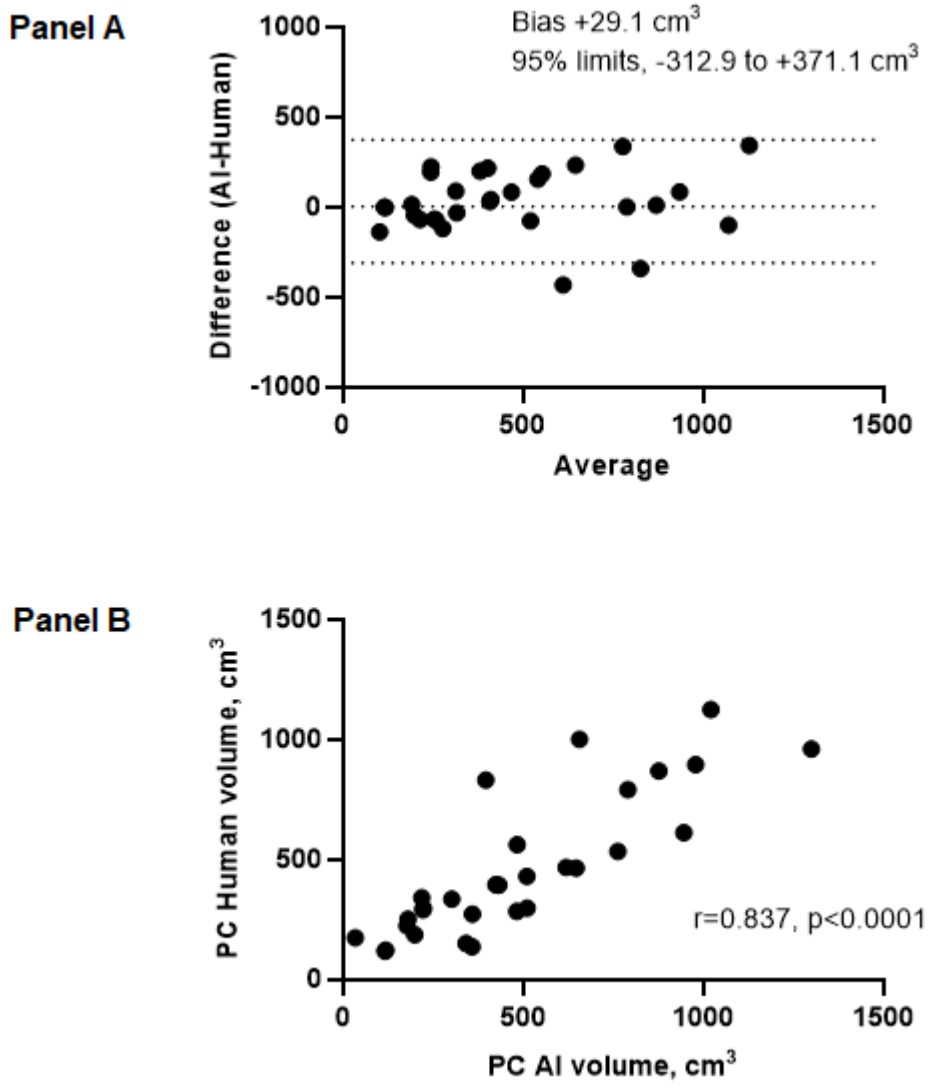

Figure 4.4 Bland-Altman analysis (Panel A) and Spearman's correlation (Panel B) between pre-chemotherapy (PC) human and AI external validation set volumes in 60 scans

4.3.3.1.2 Human versus AI response assessment volumes

At the response assessment time point, there was a mean difference between AI minus human of +32.1 cm^3 on the Bland-Altman plots (95% limits of agreement -381 to +445.2 cm^3, see Figure 4.5: Panel A). Response assessment human and AI volumes were strongly correlated (r=0.802, 95% CI 0.621 to 0.902, p<0.0001, see Figure 4.5: Panel B).

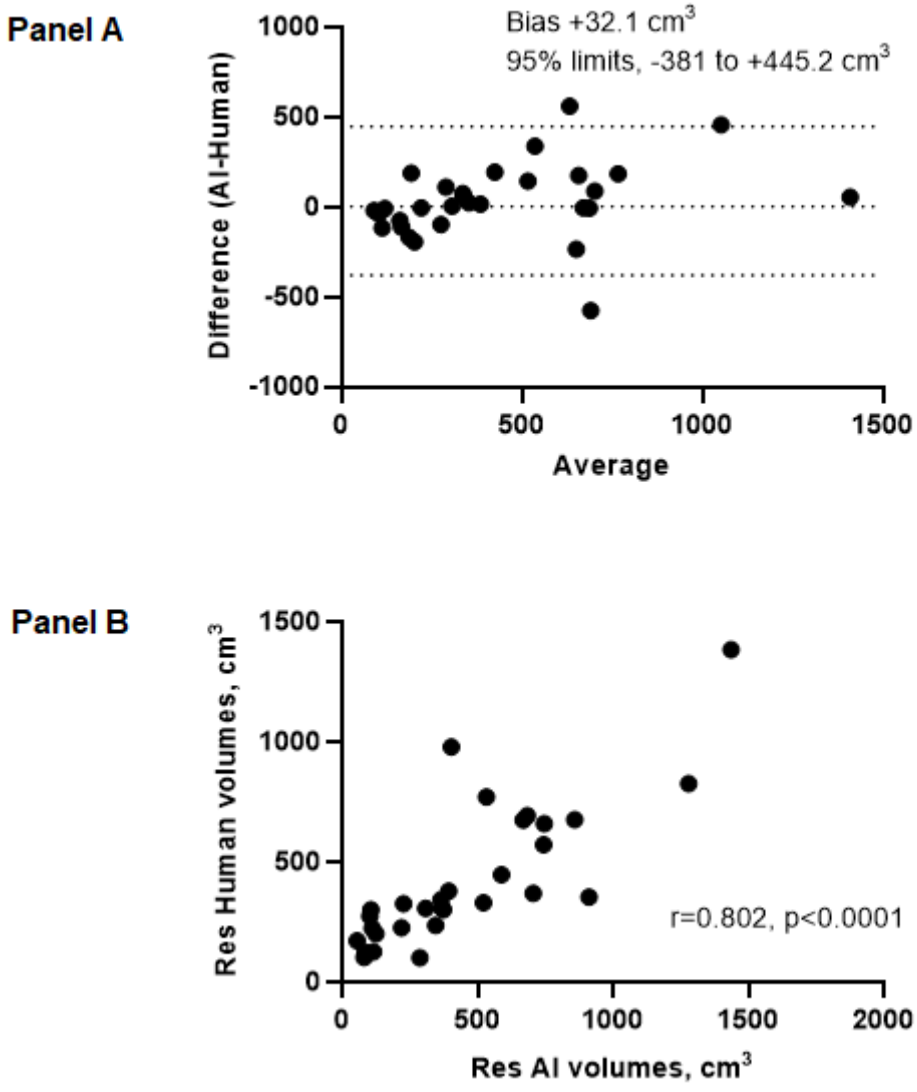

Figure 4.5 Bland-Altman analysis (Panel A) and Spearman's correlation (Panel B) between response assessment (Res) human and AI external validation set volumes in 60 scans

4.3.4 **Visual inspection of outlying volumes**

Visual inspection of the 4 datapoints out-with the 95% limits of agreement was carried out and are illustrated in Figure 4.6. These cases have been extracted from the Bland Altman plot of the 60 scans from the external validation set in Figure 4.3: Panel A.

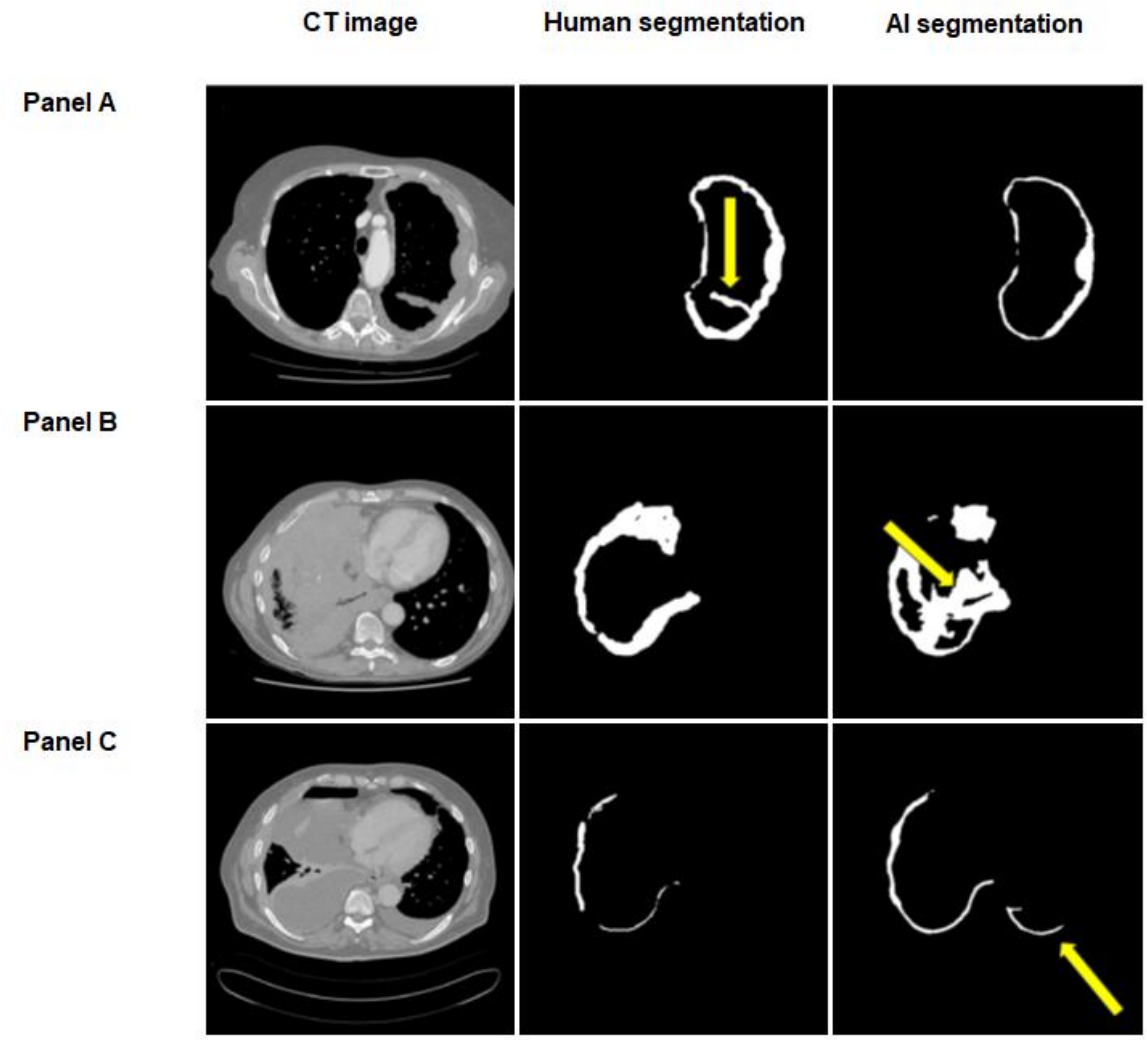

Figure 4.6 Examples of the scans out-with the 95% limits of agreement. Panel A illustrates under-segmentation by the AI in pre-chemotherapy images with tumour in the left lung fissure (yellow arrow) not included in the final volume. Panel B illustrates over-segmentation with the AI erroneously including lung atelectasis above the right hemidiaphragm (yellow arrow). Panel C illustrates over-segmentation with the AI erroneously including contralateral benign pleural thickening by the AI (yellow arrow)

4.3.5 **Changes in tumour volume following chemotherapy by human and AI**

The median human pre-chemotherapy and response assessment tumour volumes were 366 [IQR 244 to 656] cm^3 and 328 [IQR 225 to 663] cm^3, respectively (p=0.196). The median AI pre-chemotherapy and response assessment tumour volumes were 427 [IQR 220 to 682] cm^3 and 371 [IQR 122 to 689] cm^3, respectively (p=0.081). There was a mean difference between AI and human volumes of +2.1% (95% limits of agreement -59.6 to 55.5%, see Figure 4.7: Panel A). There was moderate correlation between human and AI volumetric changes (r=0.611, 95% CI 0.311 to 0.799, p=0.0003, see Figure 4.7: Panel B).

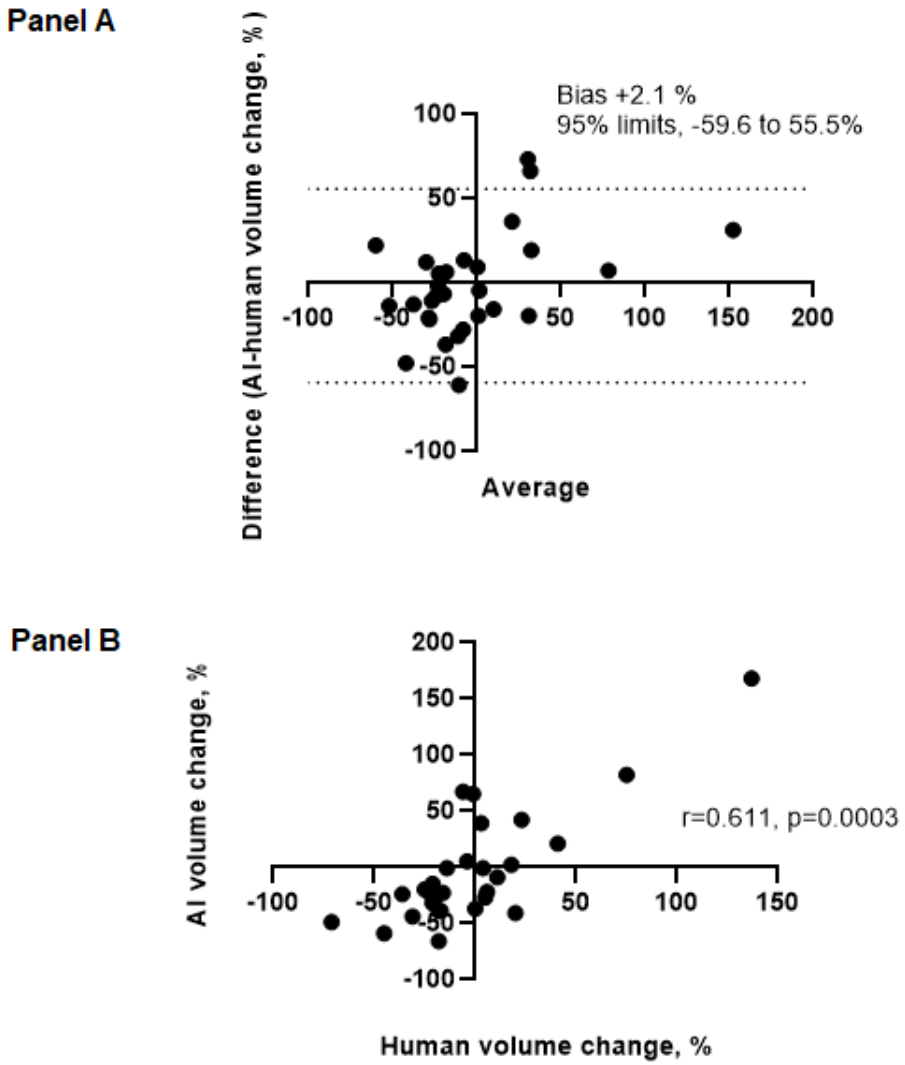

Figure 4.7 Bland-Altman analysis (Panel A) and Spearman's correlation (Panel B) between human and AI percentage volume change in the 60 volumes in the external validation set

There was agreement in 20/30 (67%) cases following classification of human and AI percentage volume changes into partial response (PR), stable disease (SD) and progressive disease (PD) (Kappa=0.439, 95% CI 0.178 to 0.700, see Figure 4.8). When dichotomised into non-PD versus PD, there was agreement in 26/30 cases (87%), kappa=0.586, 95% CI 0.227 to 0.945, see Figure 4.9.

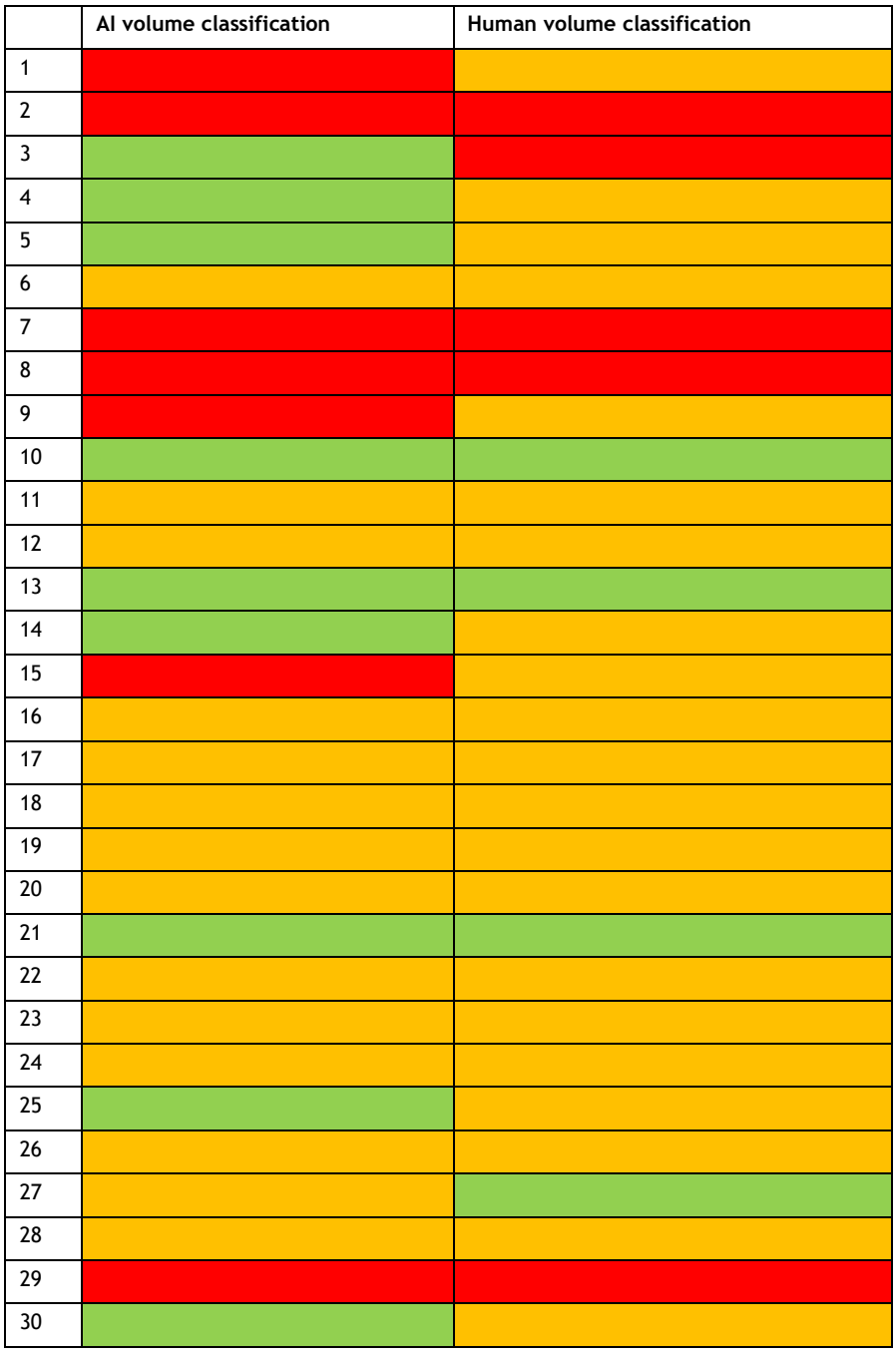

Figure 4.8 Comparison of human- and AI-defined volume responses for each patient (rows 1 to 30) in the external validation set. Partial response is green, stable disease is amber and progressive disease is red

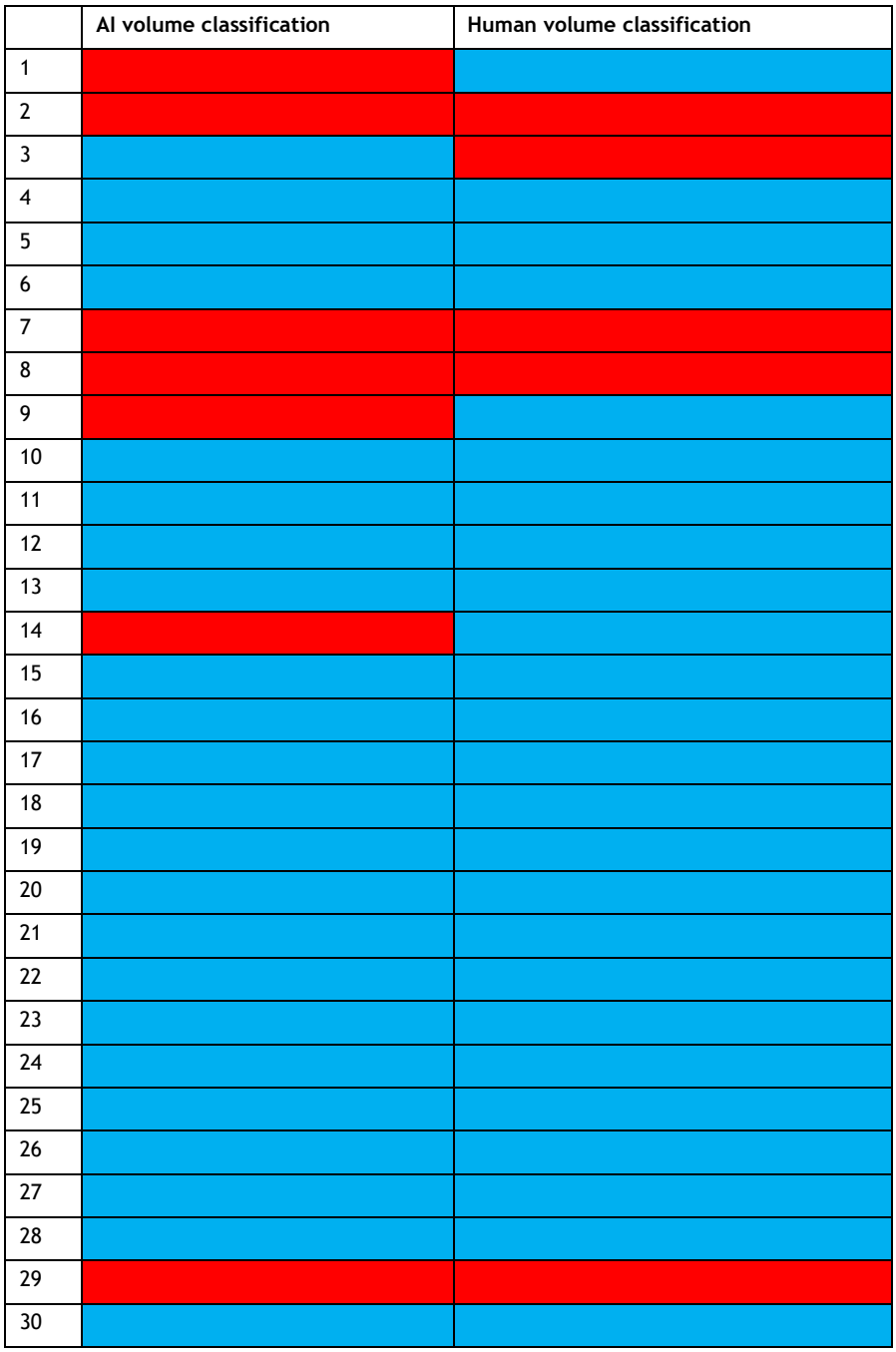

Figure 4.9 Comparison of human- and AI-defined volume responses for each patient (rows 1 to 30) in the external validation set. Progressive disease (PD) is red and Non-PD is blue

4.3.6 **mRECIST versus AI volumetric response**

There were differences between human-, AI- and mRECIST-defined treatment response classifications. These have been summarised in Table 4.3.

Table 4.3 Response to treatment defined by human and AI volumes and mRECIST in 30 patients with MPM (n=60 scans)

	Human volume n (%)	**AI volume n (%)**	**mRECIST n (%)**
PR	4/30 (13%)	9/30 (30%)	6/30 (20%)
SD	21/30 (70%)	14/30 (47%)	13/30 (43%)
PD	5/30 (17%)	7/30 (23%)	11/30 (37%)
Non-PD	25/30 (83%)	23/30 (77%)	19/30 (63%)
PD	5/30 (17%)	7/30 (23%)	11/30 (37%)
PD: progressive disease; PR: partial response, SD: stable disease			

There was agreement between mRECIST and AI response classification in 16/30 (55%) cases (Kappa=0.284, 95% CI 0.026 to 0.543, see Figure 4.10). When mRECIST and AI response classifications were classified into non-PD v PD, there was agreement in 20/30 (67%) cases (Kappa=0.223, 95% CI -0.128 to 0.574, see Figure 4.11).

	AI volume classification	mRECIST response classification
1		
2		
3		
4		
5		
6		
7		
8		
9		
10		
11		
12		
13		
14		
15		
16		
17		
18		
19		
20		
21		
22		
23		
24		
25		
26		
27		
28		
29		
30		

Figure 4.10 Comparison of mRECIST- and AI-defined volume responses for each patient (rows 1 to 30) in the external validation set. Partial response is green, stable disease is amber and progressive disease is red

	AI volume classification	mRECIST response classification
1		
2		
3		
4		
5		
6		
7		
8		
9		
10		
11		
12		
13		
14		
15		
16		
17		
18		
19		
20		
21		
22		
23		
24		
25		
26		
27		
28		
29		
30		

Figure 4.11 Comparison of mRECIST- and AI-defined volume responses for each patient (rows 1 to 30) in the external validation set. Progressive disease (PD) is red and Non-PD is blue

The median mRECIST-defined PD, SD and PR percentage volume changes were -52 cm^3, -21 cm^3 and -18 cm^3, respectively, when the human ground truth volumes were used as a reference standard. There was no significant difference in percentage volume change between the groups (p=0.072, see Figure 4.12: Panel A). The median AI-defined PD, SD and PR percentage volume changes were -18 cm^3, -15 cm^3, +23 cm^3, respectively. There was a significant difference in volume change between the groups (p=0.009, see Figure 4.12: Panel B).

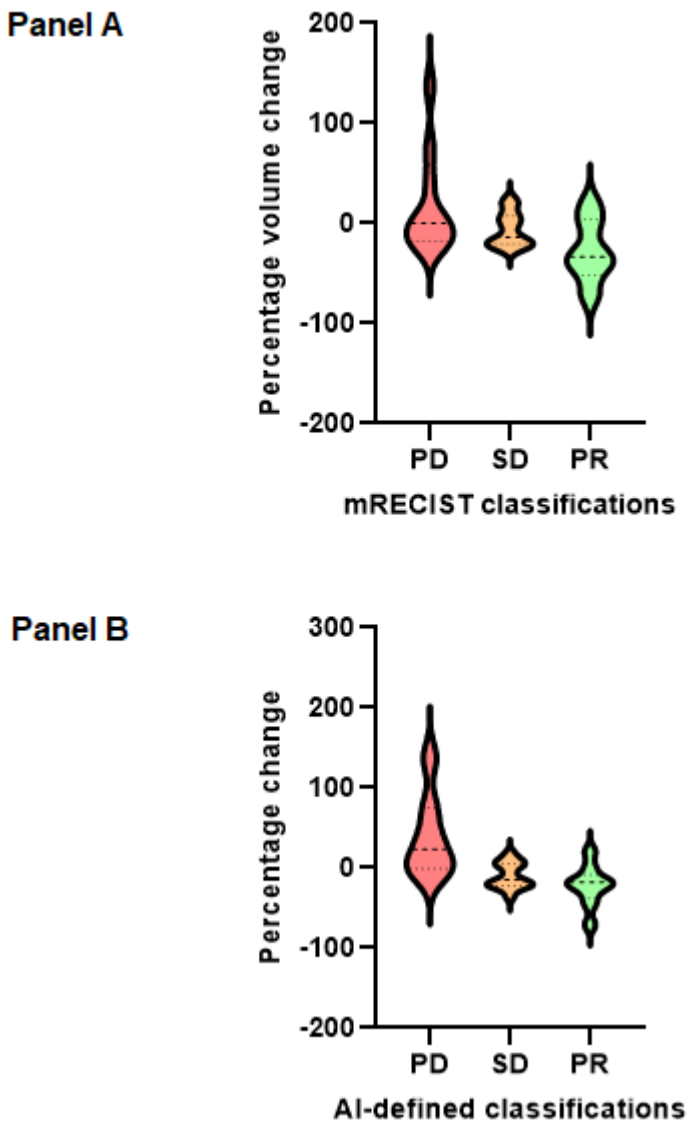

Figure 4.12 Classification of percentage human volume changes into mRECIST (Panel A) and AI-defined (Panel B) progressive disease (PD), stable disease (SD) and partial response (PR) in the external validation set

4.3.7 **Survival analyses**

The median follow-up period was 1729 days. The median overall survival (OS) in the external validation set was 377 days. When human tumour volume in the external validation set was dichotomised into high and low volume based in median volumes (366 cm^3), higher pre-chemotherapy human tumour volume was associated with shorter OS (293 versus 473 days, HR 4.01, 95% CI 1.26 to 6.48, p=0.0019, see Figure 4.13: Panel A). Similarly, when AI tumour volume in the external validation set was dichotomised into high and low volume based in median volumes (427 cm^3), higher pre-chemotherapy AI tumour volume was associated with shorter OS (299 versus 462 days, HR 2.40, 95% CI 1.07 to 5.41, p=0.0114, see Figure 4.13: Panel B). When dichotomised according to human volume-defined PD and Non-PD, there were no survival differences (379 versus 375 days, HR 0.71, 95% CI 0.28 to 1.84, p=0.403, see Figure 4.13: Panel C). Similarly, no differences were observed with AI-defined response assessment (PD 452 versus non-PD 317 days, HR 1.18, 95% CI 0.48 to 2.90, p=0.6853, see Figure 4.1: Panel D). There was a non-significant trend towards shorter OS in the mRECIST-defined PD group versus non-PD (317 versus 450 days, HR 1.98, 95% CI 0.84 to 4.69, p=0.0616, see Figure 4.13: Panel E).

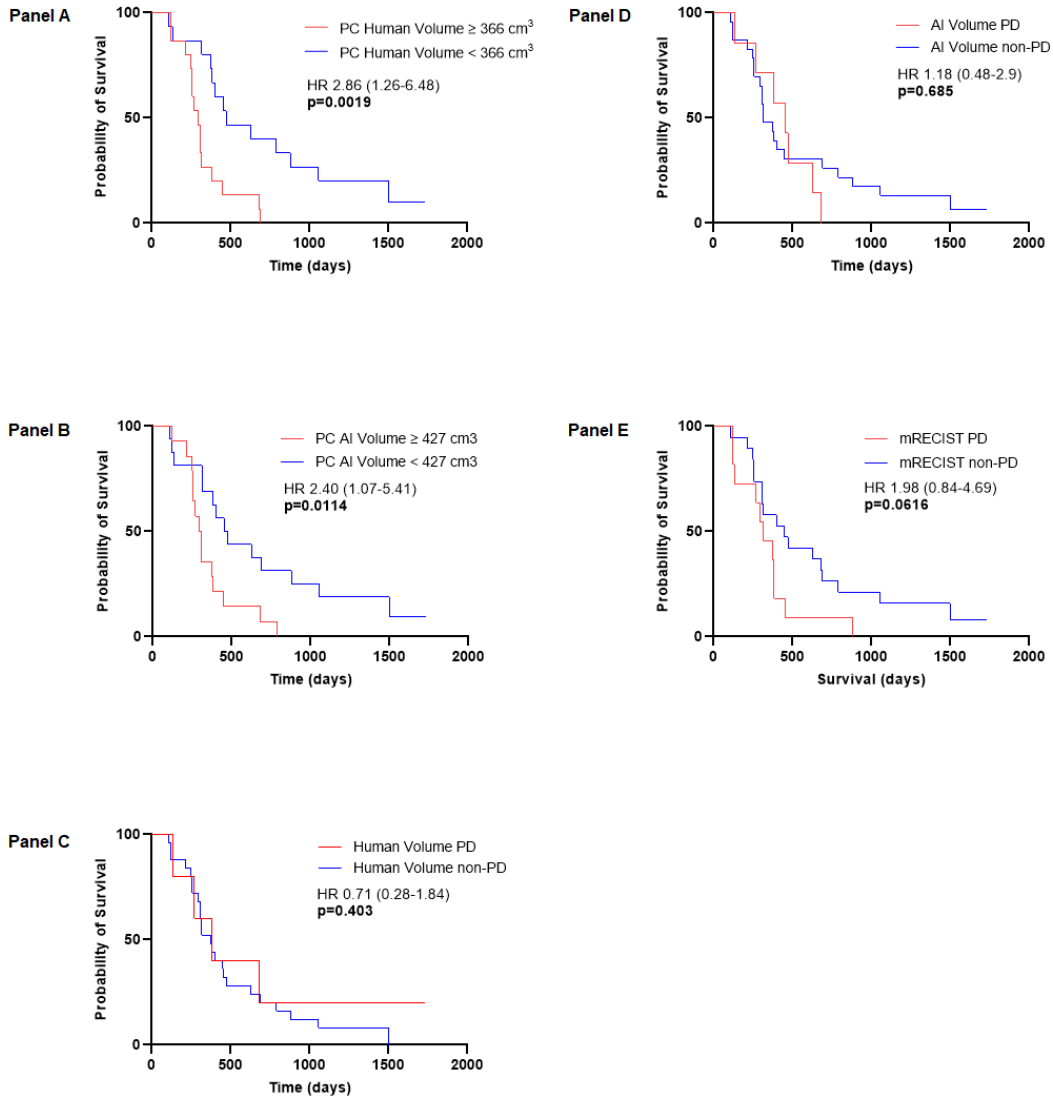

Figure 4.13 Kaplan-Meier curves and number at risk tables illustrating overall survival stratified by, Panel A) pre-chemotherapy human tumour volume ≥366 cm3 and, Panel B) pre-chemotherapy AI tumour volume ≥427 cm3, Panel C) human volume-defined progressive disease (PD) and Non-PD, Panel D) AI volume-defined PD and Non-PD, and, Panel E) mRECIST-defined PD and Non-PD

4.4 Discussion

4.4.1 **Manual CT method**

A fully automated deep learning CNN is reported in this chapter. The ground truth for the CNN was provided by manual pleural tumour volumetric segmentations following learning in Chapter 3 of this thesis. On visual inspection, the manually contoured slices were robust and consistently volumed the entirety of the parietal pleura. I reported excellent reproducibility with my repeat measurements. However, the manual contouring process was time-consuming with each scan taking approximately 2.5 hours to complete. I demonstrated moderate reproducibility between two different human readers with an absolute difference of 65.7 (SD 73.8) cm^3. However, there were absolute differences in pleural tumour volumes ranging between -124 and 158 cm^3. Gill and colleagues reported similar findings in their semi-automated assessment of pleural tumour volume in 129 patients with MPM using Vitrea Enterprise suite 6.0 (Vital Images, Minnesota, USA)(111). Although good correlation was reported between two radiologists (Spearman's Rho=0.822), with absolute volume differences of ≤200 cm^3 in 80% of the scans assessed, there was marked variability in volume estimates between the radiologists with absolute differences in volume ranging between 173.7 cm^3 and 860.6 cm^3(111). Gill and colleagues concluded that this discordance between readers reflected not only the limitations of identifying pleural tumour using contrast CT imaging, but also what the radiologists interpreted as pleural tumour, with perception, prior experience and time spent segmenting all considered to be variable between readers(111).

4.4.2 **Comparison to the MRI method**

In the present study, CT volumes were consistently smaller than MRI volumes with an average difference of 74.8 cm^3 suggesting that the MRI method was able to identify more pleural tumour than the manual CT method. The MRI method described by Tsim and colleagues was preceded by high performing detailed

perfusion studies that were tuned specifically to pleural tumour(319, 342). MRI inherently affords superior soft tissue contrast resolution with clearer demarcation of normal pleurae and pleural tumour compared to CT as well as superior definition of pleural tumour(368). MRI is also better at detecting invasion of MPM into the chest wall as well as trans-diaphragmatic tumour extension and extension into the inter-lobar fissures(336, 369). Also, unlike the HU-defined threshold limits for tumour region growing, the median MRI signal intensity value used by Tsim and colleagues was +/- 99 AU which did not overlap with adjacent thoracic structures. This has been discussed in further detail in Chapter 3, Section 3.4.2.

Although only high quality venous-phase contrast-enhanced CT scans were included in the final analyses, the retrospective nature of the study meant that contrast administration and dosimetry have not been accounted for and may not have been consistent. Tumour enhancement using CT is known to be dependent on the timing of image acquisition post-administration of intravenous contrast(370). Traditionally, the optimal timing of image acquisition is 40 to 60 seconds post-intravenous contrast administration. However, Patel and colleagues assessed increased time delays beyond this traditional interval and concluded that a time delay of 230 to 300 seconds post-intravenous contrast administration improved pleural tumour discernability(371). Another problem encountered with the CT method was that pleural tumour was often not visible despite the paired MRI scans demonstrating visible pleural tumour. I illustrated this in Chapter 2, Figure 2.6. This was particularly evident when the images were viewed in the coronal plane. Pleural tumour was also more visible on some CT scans than others which I illustrated in Table 3.4 in Chapter 3. The potential for variability in contrast enhancement may be explained by factors such as histological sub-type differences on CT imaging(365) which were not accounted for in the present study which I discuss in detail in Section 3.4.6 of Chapter 3. Regardless of these imaging limitations and pleural tumour volume differences between the two imaging modalities, the CT and MRI data reported in the present study remained moderately correlated (Pearson's r=0.524, 95% CI 0.142 to 0.769), and as such, provided reassurance that the volumes could be used to train the deep learning CNN.

4.4.3 **AI and ground truth tumour volumes**

In the training and internal validation set, the median AI pre-chemotherapy tumour volumes were larger than the volumes measured by my ground truth (330 [IQR 248.5 to 464] cm^3 versus 474.5 [IQR 354 to 694] cm^3, respectively). The mean difference between AI and human volumes was +142 cm^3. The diversity of disease stages of the cases included in the training and interval validation set may explain this as there was a predominance of patients in the PRISM study who had later-stage disease whereas the 23 patients in the DIAPHRAGM study had earlier-stage disease and scans performed at the diagnostic, rather than pre-chemotherapy, time point. The mean human and AI volumes for patients in the DIAPHRAGM study were lower (262.5 (SD 98.3) cm^3 and 358.6 (SD 160.6) cm^3, respectively).

In the external validation set, the median AI pre-chemotherapy tumour volumes were also larger than the volumes determined by my ground truth (336.5 [IQR 227.8 to 637] cm^3 versus 394 [IQR 217 to 679] cm^3, respectively). There was a mean difference of +31 cm^3 between AI and human volumes on the Bland-Altman plots in the external validation set. There may be several reasons for the higher AI volumes compared to the ground truth. Firstly, in the inter-observer work, I consistently reported higher tumour volumes compared to the other human observer with a mean difference of +65.7 cm^3. Labby and colleagues also recognised this in their study and reported that different observers consistently annotate differently with some observers consistently segmenting less tumour than others(104). Secondly, the CNN will segment images features that a human reader may not(372). Thirdly, CT is known to underestimate the extent of pleural tumour volume in MPM. A further reason could be overfitting for the CNN. Attempts were made to minimise over-fitting by training the CNN using different CT scanners as well as testing the CNN using an external validation set.

There was strong correlation between human and AI volumes in the training and internal validation ($r=0.847$, $p<0.0001$) and external validation sets ($r=0.851$, $p<0.001$). A similar finding was reported by Weikert and colleagues in their study

of patients with NSCLC with positive correlation between volumes calculated by AI algorithms and ground truth volumes (r=0.634, p<0.001)(373).

4.4.4 **Tumour volume comparison to other studies**

The pre-chemotherapy tumour volumes in this study (330 cm^3) were similar to those reported by Gill and colleagues (319 cm^3)(101) and Rusch and colleagues (most tumours were <500 cm^3)(102). Labby and colleagues reported higher mean pleural disease volume (1511 (SD 1065) cm^3)(104). Pass and colleagues reported smaller volumes, reflecting patients with earlier-stage disease who were eligible for surgery (the mean tumour volumes for pleurectomy decortication and extra-pleural pneumonectomy were 88 cm^3 and 86 cm^3, respectively(99).

4.4.5 **CNN model performance**

Region overlap between different volumetry methods was quantified using the Dice coefficient - a metric of performance in image segmentation by deep learning algorithms – which was performed separately by an EngD Research Engineer (Owen Anderson) from Canon Medical Research Europe (CMRE) and published in a conference abstract(327). The mean Dice co-efficient between the ground truth human annotation and AI segmentation in this study was 0.55 (SD 0.12), mirroring studies by Sensakovic and colleagues and Gudmundsson and colleagues who reported a median Jaccard index of 0.484 - which equates to a Dice coefficient of 0.65 - and median Dice coefficients ranging from 0.662 to 0.800, respectively(109, 136). In their studies, Chen and colleagues and Brahim and colleagues reported higher mean Dice coefficients (0.825 and of 0.88, respectively)(112, 113).

4.4.6 **Reproducibility**

The tumour segmentation method and software utilised in the present study are closest to those employed by Frauenfelder and colleagues who compared volumetric measurement of MPM pre- and post-chemotherapy according to

mRECIST criteria(108). The authors of that study reported a high inter-rater reliability (0.99) and inter-observer agreement (general κ 0.9) for absolute pleural tumour volumes on volumetric measurements. They also reported mean differences of ≤66 cm^3 between their three human readers. The inter-observer and intra- observer coefficients in this study were 0.732 and 0.997, respectively. The selection of 10 cases for inter-observer analysis was arbitrary, but similar to recent similar publications, including Brahim and colleagues who evaluated 10 cases(113) and Sensakovic and colleagues(109) and Gudmundsson and colleagues(136) who, although analysed larger patient numbers, assessed fewer CT image sections.

4.4.7 **Analysis of anatomical features associated with AI segmentation errors**

In the external validation set, 4/60 patients had segmentation errors that exceeded 95% limits of agreement. Closer examination of these cases demonstrated morphological features including adjacent atelectasis of lung, tumour in the lung fissure and contralateral pleural thickening.

Gudmundsson and colleagues experienced similar “volumetric outliers” in their study examining an automated segmentation method, reporting that 7/15 cases where their algorithm over-predicted tumour area contained pleural effusions(152). Sensakovic and colleagues reported their computerised volumes to be larger (mean volume difference 59.3 cm^2), which they attributed to “leakage of the active surface” used in the hemi-thoracic cavity segmentation method. Their segmentation errors were most likely to occur in the lung bases and intercostal spaces due to segmentation difficulties in these areas as well as pleural effusion(109). Brahim and colleagues reported a mean over-segmentation rate between their adjusted thoracic cavity segmentation method output and the ground truth of 19.55%, citing their thoracic cavity delimitation step which may have included sections of adjacent tissues(113). I provided a commentary of the anatomical complexities that I encountered when delineating pleural tumour in Chapter 3, Section 3.4.6. The segmentation errors experienced in the present study are likely to be relatively infrequent features in the training and internal validation data given the small sample size, however they will have direct

implications for the next steps in CNN development. If deep learning techniques are to be further optimised, enrichment of future data sets to include these features will be required to improve the training, and subsequent performance of, deep learning CNNs.

4.4.8 **Survival analyses**

Higher human-defined pre-chemotherapy tumour volume was associated with poorer OS which is consistent with previous volumetry studies(99, 101-103). Pass and colleagues reported that patients with pre-operative tumour volume <100cm^3 had a longer median survival (22 months versus 11 months, p=0.03)(99). Patients with pre-operative tumour volumes >52 cm^3 had shorter progression-free intervals (8 months versus 11 months, p=0.02)(99). Using the volumetric measurement methods described by Gill and colleagues(101), Rusch and colleagues divided tumour volume into tertiles with mean volumes of 91.2 cm^3, 245.3 cm^3, 511.3 cm^3, with associated median overall survival of 37, 18 and 8 months, respectively(102). Gill and colleagues measured pre-operative CT-based tumour volume in patients with MPM undergoing extra-pleural pneumonectomy and concluded that patients with tumour volume ≥500 cm^3 had poorer OS compared with those with tumour volume ≤500 cm^3 (24.4 months versus 12 months, p<0.0001)(101). Paajanen and colleagues divided tumour size - calculated by the sum of the maximal tumour thickness and tumour extent grade of the pleural circumference (measured at the level of the carina) - into tertiles with the median OS in the lowest, middle and highest tumour volume groups being 14.0, 11.1 and 5.4 months, respectively (p=0.016)(103). In the present study, patients were excluded from the response classification survival analyses if they had a pre-chemotherapy and response assessment CT scan interval period of ≥100 days. This arbitrary threshold was chosen to ensure that only cases with imaging that aligned with clinical practice were included, i.e., four cycles of chemotherapy over three weeks equates to three months, or approximately 100 days.

4.4.9 Differences in mRECIST-, human- and AI-defined volumetric response classification

The chemotherapy partial response (PR) rate by mRECIST was 20%. This is similar to previous studies by Santoro and colleagues in their expanded access program (n=1704, PR 21.7-26.3%)(374) and in a meta-analysis of chemotherapy trials by Blayney and colleagues (n=526, PR 11%)(375). In the present study, stable disease (SD) as defined by mRECIST was the most common response rate (43%). In the aforementioned studies by Santoro and Blayney and respective colleagues, similar SD rates were reported (54.1%(374) and 75%(375), respectively). The low efficacy of doublet chemotherapy in MPM most likely explains the high progressive disease (PD) rate (37%) and low PR rate (13%) in the present study. Oxnard and colleagues reported similarly low PR rates (14%)(82).

In the present study, there were differences in human volumetry- and AI-defined response assessment classifications. For example, human volumetry- and AI-defined SD, PR and PD were 21/30 (70%), 9/30 (30%) and 5/30 (17%), respectively, and 13/30 (47%), 4/30 (13%) and 7/30 (23%), respectively. Moreover, there was moderate agreement in volumetric response classifications between human and AI (general κ 0.439), which increased to 0.586 when dichotomised into progressive disease and non-progressive disease. The most likely reason for only moderate agreement was the more detailed segmentation afforded by the human reader compared to the AI, i.e., in subtle areas such as non-pleural progressive disease. Our research group has previously reported that total tumour volume error can be as high as 60% due to uncertainty of only half a voxel in the edge delineation of pleural tumour(327). In addition, different thoracic cage tissues have overlapping Hounsfield units and MPM has a complex morphology which has been described in detail in Chapter 3.

Fair agreement was observed in volumetric response classifications between mRECIST and AI (general κ 0.284). This poor agreement between mRECIST and AI-classification is most likely explained by the volumetric response thresholds chosen and may explain the differences observed between AI- and mRECIST-defined volume changes and OS (i.e., p=0.6853 and p=0.0616, respectively).

4.4.10 Thresholds for AI and mRECIST response classification

One of the most challenging aspects of this study was defining optimal volumetric thresholds for response assessment classification. Response assessment classification differs depending on the dimensionality of tumour measurement(376) and whether tumour volumetric, unidimensional or bidimensional techniques are employed in lung(331, 377, 378), breast(379, 380) and hepatocellular cancers(381). In MPM, there have been similar discrepancies between CT tumour volumetry-defined and mRECIST-defined response assessment classifications(324) as well as wide inter-observer variability with the mRECIST technique(81) and with volumetric measurements(108).

The decision to define PR as a percentage volume change of -30% and PD +20% (with SD defined as percentage volume change between -30% to +20%) was based on criteria proposed by Oxnard and colleagues(82) who modelled the impact of non-spherical growth patterns on RECIST response criteria and found these to be unchanged when a crescent-shaped prism was assumed. These criteria were selected as volumetric response thresholds in the present study as they represented a good approximation of the pleural cavity which is demonstrated in Figure 2.9 in Chapter 2 of this thesis.

Oxnard and colleagues also proposed alternative 'volume equivalent' PR and PD thresholds as a volume decrease of 65.7% and increase of 72.8%, respectively. These 'volume equivalent' criteria result in a broad SD percentage change range of 138.5%. Frauenfelder and colleagues applied by these 'volume equivalent' criteria as proposed by Oxnard and colleagues and reported mRECIST- and volumetry-defined SD in 7/30 (23%) and 20/30 (67%) cases, respectively, and PR in 16/30 (53%) and 2/30 (7%), respectively(108). A similarly broad SD range was reported in the present study with more patients classified as having SD according to human-volumetry than mRECIST (70% versus 43%). Ak and colleagues experienced the same (43% versus 33.3%) after defining PD as a tumour volume increase of ≥15% and PR as a decrease of 50%(107). Oxnard and colleagues reported RECIST and 'volume equivalent' SD of 73% and 91%, respectively(82). Volumetric measurements are sensitive to minimal change

during systemic anti-cancer therapy(334). Having such a large proportion of patients in the SD response assessment category risks equivocality and may not capture what constitutes a clinically important difference.

4.4.11 **Comparison with other computer-generated tumour volumes**

Although computer-generated volumetric measurement techniques have been reported in the MPM literature, to my knowledge, the CNN described in this chapter is the first fully automated system independent of human user input. Gudmundsson and colleagues reported a deep learning algorithm that utilised the same CNN architecture as the present study(136). However, it required manual input to define the hemi-thorax in which disease was present. Ak and colleagues reported a three-dimensional interpretation technique - termed Cavalieri's geometrical principle of stereology - by counting the number of dots placed on representative tumour on cross-sectional imaging(107). Frauenfelder and colleagues reported semi-automated linear interpolation(108) and Chen and colleagues described a random walker algorithmic approach(112).

4.4.12 **Possible clinical implications**

The clinical implications of the successful deployment of a CNN-derived volumetric approach to pleural tumour segmentation are considerable. At present, mRECIST criteria and subjective visualisation of pleural tumour are the methods employed to determine response to treatment in patients with MPM and are associated with wide inter-observer variability. Human annotations which can be accurately measured by experts in pleural tumour interpretation are not routinely performed in clinical practice or in the clinical research setting due to the time taken to manually segment pleural tumour. The present study demonstrates that the CNN generates similar measurements to expert human annotations.

Having accurate measures of disease response would improve clinical decision making, especially earlier cessation of toxic treatment if an AI-generated volume can segment more subtle interval changes compared to the traditional mRECIST

response assessment classification or subjective interpretative approaches. Moreover, the rapidity of AI algorithm volumetric processes when compared to manual human delineation could result in significant cost reductions(334). Further refinement is required to avoid variability in image quality and resultant inconsistency in response assessment classifications. Standardised image acquisition and large-scale validation are crucial in the ongoing development of automated tumour volumetry in patients with MPM.

4.4.13 **Study limitations and strengths**

The main limitation of this study has been my inability to advance the question of optimal volumetric response assessment thresholds further in the present study. This has been discussed in detail in Section 4.4.10 of this discussion. Larger studies are therefore essential to determine the optimal cut points for volumetric PR and PD in MPM.

Another limitation of this study is the small sample size of 80 fully annotated scans and 43 part-annotated scans. CNN dataset often exceeds 10,000 images. However, the present study included volumetric measurements of entire CT image series resulting in a mean total of 2250 CT slices (10 patients with a mean of 225 CT slices each) which exceeds the comparisons made in previous studies. For example, Sensakovic and colleagues assessed 5 image slices in CT scans of 31 patients(109) and Gudmundsson and colleagues assessed 69 scan slices of 27 patients(136). Moreover, expert ground truth was provided rather than relying on minimal ground truth which is often utilised in larger commercial projects, thus improving the quality of the data fed into the CNN architecture.
A third limitation was that the manual segmentation method was time-consuming, averaging approximately 2.5 hours per scan. This would not be feasible due to the heavy workloads experienced by radiologists in standard clinical practice. Additionally, the level of thoracic oncology expertise required to accurately identify pleural tumour in mesothelioma will not be available in every hospital.

A further limitation is that only one human reader provided ground truth data and only one human reader provided mRECIST data. The mRECIST criteria in MPM is associated with intra- and inter-observer variabilities as the three pleural tumour measurements required as part of these criteria can be placed at different anatomical levels(75, 81, 82). This was also evidenced by Frauenfelder and colleagues who reported low inter-observer agreement (general κ 0.33) between their three readers using unidimensional tumour measurements(108). A more robust approach would have been double reading of CT scans +/- a consensus reader to resolve any mRECIST discrepancies.

The retrospective study design is a further limitation. Disease stage, which is a key determinant of MPM prognosis, was unavailable in 41% and 20% of the patients included in the training and internal validation and external validation sets, respectively. However, both sets were broadly similar with a predominantly middle-aged, male population with good performance status receiving doublet chemotherapy, mirroring other studies assessing tumour volumetry in MPM(99, 101, 102, 108).

The performance of the algorithm was assessed on subjects from imaging centres across three different sites thus providing an unbiased assessment of performance using data from centres not involved in training the algorithm. Over the 10-year time period that the patients were recruited, a variety of scanners will have been used, resulting in important differences in the reconstruction and acquisition parameters. This lack of standardisation is common in retrospective datasets and may impact on the reliability of the results. Conversely, this multiplicity of scanners from different hospital sites will have partly off-set the potential for over-fitting compared to using a small study sample from one centre.

The present study reported tumour volume generated entirely by a CNN algorithm. Volumetric assessment of lung nodules(382) and primary lung(383, 384), pancreatic(385) and breast tumours(386) have been reported using deep learning algorithms. To my knowledge, this is the first study to do so in the MPM population.

4.5 Conclusions

In this chapter, I have described the training and internal validation and external validation of an automated CNN to segment pleural tumour in MPM using detailed human ground truth. The development of an automated approach may facilitate a more accurate and less time-consuming approach to radiological response assessment which is an important metric in decision-making regarding response to systemic anti-cancer therapy. This represents the first step towards replacing mRECIST with volumetric response assessment. Implementation of this larger goal requires calibration of optimal and validated response assessment cut-off thresholds to help define what constitutes a clinically important difference between human and AI volumetry measurements.

Chapter 5

PREVALENCE, PATTERN AND PROGNOSTIC SIGNIFICANCE OF ALTERED BODY COMPOSITION IN PATIENTS WITH CHEMOTHERAPY-TREATED MPM

5 Chapter 5: Prevalence, pattern and prognostic significance of altered body composition in patients with chemotherapy-treated MPM

5.1 Introduction

Survival prediction is important in guiding treatment decisions and identifying patients most at risk of developing toxicities to systemic anti-cancer therapy (SACT). The current survival prediction models in patients with malignant pleural mesothelioma (MPM) do not include measures of altered body composition such as the loss of skeletal muscle mass – also termed sarcopenia – which is associated with chemotherapy toxicity and poorer overall survival (OS) in other cancer cohorts(173, 175, 176). Although frequently encountered in the clinical setting, there are little data describing the prevalence of sarcopenia in patients with MPM. Recent studies utilising dual-energy X-ray absorptiometry (DEXA) have defined pre-sarcopenia and sarcopenia in patients with MPM(257, 283). However, DEXA is not routinely performed in the clinical setting and measures lean body mass which is not equivalent to muscle mass(387, 388). Computed tomography (CT) has the advantage of being available through its use in clinical practice. Sarcopenia linked to adverse outcomes in patients with other solid organ cancers have traditionally been acquired at the level of the third lumbar vertebrae (L3)(251, 305). However, CT scans acquired in patients with thoracic malignancy may not extend inferiorly to include this vertebral level and those researching thoracic malignancy have sought alternative measures of skeletal muscle area, including the fourth thoracic vertebra (T4) as a surrogate marker of sarcopenia(311, 313).

Adipopenia - or the loss of fat mass - is another feature of the cancer cachexia syndrome that is prognostically significant in patients with lung(389-392), gastrointestinal and lung(393), gastric(394, 395), breast(396) and renal cell cancers(397). Very few data exist regarding adiposity indices in MPM(190, 257).

This chapter describes a retrospective cohort study based on measures of skeletal muscle and adipose tissue at L3 and skeletal muscle at T4 in patients with chemotherapy-treated MPM to determine if altered body composition at these levels is associated with poorer OS and response to treatment.

5.2 Methods

A detailed description of the methods is provided in Chapter 2, Section 2.3.

The objectives and associated outcome measures for this study are detailed in Chapter 2, Section 2.3.1. To summarise, the primary objective was to determine the prevalence of sarcopenia and adipopenia at L3 and T4 and the prevalence of sarcopenia at T4. Secondary objectives included demonstration of any prognostic association of these measures and their reproducibility. I also addressed several exploratory objectives, including determining the frequency of asymmetrical T4 sarcopenia ipsilateral to the primary tumour and the prognostic impact of this if present. I also looked for relationships between patterns of sarcopenia and adipopenia at L3 and T4 and measures of systemic inflammation and primary tumour volume, the latter derived from the measurements I made in Chapter 4.

5.3 Results

5.3.1 Study population

147 patients were screened. 91 patients had height and weight data and an identifiable L3 on pre-chemotherapy and response assessment time points. 111 patients had height and weight data and an identifiable T4 on pre-chemotherapy and response assessment time points. 47/111 patients in the T4 group had inflammatory indices at pre-chemotherapy and response assessment time points. This is illustrated in Figure 5.1.

Table 5.1 summarises the clinicopathological characteristics of the study cohort. Patients were predominantly male (82%) with epithelioid mesothelioma (81%) and a performance status (PS) of 0 (26%) or 1 (50%). The pre-chemotherapy inflammatory indices were frequently within normal limits. Approximately 29% of patients had a response to chemotherapy. The baseline median tumour volume was 377 [IQR 279 to 524] cm^3 and median survival from the date of pre-chemotherapy CT scan to death from any cause was 389 days, or 12.8 months.

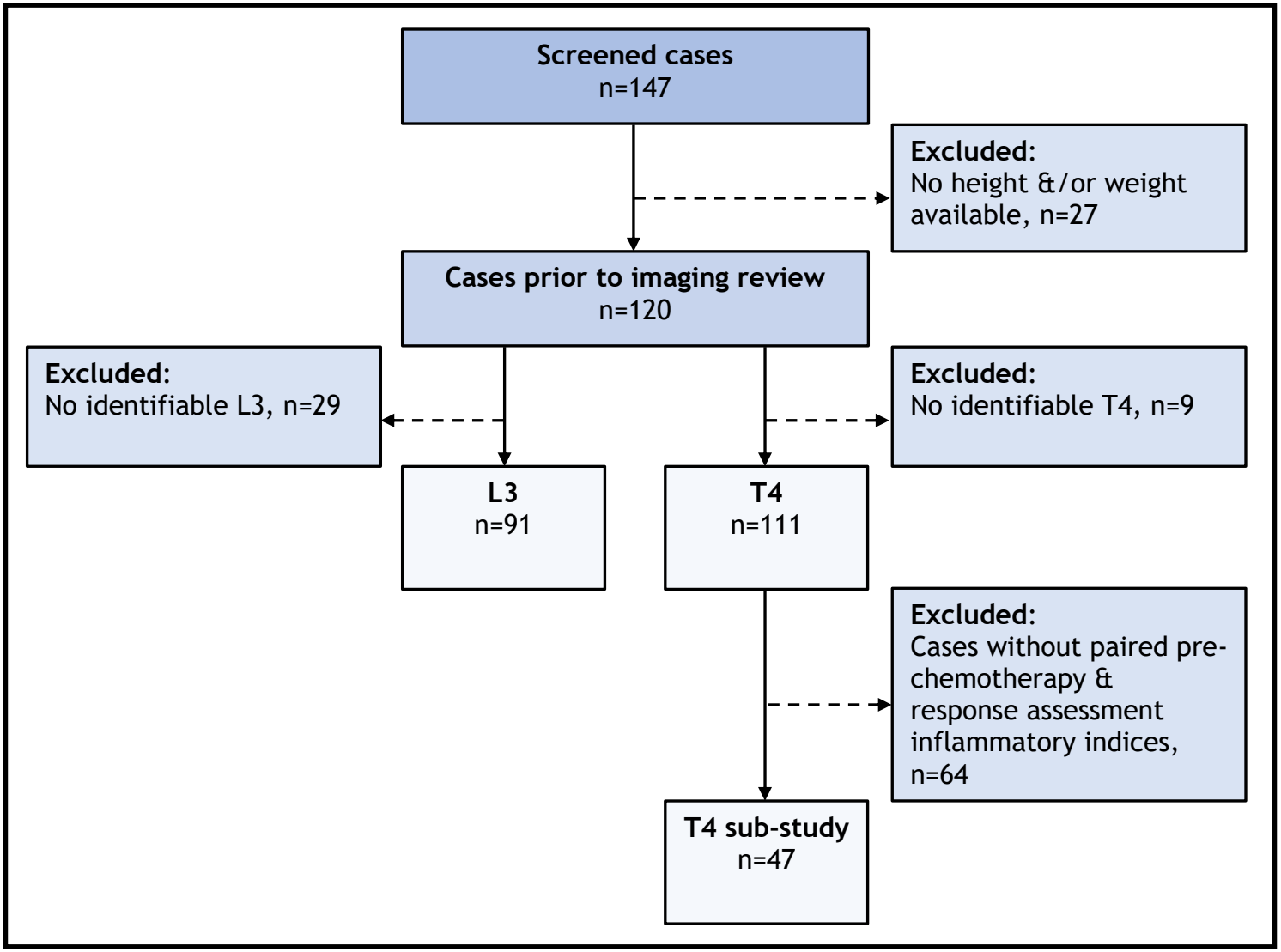

Figure 5.1 Flowchart of body composition study

Table 5.1 Clinicopathological characteristics in patients with MPM who received chemotherapy

	L3 (n=91) **Median [IQR] or n (%)**	**T4 (n=111)** **Median [IQR] or n (%)**
Age, years	69 [64-73]	69 [63–72]
Male sex	72 (80%)	91 (82%)
ECOG PS 0	26 (29%)	30 (26%)
ECOG PS 1	42 (46%)	55 (50%)
ECOG PS 2	7 (8%)	8 (7%)
ECOG PS not defined	16 (18%)	18 (16%)
Epithelioid sub-type	74 (81%)	90 (81%)
Biphasic sub-type	7 (8%)	8 (7%)
Sarcomatoid sub-type	8 (9%)	10 (8%)
Unspecified sub-type	2 (2%)	3 (3%)
Disease stage I	36 (40%)	45 (41%)
Disease stage II	16 (18%)	22 (20%)
Disease stage III	17 (19%)	12 (11%)
Disease stage IV	10 (11%)	19 (17%)
Median number of cycles	4 [3–4]	4 [3–4]
PC WCC, $x10^9$/L	8.6 [7.4–11.2]	8.6 [7.3–11.0]
PC neutrophils, $x10^9$/L	5.7 [4.9–8.1]	5.8 [4.9–8.0]
PC lymphocytes, $x10^9$/L	1.5 [1.1–2.1]	1.5 [1.0–2.0]
PC platelets, $x10^9$/L	350 [285–431]	343 [281–418]
PC NLR	4 [3–6]	4 [2–6]
PC PLR	245 [170–348]	234 [167–351]
PC albumin, g/L	36 [30–40]	35 [30–39]
PC CRP, mg/L	29 [8–57]	25 [8–49]
mRECIST: progressive disease	23 (25%)	27 (24%)
mRECIST: stable disease	36 (40%)	45 (41%)
mRECIST: partial response	25 (27%)	32 (29%)
PC tumour volume, cm^3	377 [277–520]	377 [279–524]
Survival, days	389 [251-63]	389 [279–524]

CRP: C-reactive protein; ECOG PS: Eastern Cooperative Oncology Group performance status; mRECIST: modified Response Evaluation in Solid Organ Tumours; NLR: neutrophil:lymphocyte ratio; PC: pre-chemotherapy; PLR: platelet:lymphocyte ratio; WCC: white cell count

5.3.2 **Primary objective**

5.3.2.1 Prevalence and pattern of sarcopenia and adipopenia at L3

5.3.2.1.1 Sarcopenia

The prevalence of sarcopenia - defined by the Martin and colleagues criteria(186) – was 32/91 (35%) at pre-chemotherapy and 44/91 (48%) at response assessment time points (see Table 5.2). The median pre-chemotherapy and response assessment L3SMI were 50 [IQR 44 to 57] cm^2/m^2 and 47 [IQR 42 to 57] cm^2/m^2, respectively. The median L3SMI percentage change between pre-chemotherapy and response assessment was -2.4 [IQR -9 to 1.4] %.

5.3.2.1.2 Adipopenia

The prevalence of adipopenia – defined as total fat index (TFI) mean minus 1 SD - was 13/91 (14%) at pre-chemotherapy and 14/91 (15%) at response assessment time points (see Table 5.2). The mean pre-chemotherapy and response assessment total fat indices were 126.6 (SD 57.6) cm^2/m^2 and 122 (SD 66.4) cm^2/m^2, respectively. The mean TFI percentage change between pre-chemotherapy and response assessment was -6.17 (SD 29.8) %.

5.3.2.2 Prevalence and pattern of sarcopenia at T4

The prevalence of sarcopenia at T4 – defined as T4SMI values below the 25th percentile - was 32/111 (28%) at pre-chemotherapy and 35/111 (32%) at response assessment time points (see Table 5.2). The median pre-chemotherapy and response assessment T4SMI were 54.3 [IQR 48.7 to 60.3] cm^2/m^2 and 53.1 [IQR 47.6 to 60.1] cm^2/m^2, respectively. The mean T4SMI percentage change between pre-chemotherapy and response assessment was -1.5 (SD 13.4) %.

Table 5.2 Body composition measurements at L3 (n=91) and T4 (n=111)

	Median [IQR] or mean (SD)	**n (%)**
Pre-chemotherapy		
L3SMI, cm^2/m^2	50 [44–57]	35/91 (35%)
TFI, cm^2/m^2	126.6 (57.6)	13/91 (14%)
T4SMI, cm^2/m^2	54.3 [48.7-60.3]	32/111 (28%)
Response assessment		
L3SMI, cm^2/m^2	47 [42–57]	44/91 (48%)
TFI, cm^2/m^2	122 (66.4)	14/91 (15%)
T4SMI, cm^2/m^2	53.1 [47.6-60.1]	35/111 (32%)
L3SMI: skeletal muscle index at the third lumbar vertebra; T4SMI: skeletal muscle index at the fourth thoracic vertebra; TFI: total fat index		

5.3.3 **Secondary objectives**

5.3.3.1.1L3 measures and systemic inflammation and tumour volume

Figure 5.2 illustrates associations of skeletal muscle and fat indices, inflammatory indices and tumour volume according to adjusted p-values. Patients with lower body weight had greater TFI and visceral fat index (VFI) percentage changes (r=-0.34, 95% CI -0.54 to -0.17, p<0.001, and r=-0.48, 95% CI -0.63 to -0.30, p<0.001, respectively). Similar, patients with lower BMI had higher TFI and VFI percentage changes (r=-0.41, 95% CI -0.57 to -0.22, p<0.001, and r=-0.44, 95% CI -0.59 to -0.25, p<0.001, respectively). Subcutaneous fat index (SFI) percentage change positively correlated with pre-chemotherapy weight (r=0.31, 95% CI 0.10 to 0.49, p=0.003) and BMI (r=0.36, 95% CI 0.16 to 0.53, p<0.001). VFI percentage change positively correlated with pre-chemotherapy platelets (r=0.30, 95% CI 0.08 to 0.49, p=0.006).

Tumour volume negatively correlated with pre-chemotherapy lymphocytes (r=-0.30, 95% CI -0.51 to -0.06, p=0.013) and positively correlated with pre-chemotherapy NLR (r=0.33, 95% CI 0.09 to 0.53, p=0.007), PLR (r=0.34, 95% CI 0.11 to 0.54, p=0.004) and CRP (r=0.30, 95% CI 0.02 to 0.54, p=0.032).

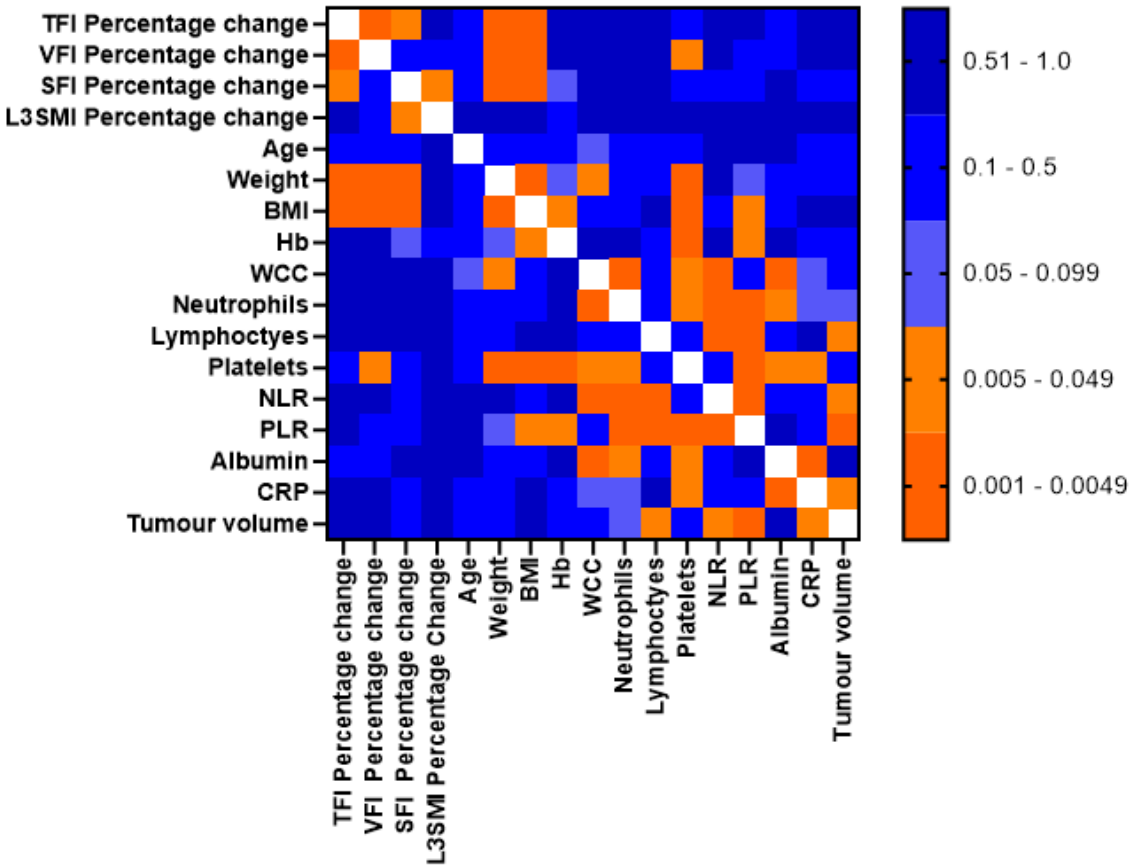

Figure 5.2 Heatmap of adjusted p-values summarising associations of L3 skeletal muscle and adipose indices and inflammatory indices and tumour volume in 91 patients with MPM

5.3.3.1.2 T4 measures and systemic inflammation and tumour volume

T4SMI percentage change did not correlate with any pre-chemotherapy inflammatory indices (see Figure 5.3, Panel A). T4SMI did not correlate with tumour volume (r=-0.03, 95% CI -0.25 to 0.20, p=0.819).

Ipsilateral T4SMI did not correlate with any pre-chemotherapy inflammatory indices (see Figure 5.3, Panel B). Ipsilateral T4SMI did not correlate with tumour volume (r=-0.14, 95% CI -0.36 to 0.087, p=0.210, see Figure 5.3, Panel B).

Tumour volume negatively correlated with pre-chemotherapy lymphocytes (r=-0.28, 95% CI -0.49 to -0.05, p=0.016) and positively correlated with pre-chemotherapy NLR (r=0.29, 95% CI 0.05 to 0.49, p=0.014), PLR (r=0.31, 95% CI 0.07 to 0.51, p=0.009) and CRP (r=0.32, 95% CI 0.05 to 0.55, p=0.018).

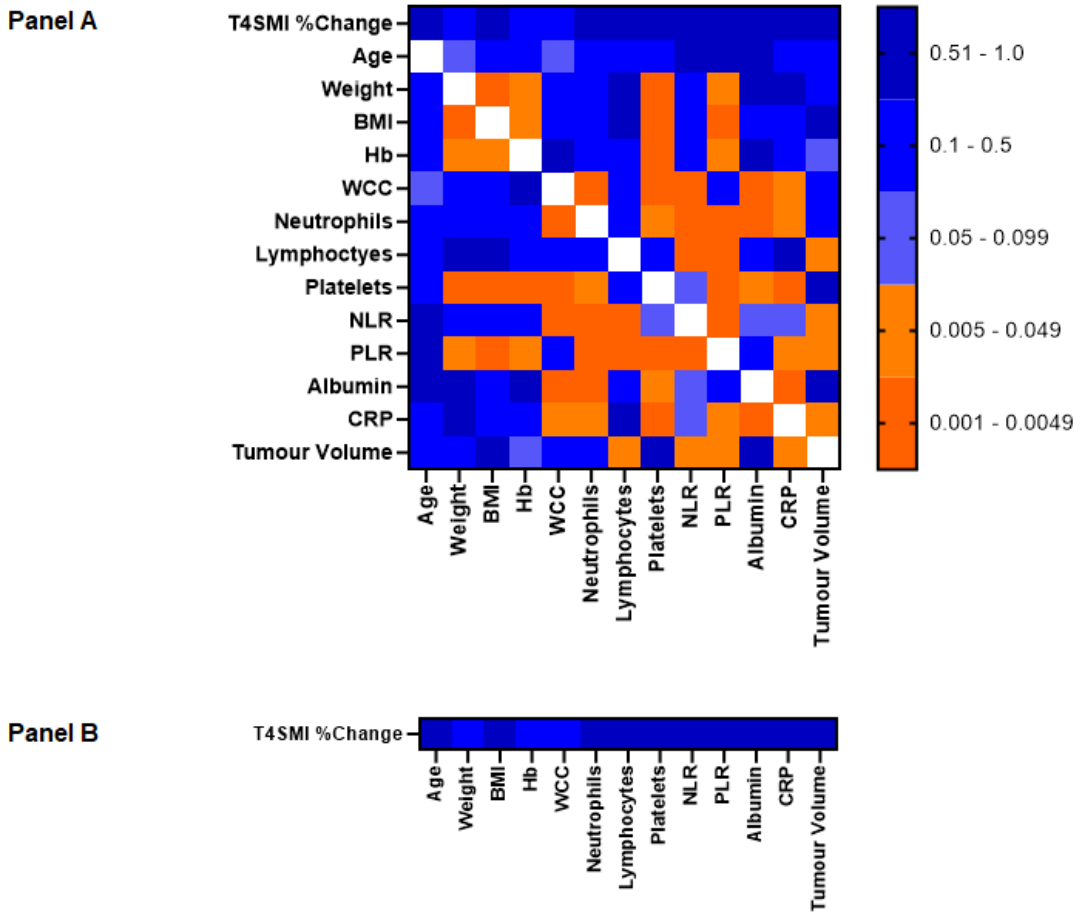

Figure 5.3 Heatmap of adjusted p-values summarising associations of total T4 skeletal muscle index percentage change (Panel A) and ipsilateral T4SMI percentage change (Panel B) and inflammatory indices and tumour volume in 111 patients with MPM

Table 5.3 summarises the pre-chemotherapy and response assessment inflammatory indices in a single centre sub-group of 47 patients. There was a weakly positive correlation between response assessment albumin and T4SMI percentage change (r=0.32, 95% CI 0.02 to 0.56, p=0.036, see Table 5.4). There were no correlations between ipsilateral T4SMI and pre-chemotherapy and response assessment inflammatory indices (see Table 5.4).

Table 5.3 Inflammatory indices between pre-chemotherapy and response assessment time points in a single centre sub-group of 47 patients with MPM

Pre-chemotherapy bloods	**Mean (SD) or median [IQR]**
WCC, $x10^9$/L	9.8 (3.2)
Neutrophils, $x10^9$/L	6.1 [5.1-8.2]
Lymphocytes, $x10^9$/L	1.7 (0.7)
Platelets, $x10^9$/L	353 [285-416]
NLR	3.9 [2.9-5.9]
PLR	249 (116)
Albumin, g/L	31.9 (6)
CRP, mg/L	33 [13.5-71.5]
Response assessment bloods	
WCC, $x10^9$/L	7.7 [5.9-11.6]
Neutrophils, $x10^9$/L	5 [2.7-8.4]
Lymphocytes, $x10^9$/L	1.2 [1.0-1.9]
Platelets, $x10^9$/L	338 [254-488]
NLR	3.9 [1.8-7.2]
PLR	264 [180-439]
Albumin, g/L	29.9 (7.0)
CRP, mg/L	62 [16-136]
CRP: C-reactive protein; NLR: neutrophil:lymphocyte ratio; PLR: platelet:lymphocyte ratio; WCC: white cell count	

Table 5.4 Correlation matrices of p-values of T4 skeletal muscle indices and inflammatory indices of a single centre sub-group of 47 patients with MPM

	Pre-chemotherapy							
	WCC	**Neutrophils**	**Lymphocytes**	**Platelets**	**NLR**	**PLR**	**Albumin**	**CRP**
T4SMI % change	0.168	0.408	0.159	0.793	0.338	0.636	0.513	0.642
Ipsilateral T4SMI % change	0.196	0.180	0.122	0.911	0.057	0.256	0.450	0.558
	Response assessment							
	WCC	**Neutrophils**	**Lymphocytes**	**Platelets**	**NLR**	**PLR**	**Albumin**	**CRP**
T4SMI % change	0.154	0.120	0.843	0.529	0.128	0.779	0.036	0.543
Ipsilateral T4SMI % change	0.106	0.072	0.835	0.634	0.095	0.747	0.206	0.638

CRP: C-reactive protein; NLR: neutrophil:lymphocyte ratio; PLR: platelet:lymphocyte ratio; T4SMI % and T4SMI Ipsilateral % change: percentage change in fourth thoracic vertebra (T4) skeletal muscle index and Ipsilateral T4SMI between pre-chemotherapy and response assessment time points; WCC: white cell count

When dichotomised into decreasing thoracic skeletal muscle index groups and increasing inflammatory indices groups, there was an association between ipsilateral T4SMI and NLR (X_2 4.97, p=0.026, see Table 5.5).

Table 5.5 Chi square of decreased T4SMI percentage change and increasing inflammatory indices between pre-chemotherapy and response assessment inflammatory indices in a single centre sub-group of 47 patients with MPM

	T4SMI		**Ipsilateral T4SMI**	
	X_2	**p-value***	X_2	**p-value***
WCC	0.015	0.901	1.091	0.296
Neutrophils	0.096	0.756	0.658	0.417
Lymphocytes	0.006	0.937	0.006	0.937
Platelets	0.643	0.423	0.672	0.412
NLR	0.018	0.894	4.968	0.026
PLR	0.073	0.787	0.006	0.937
Albumin	0.256	0.613	0.256	0.613
CRP	0.065	0.798	1.046	0.306
CRP: C-reactive protein; NLR: neutrophil:lymphocyte ratio; PLR: platelet:lymphocyte ratio; WCC: white cell count; X_2: chi square				

*Fisher's exact test

5.3.3.1.3 Survival at L3 and T4

5.3.3.1.3.1 Sarcopenia at L3

The pre-chemotherapy sarcopenia group trended towards shorter OS compared to the non-sarcopenia group (315 days versus 416 days, HR 1.49, 95% CI 0.95 to 2.52, p=0.077, see Figure 5.4: Panel A).

The response assessment sarcopenia group trended towards shorter OS compared to the non-sarcopenia group (334 days versus 420 days, HR 1.47, 95% CI 0.95 to 2.27, p=0.0702, see Figure 5.4: Panel B).

24 (26.4%) patients had a L3SMI percentage change loss of ≥9% (below 25th percentile) between pre-chemotherapy and response assessment time points. The decreased L3SMI did not have shorter OS compared to the non-sarcopenia group (369 days versus 375 days, HR 1.20, 95% CI 0.72 to 2.00, p=0.4456, see Figure 5.4: Panel C).

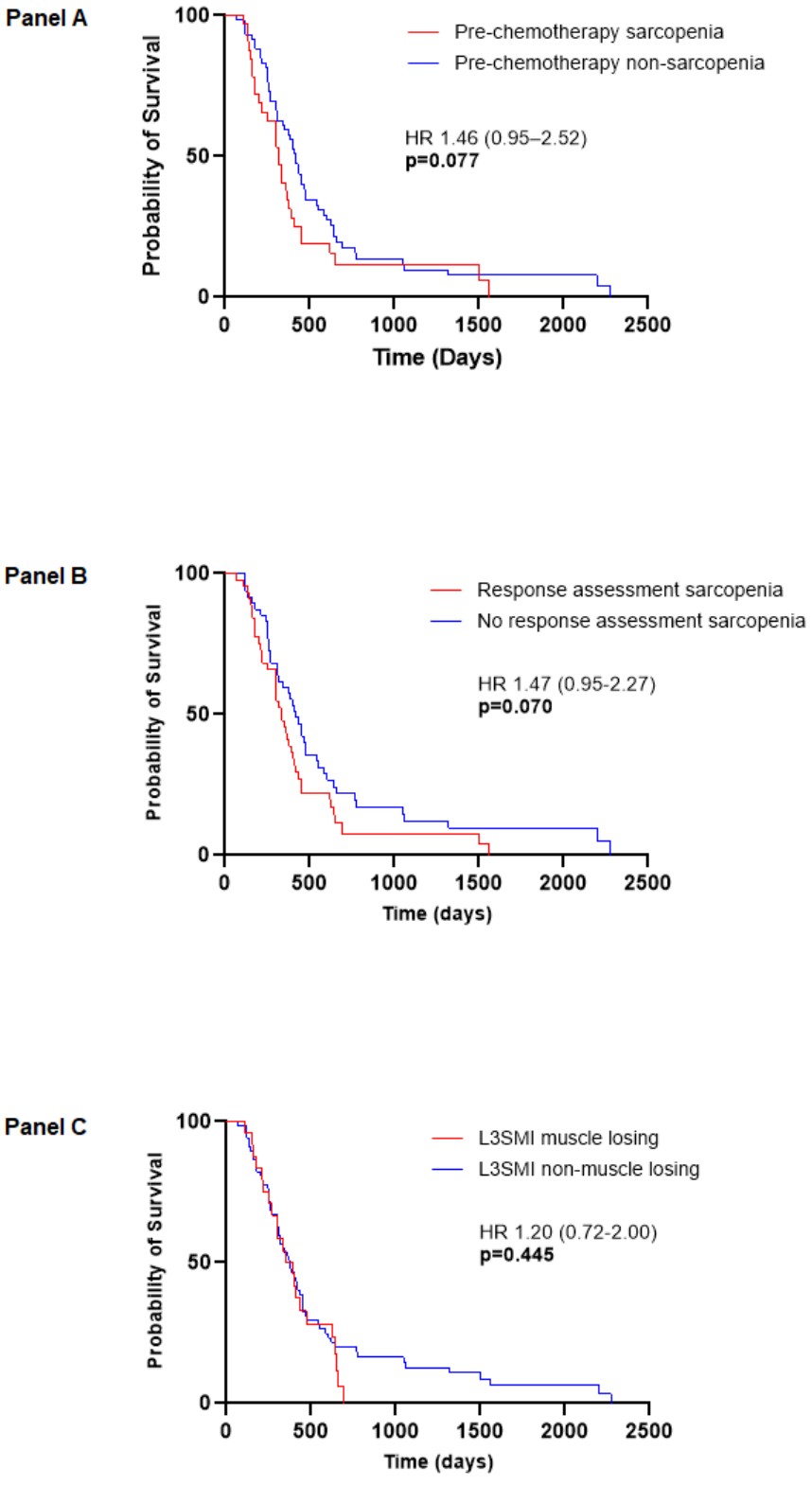

Figure 5.4 Kaplan-Meier curves and number at risk tables illustrating no survival differences in overall survival (OS) and L3 muscle index differences at pre-chemotherapy (Panel A) and response assessment (Panel B) time points and in patients who lose skeletal muscle at L3 during chemotherapy (Panel C)

5.3.3.1.3.2 Sarcopenia at T4

There was no difference in survival rates in the pre-chemotherapy T4SMI muscle losing and non-muscle losing groups (379 versus 399 days, HR 1.10, 95% CI 0.72 to 1.70, p=0.65, see Figure 5.5: Panel A).

There was no difference in survival rates in the response assessment T4SMI muscle losing and non-muscle losing groups (302 versus 438 days, HR 1.47, 95% CI 0.94 to 2.31, p=0.06, see Figure 5.5: Panel B).

Patients who had a T4SMI percentage change of -14.9% (mean minus 1 standard deviation) between pre-chemotherapy and response assessment time points were defined as losing muscle (n=15, 13.5%). The T4SMI muscle losing group had a shorter OS compared to the non-muscle losing group (215 versus 420 days, HR 2.79, 95% CI 1.22 to 6.40, p<0.0001, see Figure 5.5: Panel C).

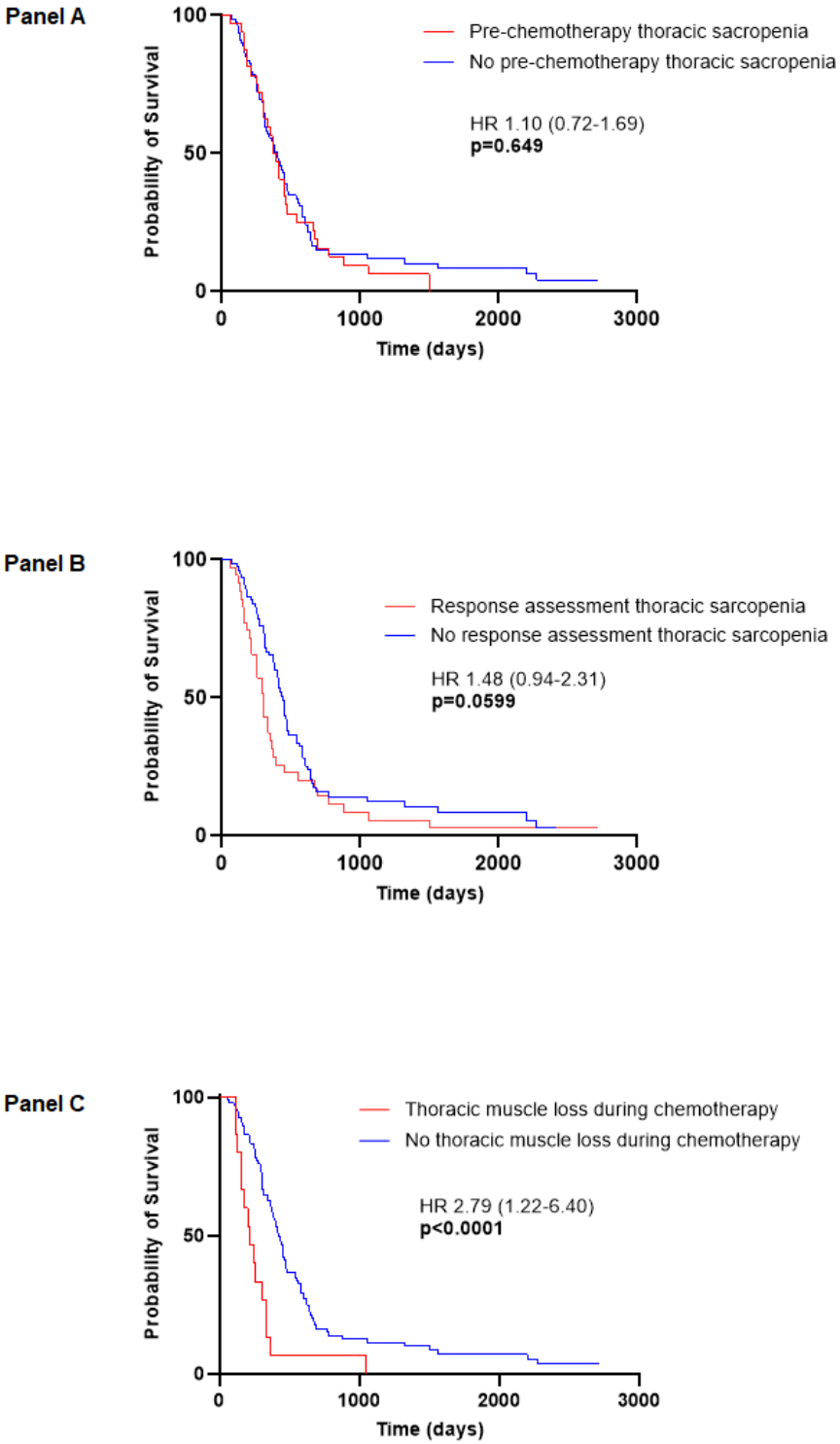

Figure 5.5 Kaplan-Meier curves and number at risk tables illustrating no survival differences in overall survival (OS) and pre-chemotherapy (Panel A) and response assessment (Panel B) fourth thoracic vertebra skeletal muscle indices. Panel C illustrates poorer OS in patients who lost thoracic skeletal muscle during chemotherapy (Panel C)

Sub-group analyses were performed with stratification by stage and pre-chemotherapy tumour volume. When stratified by stage, patients in the T4SMI muscle losing and disease stage>1 group had shorter OS than with patients who did not lose T4SMI with earlier-stage disease (253 versus 416 days, HR 2.31, 95% CI 0.91 to 5.87, p=0.0096, see Figure 5.6: Panel A). When stratified by pre-chemotherapy tumour volume, patients with in the decreased T4SMI group with tumour volume ≥377 cm3 had shorter OS than with patients who maintained T4SMI with lower tumour volume (233 versus 404 days, HR 4.58, 95% CI 0.86 to 24.46, p<0.0001, Figure 5.6: Panel B).

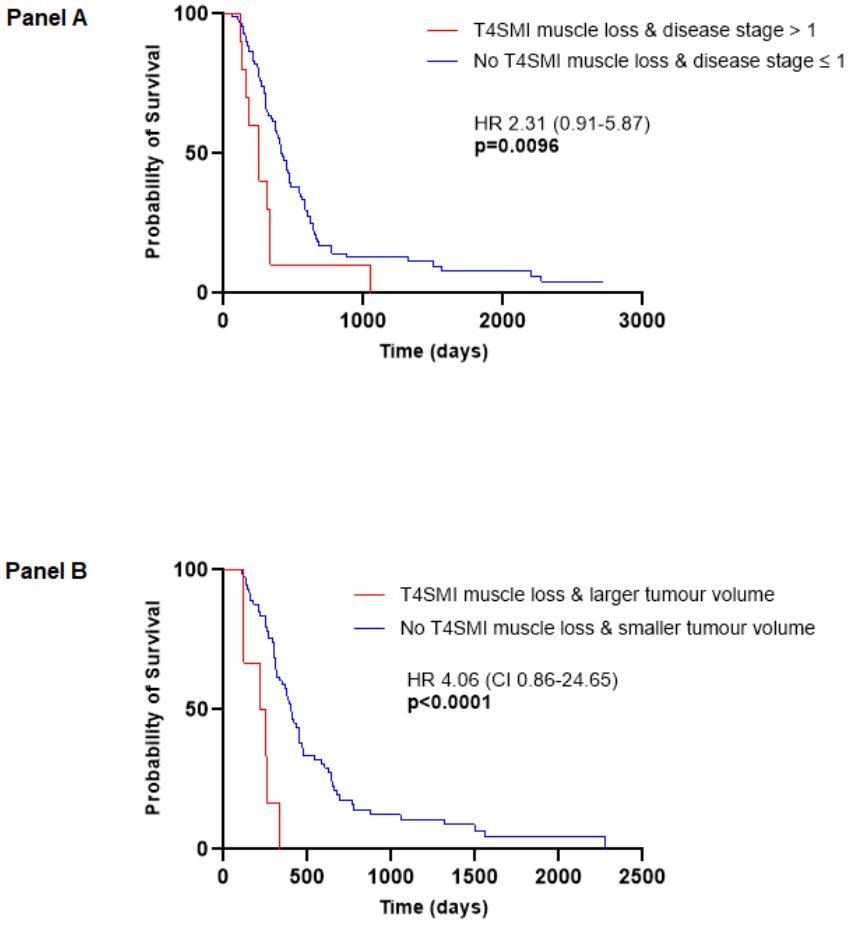

Figure 5.6 Kaplan-Meier curves and number at risk tables illustrating poorer OS in those patients with higher disease stage losing skeletal muscle at T4 during chemotherapy (Panel A) and in those patients with higher pre-chemotherapy tumour volume losing thoracic skeletal muscle during chemotherapy (Panel B)

Table 5.6 illustrates the survival differences of thoracic sarcopenia between males and females. There was no difference in survival in males or females with pre-chemotherapy thoracic sarcopenia (males 350 versus 401 days, HR 1.47, 95% CI 0.83 to 2.6, p=0.1358; and females 450 versus 266 days, HR 1.04, 95% CI 0.41 to 2.6, p=0.9364). Male patients with thoracic sarcopenia had shorter OS at the response assessment time point despite there being no survival difference when the entire cohort was assessed (293 versus 450 days, HR 1.87, 95% CI 1.08 to 3.25, p=0.0063). Male and female patients losing thoracic skeletal muscle during chemotherapy continued to have a shorter OS (males 233 versus 410 days, HR 2.48, 95% CI 1.1 to 5.61, p=0.0011; and females 155 versus 450 days, HR 21.12, 95% CI 0.003 to 136994, p<0.0001). It is important to note that only 1 event, i.e., muscle loss during chemotherapy, was available in the latter female survival analysis cohort which is reflected in the very wide confidence intervals reported.

Table 5.6 Hazard ratios from Log Rank test for T4SMI indices between males and females

	Hazard ratios	**95% CI**	**p-value**
Pre-chemotherapy			
T4SMI Males	1.47	0.83 to 2.6	0.1358
T4SMI Females	1.04	0.41 to 2.6	0.9364
Response assessment			
T4SMI Males	1.87	1.08 to 3.25	0.0063
T4SMI Females	1.18	0.48 to 2.94	0.7027
Muscle loss during chemotherapy			
T4SMI Males	2.48	1.1 to 5.61	0.0011
T4SMI Females	21.12	0.003 to 136994	<0.0001
T4SMI: skeletal muscle index at fourth thoracic vertebra			

Table 5.7 illustrates the univariate analyses of factors contributing to OS in patients with chemotherapy-treated MPM. Elevated pre-chemotherapy inflammatory markers (white cell count, neutrophils and CRP) as well as T4SMI and ipsilateral T4SMI muscle loss during chemotherapy were significant predictors for OS.

Two multivariate models are included in Table 5.7. In the first model, T4SMI muscle loss during chemotherapy (HR 2.15, 95% CI 1.02 to 4.54, p=0.045) and pre-chemotherapy neutrophils (HR 2.05, 95% CI 1.20 to 3.52, p=0.019) were significant predictors for OS. In the second model, T4SMI ipsilateral muscle loss during chemotherapy (HR 2.85, 95% CI 1.17 to 6.94, p=0.021) and higher neutrophils (HR 1.81, 95% CI 1.04 to 3.16, p=0.037) were significant predictors for OS.

Table 5.7 Univariate and multivariate analyses of factors contributing to overall survival in 111 patients with MPM

	Univariate		**Multivariate model 1**		**Multivariate model 2**	
Variables	**HR (95% CI)**	**p-value**	**HR (95% CI)**	**p-value**	**HR (95% CI)**	**p-value**
Age ≥69	1.026 (0.694–1.516)	0.899				
Male gender	1.439 (0.858–2.414)	0.168				
ECOG PS >0	1.039 (0.648–1.667)	0.874				
Epithelioid	0.611 (0.373–1.004)	0.052				
Non-epithelioid	1.611 (0.910–2.852)	0.121				
Disease stage >I	1.480 (0.971–2.256)	0.069				
Pre-chemotherapy weight ≤75.9 kg	1.188 (0.803–1.757)	0.389				
Pre-chemotherapy BMI ≥30 kg/m^2	0.639 (0.397-1.028)	0.065				
Pre-chemotherapy BMI ≤18.5 kg/m^2	1.353 (0.425-431)	0.609				
Pre-chemotherapy WCC ≥8.6 x 10^9/L	1.637 (1.079–2.484)	0.021				
Pre-chemotherapy neutrophils ≥5.7 x 10^9/L	1.841 (1.190–2.847)	0.006	2.050 (1.195-3.517)	0.019	1.809 (1.037-3.155)	0.037

Pre-chemotherapy lymphocytes ≥1.5 x 10^9/L	0.967 (0.643–1.454)	0.872				
Pre-chemotherapy platelets ≥244 x 10^9/L	1.493 (0.993–2.246)	0.054				
Pre-chemotherapy NLR ≥4.1	1.380 (0.902–2.110)	0.138				
Pre-chemotherapy PLR ≥234	1.258 (0.828–1.912)	0.283				
Pre-chemotherapy albumin ≤35 g/L	1.263 (0.834–1.914)	0.270				
Pre-chemotherapy CRP ≥25 mg/L	1.849 (1.119–3.057)	0.017	1.500 (0.889-1.500)	0.129	1.576 (0.939-2.645)	0.085
Pre-chemotherapy tumour volume ≥377 cm^3	1.563 (0.978–2.498)	0.062				
T4SMI percentage change muscle loss	2.923 (1.66-5.146)	<0.001	2.147 (1.016-4.537)	0.045		
Ipsilateral T4SMI percentage change muscle loss	3.24 (1.823-5.76)	<0.001			2.853 (1.173-6.939)	0.021

BMI: body mass index; CI: confidence interval; CRP: C-reactive protein; ECOG PS: Eastern Cooperative Oncology Group performance status; Hb: haemoglobin; HR: hazard ratio; NLR: neutrophil:lymphocyte ratio; PLR: platelet:lymphocyte ratio; T4SMI: skeletal muscle index at fourth thoracic vertebra; WCC: white cell count

5.3.3.1.3.3 Adipopenia at L3

There was a statistically significant difference in OS between the pre-chemotherapy total fat index (TFI, cm2/m2) losing and non-losing groups (336 versus 380 days, HR 1.65, 95% CI 0.91 to 3.25, p=0.0038). Pre-chemotherapy visceral fat index (VFI, cm2/m2) loss trended towards significance (339 versus 379 days, HR 1.68, 95% CI 0.88 to 3.24, p=0.051). Patients with lower pre-chemotherapy subcutaneous fat index (SFI, cm2/m2) had shorter OS compared to those with higher SFI (317 versus 394 days, HR 1.82, 95% CI 1.02 to 3.26 p=0.011). Patients with lower response assessment TFI did not have shorter OS compared to those with higher TFI (308 versus 382 days, HR 1.71, 95% CI 0.85 to 3.43, p=0.058). There was no statistically significant difference in the response assessment VFI losing and non-losing groups (320 versus 379 days, HR 1.72, 95% CI 0.85 to 3.45, p=0.057). Patients with lower response assessment SFI had shorter OS compared to those with higher SFI (307 versus 401 days, HR 1.93, 95% CI 1.07 to 3.48, p=0.005)

Table 5.8 Hazard ratios from Log Rank test for pre-chemotherapy and response assessment adipose tissue indices in 91 patients with MPM

	Hazard ratios	**95% CI**	**p-value**
Pre-chemotherapy			
TFI	1.72	0.91 to 3.25	0.038
VFI	1.68	0.88 to 3.24	0.051
SFI	1.82	1.02 to 3.26	0.011
Response assessment			
TFI	1.71	0.85 to 3.43	0.058
VFI	1.72	0.85 to 3.45	0.057
SFI	1.93	1.07 to 3.48	0.005
SFI: subcutaneous fat index; TFI: total fat index; VFI: visceral fat index			

Thresholds for low and high adipose tissue mass were determined as those patients below the 25th percentile for TFI, VFI and SFI based on distribution of percentage changes between pre-chemotherapy and response assessment time points.

There were no statistically significant differences between patients who lost TFI between pre-chemotherapy and response assessment time points and those who did not (305 versus 394 days, HR 1.54, 95% CI 0.88 to 2.69, p=0.0793, see Figure 5.7: Panel A).

Patients who lost VFI between pre-chemotherapy and response assessment time points had shorter OS compared to those with higher VFI (272 versus 401 days, HR 1.95, 95% CI 1.05 to 3.62, p=0.0067, see Figure 5.7: Panel B).

There were no statistically significant differences between patients who lost SFI between pre-chemotherapy and response assessment time points and those who did not (336 versus 380 days, HR 1.24, 95% CI 0.73 to 2.18, p=0.386), see Figure 5.7: Panel C).

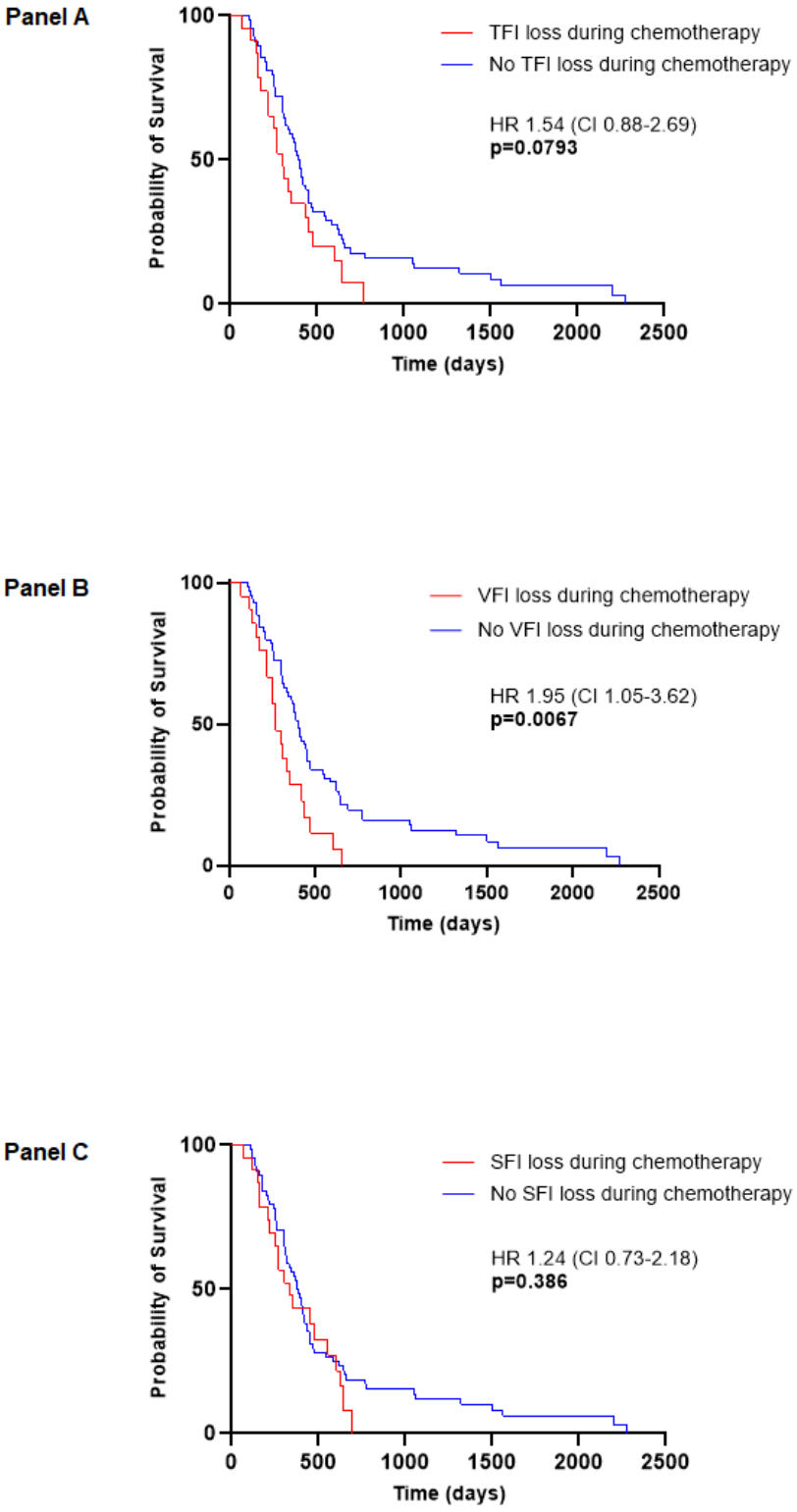

Figure 5.7 Kaplan-Meier curves and number at risk tables illustrating the survival advantage afforded by not losing total fat (Panel A) and visceral fat (Panel B) between pre-chemotherapy and response assessment time points. Subcutaneous fat tissue loss was not associated with overall survival (Panel C)

Table 5.9 illustrates the univariate and multivariate analyses of factors contributing to OS in patients with L3SMI and adipose indices. Epithelioid sub-type, elevated pre-chemotherapy BMI, visceral fat loss during chemotherapy and elevated pre-chemotherapy inflammatory markers (pre-chemotherapy lymphocytes and neutrophils) were significant predictors for OS.

The multivariate models are illustrated in Table 5.9. The multivariate models are illustrated in Table 5.9. Epithelioid subtype (HR 0.47, 95% CI 0.26 to 0.86, p=0.014), obesity (HR 0.36, 95% CI 0.20 to 0.65, p<0.001), greater VFI percentage change loss (HR 1.81, 95% CI 1.04 to 3.13, p=0.035) and higher pre-chemotherapy neutrophils (HR 1.62, 95% CI 1.01 to 1.62, p=0.048) were significant independent predictors for OS. Obesity was significant and outperformed MPM sub-type and NLR which are both established prognostic variables.

Table 5.9 Univariate and multivariate analyses of factors contributing to overall survival in 91 patients with MPM

	Univariate		**Multivariate**	
Variables	**HR (95% CI)**	**p-value**	**HR (95% CI)**	**p-value**
Age ≥69	1.14 (0.732-1.774)	0.563		
Male gender	1.564 (0.904-2.705)	0.110		
ECOG PS >0	1.139 (0.685-1.893)	0.614		
Epithelioid	0.517 (0.296-0.903)	0.020	0.472 (0.261-0.856)	0.014
Disease stage >I	1.532 (0.952-2.464)	0.077		
Pre-chemotherapy weight ≤75.9 kg	1.373 (0.888-2.123)	0.154		
Pre-chemotherapy BMI ≥30 kg/m^2	0.418 (0.240-0.730)	0.002	0.361 (0.202-0.647)	<0.001
Pre-chemotherapy BMI ≤18.5 kg/m^2	1.207 (0.378-3.859)	0.751		
Pre-chemotherapy WCC ≥8.6 $x10^9/L$	1.405 (0.891-2.215)	0.143		
Pre-chemotherapy neutrophils ≥5.7 $x10^9/L$	1.762 (1.093-2.839)	0.020	1.623 (1.005-1.621)	0.048
Pre-chemotherapy lymphocytes ≥1.5 $x10^9/L$	1.145 (0.731-1.792)	0.555		

Pre-chemotherapy platelets ≥244 x10^9/L	1.231 (0.787-1.928)	0.363		
Pre-chemotherapy NLR ≥4.1	1.246 (0.784-1.981)	0.352		
Pre-chemotherapy PLR ≥234	1.185 (0.749-1.875)	0.469		
Pre-chemotherapy albumin ≤35 g/L	1.401 (0.881-2.229)	0.155		
Pre-chemotherapy CRP ≥25 mg/L	1.672 (0.951-2.943)	0.074		
Pre-chemotherapy tumour volume ≥377 cm^3	1.595 (0.977-2.605)	0.062		
L3SMI muscle loss	1.231 (0.748-2.027)	0.423		
TFI loss (percentage change)	1.799 (0.965-3.356)	0.084		
VFI loss (percentage change)	2.048 (1.166-3.595)	0.008	1.807 (1.043-3.131)	p=0.035
BMI: body mass index; CI: confidence interval; CRP: C-reactive protein; ECOG PS: Eastern Cooperative Oncology Group performance status; Hb: haemoglobin; HR: hazard ratio; NLR: neutrophil:lymphocyte ratio; PLR: platelet:lymphocyte ratio; T4SMI: skeletal muscle index at fourth thoracic vertebra; WCC: white cell count				

5.3.3.1.4Reproducibility at L3

L3SMI intra-observer agreement was excellent (ICC 0.987, 95% CI 0.975 to 0.994, p=0.000), with a mean difference of -2.8 (SD 3.8) cm^2/m^2. L3SMI inter-observer agreement was excellent (ICC 0.985, 95% CI 0.971 to 0.992, p=0.000), with a mean difference of -3.0 (SD 2.0) cm^2/m^2.

Inter-observer agreement was excellent for VFI (ICC 0.998, 95% CI 0.997 to 0.999, p<0.0001) and SFI (ICC 0.996, 95% CI 0.992 to 0.998, p<0.0001). TFI ICC, by definition, was 1.0 as it is the sum of VFI and SFI. Intra-observer agreement was excellent for VFI (ICC 0.962, 95% CI 0.925 to 0.981, p<0.001) and SFI (ICC 0.969, 95% CI 0.938 to 0.984, p<0.001). TFI ICC, by definition, was 1.0 as it is the sum of VFI and SFI.

5.3.3.1.5Reproducibility at T4

T4SMI intra-observer agreement was excellent (ICC 0.988, 95% CI 0.977 to 0.994, p=0.000), with a mean difference of -0.7 (SD 2.2) cm^2/m^2. T4SMI inter-observer agreement was good (ICC 0.831, 95% CI 0.665 to 0.915, p=0.000), with a mean difference of 2.2 (SD 8.9) cm^2/m^2.

5.3.4 **Exploratory objectives**

5.3.4.1 Ipsilateral T4 and survival

T4SMI was divided into ipsilateral and contralateral compartments as demonstrated in Chapter 2, Section 2.3.6.3. The median pre-chemotherapy and response assessment ipsilateral T4SMI were 26.3 [IQR 23.6 to 29.8] cm^2/m^2 and 25.9 [IQR 23.1 to 29.4] cm^2/m^2, respectively. Patients with ipsilateral T4SMI muscle loss of 16.9% (mean minus 1 standard deviation) were included.

Patients in the muscle losing pre-chemotherapy group did not have improved OS than the non-losing ipsilateral T4SMI group (399 versus 382 days, HR 1.02, 95% CI 0.65 to 1.59, p=0.9245, see Figure 5.8: Panel A).

Patients in the muscle losing response assessment ipsilateral T4SMI group had shorter OS than the non-losing muscle losing group (297 versus 433 days, HR 1.78, 95% CI 1.05 to 3.02, p=0.0093, see Figure 5.8: Panel B).

Patients who had an ipsilateral T4SMI percentage change of -16.9% (mean minus 1 standard deviation) between pre-chemotherapy and response assessment time points were defined as those losing muscle (n=16, 14.4%). The ipsilateral T4SMI muscle losing group had a shorter OS compared to the non-muscle losing group (255 versus 433 days, HR 2.91, 95% CI 1.28 to 6.59, p<0.0001), Figure 5.8: Panel C).

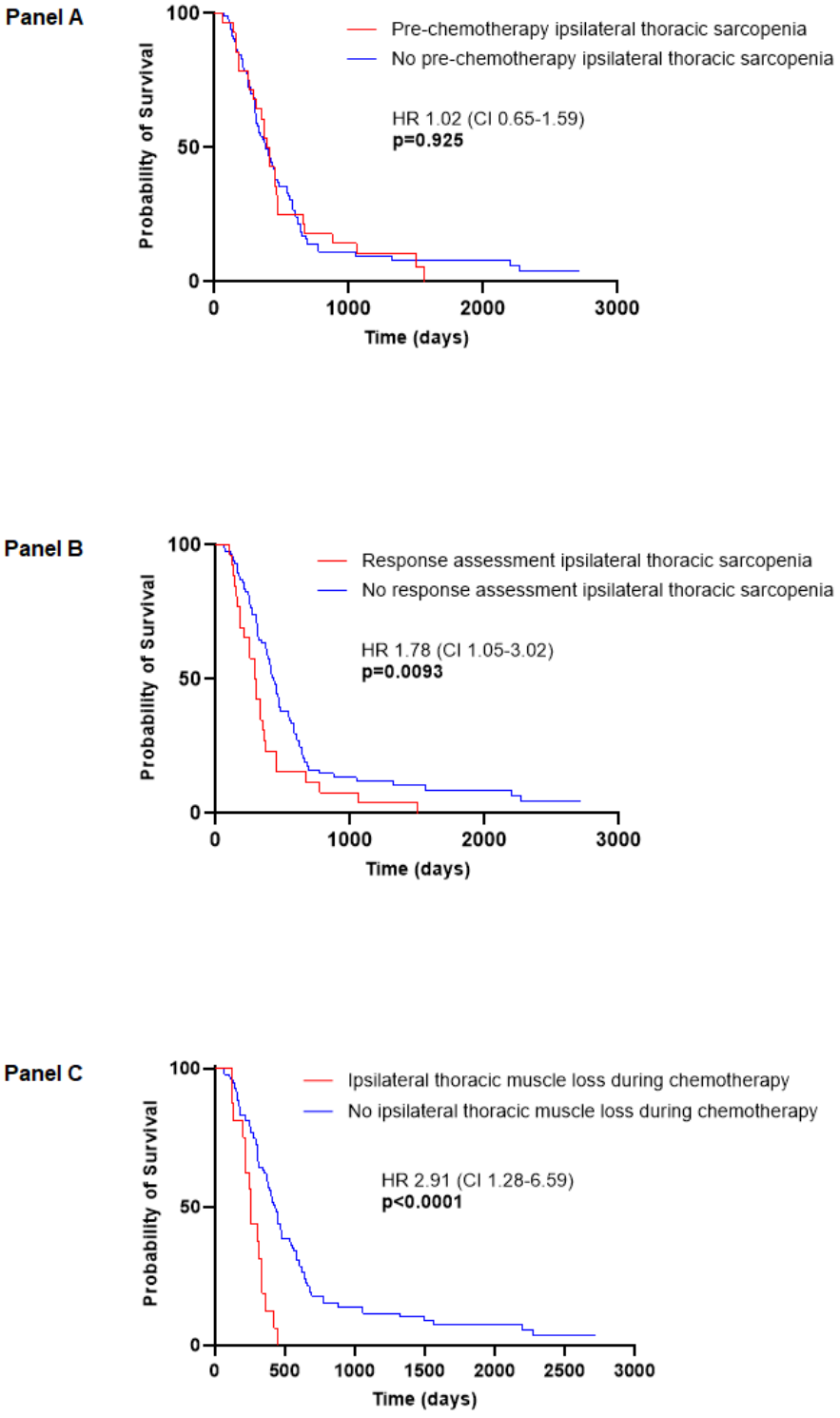

Figure 5.8 Kaplan-Meier curves and number at risk tables illustrating overall survival stratified by muscle losing and non-losing groups, Panel A) pre-chemotherapy ipsilateral (to tumour) T4SMI, Panel B), response assessment ipsilateral T4SMI, and, Panel C) ipsilateral T4SMI percentage change between pre-chemotherapy and response assessment scans

5.3.4.2 Chemotherapy treatment completion and response to treatment

5.3.4.2.1 Relationship between chemotherapy treatment completion and response to treatment at L3

33 (37.4%) patients received less than four cycles of chemotherapy due to toxicity, progression whilst on treatment or death. 8/15 (61.5%) patients in the TFI percentage change losing group received less than 4 cycles of chemotherapy. 26/78 (33.3%) patients in the TFI percentage change non-losing group received less than 4 cycles. This was not statistically significant (p=0.067, using Fisher's exact test). 9/17 (52.9%) patients in the TFI percentage change losing group received less than 4 cycles of chemotherapy. 25/74 (75.3%) patients in the TFI percentage change non-losing group received less than 4 cycles. This was not statistically significant (p=0.1697, using Fisher's exact test).

The mean percentage changes in TFI in patients who had mRECIST-defined progressive disease (PD), stable disease (SD) and partial response (PR) were -16.65 (SD 31.33) %, -2.972 (SD 24.4) % and -2.680 (SD 35.4) %, respectively. Response to chemotherapy was not associated with percentage change in TFI (p=0.1748, see Figure 5.9: Panel A). When dichotomised into mRECIST-defined PD and non-PD (SD and PR), response to chemotherapy was not associated with percentage change in TFI (-16.65 (SD 31.33) % versus -2.85 (SD 2.1) %, p=0.061). The median percentage changes in VFI in patients who had mRECIST-defined PD, SD and PR were -15 [IQR -51 to 0] %, -15.5 [IQR -27.8 to 19] % and -10 [IQR -29.5 to 26] %, respectively. Response to chemotherapy was not associated with percentage change in VFI (p=0.4491, see Figure 5.9: Panel B). When dichotomised into mRECIST-defined PD and non-PD, response to chemotherapy was not associated with percentage change in VFI (-15 [IQR -51 to 0] % versus -15 [IQR -28.5 to 21.5] %, p=0.2123).

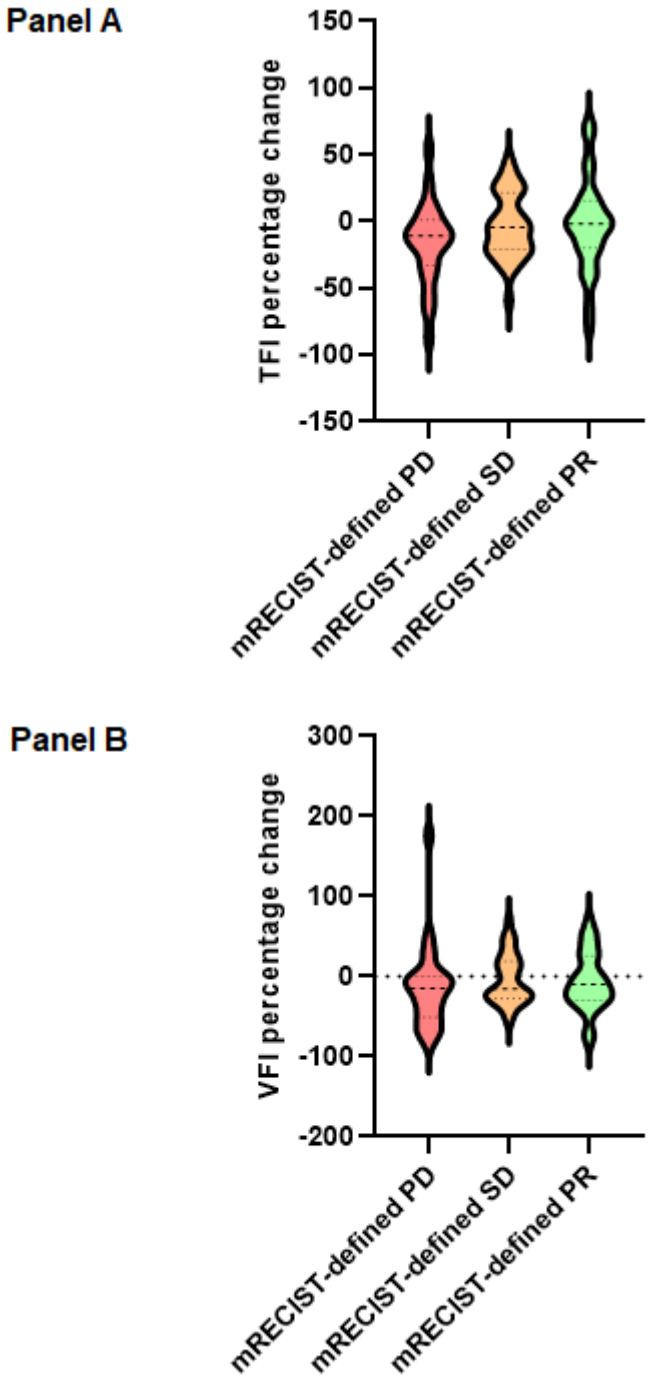

Figure 5.9 Scatterplot illustrating mRECIST-defined response assessment criteria and percentage changes between pre-chemotherapy and response assessment scans in, Panel A) total fat index (TFI), and, Panel B) visceral fat index (VFI) in 91 patients with MPM

PD: progressive disease; PR: partial response; SD: stable disease

5.3.4.2.2 Relationship between chemotherapy treatment completion and response to treatment at T4

36 (32%) patients received less than four cycles of chemotherapy due to toxicity, progression whilst on treatment or death. 6/15 (40%) patients in the T4SMI percentage change muscle losing group received less than 4 cycles of chemotherapy. 30/96 (31%) patients in the T4SMI percentage change muscle retaining group received less than 4 cycles. There was no statistically significant difference (p=0.5579, using Fisher's exact test). 7/15 (46.7%) patients in the ipsilateral T4SMI percentage change muscle losing group received less than 4 cycles of chemotherapy. 30/96 (31%) patients in the ipsilateral T4SMI percentage change muscle retaining group received less than 4 cycles. There was no statistically significant difference (p=0.3870, using Fisher's exact test).

The mean percentage changes in T4SMI in patients who had mRECIST-defined progressive disease (PD), stable disease (SD) and partial response (PR) were -3.01 (SD 14.26) %, -1.94 (SD 14.21) % and 1.09 (SD 11.97) %, respectively. Response to chemotherapy as defined by mRECIST was not associated with percentage change in T4SMI (p=0.4701, see Figure 5.10: Panel A). When dichotomised into mRECIST-defined PD and non-PD (SD and PR), response to chemotherapy was not associated with percentage change in T4SMI (-3.01 (SD 14.26) % versus -0.99 (SD 13.37) %, p=0.5084). The mean percentage changes in ipsilateral T4SMI in patients who had mRECIST-defined PD, SD and PR were -2.86 (SD 13.97) %, 3.08 (SD 20.32) % and -1.13 (SD 14.31) %, respectively. Response to chemotherapy was not associated with percentage change in ipsilateral T4SMI (p=0.3166, see Figure 5.10: Panel B). When dichotomised into mRECIST-defined PD and non-PD, response to chemotherapy was not associated with percentage change in ipsilateral T4SMI (-2.86 (SD 13.97) % versus 1.03 (SD 17.97) %, p=0.3098).

The mean percentage changes in T4SMI in patients who had human volume-defined PD, SD and PR were -7.58 (SD 12.13) %, -5.97 (SD 10.85) % and 6.73 (SD 15.17) %, respectively (n=30). Response to chemotherapy was not associated with percentage change in T4SMI (p=0.1285, see Figure 5.10: Panel C). When dichotomised into human volume-defined PD and non-PD, response to

chemotherapy was not associated with percentage change in T4SMI (-7.58 (SD 12.13) % versus -3.94 (SD 12.23) %, p=0.5474). The mean percentage changes in ipsilateral T4SMI in patients who had human volume-defined PD, SD and PR were -7.24 (SD 10.88) %, -3.44 (SD 13.82) % and -0.98 (SD 20.16) %, respectively (n=30). Response to chemotherapy was not associated with percentage change in ipsilateral T4SMI (p=0.7965, see Figure 5.10: Panel D). When dichotomised into human volume-defined PD and non-PD, response to chemotherapy was not associated with percentage change in ipsilateral T4SMI (7.24 (SD 10.88) % versus -3.04 (SD 14.52) %, p=0.5473).

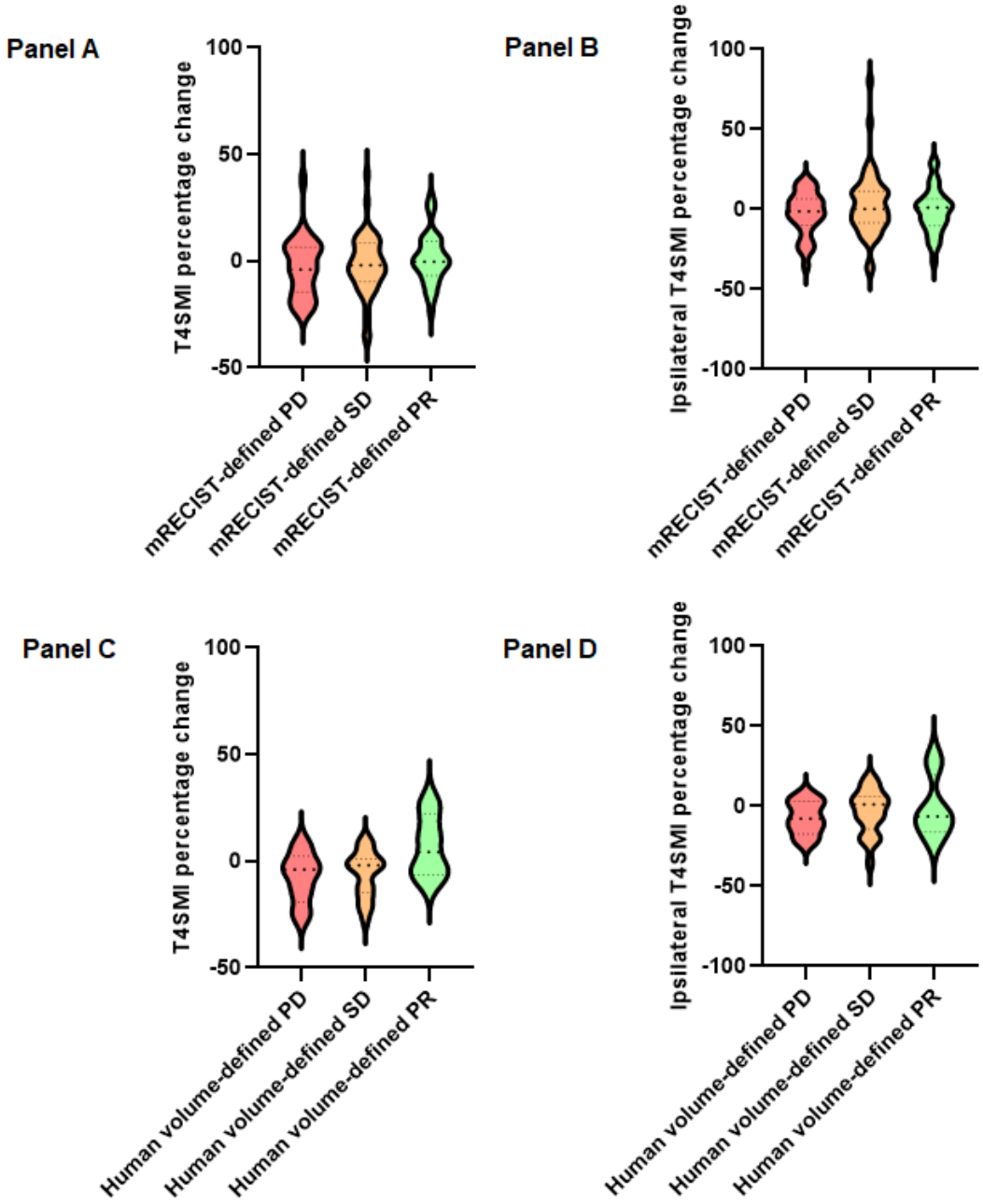

Figure 5.10 Violin plots illustrating fourth thoracic vertebra skeletal muscle index (T4SMI) and ipsilateral (to tumour) T4SMI percentage changes between pre-chemotherapy and response assessment scans and response assessment criteria according to, Panels A) and, Panel B) mRECIST, and, Panel C) and, Panel D) human volumes in 111 patients with MPM

PD: progressive disease; PR: partial response; SD: stable disease

5.3.4.3 Sex-and BMI-specific differences

5.3.4.3.1 Sex-specific differences at L3

Table 5.10 summarises the sex-specific differences in skeletal muscle and adipose tissue indices at L3. Male patients had a higher mean pre-chemotherapy L3SMI than females (52.1 (SD 7.9) cm^2/m^2 versus 45.2 (SD 8.9) cm^2/m^2, p=0.012, respectively). Males also had higher median response assessment L3SMI than females (48 [IQR 43 to 58] cm^2/m^2 versus 41 [IQR 40 to 48] cm^2/m^2, p=0.001, respectively). There was a statistically significant difference in pre-chemotherapy visceral fat indices (VFI) between male (59 [IQR 40 to 91] cm^2/m^2) and female patients (41 [IQR 8 to 66] cm^2/m^2, (p=0.0095). There was a trend towards significance in pre-chemotherapy subcutaneous fat indices (SFI) between male (58 [IQR 45 to 72] cm^2/m^2) and female patients (89 [IQR 33 to 120] cm^2/m^2), respectively (p=0.0529). There was no statistically significant difference in pre-chemotherapy total fat index (TFI) between male (124 [IQR 95 to 152] cm^2/m^2) and female patients (148 [IQR 50 to 176] cm^2/m^2), respectively (p=0.9325). There was a statistically significant difference in response assessment visceral fat index (VFI) between male (52 [IQR 34 to 79] cm^2/m^2) and female patients (32 [IQR 8 to 94] cm^2/m^2), respectively (p=0.0138). There was no statistically significant difference in response assessment subcutaneous fat index (TFI) between male (61 [IQR 38 to 78] cm^2/m^2) and female patients (82 [IQR 28 to 115] cm^2/m^2), respectively (p=0.1059). There was no statistically significant difference in response assessment total fat index (TFI) between male (116 [IQR 74 to 152] cm^2/m^2) and female patients (120 [IQR 32 to 187] cm^2/m^2), respectively (p=0.9132).

Table 5.10 Sex-specific differences in skeletal muscle and adipose indices at L3 in 91 patients with MPM

	Male Mean (SD) or median [IQR]	**Female Mean (SD) or median [IQR]**	**p-value**
Pre-chemotherapy			
Pre-chemotherapy L3SMI, cm^2/m^2	52.1 (7.9)	45.2 (8.9)	0.0012
Total fat index, cm^2/m^2	124 [95-152]	148 [50-176]	0.9325
Visceral fat index, cm^2/m^2	59 [40-91]	41 [8-66]	0.0095
Subcutaneous fat index, cm^2/m^2	58 [45-72]	89 [33-120]	0.0529
Response assessment			
Response assessment L3SMI, cm^2/m^2	48 [43–58]	41 [40–48]	0.0010
Total fat index, cm^2/m^2	116 [74-152]	120 [32-187]	0.9132
Visceral fat index, cm^2/m^2	52 [34-79]	32 [8-94]	0.0138
Subcutaneous fat index, cm^2/m^2	61 [38-78]	82 [28-115]	0.1059
SMI: skeletal muscle index, cm^2/m^2			

5.3.4.3.2 Sex-and BMI-specific differences at T4

Table 5.11 summarises the skeletal muscle indices at T4 in the study cohort. Males had a higher pre-chemotherapy weight than females (78.7 (SD 13.9) kg and 63.3 (SD 10.3) kg, respectively, p<0.0001). There were no differences in pre-chemotherapy BMI between males and females (26.7 (SD 4.1) kg/m^2 and 25.1 (SD 4.1) kg/m^2, respectively, p=0.1371).

Male patients had a higher mean pre-chemotherapy T4SMI than females (56.7 (SD 8.3) cm^2/m^2 versus 47.9 (SD 6.2) cm^2/m^2, p<0.0001). Males also had higher mean response assessment T4SMI than females (54.8 (SD 9.8) cm^2/m^2 versus 50.1 (SD 7.3) cm^2/m^2, p=0.0457).

Patients with higher BMI – defined as overweight as per the WHO definition of BMI ≥25 kg/m^2 – did not have a higher mean pre-chemotherapy T4SMI than those patients with lower BMI (54 [IQR 48 to 60] kg/m^2 versus 54 [IQR 49 to 60] kg/m^2, p=0.622). Patients with higher BMI also did not have a higher mean response assessment T4SMI than those patients with lower BMI (52 [IQR 47 to 60.5] kg/m^2 versus 53.5 [IQR 48 to 59.3] kg/m^2, p=0.868).

Table 5.11 Body composition analyses at T4 in 111 patients with MPM

	All patients (n=111) Mean (SD) or median [IQR]	**Male (n=91) Mean (SD) or median [IQR]**	**Female (n=20) Mean (SD) or median [IQR]**	**p-value**
Pre-chemotherapy				
PC Weight, kg	75.9 (14.5)	78.7 (13.9)	63.3 (10.2)	<0.0001
PC BMI, kg/m^2	26.4 (4.1)	26.7 (4.1)	25.1 (4.1)	0.1371
T4SMI, cm^2m^2	55.1 (8.6)	56.7 (8.3)	47.9 (6.1)	<0.0001
Ipsilateral T4SMI, cm^2m^2	26.8 (4.7)	28.3 (7.2)	23.1 (3.4)	0.0024
Contralateral T4SMI, cm^2m^2	28.2 (4.4)	28.9 (4.2)	25.8 (3.6)	<0.0001
Response assessment				
T4SMI, cm^2m^2	53.9 (9.5)	54.8 (9.8)	50.1 (7.3)	0.0457
Ipsilateral T4SMI, cm^2m^2	25.9 [23.1-29.4]	26.8 [23.4-29.7]	23.7 [21.1-25.8]	0.0069
Contralateral T4SMI, cm^2m^2	26.8 [23.6-30.5]	27.6 [23.8-31]	25.1 [22.6-28.8]	0.1140
Percentage change between pre-chemotherapy and response assessment				
T4SMI, %	-1.5 (13.4)	-2.9 (12.9)	5.2 (14)	0.0143
Ipsilateral T4SMI, %	-0.1 (16.8)	-1.4 (15.3)	5.5 (22)	0.0952
BMI: body mass index; T4SMI: skeletal muscle index at fourth thoracic vertebra; Ipsilateral & Contralateral T4SMI: skeletal muscle index at T4 on ipsilateral and contralateral side of tumour, respectively				

5.3.4.4 Correlation between L3 and T4

Pre-chemotherapy L3SMI and T4SMI were moderately correlated (r=0.42, 95% CI 0.23 to 0.58, p<0.0001, see Figure 5.11: Panel A). When assessed according to sex, pre-chemotherapy L3SMI and T4SMI continued to correlate in males (r=0.36, 95% CI 0.16 to 0.56, p=0.0006, Figure 5.11: Panel B), but the strength of correlation was lost in females (r=0.29, 95% CI -0.34 to 0.74, p=0.3657, see Figure 5.11: Panel C).

Response assessment T4SMI and L3SMI were also moderately correlated (r=0.45, 95% CI 0.27 to 0.61, p<0.0001, see Figure 5.11: Panel D). The correlation was made stronger in males only (r=0.48, 95% CI 0.28 to 0.65, p<0.0001, Figure 5.11: Panel E). The strength of correlation was again diminished in females (r=0.28, 95% CI -0.37 to 0.74, p=0.3786, Figure 5.11: Panel F).

Pre-chemotherapy T4SMI and L3TFI did not correlate (r=-0.07, 95% CI -0.29 to 0.16, p=0.5382). Response assessment T4SMI and L3TFI did not correlate (r=0.03, 95% CI -0.18 to 0.24, p=0.7538).

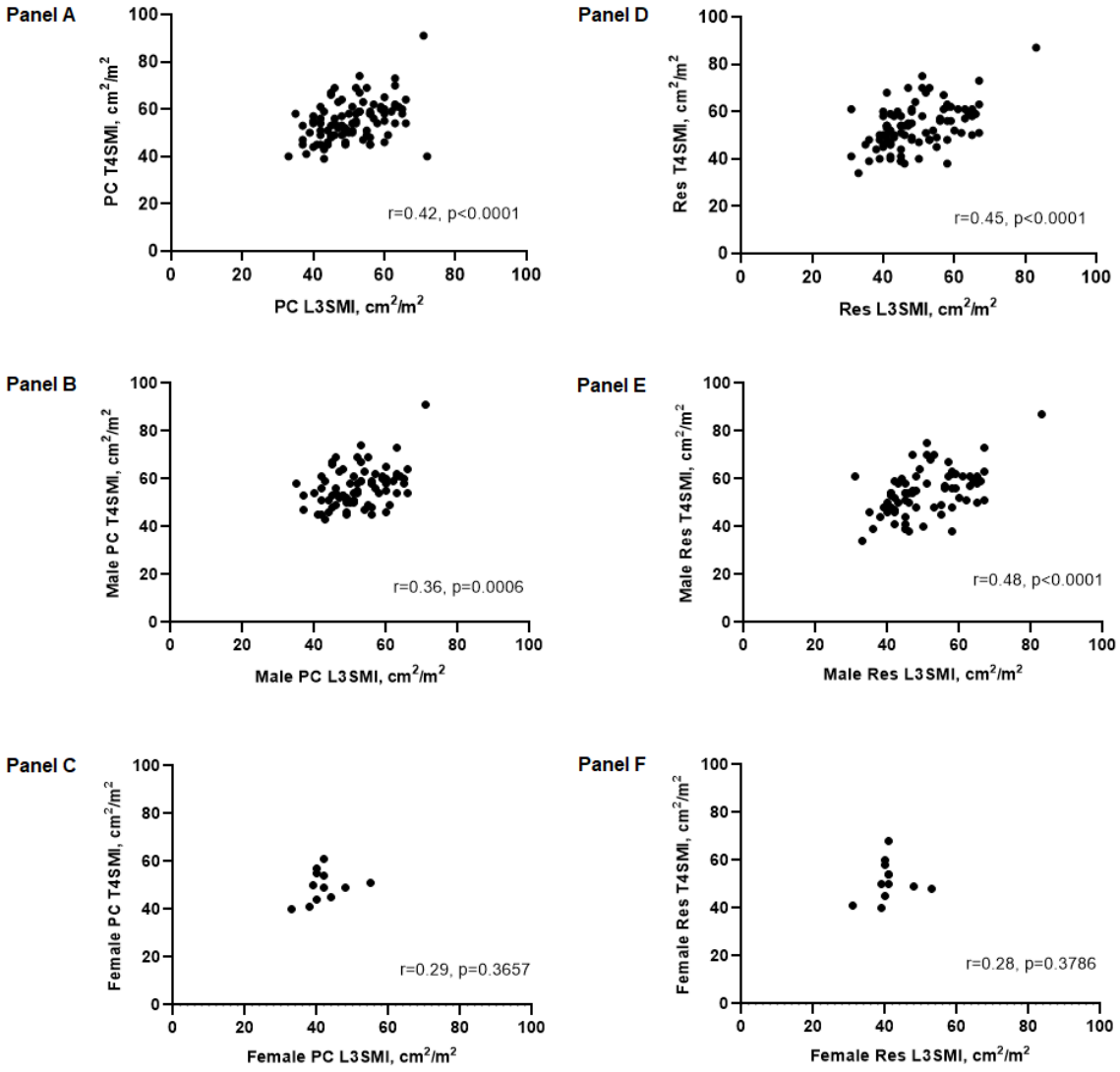

Figure 5.11 Correlations between third lumbar vertebra skeletal muscle index (L3SMI) and fourth thoracic vertebra skeletal muscle index (T4SMI) at the pre-chemotherapy time points in all patients (Panel A), male (Panel B) and female patients (Panel C), and at response assessment time points in all patients (Panel D), male (Panel E) and female patients (Panel F)

PC: pre-chemotherapy; Res: response assessment

5.4 Discussion

5.4.1 Skeletal muscle measurements at the L3 and T4

Following the work of Mourtzakis and colleagues(305) who first extrapolated data from a single cross-sectional CT image at the third lumbar vertebra (L3) to predict whole body composition of skeletal muscle mass, and Prado and colleagues who defined sex- and BMI-specific thresholds(251), sarcopenia has been associated with adverse outcomes in patients with cancer(398, 399). However, this widely validated approach to measuring skeletal muscle index using L3 has limitations in patients with thoracic malignancy as CT scans acquired during diagnostic work-up, prior to chemotherapy and response assessment may not extend inferiorly enough to capture L3. In my cohort, only 91 patients had an identifiable L3 on pre-chemotherapy and response assessment CT scans with accompanying height metrics. At the fourth thoracic vertebra (T4), 111 patients had these data. In an epidemiological survey by Sun and colleagues that included mostly patients with lung cancer, only 65% had scans in which skeletal muscle mass could be evaluated at the L3 level(308). Other studies have reported similar issues with up to one third of patients being excluded from studies due to L3 not being identifiable on CT scans(400, 401). Fourth thoracic vertebra-defined sarcopenia is being increasingly reported in the sarcopenia literature(311-313, 317). Sarcopenia has also been determined at other thoracic levels in patients with lung cancer, including at the fifth(190, 402), eighth(403) and tenth thoracic vertebrae(404, 405) as well as the sum of the eight and twelfth thoracic vertebrae(406).

5.4.2 Thresholds for sarcopenia

In their systematic review, Vangelov and colleagues reported that only 75% of studies assessing sarcopenia reported cut-off values and that authors were using different methods(310). A meta-analysis of 81 studies which determined the performance of sarcopenia cut-offs in cancer concluded that despite the variability of thresholds used, including optimal stratification, median,

percentiles and receiving operator curves, low lean muscle mass was associated with poorer prognosis(407).

I determined sarcopenia at L3 based on the well-validated sex- and BMI-specific SMI cut-offs defined by Martin and colleagues who used an optimal stratification method(186, 408). There is no consensus on specific sex- and BMI-specific thresholds for sarcopenia at T4. My two-dimensional measurements at the level of T4 were normalised for height squared to adjust for body size as per the height-based indexing described by Prado and colleagues at the third lumbar vertebra(174). I defined T4 sarcopenia groups using *a priori* definitions based on the distribution of the study sample, i.e., those patients with T4SMI mean minus 1 standard deviation if normally distributed or those with T4SMI below the 25th percentile if non-normally distributed. Skeletal muscle cut-offs have been defined as the mean minus one or two standard deviations by other authors(309, 409, 410). Sarcopenia has also been defined according to patients in lowest quartile in colorectal cancer(410, 411) and patients diagnosed with idiopathic pulmonary fibrosis(317) and post-operative pneumonia following partial hepatectomy for colorectal metastasis(312). Verhoek and colleagues defined sarcopenia according to the lowest tertile in their recent study of patients with MPM(190).

5.4.3 **Body composition differences between male and female patients**

I demonstrated that male patients had higher T4SMI compared to females and lost muscle mass between the two time points assessed. This is consistent with previous studies demonstrating that male patients have higher skeletal muscle mass(412) and strength(413) compared to females. Conversely, females gained mean muscle mass index at T4 between pre-chemotherapy and response assessment time points (2.2 cm^2/m^2). The cause for this latter observation is unclear. Stene and colleagues reported that nearly half of their patients with non-small cell lung cancer (NSCLC) had a stable or increased muscle mass after chemotherapy(414). Stable muscle or muscle gain has also been reported in patients with NSCLC by Prado and colleagues(415) with the suggestion that chemotherapy may be exerting an anti-catabolic effect in treatment

responders(415). To investigate this observation further, I performed a post-hoc analysis and demonstrated differences in the median interval period between CT scans between males (116 [IQR 82 to 174] days) and females (98 [IQR 79 to 147] days). Male patients with cancer cachexia are known to lose skeletal muscle at a greater rate than females(416, 417) and the longer interval period between scans in male patients may partly explain this. Alternatively, this finding may reflect differences in thoracic musculature between male and female patients. I demonstrated that T4 skeletal muscle measurements were larger than L3 which is likely due to the muscles at T4 being involved with arm and shoulder movement. The muscles of the shoulder, i.e., deltoid, were not included in my muscle tissue segmentations to limit this potential for confounding. I did include the pectoralis muscles in my T4 muscle areas. Males have larger pectoralis mass(418) and strength(419) compared to females. Pectoralis muscle mass is prognostic in patients with NSCLC(420, 421). Male sex and pectoralis muscle area remained significant in the proportional hazards model reported by Kinsey and colleagues(421).

The median pre-chemotherapy T4 ipsilateral muscle areas were lower than the contralateral skeletal muscle areas in both male and female patients. The decreased ipsilateral T4SMI group – stratified to muscle losing and non-losing groups according to mean minus 1 SD - had a shorter OS compared to the maintained SMI groups. Moreover, male patients had greater ipsilateral T4SMI loss, reenforcing the finding that male patients lose skeletal muscle at a higher rate than females. The reason for the differences between ipsilateral and contralateral muscle compartments is not clear. Patients with pleural malignancy frequently have altered chest wall mechanics due either to pleural effusion or tumour bulk. Survival is sufficiently long in some patients with MPM that this may translate into loco-regional changes in thoracic muscle compartments. Another reason for this observation could be that reduced muscle mass is associated with poor lung function and breathlessness which is observed in the clinical setting of MPM as well as in the chronic obstructive pulmonary disease (COPD) literature(422, 423). Sun and colleagues defined muscle losing groups according to peak expiratory flow rate-defined respiratory

strength and pectoralis muscle, reporting that pre-operative sarcopenia based upon these criteria was significantly associated with poor OS(420).

5.4.4 **Correlations between T4SMI and L3SMI**

I demonstrated moderate correlations between L3 and T4 pre-chemotherapy and response assessment skeletal muscle indices ((r=0.42 and r=0.45, respectively). In their study of patients with head and neck cancers, Van Heusden and colleagues reported a strong correlation between muscle cross-sectional area at T4 (excluding the muscles of the shoulder) and L3 (r=0.79) which was further strengthened (r=0.856) after incorporating age, sex, weight, arm positioning and weight(424). Grønberg and colleagues reported moderate agreement with intra-class correlation 0.71 in males and 0.52 in females(425).

I assessed T4SMI and L3SMI correlations in males and females with female patients having weaker correlations at both the pre-chemotherapy and response assessment scan time points (r=0.29 and r=0.28, respectively) compared to males who retained low-to-moderate r values (r=0.36 and r=0.48, respectively). My subsequent correlative analyses of total fat index (TFI) as an exploratory surrogate for adipose tissue volumes did not yield any concrete systemic reasons as to why the previously moderate L3SMI and T4SMI correlations had become uncoupled in female patients. As described earlier in this discussion, males generally have different chest musculature compared to females, particularly in respect to larger pectoralis muscle areas(426, 427). Females have different fat distribution at the level of thoracic vertebrae, including breast tissue in the anterior thoracic wall. I did not measure adipose tissue at T4 - or elsewhere in the chest - to further test this hypothesis. One study assessing adiposity at the level of T4 demonstrated that females have higher volume of adipose tissue at this level compared with males(428). The only study to date in MPM has assessed adiposity in the chest and demonstrated that males had more anterior mediastinal fat than females(190). A study assessing thoracic adipose tissue volume could shed further light on these differences.

5.4.5 **Sarcopenia survival outcomes**

The median survival time in this study was 389 days. This is similar to the outcomes reported in the South West Area Mesothelioma and Pemetrexed (SWAMP) trial(321) (368 days) and the Phase III study of pemetrexed in combination with cisplatin versus cisplatin alone in patients with malignant pleural mesothelioma study (12.1 months, or approximately 368 days)(3).

In the NSCLC population, pre-operative sarcopenia measured at L3 has been shown to be prognostically significant(245-248, 250, 429). Similar findings have been reported in advanced NSCLC(315, 430, 431) and small cell lung cancer (SCLC)(249). In the present study, the pre-chemotherapy and response assessment L3 sarcopenia groups trended towards shorter OS compared to the non-sarcopenia group, but neither reached statistical significance (p=0.077 and p=0.054, respectively).

The rate of muscle loss over time is associated with mortality and has been observed in patients with lung(414, 432), colorectal(221, 433), foregut(434), ovarian(435) and gastric cancers(436) as well as in patients with melanoma(437). I dichotomised patients into interval muscle losing and non-losing groups by calculating the percentage change in L3SMI, T4SMI and ipsilateral T4SMI from the pre-chemotherapy time point. The percentage change method is routinely used in medicine and is independent of units of measurement(438). At L3, I found no survival difference between the two groups (p=0.307). This is inconsistent with the findings of the aforementioned studies exploring longitudinal change in muscle mass in different solid organ tumour sites. This was a surprising finding as both males and females lost skeletal muscle between the interval time points assessed. Moreover, the median time between CT scans in my study was 109 [IQR 80 to 174] days, or 15 [IQR 11 to 24] weeks, which is a reasonably long interval period to assess changes in muscle mass loss. Other possible explanations for this finding are the small sample size (n=91) and the percentage change method used. The latter method has been criticised by Vickers and colleagues who suggested the use of analysis of co-variance instead(439).

In the present study, the L3 muscle losing group had a percentage change decrease of ≥9% which was similar to the thresholds applied by Blauwhoff-Buskermolen and colleagues(440) and Daly and colleagues(441). Two other studies have assessed longitudinal muscle mass loss defined by percentage change and reported no impact on survival. Firstly, Degens and colleagues determined skeletal muscle percentage change over 6-weeks using CT images of patients with advanced NSCLC and concluded that patients with decreasing skeletal muscle mass - defined as a skeletal muscle mass decrease of >1.3% - did not have shorter OS compared to those who maintained muscle(442). Similar findings were reported by Tan and colleagues who assessed patients with advanced pancreatic cancer according to 60-day percentage change skeletal muscle mass tertiles(399). The latter study did report that patients with sarcopenia and obesity had a worse prognosis(399).

When measured at the fourth thoracic vertebra, pre-chemotherapy and response assessment sarcopenia – defined as mean minus 1 SD – was not associated with poorer OS compared to the muscle retaining groups (p=0.789 and p=0.185, respectively). However, percentage change in skeletal muscle loss between pre-chemotherapy and response assessment time points was associated with shorter OS (p=0.0002). T4SMI loss was also an independent predictor of OS following multivariate analysis. When stratified by stage, patients in the T4SMI muscle losing and higher tumour volume group had shorter OS. This is not surprising as tumour volume is a recognised predictor or poorer OS in the MPM population(100). This also links to my tumour volume work which has been discussed in detail in Chapter 4.

Thoracic sarcopenia measured at T4 is prognostic in patients with breast cancer(313) as well as in patients with post-liver surgery pneumonia(312). To my knowledge, the present study is only the second study that has determined the prognostic impact of CT-measured skeletal muscle mass loss and the first study to assess longitudinal changes in the MPM population. A recent study by Verhoek and colleagues reported that patients with MPM and sarcopenia – measured at the fifth thoracic vertebra (T5) - have a higher three-year mortality compared to those who are not sarcopenic (p=0.002)(190). In the thoracic malignancy

literature, other authors have defined sarcopenia according to pectoral mass muscle(311, 420) and the twelfth thoracic vertebra groups(431, 443-445).

5.4.6 **Adipopenia**

Although there are no BMI- and sex-specific thresholds for adipose tissue measurements, the cachexia literature reports that females have higher body fat compared to BMI-matched males(446) and that females have lower visceral adipose tissue(447, 448). Results from the present study support this as males had a higher median visceral adipose index (VFI) compared to females and lower TFI compared to females. Mallio and colleagues reported similar visceral adipose tissue findings in their study of patients with NSCLC, citing hormone differences between males and females as a potential reason for this(449).

Adipopenia – the loss of fat mass - has been shown to be prognostically significant in patients with lung(389-392), gastrointestinal and lung(393), gastric(394, 395), breast(396) and renal cell cancers(397). Higher fat density has been shown to be prognostic in patients with colorectal cancer(450). Other studies have demonstrated improved outcomes with higher adipose tissue metrics, including patients with NSCLC and higher subcutaneous adipose tissue (SAT) volumes having better progression free survival compared to those with lower SAT volumes(451) and patients with advanced renal cell carcinoma and higher visceral fat area (VFA) having longer OS compared to those with lower VFA(452). Verhoek and colleagues determined pre-cardial fat mass at T5 and did not demonstrate any association with this metric and three-year survival($p=0.863$)(190). In the present study, loss of VFI measured at L3 were associated with shorter OS ($p=0.007$). Visceral fat loss was a predictor of OS in my subsequent multivariate analysis ($p=0.035$). In their study of patients with pancreatic cancer(453), Di Sebastiano and colleagues hypothesised that there is a relationship between adipose tissue loss rate and greater expression of pro-catabolic pathways associated with wasting. Visceral fat is pro-inflammatory and associated with the release of leptin, tumour necrosis factor and interleukin-6 (IL-6)(454) and greater insulin resistance, thus potentiating an environment

conducive to tumour growth(455). However, studies determining local adipose tissue inflammation in cancer are contradictory(263, 456, 457).

In addition to visceral fat loss, obesity – defined by WHO BMI criteria of ≥30 mg/m^2 – was a protective factor in my multivariate analysis ($p<0.001$). The 'obesity paradox' is the term given to describe the paradoxically protective effect of obesity in chronic diseases and cancers and has been discussed in the cachexia literature(458, 459), including in patients with lung cancer(392, 460). A recent meta-analysis of more than 6.3 million patients with cancer concluded that patients with obesity and lung and renal cancers and melanoma had improved survival compared to patients without obesity(461). Higher BMI has also been inversely associated with lung cancer development(462). However, the crudity of body mass index body as a surrogate metric for adiposity has been cited as a possible reason for this paradox. In the present study, obesity and loss of visceral fat both remained independent predictors of OS in the multivariate analysis suggesting that the distribution of fat mass is important. Moreover, fat and muscle indices did not correlate in the present study, neither did age and fat indices suggesting that obesity was not associated with higher skeletal muscle mass or younger age as postulated by Lennon and colleagues in their review article determining potential biases associated with BMI(458).

Smoking and concurrent metformin – a medication used in the management of diabetes through activated 5' adenosine monophosphate-activated protein kinase (AMPK) – have been postulated by Barbi and colleagues to be further confounders contributing to the 'obesity paradox'(390). Smoking status as a confounding variable has been explored by other authors(463-465). The same authors highlighted the importance of adipose tissue distribution - including visceral fat - rather than BMI in determining obesity in patients with NSCLC. They reported that higher VFI conferred a worse prognosis in their patient group(390). Blanc-Durand and colleagues also reported the prognostic influence of adipose tissue indices, reporting a higher VAT/SAT ratio being an independent predictor of both progression free survival and OS in their population(466). I did not have smoking status or medications available to include in my analyses to assess for potential confounding.

5.4.7 **Treatment tolerance**

In the present study, over one third of patients did not receive four cycles of chemotherapy either due to toxicity, progression whilst on treatment or death. I did not identify an association between pre-chemotherapy or response assessment sarcopenia measured at T4 and number of treatment cycles received. Chemotherapy has been shown to be causative of and contributory to muscle mass loss in patients with lung(414), colorectal(440), breast(467), gastric(468) and oesophageal cancers(469). Skeletal muscle mass correlates with increased toxicity during treatment in locally advanced oesophageal cancer(470) and gastric cancer(471). Pathophysiological mechanisms for his include chemotherapy-induced protein catabolism(186) and anorexic changes(472) as well as direct changes that chemotherapy exerts on skeletal muscle(473).

The patients in the present study received either carboplatin or cisplatin and pemetrexed chemotherapies, with most patients receiving carboplatin rather than cisplatin. Sjøblom and colleagues reported that patients with sarcopenia have increased toxicities to these agents(400). The mechanism for this is unclear, however may relate to the formulae used to dose chemotherapy. Carboplatin is dosed according to the Wright formula which places emphasis on an estimation of glomerular filtration rate (eGFR) rather than weight as it is eliminated solely by the kidneys(474). The Wright formula is calculated as: ((6500 minus 38.8 multiplied by age) multiplied by BSA multiplied by (1 minus 0.168 multiplied by sex)) divided by creatinine(474). Patients with sarcopenia will lose muscle, leading to a decrease in serum creatinine with the potential for eGFR overestimation(475), and theoretically, increased toxicities as a result of this (serum creatinine is the denominator in the Wright formula).

I did not identify associations between fat indices and treatment tolerance. There were limited data available relating to chemotherapy treatment toxicities resulting in only a small number of patients included in this analysis. The short follow-up time also precluded progression free survival analyses. It is also important to acknowledge that most patients in the present study were PS 0 and

1, representing a fit cohort. Patients who are borderline PS 1 and those who are PS 2 are most likely to have a reduced tolerance to treatment.

Although not statistically significant, less patients in the fat losing (52.9%) than non-losing groups (75.3%) did not complete the planned 4 cycles of chemotherapy. The reason for this is unclear and must be considered in the context of a small sample size with the potential for type II error. Altered adipose distribution in the context of systemic anti-cancer therapies (SACT) is important as most SACT doses are calculated using body surface area (BSA), including cisplatin and pemetrexed in patients with MPM. BSA for chemotherapy dosing is most commonly calculated using the Du Bois formula as: weight (kg)]$^{x0.425}$ multiplied by height (cm)$^{x0.725}$ multiplied by 0.007184(476). Based on this, patients who are obese will have a higher BSA than non-obese patients. Interestingly, an analysis of 25 different BSA formulae by Redlarski and colleagues demonstrated marked variation in BSA estimates, with up to 0.5 m^2 differences reported depending on the formulae used(477). Practising oncologists often dose chemotherapy according to ideal body weight rather than actual body weight, with a BSA limit set to 2.0 m^2(478). However, a recent update from the American Society of Clinical Oncologists (ASCO) recommended that chemotherapy should be dosed according to actual body weight in patients with obesity(479). However, dosing to actual body weight can result in doses being 15% to 30% greater compared to dosing according to ideal body weight(480).

A further consideration in the present study is whether patients who were obese received higher doses of chemotherapy. I did not have the doses of chemotherapy available at the time of my analyses to answer this question. It is an important consideration as changes in body composition have the potential to alter the pharmacokinetics of chemotherapy, including the volume of distribution and metabolism, which could result in sub-therapeutic dosing(481) or even toxicities(478). Patients with excess adipose tissue have a reduced water:muscle proportions(482). Carboplatin and pemetrexed are hydrophilic chemotherapies(483, 484) and distribute poorly in adipose tissue(485). As highlighted earlier, carboplatin is eliminated exclusively by the kidneys with

some studies suggesting that obese patients have higher creatinine clearance(485). Cisplatin elimination has been shown to be higher in patients with obesity compared to non-obese patients(486). Hall and colleagues highlighted the call by some authors to offer increased doses of carboplatin and cisplatin in patients with obesity(487).

In breast(488) and other solid organ malignancies including lung and colorectal cancers(489), obese patients have been demonstrated to have better tolerance to chemotherapy. This relates to the 'obesity paradox' discussed in Section 5.4.6. of this discussion. Increased energy reserves(490) and distribution of fat(491) have been reported as possible reasons for improved tolerance to chemotherapy. It is unclear whether this tolerance to chemotherapy translates into improved OS in obese patients. A press release from the European Society of Medical Oncologists (ESMO) suggested that patients who are obese receiving chemotherapy for colorectal cancer may have poorer OS due to chemotherapy dose-reductions(492). A study by Martini and colleagues concluded that although patients with prostate cancer who received higher doses of docetaxel chemotherapy due to BSA dosing, the increase OS observed was not related to the higher doses received(493). Similar conclusions were drawn in obese patients with breast cancer by Liu and colleagues in their response(494) to a study by Karatas and colleagues who postulated that dose-capping at BSA 2.0 cm^2 may have impacted on the lower survival trends observed in their study of obese chemotherapy-treated breast cancer patients(495).

5.4.8 **Response assessment**

In this study, the overall partial response rate during chemotherapy was 29% in patients with MPM which is similar to the response rate reported by the phase I study of pemetrexed and carboplatin(496), but lower than the phase III trial(3). Studies have demonstrated relationships altered body composition and response to treatment. Nattenmüller and colleagues reported that patients with NSCLC received less chemotherapy cycles than those without sarcopenia(253). Shiroyama and colleagues determined that patients without sarcopenia had a higher overall response rate to programmed cell death protein 1 (PD-1) inhibitors

in patients with NSCLC(430). Shachar and colleagues reported poorer response to capecitabine in sarcopenic patients with breast cancer(497). Higher visceral fat area is predictive of treatment response in patients with colorectal cancer(498).

In the present study, response to chemotherapy was not associated with a decrease in T4SMI. This aligns with findings in previous studies, including patients with gastric(471, 499), foregut(441) and bladder cancers(500). In patients with mesothelioma, this could reflect the limitations of accurately measuring response assessment using the mRECIST criteria which does not evaluate the complexities of the tumour growth pattern and is associated with poor reproducibility(81). More recent volumetric approaches are being investigated, including human-defined and machine learning methods. These may improve response assessment in this cohort and have been discussed in detail in Chapter 4 of this thesis. I also assessed human volume-defined response to treatment with T4SMI values. Although not statistically significant, I did observe T4SMI percentage change trends of -7.240%, -3.438% and -0.975% according to progressive disease, stable disease and partial response, respectively. However, the total number of patients assessed was small (n=30). I also did not find a statistically significant difference in fat indices and mRECIST-defined response assessment classifications.

5.4.9 **Systemic inflammation**

Studies have demonstrated that low muscularity is related to systemic inflammation, including in patients with lung(311), colorectal(501, 502) and oesophageal cancers(503). The pathogenesis of MPM is highly influenced by the systemic inflammatory response(504). In the present study, skeletal muscle index percentage change at L3, T4 and ipsilateral T4 did not correlate with pre-chemotherapy inflammatory indices. This could be due in part to missing data, for example, in the T4 analyses, only 71/111 (64%) patients had complete C-reactive protein (CRP) data. A small sub-study (n=47) was performed to examine markers of systemic inflammation at pre-chemotherapy and response assessment time points. I identified weakly negative correlations between ipsilateral T4SMI and response assessment neutrophil:lymphocyte ratio (NLR). NLR is associated

with poor outcomes in MPM. In their systematic review which included 33,432 patients, Templeton and colleagues concluded that the prognostic effect of NLR was highest in MPM compared to other solid organ cancers (HR=2.35)(163). Unsurprisingly, I also demonstrated that TFI and VFI percentage changes negatively correlated with weight (r=-0.367 and r=-0.482, respectively) and BMI (r=-0.413 and r=-0.435, respectively). Patients with MPM and low BMI have also been shown to trend towards poorer OS(505). VFI percentage change also positively correlated with pre-chemotherapy platelets (r=0.296). A meta-analysis of 3602 patients concluded that pre-treatment thrombocytosis is an adverse prognostic indicator in MPM(506). Moreover, thrombocytosis is positively associated with elevated BMI and total fat mass percentage(507) and visceral adipose tissue(508). Platelet-derived microparticles – released by activated platelets - have been associated with excessive adipose tissue(509) and are associated with malignancy(510).

5.4.10 **Tumour volume**

In the present study, L3SMI, T4SMI and ipsilateral T4SMI did not correlate with tumour volume. There are little data exploring tumour volume in the context of sarcopenia. Vohra and colleagues reported alterations in skeletal muscle properties by increased tumour burden in their murine model of pancreatic cancer(511). Other murine models examining tumour volume and skeletal muscle indices have been published(512-514).

In the wider context of the cancer cachexia syndrome, a review examining the advantage of introducing the measurement of tumour burden in the assessment of cancer cachexia concluded that the extent of cachexia increases with tumour burden(515). A study examining the extent of tumour, diet and patient-related factors including appetite, metabolic hormones, immune activation, liver function and quality of life were compared in patients with colorectal liver metastases concluded that those patients who lost weight had a higher volume of liver metastases(516). Interestingly, I demonstrated that tumour volume negatively correlated with pre-chemotherapy lymphocytes and positively correlated with pre-chemotherapy NLR, platelet:lymphocyte ratio (PLR) and

CRP. MPM tumour volume is associated with elevated inflammatory markers, including activin A(517) and complement component 4d (C4d)(518). The latter study also found a positive correlation between C4d and CRP(518). Moreover, neoangiogenesis – the proliferation of blood vessels in tumour growth - correlates with NLR(167).

5.4.11 **Potential clinical implications**

I have demonstrated that sarcopenia measured at the fourth thoracic vertebra is an independent predictor of poorer OS. It has the potential to be an additional prognostic radiological biomarker in patients with MPM receiving systemic anti-cancer therapy. Sarcopenia has been traditionally measured at the third lumbar vertebra, however CT scans in patients with thoracic malignancies often do not have third lumbar vertebral views as this level is included in abdominal image sequences. The inherent advantage of the fourth thoracic vertebra is that it will be included in pre-chemotherapy images and subsequent interval scans in patients with thoracic malignancy. The use of the T4 as a surrogate for sarcopenia could improve clinical decision-making, and ultimately outcomes, for patients with thoracic malignancies such as MPM. A larger study is required to validate these findings, especially given the sex- and BMI-specific thresholds that exist for sarcopenia determination when measured at the third lumbar vertebra.

Another interesting finding from this study has been the apparent protective effect of obesity. In the cachexia literature, this has been termed the ‘obesity paradox’. I also demonstrated that the loss of visceral adipose tissue is prognostic. The exact mechanism of this unclear. Adipose tissue is considered to be an endocrine organ(519) and has a role in inflammatory pathways(520) with suggestions that the pro-inflammatory effects of obesity can intensify the immune response through T cell activation(521-523). With immunotherapy becoming more commonplace in the treatment of solid organ cancers, including the recent approval of nivolumab and ipilimumab as first-line treatment of patients with MPM in Scotland, further investigation of the complex hormonal and inflammatory interplay that exists between the tumour and host is warranted.

The identification of thoracic sarcopenia and visceral adipopenia prior to treatment with systemic anti-cancer therapies may provide a window of opportunity for intervention to reverse or even halt the sarcopenia and adipopenia processes which are central to the cancer cachexia syndrome and associated with treatment-related toxicities and poorer prognosis. Anti-cachexia agents are already the subject of clinical trials in patients with thoracic malignancies (NCT03743064, NCT04131426, NCT04803305), including MPM(225).

5.4.12 **Study limitations and strengths**

The main limitation of this study was its retrospective study design. Despite having identifiable T4 on CT scans, 23 patients did not have available height metrics for calculation of skeletal muscle index, and as such, they were not included in the final analyses. Additionally, there was only a small sub-study of patients who had inflammatory indices at the pre-chemotherapy and response assessment time points (n=47). Moreover, I did not have weight, and subsequently BMI, measurements available at the response assessment time point. Interval changes in weight and BMI would have been useful in determining whether changes in body composition impacted on these metrics that are routinely monitored during chemotherapy. Response assessment skeletal and adipose areas were indexed according to height squared that was measured prior to chemotherapy as height was unlikely to change significantly over the interval period examined.

A further limitation was the lack of data of chemotherapy doses at the time of my analyses. This has been discussed in Section 2.4.7 of this discussion and would have facilitated an assessment of whether tolerance to treatment and survival between obese and non-obese and sarcopenic and non-sarcopenic patients were influenced by the doses administered.

A third limitation is that I did not assess fat indices at the fourth thoracic vertebra. Verhoek and colleagues assessed pre-cardial fat at T5(190). Jeffery and colleagues have assessed the relationship between skeletal muscle loss and adipose tissue changes using DEXA(257). Other studies have measured thoracic

adipose tissue volumes according to pericardial, intrathoracic and subcutaneous thoracic adipose tissue(524, 525). Combined fat and muscle indices such as those recently reported by Jeffery and colleagues may also shed further light on the importance of adiposity on outcomes.

Another important limitation relates to the definition of sarcopenia which includes skeletal muscle quantity as well as skeletal muscle strength and physical performance(526, 527). One study by Yang and colleagues demonstrated that the prognostic impact of skeletal muscle loss in patients with advanced NSCLC was improved when handgrip strength and performance status were included in their multivariable analysis(431). Treatments directed towards reversing sarcopenia often include exercise programmes to strengthen muscle and preserve function(528-530). The data for the present study was collected retrospectively and did not include skeletal muscle strength. The most validated method of muscle strength is grip strength and physical performance using gait speed or short physical performance battery(526, 531). Moreover, I did not have data relating to patients' use of anti-inflammatory medications, physical exercise regimes or access to nutritional support regimes which may have impacted on muscle mass.

A further limitation relates to the lack of data on patient ethnicity. Studies assessing sarcopenia in the thoracic malignancy literature are often confined to one ethnic group, for example, European(247), Japanese(245, 246, 248, 250) and South Korean populations(256). Muscle mass differs depending on patient ethnicity(254, 532). Having these data would enhance the knowledge of sarcopenia in different populations.

Although the sample sizes were modest (n=91 at the third lumbar vertebra and n=111 at the fourth thoracic vertebra), they are similar to a previous study assessing thoracic sarcopenia in patients with SCLC(311, 315). To my knowledge, this is the first study to assess sarcopenia at the fourth thoracic vertebra in patients with MPM, as well as the first study to assess ipsilateral sarcopenia in any solid organ cancer. Patients were recruited across three different hospital sites with different CT scanners used which improved generalisability. The

method used to quantify skeletal muscle mass was performed using freely available body composition software and had good-to-excellent intra- and inter-observer reliability.

5.5 Conclusions

In this chapter, I demonstrated the negative impact of decreasing thoracic skeletal muscle mass and visceral adipose tissue on treatment response and survival in patients with MPM receiving chemotherapy. Patients losing thoracic muscle had poorer overall survival during chemotherapy than patients who maintained thoracic skeletal muscle. This association was further strengthened when muscle losing groups were stratified according to tumour volume. I also identified that lumbar vertebra-measured adipopenia was associated with poorer OS and that pre-chemotherapy obesity may have exert a protective effect with loss of adipose tissue during treatment conferring a worse prognosis.

Chapter 6

CONCLUSIONS

6 Chapter 6: Conclusions

Prognostication in patients with malignant pleural mesothelioma (MPM) is difficult due to the heterogeneity of the disease. Our own research group have suggested that routinely available clinical data are insufficient in determining accurate prognosis in MPM with other candidate factors potentially at play, including alterations in body composition(172). The visual evaluation of MPM for the purposes of staging and monitoring response is fraught with difficulty due to the complex and unique morphology of MPM. These imaging limitations have hampered the limited accuracy of volumetric measurements which are important in determining patients' response to systemic anti-cancer therapies, including chemotherapy and immunotherapy. The development of reliable and reproducible tumour volumetric measurements would improve clinical decision-making, including earlier cessation of toxic treatment as well as advancing clinical trials. The challenges and limitations of a semi-automated approach to tumour volume measurement were reported in Chapter 3 and provided the impetus to develop a fully automated method of pleural tumour volumetry based on pleural tumour volumes measured by a physician with expertise in MPM (reported in Chapter 4). The novel artificial intelligence method reported provides the basis for future studies to assess the role of automated tumour volumetry on a larger scale. Body composition is another important prognostic factor that has been poorly studied in MPM. In other solid organ cancers, body composition metrics such as skeletal muscle loss and adipose tissue loss have prognostic implications for patients. Importantly, the reversibility of these body composition abnormalities is the subject of ongoing clinical research. Chapter 5 highlighted the importance of altered body composition in patients with MPM in a multicentre setting and has enhanced our knowledge of altered body composition in this disease.

6.1 Limitations of semi-automated tumour segmentation in MPM

In Chapter 3, volumetric assessment of tumour burden in patients with MPM was examined in a single centre observational study. I hypothesised that pleural tumour volume could be achieved accurately and reliably by using a semi-automated volumetric segmentation method on contrast-enhanced computed tomography (CT) scans extrapolated from a previously published magnetic resonance imaging (MRI) method(319). There were obvious segmentation errors on subjective visual assessment of the final segmented volumes which included under-segmentation of pleural tumour volume, i.e., incomplete inclusion of pleural tumour, and over-segmentation of tumour volume, i.e., volumes which included other thoracic soft tissue structures. Overlapping HU values between different thoracic tissues accounted for the over-segmentation of tumour volumes.

Despite multiple segmentation attempts and refinement of the semi-automated technique, including increasing the number of axial CT slices delineated, and after meeting with the Myrian Intrasense® engineers to seek a resolution to these problems, accurate threshold-based region growing could not be achieved and further semi-automated volumetry attempts using contrast-enhanced CT scans were abandoned.

6.2 Development of automated tumour volumetry in MPM

An automated approach to volumetric tumour segmentation in patients with MPM was described in Chapter 4. I hypothesised that accurate pleural tumour segmentation could be achieved through a fully automated artificial intelligence (AI) algorithm – specifically, a deep learning convolutional neural network (CNN) - based on detailed human ground truth using contrast-enhanced CT scans. My involvement in this multicentre study was as a clinician with expertise in pleural anatomy. The research group also consisted of a Consultant Radiologist (Dr Gordon Cowell) who provided the modified Response Evaluation Criteria in Solid Tumours (mRECIST) measurements and disease stage metrics and two AI scientists (Owen Anderson and Keith Goatman) who trained the deep learning

CNN to segment pleural tumour based on my tumour volumes, also termed ground truth.

Due to the failure to achieve my primary objective of developing an accurate semi-automated volumetric segmentation technique in Chapter 3, time-consuming manual delineation was required for the ground truth; as such, the time-to-annotate pleural tumour far exceeded our initial estimates. Delays were accommodated by adjusting the project timeline to make the development of the algorithm and annotation of the training and validation data concurrent processes, thus prioritising development which could be completed without annotated data. A key action was the deliberate reduction in number of annotated CT slices for a sub-section of 43 CT images to allow the completion of more scans in the time allocated to the project. The training and internal validation set sample size of 123 CT scans exceeded the original target of 90 scans. Despite the use of manually annotated ground truth, this study included the largest number of scans included in the MPM volumetry literature (n=183 annotated CT images).

The success of the AI RECIST project was that the CNN reported is the first fully automated algorithm for MPM tumour segmentation. The identification of segmentation errors in 4/30 CT scans reflected important morphological features of MPM suggesting the algorithm's performance could be further improved by enriching future training sets for these features. This work has directly informed the design of Work Package 5 (WP5) in the Pre-malignant Drivers Combined with Target-Drug Validation in Mesothelioma (PREDICT-Meso) study which I detail further in the 'Future work' section of this chapter.

6.3 The prognostic significance of altered body composition in MPM

In Chapter 5 of this thesis, I hypothesised that sarcopenia and adipopenia measured at the third lumbar vertebra (L3) and sarcopenia at the fourth thoracic (T4) vertebra would be prognostically significant in patients with MPM receiving chemotherapy.

Sarcopenia at L3 was not associated with survival, but patients who lost visceral adipose tissue between pre-chemotherapy and response assessment time points had shorter OS. Skeletal muscle and adipose assessments at L3 were hampered by the lack of abdominal views on pre-chemotherapy and response assessment CT scans. Assessment of muscle mass at T4 yielded a higher sample size as MPM is a thoracic malignancy with more readily available chest CT images. To my knowledge, this is the first study that has demonstrated the detrimental impact of losing thoracic skeletal muscle mass during chemotherapy for MPM. This is an important finding as there is the potential to intervene at the pre-chemotherapy juncture and attempt to reverse or halt the progression of skeletal muscle loss, thus improving OS independent of chemotherapy tolerance. A larger study is needed to negate the potential for type 1 error and to determine whether there is a true link to reduced chemotherapy tolerance. This would subsequently support an intervention study for patients due to receive chemotherapy. Also, immunotherapy is now a first-line treatment in MPM and an unanswered question in this study is whether patients on immunotherapy behave differently. Those who are more inflamed might lose more skeletal muscle. In the present study, patients had a higher NLR following chemotherapy. There is an unanswered question as to whether immunotherapy-treated patients will have further to gain from anti-sarcopenic interventions

Two important considerations are the lack of data relating to the optimal thoracic level for determining sarcopenia and the lack of data available relating to optimal sarcopenia cut-offs using the thoracic vertebrae. I elected to use T4 due to its inclusion in thoracic images and because it has been shown to be prognostic in patients with other solid organ cancers(311-313). I defined sarcopenia based on *a priori* threshold cut-offs based on the normality of the distribution of the study sample in the absence of a gold-standard approach to this and because it has been reported in studies examining the clinical significance of sarcopenia at this vertebral level(312, 410, 411).

6.4 Future work

The work described in this thesis will be further optimised and validated in a larger study as part of the Pre-malignant Drivers Combined with Target-Drug Validation in Mesothelioma (PREDICT-Meso) Network. This network aims to define accurate response assessment classifications based on volumetric measurements and encompasses study centres in the UK, Spain, Italy, Belgium, Canada and Brazil. The data will be optimised using CT data from the National Consortium of Intelligent Medical Imaging (NCIMI) network. A new Research Fellow and new AI Scientist will be employed in Glasgow to move this work forward with the plan to use 1000 pre-treatment and 1000 follow-up CT scans, i.e., a total of 2000 scans. Cases will be selectively chosen to manually volume to include those scans with features of over- and under-segmentation described in Chapter 4 as well as sparsely annotating scans to increase the number of cases to feed into the CNN architecture.

The manual segmentation method I developed in Chapter 4 has the potential to facilitate the identification of future radiological biomarkers, including radiomic features. Radiomics - broadly defined as the study of textural and other feature imaging analyses(533) - is an expanding radiological research area. Studies have assessed the prognostic importance of radiomic features in MPM, including assessing shape and textural features using contrast-enhanced CT and MRI imaging to help determine benign lesions from MPM(534) and the use of CT-defined radiomic signatures to aid in early response assessment(535). Radiomics has the advantage that can overcome statistical variances around a region of interest of an image voxel(536). I have been involved in drafting a research protocol with a Consultant Radiologist colleague (Dr Gordon Cowell) which aims to define radiomic imaging features that determine response to treatment and survival in patients with chemotherapy-treated MPM using the detailed volumetric ground truth described in Chapter 4 of this thesis.

Prognostication in patients with MPM is important. In the age of precision medicine, advances in imaging, staging and genomic sequencing have superseded traditional metrics of survival prediction which have been based largely on

routinely available clinical data(30, 34, 36). The clinical, inflammatory markers and disease stage data used in this thesis will be included in the PRISM study which is funded by the British Lung Foundation(322). In the PRISM study, deoxyribonucleic acid (DNA) has been extracted from MPM tumour identified by a Consultant Histopathologist on formalin-fixed paraffin embedded (FFPE) samples obtained from chemotherapy-treated patients. Subsequent analysis of somatic copy number variations (CNV) on the FFPE samples have been carried out by the NHSGGC Molecular Pathology Department. Two independent Consultant Radiologists have determined mRECIST classifications on pre-chemotherapy and response assessment CT scans in the same patients. Statistical analyses are ongoing at the time of writing this thesis. The aim of the PRISM study is to define a genomic predictor-classifier of chemotherapy resistance in MPM using these clinical, radiological and genomic data. The chemoresistance predictors identified will be externally validated in two independent patient cohorts supplied by Royal Papworth Hospital NHS Foundation Trust and Wythenshawe Hospital.

References

1. Brims FJH, Maskell NA. Prognostic factors for malignant pleural mesothelioma. Current Respiratory Care Reports. 2013;2(2):100-8.

2. Woolhouse I, Bishop L, Darlison L, De Fonseka D, Edey A, Edwards J, et al. British Thoracic Society Guideline for the investigation and management of malignant pleural mesothelioma. Thorax. 2018;73(Suppl 1):i1-i30.

3. Vogelzang NJ, Rusthoven JJ, Symanowski J, Denham C, Kaukel E, Ruffie P, et al. Phase III study of pemetrexed in combination with cisplatin versus cisplatin alone in patients with malignant pleural mesothelioma. J Clin Oncol. 2003;21(14):2636-44.

4. Consortium SM. nivolumab (Opdivo®) is accepted for use within NHS Scotland.: Scottish Medicines Consortium; 2022 [cited 2022 26/02/22]. https://www.scottishmedicines.org.uk/medicines-advice/nivolumab-opdivo-full-smc2385/].

5. England N. NHS England interim treatment options during the COVID-19 pandemic NICE: NICE; 2022 [cited 2022 26/02/2000022]. https://www.nice.org.uk/guidance/ng161/resources/interim-treatment-change-options-during-the-covid19-pandemic-endorsed-by-nhs-england-pdf-8715724381].

6. Byrne MJ, Nowak AK. Modified RECIST criteria for assessment of response in malignant pleural mesothelioma. Ann Oncol. 2004;15(2):257-60.

7. Fearon K, Strasser F, Anker SD, Bosaeus I, Bruera E, Fainsinger RL, et al. Definition and classification of cancer cachexia: an international consensus. Lancet Oncol. 2011;12(5):489-95.

8. Schumann SO, Kocher G, Minervini F. Epidemiology, diagnosis and treatment of the malignant pleural mesothelioma, a narrative review of literature. J Thorac Dis. 2021;13(4):2510-23.

9. Baumann F, Ambrosi JP, Carbone M. Asbestos is not just asbestos: an unrecognised health hazard. Lancet Oncol. 2013;14(7):576-8.

10. Tlotleng N, Sidwell Wilson K, Naicker N, Koegelenberg CF, Rees D, Phillips JI. The significance of non-occupational asbestos exposure in women with mesothelioma. Respirol Case Rep. 2019;7(1):e00386.

11. Abratt R. Malignant mesothelioma: epidemiological snapshots from around the world. Malignant Pleural Mesothelioma. 2006;19.

12. Alleman JE, Mossman BT. Asbestos Revisited. Scientific American. 1997;277(1):70-5.

13. Doll R. Mortality from lung cancer in asbestos workers. Br J Ind Med. 1955;12(2):81-6.

14. Perry KM. Diseases of the lung resulting from occupational dusts other than silica. Thorax. 1947;2(2):75-120.

15. Gorman T, Johnston R, McIvor A, Watterson A. Asbestos in Scotland. International Journal of Occupational and Environmental Health. 2004;10(2):183-92.

16. Instruments US. The Asbestos (Prohibitions) (Amendment) Regulations 1999 https://www.legislation.gov.uk/uksi/1999/2373/made1999 [

17. Commission E. COMMISSION DIRECTIVE 1999/77/EC https://eur-lex.europa.eu/LexUriServ/LexUriServ.do?uri=OJ:L:1999:207:0018:0020:EN:PDF1999 [

18. Peto J, Hodgson JT, Matthews FE, Jones JR. Continuing increase in mesothelioma mortality in Britain. Lancet. 1995;345(8949):535-9.

19. Abdel-Rahman O. Global trends in mortality from malignant mesothelioma: Analysis of WHO mortality database (1994-2013). Clin Respir J. 2018;12(6):2090-100.

20. Brims F. Epidemiology and Clinical Aspects of Malignant Pleural Mesothelioma. Cancers (Basel). 2021;13(16).

21. Hodgson JT, McElvenny DM, Darnton AJ, Price MJ, Peto J. The expected burden of mesothelioma mortality in Great Britain from 2002 to 2050. Br J Cancer. 2005;92(3):587-93.

22. Executive HaS. Mesothelioma statistics for Great Britain, 2021 Health and Safety Executive: Health and Safety Executive; 2021 [Available from: https://www.hse.gov.uk/statistics/causdis/mesothelioma/mesothelioma.pdf.

23. Odgerel CO, Takahashi K, Sorahan T, Driscoll T, Fitzmaurice C, Yoko OM, et al. Estimation of the global burden of mesothelioma deaths from incomplete national mortality data. Occup Environ Med. 2017;74(12):851-8.

24. Stayner L, Welch LS, Lemen R. The worldwide pandemic of asbestos-related diseases. Annu Rev Public Health. 2013;34:205-16.

25. Allen LP, Baez J, Stern MEC, Takahashi K, George F. Trends and the Economic Effect of Asbestos Bans and Decline in Asbestos Consumption and Production Worldwide. Int J Environ Res Public Health. 2018;15(3).

26. Rossini M, Rizzo P, Bononi I, Clementz A, Ferrari R, Martini F, et al. New Perspectives on Diagnosis and Therapy of Malignant Pleural Mesothelioma. Frontiers in Oncology. 2018;8.

27. Husain AN, Colby TV, Ordóñez NG, Allen TC, Attanoos RL, Beasley MB, et al. Guidelines for Pathologic Diagnosis of Malignant Mesothelioma 2017 Update of the Consensus Statement From the International Mesothelioma Interest Group. Archives of Pathology & Laboratory Medicine. 2017;142(1):89-108.

28. Klebe S, Brownlee NA, Mahar A, Burchette JL, Sporn TA, Vollmer RT, et al. Sarcomatoid mesothelioma: a clinical-pathologic correlation of 326 cases. Mod Pathol. 2010;23(3):470-9.

29. Asciak R, George V, Rahman NM. Update on biology and management of mesothelioma. European Respiratory Review. 2021;30(159):200226.

30. Brims FJ, Meniawy TM, Duffus I, de Fonseka D, Segal A, Creaney J, et al. A Novel Clinical Prediction Model for Prognosis in Malignant Pleural Mesothelioma Using Decision Tree Analysis. J Thorac Oncol. 2016;11(4):573-82.

31. Billè A, Okiror L, Harling L, Pernazza F, Muzio A, Roveta A, et al. Analysis of survival of patients with metastatic malignant pleural mesothelioma. Tumori Journal. 2020;107(2):110-8.

32. Blyth KG, Murphy DJ. Progress and challenges in Mesothelioma: From bench to bedside. Respiratory Medicine. 2018;134:31-41.

33. Galetta D, Catino A, Misino A, Logroscino A, Fico M. Sarcomatoid Mesothelioma: Future Advances in Diagnosis, Biomolecular Assessment, and Therapeutic Options in a Poor-Outcome Disease. Tumori Journal. 2015;102(2):127-30.

34. Curran D, Sahmoud T, Therasse P, van Meerbeeck J, Postmus PE, Giaccone G. Prognostic factors in patients with pleural mesothelioma: the European Organization for Research and Treatment of Cancer experience. J Clin Oncol. 1998;16(1):145-52.

35. Fennell DA, Parmar A, Shamash J, Evans MT, Sheaff MT, Sylvester R, et al. Statistical validation of the EORTC prognostic model for malignant pleural mesothelioma based on three consecutive phase II trials. J Clin Oncol. 2005;23(1):184-9.

36. Edwards JG, Abrams KR, Leverment JN, Spyt TJ, Waller DA, O'Byrne KJ. Prognostic factors for malignant mesothelioma in 142 patients: validation of CALGB and EORTC prognostic scoring systems. Thorax. 2000;55(9):731-5.

37. Steele JP, Klabatsa A, Fennell DA, Palläska A, Sheaff MT, Evans MT, et al. Prognostic factors in mesothelioma. Lung Cancer. 2005;49 Suppl 1:S49-52.

38. Herndon JE, Green MR, Chahinian AP, Corson JM, Suzuki Y, Vogelzang NJ. Factors predictive of survival among 337 patients with mesothelioma treated between 1984 and 1994 by the Cancer and Leukemia Group B. Chest. 1998;113(3):723-31.

39. Nowak AK, Francis RJ, Phillips MJ, Millward MJ, van der Schaaf AA, Boucek J, et al. A Novel Prognostic Model for Malignant Mesothelioma Incorporating Quantitative FDG-PET Imaging with Clinical Parameters. Clinical Cancer Research. 2010;16(8):2409-17.

40. Rusch VW, Chansky K, Kindler HL, Nowak AK, Pass HI, Rice DC, et al. The IASLC Mesothelioma Staging Project: Proposals for the M Descriptors and for Revision of the TNM Stage Groupings in the Forthcoming (Eighth) Edition of the TNM Classification for Mesothelioma. J Thorac Oncol. 2016;11(12):2112-9.

41. Flores RM, Akhurst T, Gonen M, Zakowski M, Dycoco J, Larson SM, et al. Positron emission tomography predicts survival in malignant pleural mesothelioma. The Journal of Thoracic and Cardiovascular Surgery. 2006;132(4):763-8.

42. Van Gelder T, Damhuis R, Hoogsteden H. Prognostic factors and survival in malignant pleural mesothelioma. European Respiratory Journal. 1994;7(6):1035-8.

43. Pass HI, Giroux D, Kennedy C, Ruffini E, Cangir AK, Rice D, et al. Supplementary Prognostic Variables for Pleural Mesothelioma: A Report from the IASLC Staging Committee. Journal of Thoracic Oncology. 2014;9(6):856-64.

44. Ak G, Metintas S, Metintas M, Yildirim H, Erginel S, Kurt E, et al. Prognostic Factors According to the Treatment Schedule in Malignant Pleural Mesothelioma. Journal of Thoracic Oncology. 2009;4(11):1425-30.

45. Berzenji L, Van Schil PE, Carp L. The eighth TNM classification for malignant pleural mesothelioma. Transl Lung Cancer Res. 2018;7(5):543-9.

46. Nowak A. MS25.01 Impact of Tumor Volume on Outcome: What Are the Limitations? Journal of Thoracic Oncology. 2018;13(10):S293-S4.

47. Patz EF, Jr., Shaffer K, Piwnica-Worms DR, Jochelson M, Sarin M, Sugarbaker DJ, et al. Malignant pleural mesothelioma: value of CT and MR imaging in predicting resectability. AJR Am J Roentgenol. 1992;159(5):961-6.

48. Lim E, Darlison L, Edwards J, Elliott D, Fennell DA, Popat S, et al. Mesothelioma and Radical Surgery 2 (MARS 2): protocol for a multicentre randomised trial comparing (extended) pleurectomy decortication versus no (extended) pleurectomy decortication for patients with malignant pleural mesothelioma. BMJ Open. 2020;10(9):e038892.

49. Tsim S, Stobo DB, Alexander L, Kelly C, Blyth KG. The diagnostic performance of routinely acquired and reported computed tomography imaging in patients presenting with suspected pleural malignancy. Lung Cancer. 2017;103:38-43.

50. Metintas M, Ucgun I, Elbek O, Erginel S, Metintas S, Kolsuz M, et al. Computed tomography features in malignant pleural mesothelioma and other commonly seen pleural diseases. Eur J Radiol. 2002;41(1):1-9.

51. Hallifax RJ, Haris M, Corcoran JP, Leyakathalikhan S, Brown E, Srikantharaja D, et al. Role of CT in assessing pleural malignancy prior to thoracoscopy. Thorax. 2015;70(2):192-3.

52. Hierholzer J, Luo L, Bittner RC, Stroszczynski C, Schröder RJ, Schoenfeld N, et al. MRI and CT in the differential diagnosis of pleural disease. Chest. 2000;118(3):604-9.

53. Krumbhaar EB, Krumbhaar HD. The Blood and Bone Marrow in Yelloe Cross Gas (Mustard Gas) Poisoning: Changes produced in the Bone Marrow of Fatal Cases. J Med Res. 1919;40(3):497-508.3.

54. van Meerbeeck JP, Gaafar R, Manegold C, Van Klaveren RJ, Van Marck EA, Vincent M, et al. Randomized phase III study of cisplatin with or without raltitrexed in patients with malignant pleural mesothelioma: an intergroup study of the European Organisation for Research and Treatment of Cancer Lung Cancer Group and the National Cancer Institute of Canada. J Clin Oncol. 2005;23(28):6881-9.

55. Zalcman G, Mazieres J, Margery J, Greillier L, Audigier-Valette C, Moro-Sibilot D, et al. Bevacizumab for newly diagnosed pleural mesothelioma in the Mesothelioma Avastin Cisplatin Pemetrexed Study (MAPS): a randomised, controlled, open-label, phase 3 trial. Lancet. 2016;387(10026):1405-14.

56. Krug LM, Kindler HL, Calvert H, Manegold C, Tsao AS, Fennell D, et al. Vorinostat in patients with advanced malignant pleural mesothelioma who have progressed on previous chemotherapy (VANTAGE-014): a phase 3, double-blind, randomised, placebo-controlled trial. Lancet Oncol. 2015;16(4):447-56.

57. Dubey S, Jänne PA, Krug L, Pang H, Wang X, Heinze R, et al. A phase II study of sorafenib in malignant mesothelioma: results of Cancer and Leukemia Group B 30307. J Thorac Oncol. 2010;5(10):1655-61.

58. Dudek AZ, Pang H, Kratzke RA, Otterson GA, Hodgson L, Vokes EE, et al. Phase II study of dasatinib in patients with previously treated malignant mesothelioma (cancer and leukemia group B 30601): a brief report. J Thorac Oncol. 2012;7(4):755-9.

59. Jassem J, Ramlau R, Santoro A, Schuette W, Chemaissani A, Hong S, et al. Phase III trial of pemetrexed plus best supportive care compared with best supportive care in previously treated patients with advanced malignant pleural mesothelioma. J Clin Oncol. 2008;26(10):1698-704.

60. Fennell DA, Casbard AC, Porter C, Rudd R, Lester JF, Nicolson M, et al. A randomized phase II trial of oral vinorelbine as second-line therapy for patients with malignant pleural mesothelioma. Journal of Clinical Oncology. 2021;39(15_suppl):8507-.

61. Carbone DP, Reck M, Paz-Ares L, Creelan B, Horn L, Steins M, et al. First-Line Nivolumab in Stage IV or Recurrent Non-Small-Cell Lung Cancer. N Engl J Med. 2017;376(25):2415-26.

62. Reck M, Rodríguez-Abreu D, Robinson AG, Hui R, Csőszi T, Fülöp A, et al. Pembrolizumab versus Chemotherapy for PD-L1-Positive Non-Small-Cell Lung Cancer. N Engl J Med. 2016;375(19):1823-33.

63. Antonia SJ, Villegas A, Daniel D, Vicente D, Murakami S, Hui R, et al. Overall Survival with Durvalumab after Chemoradiotherapy in Stage III NSCLC. New England Journal of Medicine. 2018;379(24):2342-50.

64. Herbst RS, Giaccone G, de Marinis F, Reinmuth N, Vergnenegre A, Barrios CH, et al. Atezolizumab for First-Line Treatment of PD-L1-Selected Patients with NSCLC. N Engl J Med. 2020;383(14):1328-39.

65. Horn L, Mansfield AS, Szczęsna A, Havel L, Krzakowski M, Hochmair MJ, et al. First-Line Atezolizumab plus Chemotherapy in Extensive-Stage Small-Cell Lung Cancer. New England Journal of Medicine. 2018;379(23):2220-9.

66. Baas P, Scherpereel A, Nowak AK, Fujimoto N, Peters S, Tsao AS, et al. First-line nivolumab plus ipilimumab in unresectable malignant pleural mesothelioma (CheckMate 743): a multicentre, randomised, open-label, phase 3 trial. Lancet. 2021;397(10272):375-86.

67. Peters S, Scherpereel A, Cornelissen R, Oulkhouir Y, Greillier L, Kaplan MA, et al. First-line nivolumab plus ipilimumab versus chemotherapy in patients with unresectable malignant pleural mesothelioma: 3-year outcomes from CheckMate 743. Annals of Oncology.

68. Quispel-Janssen J, van der Noort V, de Vries JF, Zimmerman M, Lalezari F, Thunnissen E, et al. Programmed Death 1 Blockade With Nivolumab in Patients With Recurrent Malignant Pleural Mesothelioma. J Thorac Oncol. 2018;13(10):1569-76.

69. Okada M, Kijima T, Aoe K, Kato T, Fujimoto N, Nakagawa K, et al. Clinical Efficacy and Safety of Nivolumab: Results of a Multicenter, Open-label, Single-arm, Japanese Phase II study in Malignant Pleural Mesothelioma (MERIT). Clin Cancer Res. 2019;25(18):5485-92.

70. Scherpereel A, Mazieres J, Greillier L, Lantuejoul S, Dô P, Bylicki O, et al. Nivolumab or nivolumab plus ipilimumab in patients with relapsed malignant pleural mesothelioma (IFCT-1501 MAPS2): a multicentre, open-label, randomised, non-comparative, phase 2 trial. Lancet Oncol. 2019;20(2):239-53.

71. Hassan R, Thomas A, Nemunaitis JJ, Patel MR, Bennouna J, Chen FL, et al. Efficacy and Safety of Avelumab Treatment in Patients With Advanced Unresectable Mesothelioma: Phase 1b Results From the JAVELIN Solid Tumor Trial. JAMA Oncol. 2019;5(3):351-7.

72. ASCO. CONFIRM Trial Reports Improvement in Survival With Nivolumab in Relapsed Malignant Mesothelioma https://ascopost.com/issues/march-10-2021/confirm-trial-reports-improvement-in-survival-with-nivolumab-in-relapsed-malignant-mesothelioma/2021 [

73. Bibby AC, Tsim S, Kanellakis N, Ball H, Talbot DC, Blyth KG, et al. Malignant pleural mesothelioma: an update on investigation, diagnosis and treatment. European Respiratory Review. 2016;25(142):472-86.

74. Miller AB, Hoogstraten B, Staquet M, Winkler A. Reporting results of cancer treatment. Cancer. 1981;47(1):207-14.

75. Therasse P, Arbuck SG, Eisenhauer EA, Wanders J, Kaplan RS, Rubinstein L, et al. New guidelines to evaluate the response to treatment in solid tumors. European Organization for Research and Treatment of Cancer, National Cancer Institute of the United States, National Cancer Institute of Canada. J Natl Cancer Inst. 2000;92(3):205-16.

76. Eisenhauer EA, Therasse P, Bogaerts J, Schwartz LH, Sargent D, Ford R, et al. New response evaluation criteria in solid tumours: revised RECIST guideline (version 1.1). Eur J Cancer. 2009;45(2):228-47.

77. van Klaveren RJ, Aerts JG, de Bruin H, Giaccone G, Manegold C, van Meerbeeck JP. Inadequacy of the RECIST criteria for response evaluation in patients with malignant pleural mesothelioma. Lung Cancer. 2004;43(1):63-9.

78. Ceresoli GL, Chiti A, Zucali PA, Cappuzzo F, De Vincenzo F, Cavina R, et al. Assessment of tumor response in malignant pleural mesothelioma. Cancer Treat Rev. 2007;33(6):533-41.

79. Monetti F, Casanova S, Grasso A, Cafferata MA, Ardizzoni A, Neumaier CE. Inadequacy of the new Response Evaluation Criteria in Solid Tumors (RECIST) in patients with malignant pleural mesothelioma: report of four cases. Lung Cancer. 2004;43(1):71-4.

80. Liu F, Zhao B, Krug LM, Ishill NM, Lim RC, Guo P, et al. Assessment of therapy responses and prediction of survival in malignant pleural mesothelioma through computer-aided volumetric measurement on computed tomography scans. J Thorac Oncol. 2010;5(6):879-84.

81. Armato SG, 3rd, Oxnard GR, MacMahon H, Vogelzang NJ, Kindler HL, Kocherginsky M, et al. Measurement of mesothelioma on thoracic CT scans: a comparison of manual and computer-assisted techniques. Med Phys. 2004;31(5):1105-15.

82. Oxnard GR, Armato SG, 3rd, Kindler HL. Modeling of mesothelioma growth demonstrates weaknesses of current response criteria. Lung Cancer. 2006;52(2):141-8.

83. Beaumont H, Souchet S, Labatte JM, Iannessi A, Tolcher AW. Changes of lung tumour volume on CT - prediction of the reliability of assessments. Cancer Imaging. 2015;15:17.

84. Tariq I, Chen T, Kirkby NF, Jena R. Modelling and Bayesian adaptive prediction of individual patients' tumour volume change during radiotherapy. Phys Med Biol. 2016;61(5):2145-61.

85. Farchione A, Larici AR, Masciocchi C, Cicchetti G, Congedo MT, Franchi P, et al. Exploring technical issues in personalized medicine: NSCLC survival prediction by quantitative image analysis-usefulness of density correction of volumetric CT data. Radiol Med. 2020;125(7):625-35.

86. Im HJ, Pak K, Cheon GJ, Kang KW, Kim SJ, Kim IJ, et al. Prognostic value of volumetric parameters of (18)F-FDG PET in non-small-cell lung cancer: a meta-analysis. Eur J Nucl Med Mol Imaging. 2015;42(2):241-51.

87. Ganem J, Thureau S, Gardin I, Modzelewski R, Hapdey S, Vera P. Delineation of lung cancer with FDG PET/CT during radiation therapy. Radiation Oncology. 2018;13(1):219.

88. Kolinger GD, Vállez García D, Kramer GM, Frings V, Smit EF, de Langen AJ, et al. Repeatability of [18F]FDG PET/CT total metabolic active tumour volume and total tumour burden in NSCLC patients. EJNMMI Research. 2019;9(1):14.

89. Lee JY, Choi JY, Heo JH, Han J, Jang SJ, Kim K, et al. Prognostic significance of volume-based 18F-FDG PET/CT parameter in patients with surgically resected non-small cell lung cancer. Comparison with immunohistochemical biomarkers. Nuklearmedizin. 2016;55(1):7-14.

90. Dosani M, Yang R, McLay M, Wilson D, Liu M, Yong-Hing CJ, et al. Metabolic tumour volume is prognostic in patients with non-small-cell lung cancer treated with stereotactic ablative radiotherapy. Curr Oncol. 2019;26(1):e57-e63.

91. Hyun SH, Ahn HK, Kim H, Ahn MJ, Park K, Ahn YC, et al. Volume-based assessment by (18)F-FDG PET/CT predicts survival in patients with stage III non-small-cell lung cancer. Eur J Nucl Med Mol Imaging. 2014;41(1):50-8.

92. Soussan M, Chouahnia K, Maisonobe JA, Boubaya M, Eder V, Morère JF, et al. Prognostic implications of volume-based measurements on FDG PET/CT in stage III non-small-cell lung cancer after induction chemotherapy. Eur J Nucl Med Mol Imaging. 2013;40(5):668-76.

93. Nie K, Zhang YX, Nie W, Zhu L, Chen YN, Xiao YX, et al. Prognostic value of metabolic tumour volume and total lesion glycolysis measured by 18F-fluorodeoxyglucose positron emission tomography/computed tomography in small cell lung cancer: A systematic review and meta-analysis. J Med Imaging Radiat Oncol. 2019;63(1):84-93.

94. Oh JR, Seo JH, Chong A, Min JJ, Song HC, Kim YC, et al. Whole-body metabolic tumour volume of 18F-FDG PET/CT improves the prediction of prognosis in small cell lung cancer. Eur J Nucl Med Mol Imaging. 2012;39(6):925-35.

95. van Loon J, Offermann C, Ollers M, van Elmpt W, Vegt E, Rahmy A, et al. Early CT and FDG-metabolic tumour volume changes show a significant correlation with survival in stage I-III small cell lung cancer: a hypothesis generating study. Radiother Oncol. 2011;99(2):172-5.

96. Jefferson MF, Pendleton N, Faragher EB, Dixon GR, Myskow MW, Horan MA. 'Tumour volume' as a predictor of survival after resection of non-small-cell lung cancer (NSCLC). Br J Cancer. 1996;74(3):456-9.

97. Davey A, van Herk M, Faivre-Finn C, Mistry H, McWilliam A. Is tumour sphericity an important prognostic factor in patients with lung cancer? Radiother Oncol. 2020;143:73-80.

98. Bianconi F, Fravolini ML, Bello-Cerezo R, Minestrini M, Scialpi M, Palumbo B. Evaluation of Shape and Textural Features from CT as Prognostic Biomarkers in Non-small Cell Lung Cancer. Anticancer Res. 2018;38(4):2155-60.

99. Pass HI, Temeck BK, Kranda K, Steinberg SM, Feuerstein IR. Preoperative tumor volume is associated with outcome in malignant pleural mesothelioma. J Thorac Cardiovasc Surg. 1998;115(2):310-7; discussion 7-8.

100. Kircheva DY, Husain A, Watso S, Armato S, Kindler H, Vigneswaran WT. Tumor volume is an independent predictor of survival in patients with malignant pleural mesothelioma. Journal of Cardiothoracic Surgery. 2015;10(1):A48.

101. Gill RR, Richards WG, Yeap BY, Matsuoka S, Wolf AS, Gerbaudo VH, et al. Epithelial malignant pleural mesothelioma after extrapleural pneumonectomy: stratification of survival with CT-derived tumor volume. AJR Am J Roentgenol. 2012;198(2):359-63.

102. Rusch VW, Gill R, Mitchell A, Naidich D, Rice DC, Pass HI, et al. A Multicenter Study of Volumetric Computed Tomography for Staging Malignant Pleural Mesothelioma. Ann Thorac Surg. 2016;102(4):1059-66.

103. Paajanen J, Laaksonen S, Ilonen I, Wolff H, Husgafvel-Pursiainen K, Kuosma E, et al. Computed tomography in the evaluation of malignant pleural mesothelioma-Association of tumor size to a sarcomatoid histology, a more advanced TNM stage and poor survival. Lung Cancer. 2018;116:73-9.

104. Labby ZE, Nowak AK, Dignam JJ, Straus C, Kindler HL, Armato SG, 3rd. Disease volumes as a marker for patient response in malignant pleural mesothelioma. Ann Oncol. 2013;24(4):999-1005.

105. Sobin LH, Gospodarowicz MK, Wittekind C. TNM classification of malignant tumours. 7th ed. 2009. ed. Chichester, West Sussex, UK ;: Wiley-Blackwell; 2010.

106. Zhao B, Schwartz LH, Liu F, Wang L, Krug L, Flores RM, et al. 81 Development of a computer method for volumetric response assessment in mesothelioma. Lung Cancer. 2006;54.

107. Ak G, Metintas M, Metintas S, Yildirim H, Ozkan R, Ozden H. Three-dimensional evaluation of chemotherapy response in malignant pleural mesothelioma. Eur J Radiol. 2010;74(1):130-5.

108. Frauenfelder T, Tutic M, Weder W, Götti RP, Stahel RA, Seifert B, et al. Volumetry: an alternative to assess therapy response for malignant pleural mesothelioma? Eur Respir J. 2011;38(1):162-8.

109. Sensakovic WF, Armato SG, 3rd, Straus C, Roberts RY, Caligiuri P, Starkey A, et al. Computerized segmentation and measurement of malignant pleural mesothelioma. Med Phys. 2011;38(1):238-44.

110. Chaisaowong K AC, Wilkmann C, Kraus T. A fully automatic probabilistic 3D approach for the detection and assessment of pleural thickenings from CT data. 2013 Fourth International Workshop on Computational Intelligence in Medical Imaging (CIMI). 2013:14-21.

111. Gill RR, Naidich DP, Mitchell A, Ginsberg M, Erasmus J, Armato SG, 3rd, et al. North American Multicenter Volumetric CT Study for Clinical Staging of Malignant Pleural Mesothelioma: Feasibility and Logistics of Setting Up a Quantitative Imaging Study. J Thorac Oncol. 2016;11(8):1335-44.

112. Chen M, Helm E, Joshi N, Gleeson F, Brady M. Computer-aided volumetric assessment of malignant pleural mesothelioma on CT using a random walk-based method. Int J Comput Assist Radiol Surg. 2017;12(4):529-38.

113. Brahim W, Mestiri M, Betrouni N, Hamrouni K. Malignant pleural mesothelioma segmentation for photodynamic therapy planning. Comput Med Imaging Graph. 2018;65:79-92.

114. Russel S NP. Artificial Intelligence. A modern approach. Upper Saddle River, New Jersey: Pearson Education, Inc.; 2010.

115. McCarthy J, Minsky ML, Rochester N, Shannon CE. A Proposal for the Dartmouth Summer Research Project on Artificial Intelligence, August 31, 1955. AI Magazine. 2006;27(4):12.

116. Hinton GE, Osindero S, Teh YW. A fast learning algorithm for deep belief nets. Neural Comput. 2006;18(7):1527-54.

117. Schmidhuber J. Deep learning in neural networks: An overview. Neural Networks. 2015;61:85-117.

118. What the radiologist should know about artificial intelligence - an ESR white paper. Insights Imaging. 2019;10(1):44.

119. Hosny A, Parmar C, Quackenbush J, Schwartz LH, Aerts H. Artificial intelligence in radiology. Nat Rev Cancer. 2018;18(8):500-10.

120. Këpuska V, Bohouta G, editors. Next-generation of virtual personal assistants (Microsoft Cortana, Apple Siri, Amazon Alexa and Google Home). 2018 IEEE 8th Annual Computing and Communication Workshop and Conference (CCWC); 2018 8-10 Jan. 2018.

121. Tan Q, Liu N, Hu X. Deep Representation Learning for Social Network Analysis. Frontiers in Big Data. 2019;2.

122. Fares OH, Butt I, Lee SHM. Utilization of artificial intelligence in the banking sector: a systematic literature review. Journal of Financial Services Marketing. 2022.

123. Xu L, Sanders L, Li K, Chow JCL. Chatbot for Health Care and Oncology Applications Using Artificial Intelligence and Machine Learning: Systematic Review. JMIR Cancer. 2021;7(4):e27850.

124. Shao X, Kim CS. Multi-Step Short-Term Power Consumption Forecasting Using Multi-Channel LSTM With Time Location Considering Customer Behavior. IEEE Access. 2020;8:125263-73.

125. Chaudhuri N, Gupta G, Vallurupalli V, Bose I. On the platform but will they buy? Predicting customers' purchase behavior using deep learning. Decis Support Syst. 2021;149:113622.

126. Liang H, Sun X, Sun Y, Gao Y. Text feature extraction based on deep learning: a review. EURASIP J Wirel Commun Netw. 2017;2017(1):211.

127. Seify M, Sepehri M, Hosseini-far A, Darvish A. Fraud Detection in Supply Chain with Machine Learning. IFAC-PapersOnLine. 2022;55(10):406-11.

128. Dada EG, Bassi JS, Chiroma H, Abdulhamid SiM, Adetunmbi AO, Ajibuwa OE. Machine learning for email spam filtering: review, approaches and open research problems. Heliyon. 2019;5(6):e01802.

129. Bishop C. Neural Networks for Pattern Recognition. Oxford: Clarendon Press; 1995.

130. Hahn U, Oleynik M. Medical Information Extraction in the Age of Deep Learning. Yearb Med Inform. 2020;29(1):208-20.

131. Hassanzadeh H, Karimi S, Nguyen A. Matching patients to clinical trials using semantically enriched document representation. Journal of Biomedical Informatics. 2020;105:103406.

132. Suzuki K. Overview of deep learning in medical imaging. Radiol Phys Technol. 2017;10(3):257-73.

133. Zhou N, Siegel ZD, Zarecor S, Lee N, Campbell DA, Andorf CM, et al. Crowdsourcing image analysis for plant phenomics to generate ground truth data for machine learning. PLoS Comput Biol. 2018;14(7):e1006337.

134. Willemink MJ, Koszek WA, Hardell C, Wu J, Fleischmann D, Harvey H, et al. Preparing Medical Imaging Data for Machine Learning. Radiology. 2020;295(1):4-15.

135. Brodley CE, Friedl MA. Identifying mislabeled training data. Journal of artificial intelligence research. 1999;11:131-67.

136. Gudmundsson E, Straus CM, Armato SG, 3rd. Deep convolutional neural networks for the automated segmentation of malignant pleural mesothelioma on computed tomography scans. J Med Imaging (Bellingham). 2018;5(3):034503.

137. Yamashita R, Nishio M, Do RKG, Togashi K. Convolutional neural networks: an overview and application in radiology. Insights Imaging. 2018;9(4):611-29.

138. Simonyan K, Zisserman A. Very deep convolutional networks for large-scale image recognition. arXiv preprint arXiv:14091556. 2014.

139. Szegedy C, Liu W, Jia Y, Sermanet P, Reed S, Anguelov D, et al., editors. Going deeper with convolutions. Proceedings of the IEEE conference on computer vision and pattern recognition; 2015.

140. He K, Zhang X, Ren S, Sun J. Deep Residual Learning for Image Recognition. 2016 IEEE Conference on Computer Vision and Pattern Recognition (CVPR). 2016:770-8.

141. Ronneberger O, Fischer P, Brox T, editors. U-Net: Convolutional Networks for Biomedical Image Segmentation2015; Cham: Springer International Publishing.

142. Russakovsky O, Deng J, Su H, Krause J, Satheesh S, Ma S, et al. ImageNet Large Scale Visual Recognition Challenge. International Journal of Computer Vision. 2015;115(3):211-52.

143. Deng J, Dong W, Socher R, Li LJ, Kai L, Li F-F, editors. ImageNet: A large-scale hierarchical image database. 2009 IEEE Conference on Computer Vision and Pattern Recognition; 2009 20-25 June 2009.

144. Kuznetsova A, Rom H, Alldrin N, Uijlings J, Krasin I, Pont-Tuset J, et al. The Open Images Dataset V4. International Journal of Computer Vision. 2020;128(7):1956-81.

145. Lin T-Y, Maire M, Belongie S, Hays J, Perona P, Ramanan D, et al., editors. Microsoft COCO: Common Objects in Context2014; Cham: Springer International Publishing.

146. She Q, Feng F, Hao X, Yang Q, Lan C, Lomonaco V, et al. OpenLORIS-Object: A Robotic Vision Dataset and Benchmark for Lifelong Deep Learning2020.

147. Shin HC, Roth HR, Gao M, Lu L, Xu Z, Nogues I, et al. Deep Convolutional Neural Networks for Computer-Aided Detection: CNN Architectures, Dataset Characteristics and Transfer Learning. IEEE Trans Med Imaging. 2016;35(5):1285-98.

148. Shaziya H, Shyamala K, Zaheer R, editors. Automatic Lung Segmentation on Thoracic CT Scans Using U-Net Convolutional Network. 2018 International Conference on Communication and Signal Processing (ICCSP); 2018 3-5 April 2018.

149. Baek S, He Y, Allen BG, Buatti JM, Smith BJ, Tong L, et al. Deep segmentation networks predict survival of non-small cell lung cancer. Scientific reports. 2019;9(1):1-10.

150. Grossman R, Haim O, Abramov S, Shofty B, Artzi M. Differentiating Small-Cell Lung Cancer From Non-Small-Cell Lung Cancer Brain Metastases Based on MRI Using Efficientnet and Transfer Learning Approach. Technology in Cancer Research & Treatment. 2021;20:15330338211004919.

151. Çiçek Ö, Abdulkadir A, Lienkamp SS, Brox T, Ronneberger O, editors. 3D U-Net: learning dense volumetric segmentation from sparse annotation. International conference on medical image computing and computer-assisted intervention; 2016: Springer.

152. Gudmundsson E, Straus C, Li F, Kindler H, Armato S. P1.06-04 Deep Learning-Based Segmentation of Mesothelioma on CT Scans: Application to Patient Scans Exhibiting Pleural Effusion. Journal of Thoracic Oncology. 2019;14(10):S478.

153. Metintas M, Metintas S, Ucgun I, Gibbs AR, Harmanci E, Alatas F, et al. Prognostic factors in diffuse malignant pleural mesothelioma: effects of pretreatment clinical and laboratory characteristics. Respir Med. 2001;95(10):829-35.

154. Linton A, Pavlakis N, O'Connell R, Soeberg M, Kao S, Clarke S, et al. Factors associated with survival in a large series of patients with malignant pleural mesothelioma in New South Wales. British Journal of Cancer. 2014;111(9):1860-9.

155. Ceresoli GL, Grosso F, Zucali PA, Mencoboni M, Pasello G, Ripa C, et al. Prognostic factors in elderly patients with malignant pleural mesothelioma: results of a multicenter survey. Br J Cancer. 2014;111(2):220-6.

156. Musk AW, Olsen N, Alfonso H, Reid A, Mina R, Franklin P, et al. Predicting survival in malignant mesothelioma. European Respiratory Journal. 2011;38(6):1420-4.

157. Oken MM, Creech RH, Tormey DC, Horton J, Davis TE, McFadden ET, et al. Toxicity and response criteria of the Eastern Cooperative Oncology Group. Am J Clin Oncol. 1982;5(6):649-55.

158. Karnofsky DAB BJ. The Clinical Evaluation of Chemotherapeutic Agents in Cancer. In Evaluation of Chemotherapeutic Agents. New York, NY, USA: Columbia University Press; 1949.

159. Kindler HL, Ismaila N, Armato SG, Bueno R, Hesdorffer M, Jahan T, et al. Treatment of Malignant Pleural Mesothelioma: American Society of Clinical Oncology Clinical Practice Guideline. Journal of Clinical Oncology. 2018;36(13):1343-73.

160. Popat S, Baas P, Faivre-Finn C, Girard N, Nicholson AG, Nowak AK, et al. Malignant pleural mesothelioma: ESMO Clinical Practice Guidelines for diagnosis, treatment and follow-up[†]. Annals of Oncology.

161. Cedres S, Assaf J-D, Iranzo P, Callejo A, Pardo N, Navarro A, et al. Efficacy of chemotherapy for malignant pleural mesothelioma according to histology in a real-world cohort. Scientific Reports. 2021;11(1):21357.

162. Rahouma M, Aziz H, Ghaly G, Kamel M, Loai I, Mohamed A. Survival in Good Performance Malignant Pleural Mesothelioma Patients; Prognostic Factors and Predictors of Response. Asian Pac J Cancer Prev. 2017;18(8):2073-8.

163. Templeton AJ, McNamara MG, Šeruga B, Vera-Badillo FE, Aneja P, Ocaña A, et al. Prognostic role of neutrophil-to-lymphocyte ratio in solid tumors: a systematic review and meta-analysis. J Natl Cancer Inst. 2014;106(6):dju124.

164. Kao SC, Vardy J, Harvie R, Chatfield M, van Zandwijk N, Clarke S, et al. Health-related quality of life and inflammatory markers in malignant pleural mesothelioma. Support Care Cancer. 2013;21(3):697-705.

165. Kao SC, Pavlakis N, Harvie R, Vardy JL, Boyer MJ, van Zandwijk N, et al. High blood neutrophil-to-lymphocyte ratio is an indicator of poor prognosis in malignant mesothelioma patients undergoing systemic therapy. Clin Cancer Res. 2010;16(23):5805-13.

166. Kao SC-H, Klebe S, Henderson DW, Reid G, Chatfield M, Armstrong NJ, et al. Low Calretinin Expression and High Neutrophil-To-Lymphocyte Ratio Are Poor Prognostic Factors in Patients with Malignant Mesothelioma Undergoing Extrapleural Pneumonectomy. Journal of Thoracic Oncology. 2011;6(11):1923-9.

167. Pinato DJ, Mauri FA, Ramakrishnan R, Wahab L, Lloyd T, Sharma R. Inflammation-based prognostic indices in malignant pleural mesothelioma. J Thorac Oncol. 2012;7(3):587-94.

168. Yao ZH, Tian GY, Yang SX, Wan YY, Kang YM, Liu QH, et al. Serum albumin as a significant prognostic factor in patients with malignant pleural mesothelioma. Tumour Biol. 2014;35(7):6839-45.

169. Yamagishi T, Fujimoto N, Nishi H, Miyamoto Y, Hara N, Asano M, et al. Prognostic significance of the lymphocyte-to-monocyte ratio in patients with malignant pleural mesothelioma. Lung Cancer. 2015;90(1):111-7.

170. Ghanim B, Hoda MA, Winter MP, Klikovits T, Alimohammadi A, Hegedus B, et al. Pretreatment serum C-reactive protein levels predict benefit from multimodality treatment including radical surgery in malignant pleural mesothelioma: a retrospective multicenter analysis. Ann Surg. 2012;256(2):357-62.

171. Cihan YB, Ozturk A, Mutlu H. Relationship between prognosis and neutrophil: lymphocyte and platelet:lymphocyte ratios in patients with malignant pleural mesotheliomas. Asian Pac J Cancer Prev. 2014;15(5):2061-7.

172. Kidd AC, McGettrick M, Tsim S, Halligan DL, Bylesjo M, Blyth KG. Survival prediction in mesothelioma using a scalable Lasso regression model: instructions for use and initial performance using clinical predictors. BMJ Open Respir Res. 2018;5(1):e000240.

173. Bachmann J, Heiligensetzer M, Krakowski-Roosen H, Büchler MW, Friess H, Martignoni ME. Cachexia worsens prognosis in patients with resectable pancreatic cancer. J Gastrointest Surg. 2008;12(7):1193-201.

174. Prado CM, Baracos VE, McCargar LJ, Mourtzakis M, Mulder KE, Reiman T, et al. Body composition as an independent determinant of 5-fluorouracil-based chemotherapy toxicity. Clin Cancer Res. 2007;13(11):3264-8.

175. Granda-Cameron C, DeMille D, Lynch MP, Huntzinger C, Alcorn T, Levicoff J, et al. An interdisciplinary approach to manage cancer cachexia. Clin J Oncol Nurs. 2010;14(1):72-80.

176. Kimura M, Naito T, Kenmotsu H, Taira T, Wakuda K, Oyakawa T, et al. Prognostic impact of cancer cachexia in patients with advanced non-small cell lung cancer. Support Care Cancer. 2015;23(6):1699-708.

177. Rock CL, Demark-Wahnefried W. Nutrition and survival after the diagnosis of breast cancer: a review of the evidence. J Clin Oncol. 2002;20(15):3302-16.

178. Thoresen L, Frykholm G, Lydersen S, Ulveland H, Baracos V, Birdsell L, et al. The association of nutritional assessment criteria with health-related quality of life in patients with advanced colorectal carcinoma. Eur J Cancer Care (Engl). 2012;21(4):505-16.

179. Douglas E, McMillan DC. Towards a simple objective framework for the investigation and treatment of cancer cachexia: the Glasgow Prognostic Score. Cancer Treat Rev. 2014;40(6):685-91.

180. Vigano A, Del Fabbro E, Bruera E, Borod M. The cachexia clinic: from staging to managing nutritional and functional problems in advanced cancer patients. Crit Rev Oncog. 2012;17(3):293-303.

181. Dewys WD, Begg C, Lavin PT, Band PR, Bennett JM, Bertino JR, et al. Prognostic effect of weight loss prior to chemotherapy in cancer patients. Eastern Cooperative Oncology Group. Am J Med. 1980;69(4):491-7.

182. Deans C, Wigmore SJ. Systemic inflammation, cachexia and prognosis in patients with cancer. Curr Opin Clin Nutr Metab Care. 2005;8(3):265-9.

183. Tan BH, Fearon KC. Cachexia: prevalence and impact in medicine. Curr Opin Clin Nutr Metab Care. 2008;11(4):400-7.

184. Fearon KC, Baracos VE. Cachexia in pancreatic cancer: new treatment options and measures of success. HPB (Oxford). 2010;12(5):323-4.

185. Baracos VE, Reiman T, Mourtzakis M, Gioulbasanis I, Antoun S. Body composition in patients with non-small cell lung cancer: a contemporary view of cancer cachexia with the use of computed tomography image analysis. Am J Clin Nutr. 2010;91(4):1133s-7s.

186. Martin L, Birdsell L, Macdonald N, Reiman T, Clandinin MT, McCargar LJ, et al. Cancer cachexia in the age of obesity: skeletal muscle depletion is a

powerful prognostic factor, independent of body mass index. J Clin Oncol. 2013;31(12):1539-47.

187. Prado CM, Baracos VE, McCargar LJ, Reiman T, Mourtzakis M, Tonkin K, et al. Sarcopenia as a determinant of chemotherapy toxicity and time to tumor progression in metastatic breast cancer patients receiving capecitabine treatment. Clin Cancer Res. 2009;15(8):2920-6.

188. Veasey-Rodrigues H, Parsons HA, Janku F, Naing A, Wheler JJ, Tsimberidou AM, et al. A pilot study of temsirolimus and body composition. J Cachexia Sarcopenia Muscle. 2013;4(4):259-65.

189. Harimoto N, Shirabe K, Yamashita YI, Ikegami T, Yoshizumi T, Soejima Y, et al. Sarcopenia as a predictor of prognosis in patients following hepatectomy for hepatocellular carcinoma. Br J Surg. 2013;100(11):1523-30.

190. Verhoek OG, Jungblut L, Lauk O, Blüthgen C, Opitz I, Frauenfelder T, et al. Sarcopenia, Precardial Adipose Tissue and High Tumor Volume as Outcome Predictors in Surgically Treated Pleural Mesothelioma. Diagnostics. 2022;12(1):99.

191. Muscaritoli M, Bossola M, Aversa Z, Bellantone R, Rossi Fanelli F. Prevention and treatment of cancer cachexia: new insights into an old problem. Eur J Cancer. 2006;42(1):31-41.

192. Fortunati N, Manti R, Birocco N, Pugliese M, Brignardello E, Ciuffreda L, et al. Pro-inflammatory cytokines and oxidative stress/antioxidant parameters characterize the bio-humoral profile of early cachexia in lung cancer patients. Oncol Rep. 2007;18(6):1521-7.

193. Vagnildhaug OM, Balstad TR, Almberg SS, Brunelli C, Knudsen AK, Kaasa S, et al. A cross-sectional study examining the prevalence of cachexia and areas of unmet need in patients with cancer. Support Care Cancer. 2018;26(6):1871-80.

194. Argilés JM, Busquets S, Stemmler B, López-Soriano FJ. Cancer cachexia: understanding the molecular basis. Nat Rev Cancer. 2014;14(11):754-62.

195. von Haehling S, Anker SD. Cachexia as a major underestimated and unmet medical need: facts and numbers. J Cachexia Sarcopenia Muscle. 2010;1(1):1-5.

196. Paajanen J, Ilonen I, Lauri H, Järvinen T, Sutinen E, Ollila H, et al. Elevated Circulating Activin A Levels in Patients With Malignant Pleural Mesothelioma Are Related to Cancer Cachexia and Reduced Response to Platinum-based Chemotherapy. Clin Lung Cancer. 2020;21(3):e142-e50.

197. Baracos VE, Martin L, Korc M, Guttridge DC, Fearon KCH. Cancer-associated cachexia. Nature Reviews Disease Primers. 2018;4(1):17105.

198. Porporato PE. Understanding cachexia as a cancer metabolism syndrome. Oncogenesis. 2016;5(2):e200-e.

199. Biswas AK, Acharyya S. Cancer-Associated Cachexia: A Systemic Consequence of Cancer Progression. Annual Review of Cancer Biology. 2020;4(1):391-411.

200. Loprinzi CL, Ellison NM, Goldberg RM, Michalak JC, Burch PA. Alleviation of cancer anorexia and cachexia: studies of the Mayo Clinic and the North Central Cancer Treatment Group. Semin Oncol. 1990;17(6 Suppl 9):8-12.

201. Loprinzi CL. Management of cancer anorexia/cachexia. Support Care Cancer. 1995;3(2):120-2.

202. Ross PJ, Ashley S, Norton A, Priest K, Waters JS, Eisen T, et al. Do patients with weight loss have a worse outcome when undergoing chemotherapy for lung cancers? Br J Cancer. 2004;90(10):1905-11.

203. Sanders KJ, Hendriks LE, Troost EG, Bootsma GP, Houben RM, Schols AM, et al. Early Weight Loss during Chemoradiotherapy Has a Detrimental Impact on Outcome in NSCLC. J Thorac Oncol. 2016;11(6):873-9.

204. Mytelka DS, Li L, Benoit K. Post-diagnosis weight loss as a prognostic factor in non-small cell lung cancer. J Cachexia Sarcopenia Muscle. 2018;9(1):86-92.

205. Masel EK, Berghoff AS, Füreder LM, Heicappell P, Schlieter F, Widhalm G, et al. Decreased body mass index is associated with impaired survival in lung cancer patients with brain metastases: A retrospective analysis of 624 patients. Eur J Cancer Care (Engl). 2017;26(6).

206. Patel JD, Pereira JR, Chen J, Liu J, Guba SC, John WJ, et al. Relationship between efficacy outcomes and weight gain during treatment of advanced, non-squamous, non-small-cell lung cancer patients. Ann Oncol. 2016;27(8):1612-9.

207. Meniawy TM, Creaney J, Lake RA, Nowak AK. Existing models, but not neutrophil-to-lymphocyte ratio, are prognostic in malignant mesothelioma. Br J Cancer. 2013;109(7):1813-20.

208. Rusch VW, Piantadosi S, Holmes EC. The role of extrapleural pneumonectomy in malignant pleural mesothelioma. A Lung Cancer Study Group trial. J Thorac Cardiovasc Surg. 1991;102(1):1-9.

209. De Wys W. Working conference on anorexia and cachexia of neoplastic disease. Cancer Res. 1970;30(11):2816-8.

210. Muers MF, Round CE. Palliation of symptoms in non-small cell lung cancer: a study by the Yorkshire Regional Cancer Organisation Thoracic Group. Thorax. 1993;48(4):339-43.

211. Lindsey AM, Piper BF. Anorexia and weight loss: indicators of cachexia in small cell lung cancer. Nutr Cancer. 1985;7(1-2):65-76.

212. Davis MP, Dreicer R, Walsh D, Lagman R, LeGrand SB. Appetite and cancer-associated anorexia: a review. J Clin Oncol. 2004;22(8):1510-7.

213. Ezeoke CC, Morley JE. Pathophysiology of anorexia in the cancer cachexia syndrome. J Cachexia Sarcopenia Muscle. 2015;6(4):287-302.

214. Laviano A, Inui A, Marks DL, Meguid MM, Pichard C, Rossi Fanelli F, et al. Neural control of the anorexia-cachexia syndrome. Am J Physiol Endocrinol Metab. 2008;295(5):E1000-8.

215. Rui L. Brain regulation of energy balance and body weight. Rev Endocr Metab Disord. 2013;14(4):387-407.

216. Krasnow SM, Marks DL. Neuropeptides in the pathophysiology and treatment of cachexia. Curr Opin Support Palliat Care. 2010;4(4):266-71.

217. Olson B, Diba P, Korzun T, Marks DL. Neural Mechanisms of Cancer Cachexia. Cancers. 2021;13(16):3990.

218. Molfino A, Rossi-Fanelli F, Laviano A. The interaction between pro-inflammatory cytokines and the nervous system. Nature Reviews Cancer. 2009;9(3):224-.

219. Grossberg AJ, Scarlett JM, Marks DL. Hypothalamic mechanisms in cachexia. Physiol Behav. 2010;100(5):478-89.

220. Karapanagiotou EM, Polyzos A, Dilana KD, Gratsias I, Boura P, Gkiozos I, et al. Increased serum levels of ghrelin at diagnosis mediate body weight loss in non-small cell lung cancer (NSCLC) patients. Lung Cancer. 2009;66(3):393-8.

221. Blauwhoff-Buskermolen S, Langius JA, Heijboer AC, Becker A, de van der Schueren MA, Verheul HM. Plasma Ghrelin Levels Are Associated with Anorexia but Not Cachexia in Patients with NSCLC. Front Physiol. 2017;8:119.

222. Temel JS, Abernethy AP, Currow DC, Friend J, Duus EM, Yan Y, et al. Anamorelin in patients with non-small-cell lung cancer and cachexia (ROMANA 1 and ROMANA 2): results from two randomised, double-blind, phase 3 trials. The Lancet Oncology. 2016;17(4):519-31.

223. Turcott JG, Del Rocío Guillen Núñez M, Flores-Estrada D, Oñate-Ocaña LF, Zatarain-Barrón ZL, Barrón F, et al. The effect of nabilone on appetite, nutritional status, and quality of life in lung cancer patients: a randomized, double-blind clinical trial. Support Care Cancer. 2018;26(9):3029-38.

224. Kirkham TC. Endocannabinoids in the regulation of appetite and body weight. Behav Pharmacol. 2005;16(5-6):297-313.

225. Hoon SN, Fyfe K, Peddle-McIntyre CJ, Bowyer S, Hawkins F, Jeffery E, et al. Randomised placebo-controlled cross-over study examining the role of anamorelin in mesothelioma (The ANTHEM study): rationale and protocol. BMJ Open Respiratory Research. 2020;7(1):e000551.

226. Duong L, Radley-Crabb HG, Gardner JK, Tomay F, Dye DE, Grounds MD, et al. Macrophage Depletion in Elderly Mice Improves Response to Tumor Immunotherapy, Increases Anti-tumor T Cell Activity and Reduces Treatment-Induced Cachexia. Frontiers in Genetics. 2018;9:526.

227. Luo Y, Zhou H, Krueger J, Kaplan C, Lee SH, Dolman C, et al. Targeting tumor-associated macrophages as a novel strategy against breast cancer. J Clin Invest. 2006;116(8):2132-41.

228. Zhang QW, Liu L, Gong CY, Shi HS, Zeng YH, Wang XZ, et al. Prognostic significance of tumor-associated macrophages in solid tumor: a meta-analysis of the literature. PLoS One. 2012;7(12):e50946.

229. VanderVeen BN, Murphy EA, Carson JA. The Impact of Immune Cells on the Skeletal Muscle Microenvironment During Cancer Cachexia. Frontiers in Physiology. 2020;11:1037.

230. Rausch V, Sala V, Penna F, Porporato PE, Ghigo A. Understanding the common mechanisms of heart and skeletal muscle wasting in cancer cachexia. Oncogenesis. 2021;10(1):1.

231. Tisdale MJ. Wasting in cancer. J Nutr. 1999;129(1S Suppl):243s-6s.

232. Fearon KC, Glass DJ, Guttridge DC. Cancer cachexia: mediators, signaling, and metabolic pathways. Cell Metab. 2012;16(2):153-66.

233. Emery PW, Lovell L, Rennie MJ. Protein synthesis measured in vivo in muscle and liver of cachectic tumor-bearing mice. Cancer Res. 1984;44(7):2779-84.

234. Fielitz J. Cancer cachexia-when proteasomal inhibition is not enough. J Cachexia Sarcopenia Muscle. 2016;7(3):239-45.

235. Poth KJ, Guminski AD, Thomas GP, Leo PJ, Jabbar IA, Saunders NA. Cisplatin treatment induces a transient increase in tumorigenic potential associated with high interleukin-6 expression in head and neck squamous cell carcinoma. Molecular cancer therapeutics. 2010;9(8):2430-9.

236. Quinn KM, Kartikasari AE, Cooke RE, Koldej RM, Ritchie DS, Plebanski M. Impact of age-, cancer-, and treatment-driven inflammation on T cell function and immunotherapy. Journal of Leukocyte Biology. 2020;108(3):953-65.

237. Kartikasari AER, Huertas CS, Mitchell A, Plebanski M. Tumor-Induced Inflammatory Cytokines and the Emerging Diagnostic Devices for Cancer Detection and Prognosis. Frontiers in Oncology. 2021;11(2641).

238. Braun TP, Grossberg AJ, Krasnow SM, Levasseur PR, Szumowski M, Zhu XX, et al. Cancer- and endotoxin-induced cachexia require intact glucocorticoid signaling in skeletal muscle. The FASEB Journal. 2013;27(9):3572-82.

239. Jones DP. Redefining oxidative stress. Antioxid Redox Signal. 2006;8(9-10):1865-79.

240. Manole E, Ceafalan LC, Popescu BO, Dumitru C, Bastian AE. Myokines as possible therapeutic targets in cancer cachexia. Journal of immunology research. 2018;2018.

241. Li F, Li Y, Duan Y, Hu C-AA, Tang Y, Yin Y. Myokines and adipokines: Involvement in the crosstalk between skeletal muscle and adipose tissue. Cytokine & growth factor reviews. 2017;33:73-82.

242. Raschke S, Eckardt K, Bjørklund Holven K, Jensen J, Eckel J. Identification and Validation of Novel Contraction-Regulated Myokines Released from Primary Human Skeletal Muscle Cells. PLOS ONE. 2013;8(4):e62008.

243. Costelli P, Muscaritoli M, Bonetto A, Penna F, Reffo P, Bossola M, et al. Muscle myostatin signalling is enhanced in experimental cancer cachexia. European Journal of Clinical Investigation. 2008;38(7):531-8.

244. Busquets S, Toledo M, Orpí M, Massa D, Porta M, Capdevila E, et al. Myostatin blockage using actRIIB antagonism in mice bearing the Lewis lung carcinoma results in the improvement of muscle wasting and physical performance. Journal of cachexia, sarcopenia and muscle. 2012;3(1):37-43.

245. Tsukioka T, Nishiyama N, Izumi N, Mizuguchi S, Komatsu H, Okada S, et al. Sarcopenia is a novel poor prognostic factor in male patients with pathological Stage I non-small cell lung cancer. Jpn J Clin Oncol. 2017;47(4):363-8.

246. Suzuki Y, Okamoto T, Fujishita T, Katsura M, Akamine T, Takamori S, et al. Clinical implications of sarcopenia in patients undergoing complete resection for early non-small cell lung cancer. Lung Cancer. 2016;101:92-7.

247. Hervochon R, Bobbio A, Guinet C, Mansuet-Lupo A, Rabbat A, Régnard JF, et al. Body Mass Index and Total Psoas Area Affect Outcomes in Patients Undergoing Pneumonectomy for Cancer. Ann Thorac Surg. 2017;103(1):287-95.

248. Shoji F, Matsubara T, Kozuma Y, Haratake N, Akamine T, Takamori S, et al. Relationship Between Preoperative Sarcopenia Status and Immuno-nutritional Parameters in Patients with Early-stage Non-small Cell Lung Cancer. Anticancer Res. 2017;37(12):6997-7003.

249. Kim EY, Kim YS, Park I, Ahn HK, Cho EK, Jeong YM. Prognostic Significance of CT-Determined Sarcopenia in Patients with Small-Cell Lung Cancer. J Thorac Oncol. 2015;10(12):1795-9.

250. Nakamura R, Inage Y, Tobita R, Yoneyama S, Numata T, Ota K, et al. Sarcopenia in Resected NSCLC: Effect on Postoperative Outcomes. J Thorac Oncol. 2018;13(7):895-903.

251. Prado CM, Lieffers JR, McCargar LJ, Reiman T, Sawyer MB, Martin L, et al. Prevalence and clinical implications of sarcopenic obesity in patients with solid

tumours of the respiratory and gastrointestinal tracts: a population-based study. Lancet Oncol. 2008;9(7):629-35.

252. Kazemi-Bajestani SM, Mazurak VC, Baracos V. Computed tomography-defined muscle and fat wasting are associated with cancer clinical outcomes. Semin Cell Dev Biol. 2016;54:2-10.

253. Nattenmüller J, Wochner R, Muley T, Steins M, Hummler S, Teucher B, et al. Prognostic Impact of CT-Quantified Muscle and Fat Distribution before and after First-Line-Chemotherapy in Lung Cancer Patients. PLOS ONE. 2017;12(1):e0169136.

254. Deng HY, Hou L, Zha P, Huang KL, Peng L. Sarcopenia is an independent unfavorable prognostic factor of non-small cell lung cancer after surgical resection: A comprehensive systematic review and meta-analysis. Eur J Surg Oncol. 2019;45(5):728-35.

255. Cortellini A, Verna L, Porzio G, Bozzetti F, Palumbo P, Masciocchi C, et al. Predictive value of skeletal muscle mass for immunotherapy with nivolumab in non-small cell lung cancer patients: A "hypothesis-generator" preliminary report. Thorac Cancer. 2019;10(2):347-51.

256. Kim EY, Lee HY, Kim YS, Park I, Ahn HK, Cho EK, et al. Prognostic significance of cachexia score assessed by CT in male patients with small cell lung cancer. Eur J Cancer Care (Engl). 2018;27(1).

257. Jeffery E, Lee YCG, Newton RU, Lyons-Wall P, McVeigh J, Fitzgerald DB, et al. Changes in body composition in patients with malignant pleural mesothelioma and the relationship with activity levels and dietary intake. European Journal of Clinical Nutrition. 2022.

258. Heymsfield SB, Coleman LA, Miller R, Rooks DS, Laurent D, Petricoul O, et al. Effect of Bimagrumab vs Placebo on Body Fat Mass Among Adults With Type 2 Diabetes and Obesity: A Phase 2 Randomized Clinical Trial. JAMA Network Open. 2021;4(1):e2033457-e.

259. Nowinska K, Jablonska K, Pawelczyk K, Piotrowska A, Partynska A, Gomulkiewicz A, et al. Expression of Irisin/FNDC5 in Cancer Cells and Stromal Fibroblasts of Non-Small Cell Lung Cancer. Cancers. 2019;11(10):1538.

260. Irlbeck T, Massaro JM, Bamberg F, O'Donnell CJ, Hoffmann U, Fox CS. Association between single-slice measurements of visceral and abdominal subcutaneous adipose tissue with volumetric measurements: the Framingham Heart Study. Int J Obes (Lond). 2010;34(4):781-7.

261. Murphy RA, Wilke MS, Perrine M, Pawlowicz M, Mourtzakis M, Lieffers JR, et al. Loss of adipose tissue and plasma phospholipids: Relationship to survival in advanced cancer patients. Clinical Nutrition. 2010;29(4):482-7.

262. Fouladiun M, Körner U, Bosaeus I, Daneryd P, Hyltander A, Lundholm KG. Body composition and time course changes in regional distribution of fat and lean tissue in unselected cancer patients on palliative care--correlations with food intake, metabolism, exercise capacity, and hormones. Cancer. 2005;103(10):2189-98.

263. Dahlman I, Mejhert N, Linder K, Agustsson T, Mutch DM, Kulyte A, et al. Adipose tissue pathways involved in weight loss of cancer cachexia. British journal of cancer. 2010;102(10):1541-8.

264. Sun X, Feng X, Wu X, Lu Y, Chen K, Ye Y. Fat Wasting Is Damaging: Role of Adipose Tissue in Cancer-Associated Cachexia. Frontiers in Cell and Developmental Biology. 2020;8:33.

265. Ebadi M, Mazurak VC. Evidence and mechanisms of fat depletion in cancer. Nutrients. 2014;6(11):5280-97.

266. Shellock FG, Riedinger MS, Fishbein MC. Brown adipose tissue in cancer patients: possible cause of cancer-induced cachexia. J Cancer Res Clin Oncol. 1986;111(1):82-5.

267. Fenzl A, Kiefer FW. Brown adipose tissue and thermogenesis. Horm Mol Biol Clin Investig. 2014;19(1):25-37.

268. Boström P, Wu J, Jedrychowski MP, Korde A, Ye L, Lo JC, et al. A PGC1-α-dependent myokine that drives brown-fat-like development of white fat and thermogenesis. Nature. 2012;481(7382):463-8.

269. Chondronikola M, Volpi E, Børsheim E, Porter C, Annamalai P, Enerbäck S, et al. Brown Adipose Tissue Improves Whole-Body Glucose Homeostasis and Insulin Sensitivity in Humans. Diabetes. 2014;63(12):4089-99.

270. Cao Q, Hersl J, La H, Smith M, Jenkins J, Goloubeva O, et al. A pilot study of FDG PET/CT detects a link between brown adipose tissue and breast cancer. BMC Cancer. 2014;14(1):126.

271. Huang Y-C, Chen T-B, Hsu C-C, Li S-H, Wang P-W, Lee B-F, et al. The Relationship between Brown Adipose Tissue Activity and Neoplastic Status: an 18F-FDG PET/CT Study in the Tropics. Lipids in Health and Disease. 2011;10(1):238.

272. Moley JF, Aamodt R, Rumble W, Kaye W, Norton JA. Body cell mass in cancer-bearing and anorexic patients. JPEN J Parenter Enteral Nutr. 1987;11(3):219-22.

273. Bos SA, Gill CM, Martinez-Salazar EL, Torriani M, Bredella MA. Preliminary investigation of brown adipose tissue assessed by PET/CT and cancer activity. Skeletal Radiol. 2019;48(3):413-9.

274. Fredrix EW, Soeters PB, Wouters EF, Deerenberg IM, von Meyenfeldt MF, Saris WH. Effect of different tumor types on resting energy expenditure. Cancer Res. 1991;51(22):6138-41.

275. Jatoi A, Daly BD, Hughes V, Dallal GE, Roubenoff R. The prognostic effect of increased resting energy expenditure prior to treatment for lung cancer. Lung Cancer. 1999;23(2):153-8.

276. Staal-van den Brekel AJ, Schols AM, Dentener MA, ten Velde GP, Buurman WA, Wouters EF. Metabolism in patients with small cell lung carcinoma

compared with patients with non-small cell lung carcinoma and healthy controls. Thorax. 1997;52(4):338-41.

277. Frille A, Kuhn H, Ebert T, Seyfarth H-J, Wirtz H. The influence of brown adipose tissue on the proliferation and chemosensitivity in non-small cell lung cancer cells. European Respiratory Journal. 2018;52(suppl 62):PA2844.

278. Kim J, Wang Z, Heymsfield SB, Baumgartner RN, Gallagher D. Total-body skeletal muscle mass: estimation by a new dual-energy X-ray absorptiometry method. The American journal of clinical nutrition. 2002;76(2):378-83.

279. Guglielmi G, Ponti F, Agostini M, Amadori M, Battista G, Bazzocchi A. The role of DXA in sarcopenia. Aging Clin Exp Res. 2016;28(6):1047-60.

280. Op den Kamp CM, Langen RC, Minnaard R, Kelders MC, Snepvangers FJ, Hesselink MK, et al. Pre-cachexia in patients with stages I-III non-small cell lung cancer: systemic inflammation and functional impairment without activation of skeletal muscle ubiquitin proteasome system. Lung Cancer. 2012;76(1):112-7.

281. Vigano A, Trutschnigg B, Kilgour RD, Hamel N, Hornby L, Lucar E, et al. Relationship between angiotensin-converting enzyme gene polymorphism and body composition, functional performance, and blood biomarkers in advanced cancer patients. Clin Cancer Res. 2009;15(7):2442-7.

282. Peddle-McIntyre CJ, Bell G, Fenton D, McCargar L, Courneya KS. Feasibility and preliminary efficacy of progressive resistance exercise training in lung cancer survivors. Lung Cancer. 2012;75(1):126-32.

283. Jeffery E, Lee YCG, Newton RU, Lyons-Wall P, McVeigh J, Nowak AK, et al. Body composition and nutritional status in malignant pleural mesothelioma: implications for activity levels and quality of life. European Journal of Clinical Nutrition. 2019;73(10):1412-21.

284. Buckinx F, Landi F, Cesari M, Fieding RA, Visser M, Engelke K, et al. The authors reply: Letter on: "Pitfalls in the measurement of muscle mass: a need for

a reference standard" by Clark et al. J Cachexia Sarcopenia Muscle. 2018;9(7):1272-4.

285. Goldman LW. Principles of CT and CT technology. J Nucl Med Technol. 2007;35(3):115-28; quiz 29-30.

286. Lee JK, Evens RG. Computed tomography of the body. Disease-a-month : DM. 1980;26 7:1-56.

287. Rössner S, Bo WJ, Hiltbrandt E, Hinson W, Karstaedt N, Santago P, et al. Adipose tissue determinations in cadavers--a comparison between cross-sectional planimetry and computed tomography. Int J Obes. 1990;14(10):893-902.

288. Mitsiopoulos N, Baumgartner RN, Heymsfield SB, Lyons W, Gallagher D, Ross R. Cadaver validation of skeletal muscle measurement by magnetic resonance imaging and computerized tomography. J Appl Physiol (1985). 1998;85(1):115-22.

289. Irving BA, Weltman JY, Brock DW, Davis CK, Gaesser GA, Weltman A. NIH ImageJ and Slice-O-Matic computed tomography imaging software to quantify soft tissue. Obesity (Silver Spring). 2007;15(2):370-6.

290. Wu GA, Bogie K. Assessment of gluteus maximus muscle area with different image analysis programs. Arch Phys Med Rehabil. 2009;90(6):1048-54.

291. Strandberg S, Wretling ML, Wredmark T, Shalabi A. Reliability of computed tomography measurements in assessment of thigh muscle cross-sectional area and attenuation. BMC Med Imaging. 2010;10:18.

292. van Vugt JL, Levolger S, Gharbharan A, Koek M, Niessen WJ, Burger JW, et al. A comparative study of software programmes for cross-sectional skeletal muscle and adipose tissue measurements on abdominal computed tomography scans of rectal cancer patients. J Cachexia Sarcopenia Muscle. 2017;8(2):285-97.

293. Fortin M, Battié MC. Quantitative Paraspinal Muscle Measurements: Inter-Software Reliability and Agreement Using OsiriX and ImageJ. Physical Therapy. 2012;92(6):853-64.

294. Jamal-Hanjani M, Wilson GA, McGranahan N, Birkbak NJ, Watkins TBK, Veeriah S, et al. Tracking the Evolution of Non–Small-Cell Lung Cancer. New England Journal of Medicine. 2017;376(22):2109-21.

295. Franklin BR, Patel KM, Nahabedian MY, Baldassari LE, Cohen EI, Bhanot P. Predicting abdominal closure after component separation for complex ventral hernias: maximizing the use of preoperative computed tomography. Ann Plast Surg. 2013;71(3):261-5.

296. Yun CH, Bezerra HG, Wu TH, Yang FS, Liu CC, Wu YJ, et al. The normal limits, subclinical significance, related metabolic derangements and distinct biological effects of body site-specific adiposity in relatively healthy population. PLoS One. 2013;8(4):e61997.

297. van Vledder MG, Levolger S, Ayez N, Verhoef C, Tran TC, Ijzermans JN. Body composition and outcome in patients undergoing resection of colorectal liver metastases. Br J Surg. 2012;99(4):550-7.

298. Nishikawa D, Hanai N, Suzuki H, Koide Y, Beppu S, Hasegawa Y. The Impact of Skeletal Muscle Depletion on Head and Neck Squamous Cell Carcinoma. ORL J Otorhinolaryngol Relat Spec. 2018;80(1):1-9.

299. Rollins KE, Awwad A, Macdonald IA, Lobo DN. A comparison of two different software packages for analysis of body composition using computed tomography images. Nutrition. 2019;57:92-6.

300. Pezaro C, Mukherji D, Tunariu N, Cassidy AM, Omlin A, Bianchini D, et al. Sarcopenia and change in body composition following maximal androgen suppression with abiraterone in men with castration-resistant prostate cancer. Br J Cancer. 2013;109(2):325-31.

301. GroΔ JP, Nattenmüller J, Hemmer S, Tichy D, Krzykalla J, Goldschmidt H, et al. Body fat composition as predictive factor for treatment response in patients with newly diagnosed multiple myeloma - subgroup analysis of the prospective GMMG MM5 trial. Oncotarget. 2017;8(40):68460-71.

302. Cespedes Feliciano EM, Popuri K, Cobzas D, Baracos VE, Beg MF, Khan AD, et al. Evaluation of automated computed tomography segmentation to assess body composition and mortality associations in cancer patients. Journal of Cachexia, Sarcopenia and Muscle. 2020;11(5):1258-69.

303. Kashiwagi E, Shiota M, Masaoka H, Imada K, Monji K, Takeuchi A, et al. Relationship between body composition and hormone sensitivity for androgen deprivation therapy in patients with metastatic prostate cancer. Prostate Int. 2020;8(1):22-6.

304. Ozola-Zālīte I, Mark EB, Gudauskas T, Lyadov V, Olesen SS, Drewes AM, et al. Reliability and validity of the new VikingSlice software for computed tomography body composition analysis. Eur J Clin Nutr. 2019;73(1):54-61.

305. Mourtzakis M, Prado CM, Lieffers JR, Reiman T, McCargar LJ, Baracos VE. A practical and precise approach to quantification of body composition in cancer patients using computed tomography images acquired during routine care. Appl Physiol Nutr Metab. 2008;33(5):997-1006.

306. Fujiwara N, Nakagawa H, Kudo Y, Tateishi R, Taguri M, Watadani T, et al. Sarcopenia, intramuscular fat deposition, and visceral adiposity independently predict the outcomes of hepatocellular carcinoma. J Hepatol. 2015;63(1):131-40.

307. van Dijk DP, Bakens MJ, Coolsen MM, Rensen SS, van Dam RM, Bours MJ, et al. Low skeletal muscle radiation attenuation and visceral adiposity are associated with overall survival and surgical site infections in patients with pancreatic cancer. J Cachexia Sarcopenia Muscle. 2017;8(2):317-26.

308. Sun L, Quan XQ, Yu S. An Epidemiological Survey of Cachexia in Advanced Cancer Patients and Analysis on Its Diagnostic and Treatment Status. Nutr Cancer. 2015;67(7):1056-62.

309. Derstine BA, Holcombe SA, Ross BE, Wang NC, Su GL, Wang SC. Skeletal muscle cutoff values for sarcopenia diagnosis using T10 to L5 measurements in a healthy US population. Sci Rep. 2018;8(1):11369.

310. Vangelov B, Bauer J, Kotevski D, Smee RI. The use of alternate vertebral levels to L3 in computed tomography scans for skeletal muscle mass evaluation and sarcopenia assessment in patients with cancer: a systematic review. Br J Nutr. 2021:1-14.

311. Go SI, Park MJ, Song HN, Kang MH, Park HJ, Jeon KN, et al. Sarcopenia and inflammation are independent predictors of survival in male patients newly diagnosed with small cell lung cancer. Support Care Cancer. 2016;24(5):2075-84.

312. van der Kroft G, van Dijk DPJ, Rensen SS, Van Tiel FH, de Greef B, West M, et al. Low thoracic muscle radiation attenuation is associated with postoperative pneumonia following partial hepatectomy for colorectal metastasis. HPB (Oxford). 2020;22(7):1011-9.

313. Hua X, Deng JP, Long ZQ, Zhang WW, Huang X, Wen W, et al. Prognostic significance of the skeletal muscle index and an inflammation biomarker in patients with breast cancer who underwent postoperative adjuvant radiotherapy. Curr Probl Cancer. 2020;44(2):100513.

314. Sealy MJ, Dechaphunkul T, van der Schans CP, Krijnen WP, Roodenburg JLN, Walker J, et al. Low muscle mass is associated with early termination of chemotherapy related to toxicity in patients with head and neck cancer. Clin Nutr. 2020;39(2):501-9.

315. Wysham NG, Nipp RD, LeBlanc TW, Wolf SP, Ekstrom MP, Currow DC. A practical measurement of thoracic sarcopenia: correlation with clinical

parameters and outcomes in advanced lung cancer. ERJ Open Research. 2016;2(2):00085-2015.

316. Rozenberg D, Mathur S, Herridge M, Goldstein R, Schmidt H, Chowdhury NA, et al. Thoracic muscle cross-sectional area is associated with hospital length of stay post lung transplantation: a retrospective cohort study. Transpl Int. 2017;30(7):713-24.

317. Moon SW, Choi JS, Lee SH, Jung KS, Jung JY, Kang YA, et al. Thoracic skeletal muscle quantification: low muscle mass is related with worse prognosis in idiopathic pulmonary fibrosis patients. Respiratory Research. 2019;20(1):35.

318. Tsim S, Kelly C, Alexander L, Shaw A, Paul J, Woodward R, et al. The DIAPHRAGM study: Diagnostic and prognostic biomarkers in the rational assessment of Mesothelioma. European Respiratory Journal. 2018;52(suppl 62):OA493.

319. Tsim S, Cowell GW, Kidd A, Woodward R, Alexander L, Kelly C, et al. A comparison between MRI and CT in the assessment of primary tumour volume in mesothelioma. Lung Cancer. 2020;150:12-20.

320. Buccheri G, Ferrigno D, Tamburini M. Karnofsky and ECOG performance status scoring in lung cancer: a prospective, longitudinal study of 536 patients from a single institution. Eur J Cancer. 1996;32a(7):1135-41.

321. Hooper CE, Lyburn ID, Searle J, Darby M, Hall T, Hall D, et al. The South West Area Mesothelioma and Pemetrexed trial: a multicentre prospective observational study evaluating novel markers of chemotherapy response and prognostication. British Journal of Cancer. 2015;112(7):1175-82.

322. Blyth K, Kidd AC, Winter A, Baird W, Dick C, Hair J, et al. An update regarding the Prediction of ResIstance to chemotherapy using Somatic copy number variation in Mesothelioma (PRISM) study. Lung Cancer. 2018;115:S26-S7.

323. Stewart D, Waller D, Edwards J, Jeyapalan K, Entwisle J. Is there a role for pre-operative contrast-enhanced magnetic resonance imaging for radical

surgery in malignant pleural mesothelioma? European Journal of Cardio-Thoracic Surgery. 2003;24(6):1019-24.

324. Plathow C, Klopp M, Thieke C, Herth F, Thomas A, Schmaehl A, et al. Therapy response in malignant pleural mesothelioma-role of MRI using RECIST, modified RECIST and volumetric approaches in comparison with CT. Eur Radiol. 2008;18(8):1635-43.

325. Tsao AS, Gladish GW, Gill RR. Revised Modified RECIST Criteria in Malignant Pleural Mesothelioma (Version 1.1): A Step Forward in a Long Race. J Thorac Oncol. 2018;13(7):871-3.

326. Nackaerts K, Vansteenkiste J, Nafteux P. A practical guide to measure "all" malignant pleural mesothelioma tumors by modified RECIST criteria? J Thorac Oncol. 2011;6(12):2143-4; author reply 4-5.

327. Anderson O, Kidd A, Goatman K, Weir A, Voisey J, Dilys V, et al. Fully Automated Volumetric Measurement of Malignant Pleural Mesothelioma from Computed Tomography Images by Deep Learning: Preliminary Results of an Internal Validation2020. 64-73 p.

328. Proctor MJ, Morrison DS, Talwar D, Balmer SM, O'Reilly DS, Foulis AK, et al. An inflammation-based prognostic score (mGPS) predicts cancer survival independent of tumour site: a Glasgow Inflammation Outcome Study. Br J Cancer. 2011;104(4):726-34.

329. Nuttall FQ. Body Mass Index: Obesity, BMI, and Health: A Critical Review. Nutr Today. 2015;50(3):117-28.

330. Health NIo. ImageJ 2021 [Available from: https://imagej.nih.gov/ij/docs/intro.html.

331. Mozley PD, Bendtsen C, Zhao B, Schwartz LH, Thorn M, Rong Y, et al. Measurement of tumor volumes improves RECIST-based response assessments in advanced lung cancer. Transl Oncol. 2012;5(1):19-25.

332. Spira D, Sökler M, Vogel W, Löffler S, Spira SM, Brodoefel H, et al. Volume and attenuation computed tomography measurements for interim evaluation of Hodgkin and follicular lymphoma as an additional surrogate parameter for more confident response monitoring: a pilot study. Cancer Imaging. 2011;11(1):155-62.

333. Mueller S, Wichmann G, Dornheim L, Roessling I, Bertolini J, Preim B, et al. Different approaches to volume assessment of lymph nodes in computer tomography scans of head and neck squamous cell carcinoma in comparison with a real gold standard. ANZ J Surg. 2012;82(10):737-41.

334. Goldmacher GV, Conklin J. The use of tumour volumetrics to assess response to therapy in anticancer clinical trials. Br J Clin Pharmacol. 2012;73(6):846-54.

335. Berger A. Magnetic resonance imaging. BMJ (Clinical research ed). 2002;324(7328):35-.

336. Heelan RT, Rusch VW, Begg CB, Panicek DM, Caravelli JF, Eisen C. Staging of malignant pleural mesothelioma: comparison of CT and MR imaging. AJR Am J Roentgenol. 1999;172(4):1039-47.

337. Armato SG, 3rd, Oxnard GR, Kocherginsky M, Vogelzang NJ, Kindler HL, MacMahon H. Evaluation of semiautomated measurements of mesothelioma tumor thickness on CT scans. Acad Radiol. 2005;12(10):1301-9.

338. Armato SG, 3rd, Blyth KG, Keating JJ, Katz S, Tsim S, Coolen J, et al. Imaging in pleural mesothelioma: A review of the 13th International Conference of the International Mesothelioma Interest Group. Lung Cancer. 2016;101:48-58.

339. Corson N, Sensakovic WF, Straus C, Starkey A, Armato SG, 3rd. Characterization of mesothelioma and tissues present in contrast-enhanced thoracic CT scans. Med Phys. 2011;38(2):942-7.

340. Mirvis S, Dutcher JP, Haney PJ, Whitley NO, Aisner J. CT of malignant pleural mesothelioma. AJR Am J Roentgenol. 1983;140(4):665-70.

341. Luerken L, Thurn PL, Zeman F, Stroszczynski C, Hamer OW. Conspicuity of malignant pleural mesothelioma in contrast enhanced MDCT – arterial phase or late phase? BMC Cancer. 2021;21(1):1144.

342. Tsim S, Humphreys CA, Cowell GW, Stobo DB, Noble C, Woodward R, et al. Early Contrast Enhancement: A novel magnetic resonance imaging biomarker of pleural malignancy. Lung Cancer. 2018;118:48-56.

343. Yankeelov TE, Gore JC. Dynamic Contrast Enhanced Magnetic Resonance Imaging in Oncology: Theory, Data Acquisition, Analysis, and Examples. Curr Med Imaging Rev. 2009;3(2):91-107.

344. Giesel FL, Bischoff H, von Tengg-Kobligk H, Weber MA, Zechmann CM, Kauczor HU, et al. Dynamic contrast-enhanced MRI of malignant pleural mesothelioma: a feasibility study of noninvasive assessment, therapeutic follow-up, and possible predictor of improved outcome. Chest. 2006;129(6):1570-6.

345. Cicero G, Mazziotti S, Blandino A, Granata F, Gaeta M. Magnetic Resonance Imaging of the Diaphragm: From Normal to Pathologic Findings. J Clin Imaging Sci. 2020;10:1-.

346. Ball L, Braune A, Spieth P, Herzog M, Chandrapatham K, Hietschold V, et al. Magnetic Resonance Imaging for Quantitative Assessment of Lung Aeration: A Pilot Translational Study. Frontiers in Physiology. 2018;9.

347. Vivoda Tomšič M, Bisdas S, Kovač V, Serša I, Šurlan Popovič K. Dynamic contrast-enhanced MRI of malignant pleural mesothelioma: a comparative study of pharmacokinetic models and correlation with mRECIST criteria. Cancer imaging : the official publication of the International Cancer Imaging Society. 2019;19(1):10-.

348. Gudmundsson E, Labby Z, Straus CM, Sensakovic WF, Li F, Rose B, et al. Dynamic contrast-enhanced CT for the assessment of tumour response in malignant pleural mesothelioma: a pilot study. European Radiology. 2019;29(2):682-8.

349. Meijerink MR, van Cruijsen H, Hoekman K, Kater M, van Schaik C, van Waesberghe JH, et al. The use of perfusion CT for the evaluation of therapy combining AZD2171 with gefitinib in cancer patients. Eur Radiol. 2007;17(7):1700-13.

350. Armato SG, Labby ZE, Coolen J, Klabatsa A, Feigen M, Persigehl T, et al. Imaging in pleural mesothelioma: A review of the 11th International Conference of the International Mesothelioma Interest Group. Lung Cancer. 2013;82(2):190-6.

351. Miles KA. Measurement of tissue perfusion by dynamic computed tomography. Br J Radiol. 1991;64(761):409-12.

352. Murray JG, Patz EF, Jr., Erasmus JJ, Gilkeson RC. CT appearance of the pleural space after talc pleurodesis. AJR Am J Roentgenol. 1997;169(1):89-91.

353. Kwek BH, Aquino SL, Fischman AJ. Fluorodeoxyglucose positron emission tomography and CT after talc pleurodesis. Chest. 2004;125(6):2356-60.

354. Mahesh M. The Essential Physics of Medical Imaging, Third Edition. Med Phys. 2013;40(7).

355. Lauk O, Patella M, Neuer T, Battilana B, Frauenfelder T, Nguyen-Kim TDL, et al. Implementing CT tumor volume and CT pleural thickness into future staging systems for malignant pleural mesothelioma. Cancer Imaging. 2021;21(1):48.

356. Seely JM, Nguyen ET, Churg AM, Müller NL. Malignant pleural mesothelioma: computed tomography and correlation with histology. Eur J Radiol. 2009;70(3):485-91.

357. Choi Y, Gil BM, Chung MH, Yoo WJ, Jung NY, Kim YH, et al. Comparing attenuations of malignant and benign solitary pulmonary nodule using semi-automated region of interest selection on contrast-enhanced CT. Journal of thoracic disease. 2019;11(6):2392-401.

358. Tamura M, Matsumoto I, Saito D, Yoshida S, Kakegawa S, Takemura H. Mean Computed Tomography Value to Predict the Tumor Invasiveness in Clinical Stage IA Lung Cancer. The Annals of Thoracic Surgery. 2017;104(1):261-6.

359. Tamura M, Matsumoto I, Tanaka Y, Saito D, Yoshida S, Takata M. Predicting recurrence of non-small cell lung cancer based on mean computed tomography value. Journal of Cardiothoracic Surgery. 2021;16(1):128.

360. Veeratterapillay R, r i, Heer R, Haslam P. Can the degree of contrast enhancement measured in Hounsfield units on CT scanning for renal cell cancer correlate with tumour aggressiveness or survival?2011.

361. Nakasu S, Onishi T, Kitahara S, Oowaki H, Matsumura K-I. CT Hounsfield Unit Is a Good Predictor of Growth in Meningiomas. Neurol Med Chir (Tokyo). 2019;59(2):54-62.

362. Md SC, Md SO, Md SSE. Does the Computed Tomography Hounsfield Units Change Predict Response to Perioperative Chemotherapy in Patients with Gastric Adenocarcinoma. Journal of Cancer. 2022;13(5):1449-55.

363. Alexander ES, Xiong L, Baird GL, Fernando H, Dupuy DE. CT Densitometry and Morphology of Radiofrequency-Ablated Stage IA Non-Small Cell Lung Cancer: Results from the American College of Surgeons Oncology Group Z4033 (Alliance) Trial. J Vasc Interv Radiol. 2020;31(2):286-93.

364. Senyiğit A, Bayram H, Babayiğit C, Topçu F, Nazaroğlu H, Bilici A, et al. Malignant pleural mesothelioma caused by environmental exposure to asbestos in the Southeast of Turkey: CT findings in 117 patients. Respiration. 2000;67(6):615-22.

365. Escalon JG, Harrington KA, Plodkowski AJ, Zheng J, Capanu M, Zauderer MG, et al. Malignant Pleural Mesothelioma: Are There Imaging Characteristics Associated With Different Histologic Subtypes on Computed Tomography? J Comput Assist Tomogr. 2018;42(4):601-6.

366. Ching BC, Tan HS, Tan PH, Toh CK, Kanesvaran R, Ng QS, et al. Differential radiologic characteristics of renal tumours on multiphasic computed tomography. Singapore Med J. 2017;58(5):262-6.

367. Wienbeck S, Fischer U, Perske C, Wienke A, Meyer H-J, Lotz J, et al. Cone-beam Breast Computed Tomography: CT Density Does Not Reflect Proliferation Potential and Receptor Expression of Breast Carcinoma. Translational Oncology. 2017;10:599-603.

368. Wang ZJ, Reddy GP, Gotway MB, Higgins CB, Jablons DM, Ramaswamy M, et al. Malignant pleural mesothelioma: evaluation with CT, MR imaging, and PET. Radiographics. 2004;24(1):105-19.

369. Yamamuro M, Gerbaudo VH, Gill RR, Jacobson FL, Sugarbaker DJ, Hatabu H. Morphologic and functional imaging of malignant pleural mesothelioma. Eur J Radiol. 2007;64(3):356-66.

370. Armato SG, 3rd, Francis RJ, Katz SI, Ak G, Opitz I, Gudmundsson E, et al. Imaging in pleural mesothelioma: A review of the 14th International Conference of the International Mesothelioma Interest Group. Lung Cancer. 2019;130:108-14.

371. Patel A, Roshkovan L, McNulty S, Alley E, Torigian DA, Nachiappan AC, et al. Delayed-Phase Enhancement for Evaluation of Malignant Pleural Mesothelioma on Computed Tomography: A Prospective Cohort Study. Clin Lung Cancer. 2021;22(3):210-7.e1.

372. Nowak AK, Chansky K, Rice DC, Pass HI, Kindler HL, Shemanski L, et al. The IASLC Mesothelioma Staging Project: Proposals for Revisions of the T Descriptors in the Forthcoming Eighth Edition of the TNM Classification for Pleural Mesothelioma. J Thorac Oncol. 2016;11(12):2089-99.

373. Weikert T, Akinci D'Antonoli T, Bremerich J, Stieltjes B, Sommer G, Sauter AW. Evaluation of an AI-Powered Lung Nodule Algorithm for Detection

and 3D Segmentation of Primary Lung Tumors. Contrast Media & Molecular Imaging. 2019;2019:1545747.

374. Santoro A, O'Brien ME, Stahel RA, Nackaerts K, Baas P, Karthaus M, et al. Pemetrexed plus cisplatin or pemetrexed plus carboplatin for chemonaïve patients with malignant pleural mesothelioma: results of the International Expanded Access Program. J Thorac Oncol. 2008;3(7):756-63.

375. Blayney JK, Ceresoli GL, Castagneto B, O'Brien ME, Hasan B, Sylvester R, et al. Response to chemotherapy is predictive in relation to longer overall survival in an individual patient combined-analysis with pleural mesothelioma. Eur J Cancer. 2012;48(16):2983-92.

376. Hopper KD, Kasales CJ, Eggli KD, TenHave TR, Belman NM, Potok PS, et al. The impact of 2D versus 3D quantitation of tumor bulk determination on current methods of assessing response to treatment. J Comput Assist Tomogr. 1996;20(6):930-7.

377. Erasmus JJ, Gladish GW, Broemeling L, Sabloff BS, Truong MT, Herbst RS, et al. Interobserver and intraobserver variability in measurement of non-small-cell carcinoma lung lesions: implications for assessment of tumor response. J Clin Oncol. 2003;21(13):2574-82.

378. Hayes SA, Pietanza MC, O'Driscoll D, Zheng J, Moskowitz CS, Kris MG, et al. Comparison of CT volumetric measurement with RECIST response in patients with lung cancer. European journal of radiology. 2016;85(3):524-33.

379. Prasad SR, Jhaveri KS, Saini S, Hahn PF, Halpern EF, Sumner JE. CT tumor measurement for therapeutic response assessment: comparison of unidimensional, bidimensional, and volumetric techniques initial observations. Radiology. 2002;225(2):416-9.

380. Zimmermann M, Kuhl C, Engelke H, Bettermann G, Keil S. Volumetric measurements of target lesions: does it improve inter-reader variability for

oncological response assessment according to RECIST 1.1 guidelines compared to standard unidimensional measurements? Pol J Radiol. 2021;86:e594-e600.

381. Winter KS, Hofmann FO, Thierfelder KM, Holch JW, Hesse N, Baumann AB, et al. Towards volumetric thresholds in RECIST 1.1: Therapeutic response assessment in hepatic metastases. Eur Radiol. 2018;28(11):4839-48.

382. Huang P, Lin CT, Li Y, Tammemagi MC, Brock MV, Atkar-Khattra S, et al. Prediction of lung cancer risk at follow-up screening with low-dose CT: a training and validation study of a deep learning method. The Lancet Digital Health. 2019;1(7):e353-e62.

383. Xu Y, Hosny A, Zeleznik R, Parmar C, Coroller T, Franco I, et al. Deep Learning Predicts Lung Cancer Treatment Response from Serial Medical Imaging. Clinical Cancer Research. 2019;25(11):3266-75.

384. Hosny A, Parmar C, Coroller TP, Grossmann P, Zeleznik R, Kumar A, et al. Deep learning for lung cancer prognostication: A retrospective multi-cohort radiomics study. PLoS Med. 2018;15(11):e1002711.

385. Liu K-L, Wu T, Chen P-T, Tsai YM, Roth H, Wu M-S, et al. Deep learning to distinguish pancreatic cancer tissue from non-cancerous pancreatic tissue: a retrospective study with cross-racial external validation. The Lancet Digital Health. 2020;2(6):e303-e13.

386. Koh J, Yoon Y, Kim S, Han K, Kim EK. Deep Learning for the Detection of Breast Cancers on Chest Computed Tomography. Clin Breast Cancer. 2022;22(1):26-31.

387. Lewandowicz A, Sławiński P, Kądalska E, Targowski T. Some clarifications of terminology may facilitate sarcopenia assessment. Archives of Medical Science. 2020;16(1):225-32.

388. Heymsfield SB, Smith R, Aulet M, Bensen B, Lichtman S, Wang J, et al. Appendicular skeletal muscle mass: measurement by dual-photon absorptiometry. Am J Clin Nutr. 1990;52(2):214-8.

389. Choi H, Park YS, Na KJ, Park S, Park IK, Kang CH, et al. Association of Adipopenia at Preoperative PET/CT with Mortality in Stage I Non–Small Cell Lung Cancer. Radiology. 2021;301(3):645-53.

390. Barbi J, Patnaik SK, Pabla S, Zollo R, Smith RJ, Jr., Sass SN, et al. Visceral Obesity Promotes Lung Cancer Progression—Toward Resolution of the Obesity Paradox in Lung Cancer. Journal of Thoracic Oncology. 2021;16(8):1333-48.

391. Leung CC, Lam TH, Yew WW, Chan WM, Law WS, Tam CM. Lower lung cancer mortality in obesity. Int J Epidemiol. 2011;40(1):174-82.

392. Yang R, Cheung MC, Pedroso FE, Byrne MM, Koniaris LG, Zimmers TA. Obesity and weight loss at presentation of lung cancer are associated with opposite effects on survival. J Surg Res. 2011;170(1):e75-83.

393. Ebadi M, Martin L, Ghosh S, Field CJ, Lehner R, Baracos VE, et al. Subcutaneous adiposity is an independent predictor of mortality in cancer patients. Br J Cancer. 2017;117(1):148-55.

394. Matsui R, Inaki N, Tsuji T. Impact of visceral adipose tissue on long-term outcomes after gastrectomy for advanced gastric cancer. Nutrition. 2022:111619.

395. Feng W, Huang M, Zhao X, Chen S, Wang C, Chang J, et al. Severe loss of visceral fat and skeletal muscle after chemotherapy predicts poor prognosis in metastatic gastric cancer patients without gastrectomy. Journal of Cancer. 2020;11(11):3310-7.

396. Iwase T, Sangai T, Nagashima T, Sakakibara M, Sakakibara J, Hayama S, et al. Impact of body fat distribution on neoadjuvant chemotherapy outcomes in advanced breast cancer patients. Cancer Med. 2016;5(1):41-8.

397. Mizuno R, Miyajima A, Hibi T, Masuda A, Shinojima T, Kikuchi E, et al. Impact of baseline visceral fat accumulation on prognosis in patients with

metastatic renal cell carcinoma treated with systemic therapy. Medical Oncology. 2017;34(4):47.

398. Lieffers JR, Bathe OF, Fassbender K, Winget M, Baracos VE. Sarcopenia is associated with postoperative infection and delayed recovery from colorectal cancer resection surgery. Br J Cancer. 2012;107(6):931-6.

399. Tan BH, Birdsell LA, Martin L, Baracos VE, Fearon KC. Sarcopenia in an overweight or obese patient is an adverse prognostic factor in pancreatic cancer. Clin Cancer Res. 2009;15(22):6973-9.

400. Sjøblom B, Benth J, Grønberg BH, Baracos VE, Sawyer MB, Fløtten Ø, et al. Drug Dose Per Kilogram Lean Body Mass Predicts Hematologic Toxicity From Carboplatin-Doublet Chemotherapy in Advanced Non-Small-Cell Lung Cancer. Clin Lung Cancer. 2017;18(2):e129-e36.

401. Srdic D, Plestina S, Sverko-Peternac A, Nikolac N, Simundic AM, Samarzija M. Cancer cachexia, sarcopenia and biochemical markers in patients with advanced non-small cell lung cancer-chemotherapy toxicity and prognostic value. Support Care Cancer. 2016;24(11):4495-502.

402. Fintelmann FJ, Troschel FM, Mario J, Chretien YR, Knoll SJ, Muniappan A, et al. Thoracic Skeletal Muscle Is Associated With Adverse Outcomes After Lobectomy for Lung Cancer. Ann Thorac Surg. 2018;105(5):1507-15.

403. Troschel FM, Kuklinski MW, Knoll SJ, Best TD, Muniappan A, Gaissert HA, et al. Preoperative thoracic muscle area on computed tomography predicts long-term survival following pneumonectomy for lung cancer. Interact Cardiovasc Thorac Surg. 2019;28(4):542-9.

404. Cury SS, de Moraes D, Freire PP, de Oliveira G, Marques DVP, Fernandez GJ, et al. Tumor Transcriptome Reveals High Expression of IL-8 in Non-Small Cell Lung Cancer Patients with Low Pectoralis Muscle Area and Reduced Survival. Cancers (Basel). 2019;11(9).

405. Goncalves MD, Taylor S, Halpenny DF, Schwitzer E, Gandelman S, Jackson J, et al. Imaging skeletal muscle volume, density, and FDG uptake before and after induction therapy for non-small cell lung cancer. Clin Radiol. 2018;73(5):505.e1-.e8.

406. Madariaga MLL, Troschel FM, Best TD, Knoll SJ, Gaissert HA, Fintelmann FJ. Low Thoracic Skeletal Muscle Area Predicts Morbidity After Pneumonectomy for Lung Cancer. Ann Thorac Surg. 2020;109(3):907-13.

407. Li HL, Au PC, Lee GK, Li GH, Chan M, Cheung BM, et al. Different definition of sarcopenia and mortality in cancer: A meta-analysis. Osteoporos Sarcopenia. 2021;7(Suppl 1):S34-s8.

408. Williams B, Mandrekar J, Mandrekar S, Cha S, Furth A. Finding Optimal Cutpoints for Continuous Covariates with Binary and Time-to-Event Outcomes. Technical Report Series. 2006;79.

409. Zhang X-M, Dou Q-L, Zeng Y, Yang Y, Cheng ASK, Zhang W-W. Sarcopenia as a predictor of mortality in women with breast cancer: a meta-analysis and systematic review. BMC Cancer. 2020;20(1):172.

410. Miyamoto Y, Baba Y, Sakamoto Y, Ohuchi M, Tokunaga R, Kurashige J, et al. Sarcopenia is a Negative Prognostic Factor After Curative Resection of Colorectal Cancer. Ann Surg Oncol. 2015;22(8):2663-8.

411. Jung HW, Kim JW, Kim JY, Kim SW, Yang HK, Lee JW, et al. Effect of muscle mass on toxicity and survival in patients with colon cancer undergoing adjuvant chemotherapy. Support Care Cancer. 2015;23(3):687-94.

412. Janssen I, Heymsfield SB, Wang Z, Ross R. Skeletal muscle mass and distribution in 468 men and women aged 18–88 yr. Journal of Applied Physiology. 2000;89(1):81-8.

413. Miller AEJ, MacDougall JD, Tarnopolsky MA, Sale DG. Gender differences in strength and muscle fiber characteristics. European Journal of Applied Physiology and Occupational Physiology. 1993;66(3):254-62.

414. Stene GB, Helbostad JL, Amundsen T, Sørhaug S, Hjelde H, Kaasa S, et al. Changes in skeletal muscle mass during palliative chemotherapy in patients with advanced lung cancer. Acta Oncol. 2015;54(3):340-8.

415. Prado CM, Sawyer MB, Ghosh S, Lieffers JR, Esfandiari N, Antoun S, et al. Central tenet of cancer cachexia therapy: do patients with advanced cancer have exploitable anabolic potential? The American Journal of Clinical Nutrition. 2013;98(4):1012-9.

416. Du Y, Wang X, Xie H, Zheng S, Wu X, Zhu X, et al. Sex differences in the prevalence and adverse outcomes of sarcopenia and sarcopenic obesity in community dwelling elderly in East China using the AWGS criteria. BMC Endocrine Disorders. 2019;19(1):109.

417. Zhong X, Zimmers TA. Sex Differences in Cancer Cachexia. Current Osteoporosis Reports. 2020;18(6):646-54.

418. Bartolomei S, Grillone G, Di Michele R, Cortesi M. A Comparison between Male and Female Athletes in Relative Strength and Power Performances. J Funct Morphol Kinesiol. 2021;6(1).

419. Chen G, Liu L, Yu J. A Comparative Study on Strength between American College Male and Female Students in Caucasian and Asian Populations. Sport Science Review. 2012;XXI.

420. Sun C, Anraku M, Kawahara T, Karasaki T, Kitano K, Nagayama K, et al. Respiratory strength and pectoralis muscle mass as measures of sarcopenia: Relation to outcomes in resected non-small cell lung cancer. J Thorac Cardiovasc Surg. 2020.

421. Kinsey CM, San José Estépar R, van der Velden J, Cole BF, Christiani DC, Washko GR. Lower Pectoralis Muscle Area Is Associated with a Worse Overall Survival in Non–Small Cell Lung Cancer. Cancer Epidemiology Biomarkers & Prevention. 2017;26(1):38-43.

422. Di Marco F, Terraneo S, Roggi MA, Repossi AC, Pellegrino GM, Veronelli A, et al. Physical activity impairment in depressed COPD subjects. Respir Care. 2014;59(5):726-34.

423. Vaz Fragoso CA, Beavers DP, Hankinson JL, Flynn G, Berra K, Kritchevsky SB, et al. Respiratory impairment and dyspnea and their associations with physical inactivity and mobility in sedentary community-dwelling older persons. J Am Geriatr Soc. 2014;62(4):622-8.

424. van Heusden HC, Swartz JE, Chargi N, de Jong PA, van Baal MCPM, Wegner I, et al. Feasibility of assessment of skeletal muscle mass on a single cross-sectional image at the level of the fourth thoracic vertebra. European Journal of Radiology. 2021;142.

425. Grønberg BH, Sjøblom B, Wentzel-Larsen T, Baracos VE, Hjermstad MJ, Aass N, et al. A comparison of CT based measures of skeletal muscle mass and density from the Th4 and L3 levels in patients with advanced non-small-cell lung cancer. Eur J Clin Nutr. 2019;73(7):1069-76.

426. Lim WH, Park CM. Validation for measurements of skeletal muscle areas using low-dose chest computed tomography. Scientific Reports. 2022;12(1):463.

427. McDonald ML, Diaz AA, Ross JC, San Jose Estepar R, Zhou L, Regan EA, et al. Quantitative computed tomography measures of pectoralis muscle area and disease severity in chronic obstructive pulmonary disease. A cross-sectional study. Ann Am Thorac Soc. 2014;11(3):326-34.

428. Mishra A, Bigam KD, Extermann M, Faramand R, Thomas K, Pidala JA, et al. Sarcopenia and low muscle radiodensity associate with impaired FEV(1) in allogeneic haematopoietic stem cell transplant recipients. Journal of cachexia, sarcopenia and muscle. 2020;11(6):1570-9.

429. Kim EY, Lee HY, Kim KW, Lee JI, Kim YS, Choi WJ, et al. Preoperative Computed Tomography-Determined Sarcopenia and Postoperative Outcome After Surgery for Non-Small Cell Lung Cancer. Scand J Surg. 2018;107(3):244-51.

430. Shiroyama T, Nagatomo I, Koyama S, Hirata H, Nishida S, Miyake K, et al. Impact of sarcopenia in patients with advanced non–small cell lung cancer treated with PD-1 inhibitors: A preliminary retrospective study. Scientific Reports. 2019;9(1):2447.

431. Yang M, Tan L, Xie L, Hu S, Liu D, Wang J, et al. Factors That Improve Chest Computed Tomography-Defined Sarcopenia Prognosis in Advanced Non-Small Cell Lung Cancer. Front Oncol. 2021;11:754975.

432. Lee J, Kim EY, Kim E, Kim KG, Kim YJ, Kim YS, et al. Longitudinal changes in skeletal muscle mass in patients with advanced squamous cell lung cancer. Thorac Cancer. 2021;12(11):1662-7.

433. Miyamoto Y, Baba Y, Sakamoto Y, Ohuchi M, Tokunaga R, Kurashige J, et al. Negative Impact of Skeletal Muscle Loss after Systemic Chemotherapy in Patients with Unresectable Colorectal Cancer. PLoS One. 2015;10(6):e0129742.

434. Daly LE, Ní Bhuachalla ÉB, Power DG, Cushen SJ, James K, Ryan AM. Loss of skeletal muscle during systemic chemotherapy is prognostic of poor survival in patients with foregut cancer. Journal of cachexia, sarcopenia and muscle. 2018;9(2):315-25.

435. Rutten IJ, van Dijk DP, Kruitwagen RF, Beets-Tan RG, Olde Damink SW, van Gorp T. Loss of skeletal muscle during neoadjuvant chemotherapy is related to decreased survival in ovarian cancer patients. J Cachexia Sarcopenia Muscle. 2016;7(4):458-66.

436. Kugimiya N, Harada E, Oka K, Kawamura D, Suehiro Y, Takemoto Y, et al. Loss of skeletal muscle mass after curative gastrectomy is a poor prognostic factor. Oncol Lett. 2018;16(1):1341-7.

437. Daly LE, Power DG, O'Reilly Á, Donnellan P, Cushen SJ, O'Sullivan K, et al. The impact of body composition parameters on ipilimumab toxicity and survival in patients with metastatic melanoma. Br J Cancer. 2017;116(3):310-7.

438. Törnqvist L, Vartia P, Vartia YO. How Should Relative Changes be Measured? The American Statistician. 1985;39(1):43-6.

439. Vickers AJ. The use of percentage change from baseline as an outcome in a controlled trial is statistically inefficient: a simulation study. BMC Med Res Methodol. 2001;1:6-.

440. Blauwhoff-Buskermolen S, Versteeg KS, de van der Schueren MA, den Braver NR, Berkhof J, Langius JA, et al. Loss of Muscle Mass During Chemotherapy Is Predictive for Poor Survival of Patients With Metastatic Colorectal Cancer. J Clin Oncol. 2016;34(12):1339-44.

441. Daly LE, ÉB NB, Power DG, Cushen SJ, James K, Ryan AM. Loss of skeletal muscle during systemic chemotherapy is prognostic of poor survival in patients with foregut cancer. J Cachexia Sarcopenia Muscle. 2018;9(2):315-25.

442. Degens JHRJ, Sanders KJC, de Jong EEC, Groen HJM, Smit EF, Aerts JG, et al. The prognostic value of early onset, CT derived loss of muscle and adipose tissue during chemotherapy in metastatic non-small cell lung cancer. Lung Cancer. 2019;133:130-5.

443. Tanaka S, Ozeki N, Mizuno Y, Nakajima H, Hattori K, Inoue T, et al. Preoperative paraspinous muscle sarcopenia and physical performance as prognostic indicators in non-small-cell lung cancer. J Cachexia Sarcopenia Muscle. 2021;12(3):646-56.

444. Dong X, Dan X, Yawen A, Haibo X, Huan L, Mengqi T, et al. Identifying sarcopenia in advanced non-small cell lung cancer patients using skeletal muscle CT radiomics and machine learning. Thoracic Cancer. 2020;11(9):2650-9.

445. Matsuyama R, Maeda K, Yamanaka Y, Ishida Y, Kato R, Nonogaki T, et al. Assessing skeletal muscle mass based on the cross-sectional area of muscles at the 12th thoracic vertebra level on computed tomography in patients with oral squamous cell carcinoma. Oral Oncol. 2021;113:105126.

446. Jackson AS, Stanforth PR, Gagnon J, Rankinen T, Leon AS, Rao DC, et al. The effect of sex, age and race on estimating percentage body fat from body mass index: The Heritage Family Study. International Journal of Obesity. 2002;26(6):789-96.

447. Demerath EW, Sun SS, Rogers N, Lee M, Reed D, Choh AC, et al. Anatomical patterning of visceral adipose tissue: race, sex, and age variation. Obesity (Silver Spring, Md). 2007;15(12):2984-93.

448. Després JP, Couillard C, Gagnon J, Bergeron J, Leon AS, Rao DC, et al. Race, visceral adipose tissue, plasma lipids, and lipoprotein lipase activity in men and women: the Health, Risk Factors, Exercise Training, and Genetics (HERITAGE) family study. Arterioscler Thromb Vasc Biol. 2000;20(8):1932-8.

449. Mallio CA, Greco F, Pacella G, Schena E, Beomonte Zobel B. Gender-based differences of abdominal adipose tissue distribution in non-small cell lung cancer patients. Shanghai Chest. 2018;2(4).

450. Charette N, Vandeputte C, Ameye L, Bogaert CV, Krygier J, Guiot T, et al. Prognostic value of adipose tissue and muscle mass in advanced colorectal cancer: a post hoc analysis of two non-randomized phase II trials. BMC Cancer. 2019;19(1):134.

451. Lee J, Lee H, Na J, Lee SM. Effect of adipose tissue volume on prognosis in patients with non-small cell lung cancer. Clinical Imaging. 2018;50.

452. Lee HW, Jeong BC, Seo SI, Jeon SS, Lee HM, Choi HY, et al. Prognostic significance of visceral obesity in patients with advanced renal cell carcinoma undergoing nephrectomy. International journal of urology. 2015;22(5):455-61.

453. Di Sebastiano KM, Yang L, Zbuk K, Wong RK, Chow T, Koff D, et al. Accelerated muscle and adipose tissue loss may predict survival in pancreatic cancer patients: the relationship with diabetes and anaemia. Br J Nutr. 2013;109(2):302-12.

454. Shuster A, Patlas M, Pinthus JH, Mourtzakis M. The clinical importance of visceral adiposity: a critical review of methods for visceral adipose tissue analysis. The British journal of radiology. 2012;85(1009):1-10.

455. Doyle SL, Donohoe CL, Lysaght J, Reynolds JV. Visceral obesity, metabolic syndrome, insulin resistance and cancer. Proc Nutr Soc. 2012;71(1):181-9.

456. Batista ML, Jr., Neves RX, Peres SB, Yamashita AS, Shida CS, Farmer SR, et al. Heterogeneous time-dependent response of adipose tissue during the development of cancer cachexia. J Endocrinol. 2012;215(3):363-73.

457. Batista ML, Jr., Olivan M, Alcantara PS, Sandoval R, Peres SB, Neves RX, et al. Adipose tissue-derived factors as potential biomarkers in cachectic cancer patients. Cytokine. 2013;61(2):532-9.

458. Lennon H, Sperrin M, Badrick E, Renehan AG. The Obesity Paradox in Cancer: a Review. Curr Oncol Rep. 2016;18(9):56-.

459. Strulov Shachar S, Williams GR. The Obesity Paradox in Cancer-Moving Beyond BMI. Cancer Epidemiol Biomarkers Prev. 2017;26(1):13-6.

460. Lam VK, Bentzen SM, Mohindra P, Nichols EM, Bhooshan N, Vyfhuis M, et al. Obesity is associated with long-term improved survival in definitively treated locally advanced non-small cell lung cancer (NSCLC). Lung Cancer. 2017;104:52-7.

461. Petrelli F, Cortellini A, Indini A, Tomasello G, Ghidini M, Nigro O, et al. Association of Obesity With Survival Outcomes in Patients With Cancer: A Systematic Review and Meta-analysis. JAMA Network Open. 2021;4(3):e213520-e.

462. Abdel-Rahman O. Pre-diagnostic body mass index trajectory in relationship to lung cancer incidence and mortality; findings from the PLCO trial. Expert Rev Respir Med. 2019;13(10):1029-35.

463. Calle EE, Rodriguez C, Walker-Thurmond K, Thun MJ. Overweight, obesity, and mortality from cancer in a prospectively studied cohort of U.S. adults. N Engl J Med. 2003;348(17):1625-38.

464. Reeves GK, Pirie K, Beral V, Green J, Spencer E, Bull D. Cancer incidence and mortality in relation to body mass index in the Million Women Study: cohort study. Bmj. 2007;335(7630):1134.

465. Prospective Studies C. Body-mass index and cause-specific mortality in 900 000 adults: collaborative analyses of 57 prospective studies. The Lancet. 2009;373(9669):1083-96.

466. Blanc-Durand P, Campedel L, Mule S, Jegou S, Luciani A, Pigneur F, et al. Prognostic value of anthropometric measures extracted from whole-body CT using deep learning in patients with non-small-cell lung cancer. Eur Radiol. 2020;30(6):3528-37.

467. Freedman RJ, Aziz N, Albanes D, Hartman T, Danforth D, Hill S, et al. Weight and body composition changes during and after adjuvant chemotherapy in women with breast cancer. J Clin Endocrinol Metab. 2004;89(5):2248-53.

468. Yamaoka Y, Fujitani K, Tsujinaka T, Yamamoto K, Hirao M, Sekimoto M. Skeletal muscle loss after total gastrectomy, exacerbated by adjuvant chemotherapy. Gastric Cancer. 2015;18(2):382-9.

469. Awad S, Tan BH, Cui H, Bhalla A, Fearon KC, Parsons SL, et al. Marked changes in body composition following neoadjuvant chemotherapy for oesophagogastric cancer. Clin Nutr. 2012;31(1):74-7.

470. Panje CM, Höng L, Hayoz S, Baracos VE, Herrmann E, Garcia Schüler H, et al. Skeletal muscle mass correlates with increased toxicity during neoadjuvant radiochemotherapy in locally advanced esophageal cancer: A SAKK 75/08 substudy. Radiat Oncol. 2019;14(1):166.

471. Park SE, Choi JH, Park JY, Kim BJ, Kim JG, Kim JW, et al. Loss of skeletal muscle mass during palliative chemotherapy is a poor prognostic factor in patients with advanced gastric cancer. Sci Rep. 2020;10(1):17683.

472. Garcia JM, Scherer T, Chen JA, Guillory B, Nassif A, Papusha V, et al. Inhibition of cisplatin-induced lipid catabolism and weight loss by ghrelin in male mice. Endocrinology. 2013;154(9):3118-29.

473. Bozzetti F. Chemotherapy-Induced Sarcopenia. Curr Treat Options Oncol. 2020;21(1):7.

474. Wright JG, Boddy AV, Highley M, Fenwick J, McGill A, Calvert AH. Estimation of glomerular filtration rate in cancer patients. Br J Cancer. 2001;84(4):452-9.

475. Stevens LA, Levey AS. Measured GFR as a Confirmatory Test for Estimated GFR. Journal of the American Society of Nephrology. 2009;20(11):2305.

476. Du Bois D, Du Bois EF. A formula to estimate the approximate surface area if height and weight be known. 1916. Nutrition. 1989;5(5):303-11; discussion 12-3.

477. Redlarski G, Palkowski A, Krawczuk M. Body surface area formulae: an alarming ambiguity. Scientific Reports. 2016;6(1):27966.

478. Furlanetto J, Eiermann W, Marmé F, Reimer T, Reinisch M, Schmatloch S, et al. Higher rate of severe toxicities in obese patients receiving dose-dense (dd) chemotherapy according to unadjusted body surface area: results of the prospectively randomized GAIN study. Annals of Oncology. 2016;27(11):2053-9.

479. Griggs JJ, Bohlke K, Balaban EP, Dignam JJ, Hall ET, Harvey RD, et al. Appropriate Systemic Therapy Dosing for Obese Adult Patients With Cancer: ASCO Guideline Update. Journal of Clinical Oncology. 2021;39(18):2037-48.

480. Faisal W, Tang H-M, Tiley S, Kukard C. Not All Body Surface Area Formulas Are the Same, but Does It Matter? Journal of Global Oncology. 2016;2(6):436-7.

481. Wright JD, Tian C, Mutch DG, Herzog TJ, Nagao S, Fujiwara K, et al. Carboplatin dosing in obese women with ovarian cancer: a Gynecologic Oncology Group study. Gynecol Oncol. 2008;109(3):353-8.

482. Blouin RA, Warren GW. Pharmacokinetic considerations in obesity. J Pharm Sci. 1999;88(1):1-7.

483. Mittal A, Chitkara D, Kumar N. HPLC method for the determination of carboplatin and paclitaxel with cremophorEL in an amphiphilic polymer matrix. Journal of Chromatography B. 2007;855(2):211-9.

484. Zhu X, Peng Y, Qiu L. Amino-functionalized nano-vesicles for enhanced anticancer efficacy and reduced myelotoxicity of carboplatin. Colloids and Surfaces B: Biointerfaces. 2017;157:56-64.

485. Ekhart C, Rodenhuis S, Schellens JHM, Beijnen JH, Huitema ADR. Carboplatin dosing in overweight and obese patients with normal renal function, does weight matter? Cancer Chemotherapy and Pharmacology. 2009;64(1):115-22.

486. Sparreboom A, Wolff AC, Mathijssen RH, Chatelut E, Rowinsky EK, Verweij J, et al. Evaluation of alternate size descriptors for dose calculation of anticancer drugs in the obese. J Clin Oncol. 2007;25(30):4707-13.

487. Hall RG, Jean GW, Sigler M, Shah S. Dosing Considerations for Obese Patients Receiving Cancer Chemotherapeutic Agents. Annals of Pharmacotherapy. 2013;47(12):1666-74.

488. Carroll J, Protani M, Walpole E, Martin JH. Effect of obesity on toxicity in women treated with adjuvant chemotherapy for early-stage breast cancer: a systematic review. Breast Cancer Res Treat. 2012;136(2):323-30.

489. Dotan E, Tew WP, Mohile SG, Ma H, Kim H, Sun C-L, et al. Associations between nutritional factors and chemotherapy toxicity in older adults with solid tumors. Cancer. 2020;126(8):1708-16.

490. Anderson AS, Martin RM, Renehan AG, Cade J, Copson ER, Cross AJ, et al. Cancer survivorship, excess body fatness and weight-loss intervention—where are we in 2020? British Journal of Cancer. 2021;124(6):1057-65.

491. Kovarik M, Hronek M, Zadak Z. Clinically relevant determinants of body composition, function and nutritional status as mortality predictors in lung cancer patients. Lung Cancer. 2014;84(1):1-6.

492. ESMO. Poorer survival in obese colorectal cancer patients possibly linked to lower chemotherapy doses (ESMO World GI 2021 Press Release) 2021 [Available from: https://www.esmo.org/newsroom/press-releases/poorer-survival-in-obese-colorectal-cancer-patients-possibly-linked-to-lower-chemotherapy-doses.

493. Martini A, Shah QN, Waingankar N, Sfakianos JP, Tsao CK, Necchi A, et al. The obesity paradox in metastatic castration-resistant prostate cancer. Prostate Cancer Prostatic Dis. 2021.

494. Liu YL, Connolly EP, Kalinsky K. Obesity's impact on survival is independent of dose adjustments in neoadjuvant chemotherapy in women with breast cancer. Breast Cancer Research and Treatment. 2018;168(1):285-.

495. Karatas F, Erdem GU, Sahin S, Aytekin A, Yuce D, Sever AR, et al. Obesity is an independent prognostic factor of decreased pathological complete response to neoadjuvant chemotherapy in breast cancer patients. Breast. 2017;32:237-44.

496. Hughes A, Calvert P, Azzabi A, Plummer R, Johnson R, Rusthoven J, et al. Phase I clinical and pharmacokinetic study of pemetrexed and carboplatin in patients with malignant pleural mesothelioma. J Clin Oncol. 2002;20(16):3533-44.

497. Shachar SS, Deal AM, Weinberg M, Williams GR, Nyrop KA, Popuri K, et al. Body Composition as a Predictor of Toxicity in Patients Receiving Anthracycline and Taxane-Based Chemotherapy for Early-Stage Breast Cancer. Clin Cancer Res. 2017;23(14):3537-43.

498. Guiu B, Petit JM, Bonnetain F, Ladoire S, Guiu S, Cercueil J-P, et al. Visceral fat area is an independent predictive biomarker of outcome after first-line bevacizumab-based treatment in metastatic colorectal cancer. Gut. 2010;59(3):341-7.

499. Hwang IG, Park SE, Lee SC, Choi JH. Loss of skeletal muscle mass during palliative chemotherapy is a poor prognostic factor in patients with advanced gastric cancer. Annals of Oncology. 2019;30:v727.

500. Lyon TD, Frank I, Takahashi N, Boorjian SA, Moynagh MR, Shah PH, et al. Sarcopenia and Response to Neoadjuvant Chemotherapy for Muscle-Invasive Bladder Cancer. Clin Genitourin Cancer. 2019;17(3):216-22.e5.

501. Feliciano EMC, Kroenke CH, Meyerhardt JA, Prado CM, Bradshaw PT, Kwan ML, et al. Association of Systemic Inflammation and Sarcopenia With Survival in Nonmetastatic Colorectal Cancer: Results From the C SCANS Study. JAMA Oncol. 2017;3(12):e172319.

502. Malietzis G, Lee GH, Bernardo D, Blakemore AI, Knight SC, Moorghen M, et al. The prognostic significance and relationship with body composition of CCR7-positive cells in colorectal cancer. J Surg Oncol. 2015;112(1):86-92.

503. Matsunaga T, Miyata H, Sugimura K, Motoori M, Asukai K, Yanagimoto Y, et al. Prognostic Significance of Sarcopenia and Systemic Inflammatory Response in Patients With Esophageal Cancer. Anticancer Res. 2019;39(1):449-58.

504. Vogl M, Rosenmayr A, Bohanes T, Scheed A, Brndiar M, Stubenberger E, et al. Biomarkers for Malignant Pleural Mesothelioma-A Novel View on Inflammation. Cancers (Basel). 2021;13(4).

505. Enewold L, Sharon E, Thomas A. Patterns of care and survival among patients with malignant mesothelioma in the United States. Lung Cancer. 2017;112:102-8.

506. Zhuo Y, Lin L, Zhang M. Pretreatment thrombocytosis as a significant prognostic factor in malignant mesothelioma: a meta-analysis. Platelets. 2017;28(6):560-6.

507. Han S, Gan D, Wang G, Ru Y, Huang C, Lin J, et al. Associations of Platelet Indices with Body Fat Mass and Fat Distribution. Obesity (Silver Spring). 2018;26(10):1637-43.

508. Yu J-Y, Choi W-J, Lee H-S, Lee J-W. Relationship between inflammatory markers and visceral obesity in obese and overweight Korean adults: An observational study. Medicine. 2019;98(9).

509. Murakami T, Horigome H, Tanaka K, Nakata Y, Ohkawara K, Katayama Y, et al. Impact of weight reduction on production of platelet-derived microparticles and fibrinolytic parameters in obesity. Thromb Res. 2007;119(1):45-53.

510. Lazar S, Goldfinger LE. Platelet Microparticles and miRNA Transfer in Cancer Progression: Many Targets, Modes of Action, and Effects Across Cancer Stages. Frontiers in Cardiovascular Medicine. 2018;5.

511. Vohra R, Campbell MD, Park J, Whang S, Gravelle K, Wang YN, et al. Increased tumour burden alters skeletal muscle properties in the KPC mouse model of pancreatic cancer. JCSM Rapid Commun. 2020;3(2):44-55.

512. Michaelis KA, Zhu X, Burfeind KG, Krasnow SM, Levasseur PR, Morgan TK, et al. Establishment and characterization of a novel murine model of pancreatic cancer cachexia. J Cachexia Sarcopenia Muscle. 2017;8(5):824-38.

513. Grippo PJ, Sandgren EP. Modeling pancreatic cancer in animals to address specific hypotheses. Methods Mol Med. 2005;103:217-43.

514. Capellá G, Farré L, Villanueva A, Reyes G, García C, Tarafa G, et al. Orthotopic models of human pancreatic cancer. Ann N Y Acad Sci. 1999;880:103-9.

515. De Lerma Barbaro A. The complex liaison between cachexia and tumor burden (Review). Oncol Rep. 2015;34(4):1635-49.

516. Fordy C, Glover C, Henderson DC, Summerbell C, Wharton R, Allen-Mersh TG. Contribution of diet, tumour volume and patient-related factors to weight loss in patients with colorectal liver metastases. Br J Surg. 1999;86(5):639-44.

517. Hoda MA, Dong Y, Rozsas A, Klikovits T, Laszlo V, Ghanim B, et al. Circulating activin A is a novel prognostic biomarker in malignant pleural mesothelioma – A multi-institutional study. European Journal of Cancer. 2016;63:64-73.

518. Klikovits T, Stockhammer P, Laszlo V, Dong Y, Hoda MA, Ghanim B, et al. Circulating complement component 4d (C4d) correlates with tumor volume, chemotherapeutic response and survival in patients with malignant pleural mesothelioma. Scientific Reports. 2017;7(1):16456.

519. Coelho M, Oliveira T, Fernandes R. Biochemistry of adipose tissue: an endocrine organ. Arch Med Sci. 2013;9(2):191-200.

520. Lengyel E, Makowski L, DiGiovanni J, Kolonin MG. Cancer as a Matter of Fat: The Crosstalk between Adipose Tissue and Tumors. Trends in Cancer. 2018;4(5):374-84.

521. Borisov AN, Blum CA, Christ-Crain M, Ebrahimi F. No obesity paradox in patients with community-acquired pneumonia – secondary analysis of a randomized controlled trial. Nutrition & Diabetes. 2022;12(1):12.

522. Wang Q, Wu H. T Cells in Adipose Tissue: Critical Players in Immunometabolism. Frontiers in Immunology. 2018;9.

523. Aguilar EG, Murphy WJ. Obesity induced T cell dysfunction and implications for cancer immunotherapy. Current Opinion in Immunology. 2018;51:181-6.

524. Rosito GA, Massaro JM, Hoffmann U, Ruberg FL, Mahabadi AA, Vasan RS, et al. Pericardial fat, visceral abdominal fat, cardiovascular disease risk factors, and vascular calcification in a community-based sample: the Framingham Heart Study. Circulation. 2008;117(5):605-13.

525. Kwack WG, Kang Y-S, Jeong YJ, Oh JY, Cha YK, Kim JS, et al. Association between thoracic fat measured using computed tomography and lung function in a population without respiratory diseases. Journal of thoracic disease. 2019;11(12):5300-9.

526. Cruz-Jentoft AJ, Bahat G, Bauer J, Boirie Y, Bruyère O, Cederholm T, et al. Sarcopenia: revised European consensus on definition and diagnosis. Age and Ageing. 2019;48(1):16-31.

527. Reginster JY, Cooper C, Rizzoli R, Kanis JA, Appelboom G, Bautmans I, et al. Recommendations for the conduct of clinical trials for drugs to treat or prevent sarcopenia. Aging Clin Exp Res. 2016;28(1):47-58.

528. Solheim TS, Laird BJA, Balstad TR, Stene GB, Bye A, Johns N, et al. A randomized phase II feasibility trial of a multimodal intervention for the management of cachexia in lung and pancreatic cancer. J Cachexia Sarcopenia Muscle. 2017;8(5):778-88.

529. Adams SC, Segal RJ, McKenzie DC, Vallerand JR, Morielli AR, Mackey JR, et al. Impact of resistance and aerobic exercise on sarcopenia and dynapenia in breast cancer patients receiving adjuvant chemotherapy: a multicenter randomized controlled trial. Breast Cancer Res Treat. 2016;158(3):497-507.

530. Yoh K, Nishikawa H, Enomoto H, Ishii N, Iwata Y, Ishii A, et al. Effect of exercise therapy on sarcopenia in pancreatic cancer: a study protocol for a randomised controlled trial. BMJ Open Gastroenterology. 2018;5(1):e000194.

531. Mijnarends DM, Meijers JMM, Halfens RJG, ter Borg S, Luiking YC, Verlaan S, et al. Validity and Reliability of Tools to Measure Muscle Mass, Strength, and Physical Performance in Community-Dwelling Older People: A Systematic

Review. Journal of the American Medical Directors Association. 2013;14(3):170-8.

532. Gallagher D, Visser M, De Meersman RE, Sepúlveda D, Baumgartner RN, Pierson RN, et al. Appendicular skeletal muscle mass: effects of age, gender, and ethnicity. Journal of Applied Physiology. 1997;83(1):229-39.

533. Lambin P, Leijenaar RTH, Deist TM, Peerlings J, de Jong EEC, van Timmeren J, et al. Radiomics: the bridge between medical imaging and personalized medicine. Nature Reviews Clinical Oncology. 2017;14(12):749-62.

534. Pena E, Ojiaku M, Inacio JR, Gupta A, Macdonald DB, Shabana W, et al. Can CT and MR Shape and Textural Features Differentiate Benign Versus Malignant Pleural Lesions? Acad Radiol. 2017;24(10):1277-87.

535. Catino A, Fanizzi A, Perrotti PPS, Pizzutilo P, Montrone M, Galetta D, et al. 125P Radiomic signature from baseline CT Scan to predict initial response to treatment in advanced/unresectable pleural mesothelioma: Preliminary data. Annals of Oncology. 2022;33:S89-S90.

536. Fontaine P, Acosta O, Castelli J, De Crevoisier R, Müller H, Depeursinge A. The importance of feature aggregation in radiomics: a head and neck cancer study. Scientific reports. 2020;10(1):19679-.